Optimization of thruster allocation for dynamically positioned marine vessels

Valčić, Marko

Doctoral thesis / Disertacija

2020

Degree Grantor / Ustanova koja je dodijelila akademski / stručni stupanj: **University of Rijeka, Faculty of Engineering / Sveučilište u Rijeci, Tehnički fakultet**

Permanent link / Trajna poveznica: https://urn.nsk.hr/urn:nbn:hr:190:415941

Rights / Prava: In copyright / Zaštićeno autorskim pravom.

Download date / Datum preuzimanja: **2024-11-30**

Repository / Repozitorij:

Repository of the University of Rijeka, Faculty of Engineering

UNIVERSITY OF RIJEKA
FACULTY OF ENGINEERING
Department of Naval Architecture and Ocean Engineering

Marko Valčić

OPTIMIZATION OF THRUSTER ALLOCATION FOR DYNAMICALLY POSITIONED MARINE VESSELS

DOCTORAL THESIS

Rijeka, 2020

UNIVERSITY OF RIJEKA
FACULTY OF ENGINEERING
Department of Naval Architecture and Ocean Engineering

Marko Valčić

OPTIMIZATION OF THRUSTER ALLOCATION FOR DYNAMICALLY POSITIONED MARINE VESSELS

DOCTORAL THESIS

Supervisor: Prof. D. Sc. Jasna Prpić-Oršić

Rijeka, 2020

SVEUČILIŠTE U RIJECI
TEHNIČKI FAKULTET
Zavod za brodogradnju i inženjerstvo morske tehnologije

Marko Valčić

OPTIMIZACIJA ALOKACIJE PROPULZORA KOD DINAMIČKI POZICIONIRANIH PLOVNIH OBJEKATA

DOKTORSKI RAD

Mentorica: prof. dr. sc. Jasna Prpić-Oršić

Rijeka, 2020.

Thesis Supervisor: Prof. D. Sc. Jasna Prpić-Oršić
University of Rijeka, Faculty of Engineering, Rijeka, Croatia

This doctoral thesis was defended on 6 March 2020 at the University of Rijeka, Faculty of Engineering, Rijeka, Croatia, in front of the following Evaluation Committee:

1 Prof. D. Sc. Roko Dejhalla, Chairman of the Committee
University of Rijeka, Faculty of Engineering, Rijeka, Croatia

2 Prof. D. Sc. Senka Maćešić, Member of the Committee
University of Rijeka, Faculty of Engineering, Rijeka, Croatia

3 Prof. D. Sc. Nastia Degiuli, Member of the Committee
University of Zagreb, Faculty of Mechanical Engineering and Naval Architecture, Zagreb, Croatia

Dedicated to my parents, Dora and Šime.

"Truth is much too complicated to allow anything but approximations."

John von Neumann

Acknowledgments

This work has been supported in part by the Croatian Science Foundation under the projects HRZZ-IP-2013-11-8722 (Greener Approach to Ship Design and Optimal Route Planning) and HRZZ-IP-2018-01-3739 (Decision Support System for Green and Safe Ship Routing). This work has also been supported in part by the University of Rijeka under the projects uniri-tehnic-18-266 (The impact of environmental loads on the characteristics of dynamic positioning systems for marine vessels) and uniri-tehnic-18-18 (Uncertainties of ship speed loss evaluation under real weather conditions), and by the University of Rijeka, Faculty of Engineering, Rijeka, Croatia.

During this PhD Study, I was fortunate enough to interact and discuss with a number of researchers from whom I have benefited substantially. Therefore, I would like to express my appreciation to all of them who have offered their time, advice, assistance, support and encouragement.

Most of all I would like to thank my supervisor, Professor Jasna Prpić-Oršić from the Faculty of Engineering, University of Rijeka, Rijeka, Croatia, for taking me in as a PhD Candidate, for believing in me, and for being such a great advisor and a great friend during all these years. Your encouragement and support were the key to solving every single problem or obstacle that came up during this research. Special thanks also goes to Professor Radoslav Nabergoj from the Faculty of Engineering, University of Trieste, Trieste, Italy, for the motivation received to accomplish this work and for lots of valuable discussions about initial key ideas related to dynamic positioning and thruster interactions.

Particularly motivating periods during this PhD study were my research visits to the Centre for Autonomous Marine Operations and Systems (AMOS), Department of Marine Technology, Norwegian University of Science and Technology (NTNU), Trondheim, Norway, from 2015 to 2017. Hence, I would like to express my sincere gratitude to my hosts, Professor Odd M. Faltinsen, Scientific advisor of AMOS, Professor Asgeir J. Sørensen, Director of AMOS, and Professor Sverre Steen, Head of Department of Marine Technology. Special thanks goes to Professor Sverre Steen and his former MSc student Mikal H. Espedal, for very valuable discussions on the thruster-thruster interactions and for providing me great support in extending the thruster-thruster interaction model based on the results of Mr. Erik Lehn, to whom I am also very grateful.

Due to the limited space, it is not quite possible to mention all the people I would still like to thank. However, at least I can say a sincere thanks to all my dear professors, colleagues and friends from the University of Rijeka, Faculty of Maritime Studies and Faculty of Engineering, for their great support and friendship.

At last, but not least, I especially have to point out that my family has always been with me and supported me from the very beginning in every way possible. I thank them immensely for their love and support, because without them this kind of work would not be possible to complete. A special gratitude goes to my wife Sonja for all those years of understanding, encouragement and support.

Abstract

Existing strategies and proposed methods for optimal thruster allocation in dynamic positioning systems of marine vessels are primarily focused on minimization of power consumption with handling of numerous constraints and limitations that should be satisfied at the same time. This particularly applies to thruster saturation and forbidden zones that are usually used in order to avoid or reduce thrust losses due to thruster-thruster interactions. By defining a forbidden zone for an azimuth thruster, generally a non-convex thrust region is left over which consequently can cause the significant deviations in allocated thruster azimuth angles and increase the time required for thrust and azimuth angle allocation. On the other hand, one can notice that thruster interaction effects such as axial and transverse current, thruster-hull interaction, thruster-thruster interaction and ventilation are rarely taken into account. These effects, whether they occur separately or in combinations, can cause significant thrust losses, which without appropriate reallocation strategy would consequently lead to degradation of vessel position and heading, as well as to increase of response time and power consumption.

In dynamic positioning systems, nonlinear objective functions, and nonlinear equality and inequality constraints within optimal thrust allocation procedures cannot be handled directly by means of the solvers like industry-standardized quadratic programing, at least not without appropriate linearization technique applied, which can be computationally very expensive. Thus, if optimization requirements are strict and problem should be solved for nonlinear objective function with nonlinear equality and inequality constraints, than one should use some appropriate nonlinear optimization technique. In addition, implementation of thruster interactions in optimal thrust allocation can easily transform the optimization problem into nonlinear and non-convex, which can become very demanding. In this context, two optimization approaches have been proposed. The first one is based on the weighted generalized inverse matrix approach, and the other one on the hybrid approach using sequential quadratic programing and direct search algorithms coupled with generalized regression neural network. The latter one is particularly convenient for handling non-convex and nonlinear optimization issues related to generally nonlinear power-thrust relationship and to non-convex nature of forbidden zones and thruster interaction effects. Moreover, both optimization approaches can handle selected thruster interaction effects with negligible increase in total power consumption, compared to the strategy based on forbidden zones only, while minimizing the tear and wear of thrusters at the same time. Obtained results were evaluated with numerous simulations involving different initial conditions and with direct comparison of analysed strategies that include forbidden zones, i.e. thruster-thruster interactions.

Key words

Dynamic positioning systems, thruster interactions, thrust losses, thruster allocation, nonlinear optimization

Sažetak

Postojeće strategije i predložene metode optimalne alokacije propulzora u sustavima za dinamičko pozicioniranje plovnih objekata su primarno usredotočene na minimizaciju potrošnje električne energije uz istovremeno zadovoljavanje brojnih ograničenja i uvjeta. To se posebno odnosi na zasićenje propulzora, kao i na zabranjene zone koje se uobičajeno koriste kako bi se izbjegli ili smanjili gubici poriva uzrokovani međudjelovanjem propulzora. Uvođenjem zabranjene zone za neki azimutni propulzor, skup mogućih rješenja tog propulzora općenito će postati ne-konveksan, što posljedično može rezultirati značajnim promjenama u alociranim azimutima te povećanjem vremena potrebnog za alokaciju propulzora. S druge strane, može se primijetiti da se učinci međudjelovanja propulzora poput aksijalnog i poprečnog sustrujanja, međudjelovanja propulzor-trup, međudjelovanja propulzor-propulzor i ventilacije, vrlo rijetko uzimaju u obzir. Ovi učinci, neovisno da li se javljaju svaki posebno ili u kombinacijama, mogu uzrokovati značajno smanjenje poriva, što bez odgovarajuće realokacijske strategije posljedično može dovesti do degradacije pozicije i smjera napredovanja plovnog objekta, te do povećanja vremena odziva i potrošnje električne energije.

U sustavima za dinamičko pozicioniranje, nelinearne funkcije cilja te nelinearna ograničenja u obliku jednakosti i nejednakosti ne mogu se izravno uzeti u obzir u optimalnoj alokaciji poriva. Kod industrijski prihvaćene metode kvadratičnog programiranja potrebno je provesti odgovarajuću linearizaciju koja može cijelu optimizaciju učiniti vrlo zahtjevnom u računalnom smislu. Stoga, ukoliko su zahtjevi optimizacije strogi, i problem je potrebno riješiti za slučaj nelinearne funkcije cilja uz nelinearna ograničenja u obliku jednakosti i nejednakosti, nužno je primijeniti odgovarajuću nelinearnu optimizacijsku metodu. Uzimanje u obzir međudjelovanja propulzora u optimizaciji alokacije poriva može optimizacijski problem dodatno transformirati u nelinearan i ne-konveksan, što može biti iznimno zahtjevno. U tom kontekstu, u ovom radu su predložena dva optimizacijska pristupa. Prvi se temelji na otežanoj generaliziranoj inverznoj matrici, a drugi na hibridnom pristupu koji uključuje sekvencijalno kvadratično programiranje, metode direktnog traženja i generaliziranu regresijsku neuronsku mrežu. Potonji pristup je posebno prikladan za rješavanje problema optimalne alokacije poriva vezanih uz općenito nelinearnu ovisnost snage i poriva propulzora, kao i uz ne-konveksnu prirodu zabranjenih zona i međudjelovanja propulzor-propulzor. U odnosu na optimizacijsku strategiju temeljenu isključivo na zabranjenim zonama, oba predložena optimizacijska pristupa mogu uzeti u obzir efekte međudjelovanja propulzora sa zanemarivim povećanjem ukupno utrošene snage, dok se njihovim korištenjem istovremeno minimizira trošenje i habanje propulzora. Dobiveni rezultati su evaluirani kroz brojne simulacije s različitim početnim uvjetima, uz direktnu usporedbu strategija sa zabranjenim zonama i s međudjelovanjem propulzora.

Ključne riječi

Sustavi za dinamičko pozicioniranje, međudjelovanja propulzora, smanjenje poriva, alokacija propulzora, nelinearna optimizacija

Contents

Acknowledgments viii

Abstract ix

Sažetak x

Nomenclature xiv

1 Introduction 1
- 1.1 Background and previous work 1
- 1.2 Motivation and objectives 6
- 1.3 Problem statement 9
- 1.4 Organization of the thesis 9
- 1.5 Scientific contributions 11

2 Dynamic positioning systems 12
- 2.1 General features and modelling characteristics of dynamically positioned marine vessels 12
- 2.2 Kinematics and dynamics of marine vessels 16
- 2.3 Environmental loads 18
  - 2.3.1 Wind loads 20
  - 2.3.2 Sea current loads 23
  - 2.3.3 Mean and slowly varying wave drift forces 24
- 2.4 Thrusters in dynamic positioning systems 30
  - 2.4.1 General features of azimuth thrusters 31
  - 2.4.2 Empirical modelling of ducted propeller hydrodynamic characteristics 33

3 Modelling of thrust and thruster interaction effects 37
- 3.1 Modelling of thrust in propulsion system of a dynamically positioned marine vessel 37
- 3.2 Thruster interaction effects and thrust reduction 40
  - 3.2.1 The problem of incoming current 40
  - 3.2.2 Thruster-thruster interaction 47
  - 3.2.3 Thruster-hull interaction and Coanda effect 55
  - 3.2.4 Ventilation and in-and-out-of-water effects 56

4 Thrust allocation and optimality considerations 57
- 4.1 Thrust allocation problem 57
  - 4.1.1 Thrust regions 59
  - 4.1.2 Constraints and limitations 60
    - 4.1.2.1 Thruster saturation 60

4.1.2.2 Forbidden zones 64
4.1.2.3 Other constraints and limitations 67
4.2 General considerations about optimal thrust allocation 68
4.2.1 Objective functions 68
4.2.2 Linear equality constraints 73
4.2.3 Linear inequality constraints 74

5 Optimization methods for optimal thrust allocation 76
5.1 Gradient-based optimization methods 76
5.1.1 Lagrange multiplier method 77
5.1.2 Quadratic programming 79
5.1.3 Sequential quadratic programming 83
5.2 Derivative free optimization methods based on direct search algorithms 88
5.2.1 Coordinate search algorithm 89
5.2.2 Generalized pattern search algorithm 91
5.2.3 Generating set search algorithm with augmented Lagrangian 93
5.2.4 Mesh adaptive direct search algorithm 95

6 Impact of thruster-thruster interaction effects on optimal thrust allocation 98
6.1 Setup for numerical simulations and examples 98
6.1.1 Characteristics of the reference vessel 98
6.1.2 Environmental load modelling for the reference vessel 99
6.1.3 Considerations about thruster-thruster interaction effects for the reference vessel 103
6.2 Direct solution approach for thruster-thruster interactions 104
6.2.1 Moore-Penrose pseudo-inverse and generalized inverse matrix 105
6.2.2 Thruster saturation with pseudo and generalized inverse matrix approach 106
6.2.3 Further applications of the weighting matrix 107
6.2.4 Handling of thrust losses with generalized inverse matrix approach 109
6.2.5 Numerical example on implementation and analysis of thruster-thruster interaction 110
6.3 Forbidden zone handling in optimal thrust allocation 114
6.3.1 Generalized inverse matrix approach 114
6.3.2 Quadratic programming with thruster saturation and forbidden zones included 114
6.3.3 Numerical example with comparative analysis 116

7 Nonlinear optimization of thrust allocation 125
7.1 Considerations about nonlinear optimal thrust allocation 125
7.1.1 Compatibilities and disparities of gradient based and derivative free optimization algorithms 125
7.1.2 Power consumption as a nonlinear objective function 126
7.1.3 Nonlinear inequality constraints for thruster saturation and handling of forbidden zones 128

7.1.4 Nonlinear and non-convex equality constraints for handling of thruster interaction effects 129
7.1.5 Linear equality and inequality constraints 131
7.2 Nonlinear optimal thrust allocation 131
7.2.1 Problem definition and two-step solution approach 131
7.2.2 Numerical examples and discussion of results 134
7.3 Hybrid approach to nonlinear optimal thrust allocation 138
7.3.1 Convergence and computational cost issues 138
7.3.2 Hybrid optimization with sensitivity analysis 139
7.3.3 Numerical examples and analysis of results 143

8 Conclusions and recommendations 147
8.1 Conclusions 147
8.2 Recommendations for future work 150

Bibliography 151

List of figures 157

List of tables 159

Appendixes 160
Appendix 1 Pseudo-code of optimization algorithms 161
Appendix 2 Non-dimensional wave load coefficients for the reference vessel 167
Appendix 3 Polar thrust distribution of azimuth thrusters with respect to the wind angle of attack and various environmental conditions 168
Appendix 4 Resulting thrusts and azimuth angles with respect to the wind angle of attack for all azimuth thrusters under specific environmental conditions (WGIM/QP approach) 172
Appendix 5 Resulting thrusts and azimuth angles with respect to the wind angle of attack for all azimuth thrusters under specific environmental conditions (SQP/DS approach) 175
Appendix 6 Quantitative indicators of demanded power for analysed cases obtained with FZ and TTI optimization approaches for analysed thrusters 178

Curriculum Vitae 179

Nomenclature

Abbreviations

AGA	Adaptive genetic algorithm
ALPS	Augmented Lagrangian pattern search
BCQP	Box constrained quadratic program
BFGS	Broyden-Fletcher-Goldfarb-Shanno
CB	Centre of buoyancy
CF	Centre of floatation
CFD	Computational fluid dynamics
CG	Centre of gravity
CPP	Controllable pitch propeller
CS	Coordinate search
DFO	Derivative free optimization
DOF	Degree of freedom
DP	Dynamic positioning
DS	Direct search
E	East
ECEF	Earth-centred Earth-fixed
ECI	Earth-centred inertial
EKF	Extended Kalman filter
FPP	Fixed-pitch propeller
FS	Feasible set
FZ	Forbidden zone
GA	Genetic algorithm
GIM	Generalized inverse matrix
GNC	Guidance, navigation and control
GPS	Generalized pattern search
GRNN	Generalised regression neural network
GSS	Generating set search
HF	High frequency
HMI	Human machine interface
KF	Kalman filter
KKT	Karush-Kuhn-Tucker
LF	Low frequency
LP	Linear programming
MADS	Mesh adaptive direct search
mp-QP	Multi-parameter quadratic programming
MSE	Mean squared error
N	North
NED	North-East-Down
NM	Nelder-Mead
PMS	Power management system
pQP	Parametric quadratic programming
PS	Pattern search
PSO	Particle swarm optimization
QP	Quadratic programming
RAO	Response amplitude operator
RB	Rigid body
SA	Simulated annealing
SQP	Sequential quadratic programming
SVD	Singular values decomposition
TTI	Thruster-thruster interaction
WGIM	Weighted generalized inverse matrix

Lowercase

$\mathbf{a}_i$	Linear equality or inequality constraint
b	Jet width, m
$\{b\}$	Body reference frame
b_{i1}	Intercept in a polygon, N
$\mathbf{b}$	Bias vector of slowly varying loads
$\mathbf{b}_{\text{eq}}$	Linear equality constraint vector
$\mathbf{b}_i$	Linear inequality constraint vector related to thruster saturation and forbidden zones
$\mathbf{b}_i^{\text{TS}}$	Linear inequality constraint vector related to thruster saturation
$\mathbf{b}_{\text{ineq}}$	Linear inequality constraint vector
$\mathbf{c}(\mathbf{x})$	Vector of equality constraints
$\mathbf{c}_i(\mathbf{x})$	i-th general nonlinear equality/inequality constraints
$\mathbf{d}$	Poll direction
$d(\mathbf{x},\mathbf{y})$	Euclidean distance between vectors $\mathbf{x}$ and $\mathbf{y}$
$d(\mathbf{X},\mathbf{Y})$	Euclidean distance between matrices $\mathbf{X}$ and $\mathbf{Y}$
$\{e\}$	ECEF coordinate system
$\mathbf{e}_i$	Unit vector
$\mathbf{e}$	Vector of unit vectors

$\mathbf{e}_{exc}$ Vector of environmental conditions and loads (GRNN excitation)

f Objective (cost) function

g Gravitational acceleration, m/s^2

$g_j(\mathbf{x})$ i-th inequality constraint

$\mathbf{g}$ Vector of generalized gravitational and buoyancy forces

$\mathbf{g}(\mathbf{u})$ Vector of inequality constraints

$\mathbf{g}(\mathbf{x})$ Inequality constraint

$\mathbf{g}_j(\mathbf{u})$ j-th inequality constraint

$\mathbf{g}_0$ Static recuperation forces and moments

$h_i(\mathbf{x})$ i-th equality constraint

$\mathbf{h}(\mathbf{u})$ Vector of equality constraints

$\mathbf{h}(\mathbf{x})$ Equality constraint

$\mathbf{h}_i(\mathbf{u})$ i-th equality constraint

i Step, counter

$\{i\}$ ECI coordinate system

j Step, counter

k Step, counter, class

l_{ix} x coordinate of the i-th thruster in $\{b\}$, m

l_{iy} y coordinate of the i-th thruster in $\{b\}$, m

$\mathbf{l}_B$ Lower boundary

m_i Power exponent associated to i-th thruster

n Propeller (shaft) speed, s^{-1}

$\{n\}$ NED coordinate system

n_{d} Demanded shaft speed, s^{-1}

p Angular velocity about the x axis in terms of $\{b\}$, rad/s

$\mathbf{p}$ Improving direction

q Angular velocity about the y axis in terms of $\{b\}$, rad/s

r Angular velocity about the z axis in terms of $\{b\}$, rad/s; Radial distance, m; Total number of thrusters;

r_i Inner radius of i-th azimuth thruster, N

$s(\mathbf{x},\mathbf{y})$ Similarity measure between vectors $\mathbf{x}$ and $\mathbf{y}$

$s(\mathbf{X},\mathbf{Y})$ Similarity measure between matrices $\mathbf{X}$ and $\mathbf{Y}$

s_{i1} Polygon side, N

s_{ij} Polygon side, N

s_j Slack variable associated with j-th inequality constraint

$s_{tol}(\mathbf{x},\mathbf{y})$ Threshold value for similarity measure between vectors $\mathbf{x}$ and $\mathbf{y}$

$\mathbf{s}$ Vector of slack variables associated with inequality constraints

$\mathbf{s}_k$ Step vector

t Thrust reduction ratio, -

t_0 Thrust reduction ratio, -

t_{1a} Thrust reduction ratio, -

$t_{elapsed}$ Elapsed time during convergence (training), s

t_{resp} Response time of trained GRNN, s

t_{train} Elapsed time during GRNN training, s

$\mathbf{t}$ Set of evaluation (trial) points from the poll set

u Linear surge velocity in the x direction in terms of $\{b\}$, m/s; Centreline velocity, m/s

u_0 Velocity at the nozzle outlet, m/s

u_{ix} Component of the thrust T_i in surge direction, N

$u_{ix}^{(k)}$ Value of x-component of i-th thruster in k-th class, N

u_{iy} Component of the thrust T_i in sway direction, N

$u_{iy}^{(k)}$ Value of y-component of i-th thruster in k-th class, N

u_m Maximum axial velocity, m/s

u_{wind} Longitudinal component of absolute wind speed, m/s

$\mathbf{u}$ Design vector of thrust components in Cartesian coordinates

$\mathbf{u}^*$ Optimal solution in terms of vector $\mathbf{u}$

$\mathbf{u}_0$ Initial solution

$\mathbf{u}_{0j}$ j-th randomly chosen initial solution

$\mathbf{u}_{\mathrm{a}}$ Vector of actual thrust

$\mathbf{u}_B$ Upper boundary

$\mathbf{u}_{\mathrm{d}}$ Vector of demanded (desired) thrust

$\mathbf{u}_{\mathrm{DS}}$	Optimal solution $\mathbf{u}$ obtained with DS approach
$\mathbf{u}_{ix}^{(k)}$	Vector of x-components of i-th thruster in k-th class
$\mathbf{u}_{iy}^{(k)}$	Vector of x-components of i-th thruster in k-th class
$\mathbf{u}_{\mathrm{I,GRNN}}$	First class direct GRNN solution
$\mathbf{u}_{\mathrm{II,GRNN}}$	Second class direct GRNN solution
$\mathbf{u}_{\mathrm{I,SQP}}$	First class SQP optimal solution
$\mathbf{u}_{\mathrm{II,SQP}}$	Second class SQP optimal solution
$\mathbf{u}_{\mathrm{SQP}}$	Optimal solution $\mathbf{u}$ obtained with SQP approach
v	Linear sway velocity in the y direction in terms of $\{b\}$, m/s
v_{wind}	Lateral component of absolute wind speed, m/s
w	Linear heave velocity in the z direction in terms of $\{b\}$, m/s
w_i	Weighting coefficient associated to i-th thruster
$\mathbf{w}$	Vector of weighting coefficients
x	Position in N, m (°); Distance between rear and front thruster, m
x_b	x axis of $\{b\}$
x_1^k	Coordinate of a current point
x_2^k	Coordinate of a current point
$\mathbf{x}$	Design vector
$\mathbf{x}^*$	Optimal solution
$\tilde{\mathbf{x}}$	Estimate of initial point
$\mathbf{x}_0$	Initial point
$\mathbf{x}_k$	Current point
y	Position in E, m (°)
y_b	y axis of $\{b\}$
$\mathbf{y}_k$	Step vector

Uppercase

$\mathbf{0}_i^{\mathrm{FZ}_{ik}}$	Linear inequality constraint vector related to forbidden zones
$A_E \,/\, A_0$	Expanded-area ratio, -
$A_{F,curr}$	Frontal projected area below the water line, m²
$A_{F,wind}$	Vessel's frontal projected area above the water line, m²
$A_{L,curr}$	Lateral projected area below the water line, m²
$A_{L,wind}$	Vessel's lateral projected area above the water line, m²
$A_{x,y}$	Regression coefficients for K_T
$\mathbf{A}$	Matrix of coefficients $A_{x,y}$
$\mathbf{A}_{\mathrm{eq}}$	Linear equality constraint matrix
$\mathbf{A}_i$	Linear inequality constraint matrix related to thruster saturation and forbidden zones
$\mathbf{A}_i^{\mathrm{FZ}_{ik}}$	Linear inequality constraint matrix related to forbidden zones
$\mathbf{A}_{\mathrm{ineq}}$	Linear inequality constraint matrix
$\mathbf{A}_i^{\mathrm{TS}}$	Linear inequality constraint matrix related to thruster saturation
B	Beam, m
$B_{x,y}$	Regression coefficients for K_{TN}
$\mathbf{B}$	Matrix of coefficients; Configuration matrix
$\mathbf{B}_k$	Symmetric positive definite matrix
$\mathbf{B}^{\dagger}$	Moore-Penrose pseudo-inverse matrix
$\mathbf{B}_w^{\dagger}$	Generalized inverse matrix
$C_{N,curr}$	Non-dimensional sea current load coefficient in yaw direction, -
$C_{N,wave}$	Non-dimensional coefficient of wave moment in yaw, -
$C_{N,wind}$	Non-dimensional wind load coefficient in yaw direction, -
$C_{x,y}$	Regression coefficients for K_Q
$C_{X,curr}$	Non-dimensional sea current load coefficient in surge direction, -

$C_{X,wave}$ Non-dimensional coefficient of longitudinal wave force, -

$C_{X,wind}$ Non-dimensional wind load coefficient in surge direction, -

$C_{Y,curr}$ Non-dimensional sea current load coefficient in sway direction, -

$C_{Y,wave}$ Non-dimensional coefficient of lateral wave force, -

$C_{Y,wind}$ Non-dimensional wind load coefficient in sway direction, -

$\mathbf{C}$ Matrix of Coriolis and centripetal forces; Matrix of coefficients

$\mathbf{C}_{\text{eq}}$ Linear equality constraint matrix related to tunnel thrusters

D Propeller (thruster) diameter, m

$\mathbf{D}$ Damping matrix; Fixed finite set of p mesh directions

E Finite sets of integers

$\mathbf{E}_{in}$ Environmental conditions and loads (GRNN inputs)

F_k Frame

F_{loads} Resulting force, N

$\mathbf{F}_x$ Vector of forces in surge direction

$F_{x,curr}$ Longitudinal sea current force, N

$F_{x,loads}$ Surge force of environmental loads, N

$\overline{F}_{x,wave}$ Longitudinal mean wave drift force, N

$F_{x,wave}^{\text{model}}$ Longitudinal mean wave drift forces for a model, N

$\mathbf{F}_y$ Vector of forces in sway direction

$F_{x,wind}$ Longitudinal wind force, N

$F_{y,curr}$ Transverse sea current force, N

$F_{y,loads}$ Sway force of environmental loads, N

$\overline{F}_{y,wave}$ Lateral mean wave drift force, N

$F_{y,wave}^{\text{model}}$ Lateral mean wave drift forces for a model, N

$F_{y,wind}$ Transverse wind force, N

H_s Significant wave height, m

$\mathbf{H}_s$ Vector of significant wave heights

I Finite sets of integers

$\mathbf{I}$ Unit matrix

J Advance coefficient, -

J_0 Advance coefficient at bollard pull conditions, -

J_{rear} Advance coefficient of the rear thruster, -

$\mathbf{J}$ Transformation matrix; Vector of J values

K Roll moment about the *x* axis in terms of {*b*}, Nm

K_Q Torque coefficient, -

K_{Q0} Nominal torque coefficient, -

K_T Thrust coefficient, -

K_{T0} Nominal thrust coefficient, -

$K_{T0,rear}$ Thrust coefficient of the rear thruster in bollard pull conditions, -

K_{TN} Nozzle thrust coefficient, -

$K_{T,rear}$ Thrust coefficient of the rear thruster, -

L Nozzle length, m

L_{oa} Vessel's length overall, m

L_{pp} Length between perpendiculars, m

L_{WL} Length of the vessel on the waterline, m

L_{WL}^{model} Length of the model at waterline, m

M Pitch moment about the *y* axis in terms of {*b*}, Nm; Counter

M_0 Number of randomly chosen initial solutions

$M_{z,curr}$ Yawing sea current moment, Nm

$M_{z,loads}$ Yawing moment of environmental loads, Nm

$\overline{M}_{z,wave}$ Mean wave moment around vertical axis, Nm

$M_{z,wave}^{\text{model}}$ Model moment of rotation about the vertical axis, N

$M_{z,wind}$ Yawing wind moment, Nm

$\mathbf{M}$ System inertia matrix

$\mathbf{M}_z$ Vector of moments in yaw rotation

N Yaw moment about the *z* axis in terms of {*b*}, Nm; Total number of some arbitrarily sample; Propeller (shaft) speed, min^{-1}

N_{eval} Number of objective function evaluations

N_i Number of polygon sides, i.e. linear inequalities

$N_{i,\min}$ Minimum number of polygon sides

N_{iter} Number of iterations

P Total power demand, W

P/D Pitch ratio

$(P/D)_{\mathrm{d}}$ Demanded propeller pitch ratio

P_0 Delivered power at bollard pull conditions, W

P_{a} Propeller actual power consumption, W

P_{GIM} Demanded power in GIM approach

P_i Power demand for *i*-th thruster, W

$P_{i,\max}$ Maximal power of *i*-th thruster unit, W

$P_{i,\min}$ Minimal power of *i*-th thruster unit, W

P_k Poll set

P_{QP} Demanded power in QP approach

$P_{\mathrm{SQP/DS}}$ Demanded power in SQP/DS approach without FZ or TTI

$P_{\mathrm{SQP/DS}}^{\mathrm{FZ}}$ Demanded power in SQP/DS approach with FZ

$P_{\mathrm{SQP/DS}}^{\mathrm{TTI}}$ Demanded power in SQP/DS approach with TTI

P_{WGIM} Demanded power in WGIM approach

$\mathbf{P}$ Vector of P/D values

Q Torque, Nm

Q_0 Propeller torque at bollard pull conditions, Nm

Q_{a} Actual torque, Nm

R_{AW} Added resistance in regular waves, N

$\overline{R}_{AW}$ Mean added resistance in irregular waves, N

R_i Radius of a circle that defines thrust region of *i*-th azimuth thruster, N

$\mathbf{R}$ Rotation matrix

$S(\omega)$ Wave energy spectrum, kJsm^{-2}

T Thrust, N; Summer draft, m

T_0 Peak wave period, s; Propeller thrust at bollard pull conditions, N

T_1 Average wave period, s

T_{a} Actual thrust, N

T_{d} Demanded thrust, N

T_F Thrust of the front thruster, N

T_i Thrust magnitude of *i*-th thruster, N

$\dot{T}_i$ Rate of change in thrust magnitude, N/s

$T_{i,\max}$ Maximum thrust of *i*-th thruster, N

$T_{i,\min}$ Minimum thrust of *i*-th thruster, N

T_N Nozzle thrust, N

T_R Thrust of the rear thruster, N

T_z Average zero-crossing wave period, s

$\mathbf{T}$ Transformation matrix of angular velocities

$\mathbf{T}_0$ Vector of wave peak periods

U Resulting speed of the vessel, m/s; Set of feasible thrust region

$\mathbf{U}$ Target matrix

$\hat{\mathbf{U}}$ GRRN response matrix

$\mathbf{U}_{\mathrm{I}}$ First class optimal solutions (GRNN targets)

$\mathbf{U}_{\mathrm{II}}$ Second class optimal solutions (GRNN targets)

$\mathbf{U}_k$ Target matrix of *k*-th class

V_{A} Speed of advance, m/s

$V_{A,rear}$ Advance velocity for the rear thruster, m/s

V_{wind} Absolute wind speed, m/s

$\mathbf{V}_{curr}$ Vector of sea current velocities

$\mathbf{V}_{wind}$ Vector of wind velocities

W_0 Initial working set

W_k Working set

$\mathbf{W}$ Weighting matrix

$\mathbf{W}_0$ Weighting matrix of thruster constants w_i

$\mathbf{W}_1$ Weighting matrix for excluding of tunnel thrusters

$\mathbf{W}_2$ Weighting matrix for implementation of thrust reduction ratios

$\mathbf{W}_j$ General weighting matrix

X	Surge force in the *x* direction in terms of {*b*}, N
X_L	Trust region
Y	Sway force in the *y* direction in terms of {*b*}, N
Z	Heave force in the *z* direction in terms of {*b*}, N; Number of blades

Greek

α_i	Azimuth angle of *i*-th thruster
$\dot{\alpha}_i$	Rate of change in thruster azimuth angle, rad/s (°/s)
$\alpha_{i,\max}$	Maximum azimuth angle, ° (rad)
$\alpha_{i,\min}$	Minimum azimuth angle, ° (rad)
α_k	Step length
β_{wave}	Wave propagation direction, ° (rad)
γ	Peak-shape parameter, ° (rad)
γ_{curr}	Sea current angle of attack, ° (rad)
$\gamma_{rel,wind}$	Relative wind direction, ° (rad)
γ_{wind}	Absolute wind direction (encounter angle), ° (rad)
$\gamma_{wind,\text{peak}}$	Peak value of γ_{wind} for which δP is maximal
$\boldsymbol{\gamma}_{wind}$	Vector of wind encounter angles
δ	Interaction angle of the rear thruster, °
δe_i	Relative approximation error
δP	Relative deviation of power P
δP_{FZ}	Relative deviation of power P with FZ approach
δP_{peak}	Maximum value of δP
δP_{QP}	Relative deviation of power P in QP approach
δP_{TTI}	Relative deviation of power P with TTI approach
δP_{WGIM}	Relative deviation of power P in WGIM approach
Δ	Displacement, t
Δ_0	Initial step length
Δ_k	Step length (mesh size parameter)
Δe_i	Absolute approximation error, N
ΔP	Change in power, W
Δr_{i1}	Slope of the first inner radius in a polygon
ΔT	Change in thrust T, N
ε	Threshold value
ε_k	Random phase angle of wave component *k*, rad
ζ_a	Amplitude of a regular wave, m
ζ	Wave elevation, m
$\zeta_{a,k}$	Wave amplitude, m
η_0	Open water efficiency of a propeller, -
$\boldsymbol{\eta}$	Vector of position and heading
ϑ_i	Exterior angle of a polygon, °
θ	Pitch angle, ° (rad); Wave encounter angle, ° (rad)
Θ_k	Frame size parameter
Θ_k^p	Poll size parameter
$\boldsymbol{\Theta}$	Vector of Euler angles
λ	Wavelength, m
$\overline{\lambda}$	Relative wavelength, m
λ_i	Lagrange multiplier associated with *i*-th equality constraint
$\boldsymbol{\lambda}$	Vector of Lagrange multipliers associated with equality constraints
$\boldsymbol{\mu}$	Vector of Lagrange multipliers associated with inequality constraints
$\mu(x)$	Mean value of variable x
μ_j	Lagrange multiplier associated with *j*-th inequality constraint
$\boldsymbol{\nu}$	Vector of linear and angular velocities
ρ_{air}	Air density, kg/m^3
ρ	Seawater density, kg/m^3; Positive penalty parameter
ρ_{water}	Water density, kg/m^3
$\sigma(x)$	Standard deviation of variable x
$\boldsymbol{\tau}$	Vector of generalized forces and moments in three or six DOF

$\boldsymbol{\tau}_{\mathrm{c}}$	Vector of generalized forces and moment
$\boldsymbol{\tau}_{current}$	Vector of sea current loads
$\boldsymbol{\tau}_{red}$	Reduced load vector $\boldsymbol{\tau}$
$\boldsymbol{\tau}_{wave}$	Vector of wave loads
$\boldsymbol{\tau}_{wave1}$	First order wave induced forces
$\boldsymbol{\tau}_{wave2}$	Second order wave induced forces
$\overline{\boldsymbol{\tau}}_{wave,\,\mathrm{m}}$	Mean component of $\boldsymbol{\tau}_{wave2}$
$\boldsymbol{\tau}_{wave,\,\mathrm{sv}}$	Slowly varying component of $\boldsymbol{\tau}_{wave2}$
$\boldsymbol{\tau}_{wind}$	Vector of wind loads
ϕ	Interaction angle of the front thruster, °; Roll angle, ° (rad); Merit function;
φ	Roll angle, ° (rad); Angle, ° (rad)
$\varphi(J)$	Iteration function
$\varphi_{\mathrm{end}}^{\mathrm{FS}_{ik}}$	Ending angle of *k*-th feasible set for *i*-th thruster, ° (rad)
$\varphi_{\mathrm{start}}^{\mathrm{FS}_{ik}}$	Starting angle of *k*-th feasible set for *i*-th thruster, ° (rad)
$\varphi_{\mathrm{end}}^{\mathrm{FZ}_{i}}$	Ending angle of forbidden zone for *i*-th thruster, ° (rad)
$\varphi_{\mathrm{start}}^{\mathrm{FZ}_{i}}$	Starting angle of forbidden zone for *i*-th thruster, ° (rad)
ψ	Yaw angle (heading), ° (rad)
ω_0	Peak frequency of the spectrum, s^{-1}
ω_k	Wave frequency, s^{-1}

Other

$\left\|\cdot\right\|_1$	ℓ^1 norm
$\left\|\cdot\right\|_2$	ℓ^2 norm
$\left\|\cdot\right\|_\infty$	ℓ_∞ norm
L	Lagrangian
$\nabla\mathbf{c}$	Jacobian of equality constraint vector $\mathbf{c}$
∇L	Jacobian of the Lagrangian L
$\nabla^2 L$	Hessian matrix of the Lagrangian L
$\mathbb{R}$	Set of real numbers
$\mathbb{D}_k$	Set of poll directions
$\max(\mathbf{x})$	Maximum component in vector $\mathbf{x}$
$\min(\mathbf{x})$	Minimum component in vector $\mathbf{x}$

1 INTRODUCTION

1.1 Background and previous work

Dynamic positioning (DP) systems are nowadays mostly used for classical station-keeping, maintaining of a predefined path or track, position mooring, etc. In order to perform these operations it is necessary to ensure the following (Sørensen, 2012):

- determination of accurate estimation of the position, heading and speed of the vessel,
- calculation of the required reaction forces and moments in order to compensate the action effects of environmental loads and other external disturbances, i.e. to eliminate the deviation from a predetermined position, path or track,
- operation of a subsystem that will generate the previously calculated forces and moment by means of the vessel's propulsion system.

As far as the propulsion systems of marine vessels are concerned, a number of thruster types have been developed up to date for the requirements of the maritime industry, but when it comes to their application in dynamic positioning systems, the non-retractable and retractable azimuth thrusters, in eventual combination with tunnel thrusters, are mostly used. This choice is quite understandable, and is justified by the fact that due to the different directions of external disturbances, thrusters should be able to operate in 360° at all times. Somewhat less common application is the Voith Schneider cycloid propulsor and combinations that include main propeller(s) with rudder(s).

The orientation, i.e. the angle or azimuth of each thruster, as well as the required thrust it generates, are determined by the control logic of dynamic positioning systems. This whole process is called the thrust allocation and represents a very complex mapping of the previously calculated or estimated environmental forces and moment to the set of referent states of the available thrusters.

Since DP vessels usually have fixed and azimuth thrusters, the vector of design variables must have one variable for fixed (e.g. tunnel) thrusters and two for azimuth thrusters. The basic constraints on the objective function are (at least) three equalities stemming from the fact that the generated thrust forces (F_x and F_y) and moment (M_z) should be equal with environmental loads for all three horizontal degrees of freedom. This simplified optimization approach can be reduced on finding the conditional extremes of the Lagrange's objective function. If additional constraints, usually

expressed by the matrix inequalities (e.g. thruster saturation, thruster efficiency, electrical power limitation, etc.), are added to the basic constraints, the optimization task becomes considerably more complex and is usually solved by the quadratic programming algorithms or so-called QP solvers (Jenssen and Realfsen, 2006). From a theoretical point of view, the problem of the thrust allocation could be solved by linear programming (LP solvers), but due to the approximation of the relation between the electrical power consumption (kW) and the generated thrust (kN) by the quadratic function, some of the variants of the quadratic programming are usually used (Snijders, 2005; Wit, 2009).

If the problem of the quadratic programming of the thrust allocation is set correctly, it can be explicitly solved, i.e. it is possible to determine the global minimum (Leavitt, 2008). In general, the QP consists of the quadratic objective function and linear equalities and inequalities representing the conditions, i.e. the constraints. The classic approach of solving the thrust allocation problem is reduced on solving the optimization task with the purpose of minimizing the static quadratic objective function with the new conditions in each successive moment (Jenssen, 1980; Lindfors, 1993). The basic assumption used by Jenssen (1980) and Lindfors (1993) in their papers is that the action of each azimuth thruster is replaced by the action of two independent and perpendicularly fixed thrusters without constraints on the rotation speed, which is also one of the biggest disadvantages of the classic QP approach in the thrust allocation.

Sørdalen (1997) has shown that this assumption is inappropriate in practice, both because of the mechanical and the operational limitations. He has also shown that the constraints on azimuth thrusters can lead to singular configurations, which he solved using the method of singular values decomposition (SVD). This approach provided significantly lower power consumption, effectively eliminated the issue of the forbidden zones, reduced tear and wear of thrusters. With the application of so-called logical inequalities and Moore-Penrose pseudo-inverse matrix (SVD method), it is possible to directly determine the vector of demanded forces and moment (Gierusz and Tomera, 2006; Yang et al., 2011b). This approach has given the expectedly faster results in the computational sense compared to optimization tasks based on programming, as well as much less oscillations in azimuth changes of the thrusters (Gierusz and Tomera, 2006). Although there are certain implementation limitations, such an approach can also take constraints like forbidden zones into account (Yang et al., 2011b).

If the constraints in the quadratic optimization task become nonlinear, it is no longer possible to use the QP solvers directly. One of the possible solutions to this problem is the application of the so-called sequential quadratic programming (SQP) technique that is generally used to minimize an arbitrarily selected objective function regarding the nonlinear constraint set in the form of equalities and inequalities. The possible applications of SQP approach in optimal thrust allocation were investigated by Liang and Cheng (2004) and Johansen et al. (2004). Although tested only on simulation models, the obtained results (Liang and Cheng, 2004) indicate very good capabilities of the SQP solver which in a computational sense can execute the allocation very fast with a small thrusters' azimuth change. Johansen et al. (2004) have further expanded the application possibilities of the SQP approach with the emphasis on avoiding possible singularities that are unacceptable in control sense.

Apart from the analysis of the possible applications of the SQP solver, the application of the so-called multi-parameter quadratic programming (mp-QP) has been analysed in several studies, in which the QP task is parameterized with the data such as the demanded thrust, certain limitations, criteria for particular parameters, etc. (Johansen et al., 2005; Leavitt, 2008). It has been shown that the solution of the mp-QP problem can be determined quickly and explicitly in the off-line mode of operation, and then evaluated in the on-line mode of operation (Johansen et al., 2005). Certain drawbacks in this approach are outlined by Leavitt (2008). Namely, according to his research, such an approach in off-line mode of operation is only suitable for certain types of vessels, without azimuth thrusters, so he suggests a certain generalization of the mp-QP algorithm through the so-called BCQP (Box Constrained Quadratic Program) algorithm. It is a hybrid algorithm that works both in the on-line and off-line mode of operation, and eventually is simpler than other typical on-line algorithms such as the SQP.

In addition to the SQP approach for solving the problem of nonlinear constraints of the optimization task, most recently the genetic algorithms (GA) have been increasingly used as a robust solution that ensures a good convergence of the global optimization process (Yang et al., 2011a; Zhao et al., 2010). The tests that have been carried out by Yang et al. (2011a) indicate the promising results on using these algorithms, although the authors point out the problem of possible application of GA in thruster allocation regarding the slow convergence. A better solution was suggested by Zhao et al. (2010) using the so-called adaptive GA (AGA) which equally well solves the optimization tasks with nonlinear constraints, but in a considerably shorter time interval than the simple GA.

An excellent review of the majority of optimal thrust allocation methods proposed in the literature so far is given by Johansen and Fossen (2013). The authors particularly emphasize and conclude that numerical optimization is much more challenging than classic linear and quadratic programming, mostly because of the risk that algorithm converges to some local minimum. Computational complexity, numerical sensitivity, the lack of capability for verification and validation, represent just a few additional challenges.

In the exploitation of the DP systems, regardless of the usually high level of the redundancy, there is a possibility of both the hardware and software failures of the thruster units, which directly affects the thrusters' configuration. A relatively small number of researchers have dealt with these issues so far. The highlighted ones are the paper of Spjøtvold and Johansen (2009), in which the authors developed an explicit solution of the optimal thrust allocation with the tolerance to the hardware failures based on the parametric quadratic programming (pQP), and the paper of Shi et al. (2011), in which the authors developed the strategy of the group biasing, i.e. the methodology by which the available thrusters are grouped into certain clusters which act independently as one thruster, thus increasing the performance of the entire propulsion system and reducing the possibility that programming errors may cause problems to the control logic of the DP system.

The research part that is least represented in the papers on the optimal thrust allocation are certainly the various forms and effects of interactions between the thruster and its environment, which consequently cause various thrust losses, particularly in hydrodynamic sense. As the most important thrust loss effects one can differ: transverse and longitudinal forces – the interaction of jet and sea current, the thruster-hull interaction with Coanda effect, thruster-thruster interaction, and thruster ventilation combined with in-and-out-water effects (Ekstrom and Brown, 2002; Lehn, 1992).

It should be noted that the number of papers, i.e. researchers that are dealing with these issues is relatively small, and generally this research field itself is insufficiently studied. However, the launch of large-scale projects led by the internationally renowned marine technology research centres, such as Marin (Netherlands, Project Trust JIP) and Marintek (Norway, in collaboration with Rolls-Royce Marine), with topics regarding the thruster interaction effects, over the last few years clearly shows that this research area is actually a hot topic. Their researchers have also laid the foundations for further investigation in this area. Thus all other new papers are mostly

referred to underlying papers e.g. of Lehn (1992, 1985) and Nienhuis (1992). In his research, Lehn analysed and suggested theoretical and practical methods for estimating thrust losses in the case of longitudinal and transverse currents, ventilation, losses due to regular and irregular waves, thruster-thruster interaction, thruster-hull and Coanda effect (Lehn, 1992, 1985). In the discussions of the obtained results, Lehn points out that the losses are in that extent that they should not be neglected at the DP vessels. In his PhD dissertation, Nienhuis has systematically processed and analysed the thrusters usability in dynamic positioning systems and low-speed manoeuvring, with a special emphasis on the induced flow and on the interaction effects for azimuth and tunnel thrusters (Nienhuis, 1992). Particularly important results, both of Lehn and Nienhuis, are proposed methods for estimating the thruster-thruster and thruster-hull interactions.

A few authors continued their work. Thus Wichers et al. (1998) described the procedures for the thruster-hull and thruster-thruster interaction testing using the DPSIM computer program combined with model testing. Brandner and Renilson (1998) have made a series of experimental model measurements of the force impact on one thruster, as well as the mutual impact between two relatively close thrusters. Cozijn et al. (1999) point out the need to take dynamic effects into account as well. They critically discuss the results obtained exclusively by means of model basin measurements and emphasize the necessity of full-scale measurements and testing in order to get more accurate results on the possible losses and interaction effects. Van Dijk and Aalbers (2001) further quantified the wave drift forces and the abovementioned losses for the control logic requirements. Instead of a classical feedforward control based on the wind, they suggested feedforward control based on the waves whose effects on the vessel are previously estimated.

Vartdal and Garen (2001) presented new technical solutions with the thrusters that have the possibility of vertical tilting, either as the tilting of the entire thruster with a nozzle or as tilting of the nozzle alone. The conducted tests clearly indicate that such an approach can significantly reduce the propulsion losses due to the thruster-hull interaction. In their work, Dang and Laheij (2004) analysed comprehensively and in detail almost all hydrodynamic characteristics of azimuth thrusters, including the associated losses that can occur. Nordtveit et al. (2007) presented the results of the thrust reduction tests carried out both as basin tests and full-scale tests on DP vessels, for tunnel and azimuth thrusters and for the main propeller with rudder. The obtained results indicate the need for thrust losses to be taken into account even during the project phase and in the DP capability analysis. Fjørtoft (2010) has analysed the losses

of the azimuth thrusters caused by the Coanda effect and found out that it is possible to significantly reduce them by adequate vertical and horizontal variation of thrusters' position.

Finally, among the papers that take this issues into the consideration in the thrust allocation, only (Smogeli, 2006), (Ruth et al., 2009), (Yang et al., 2011a), (Valčić et al., 2014) and (Valčić and Prpić-Oršić, 2017) can be found of interest. Smogeli (2006) and Ruth et al. (2009) have identified a thruster ventilation problem which is very common at extreme weather conditions, i.e. in the heavy sea conditions. Ruth et al. (2009) proposed an appropriate QP solver-based thrust allocation strategy, the so-called antispin allocation, otherwise a kind of analogy to the anti-slip system in the cars, which improves the thrust recuperation process and positioning accuracy while simultaneously reducing ventilation-induced thrust losses. Yang et al. (2011a) have applied the previously mentioned methods of nonlinear programming (SQP, GA) in order to optimize the thrust allocation, but with an important difference because they modelled some thrust losses (thruster-thruster interaction) and forbidden zones as well. Valčić et al. (2014) performed a quantification of selected thrust loss effects and proposed their implementation in optimal thrust allocation strategies based on Moore-Penrose pseudoinverse matrix. Valčić and Prpić-Oršić (2017) compared two optimal thrust allocation procedures, i.e. the one performed with forbidden zones included but without the implementation of thrust loss effects and the other one without forbidden zones but with implemented thrust loss effects. Obtained results suggest that the strategy with implemented thrust loss effects with forbidden zones excluded can have significant advantages with respect to the strategy with forbidden zones included.

1.2 Motivation and objectives

The research scope in this thesis included the analysis of the selected thrust losses, particularly important in DP systems, as well as their implementation in the optimization tasks of the thrust allocation. Since both the testing of thrust losses in model basin and full-scale testing are virtually unfeasible for the purpose of this research, the results of the most important research papers and reports on the effects of the thrust losses were used in this thesis (Brandner and Renilson, 1998; Cozijn et al., 1999; Dang and Laheij, 2004; Ekstrom and Brown, 2002; Fjørtoft, 2010; Lehn, 1992, 1985, 1980; Nienhuis, 1992; Nordtveit et al., 2007; Vartdal and Garen, 2001). Moreover, since the results of these papers have been tested and verified in the basins of the referent and renowned research marine technology centres (Marin, Marintek,

HSVA, etc.), they are considered to be a good reference point in modelling the effects of thrust losses for the needs of optimal thrust allocation. Among the effects causing thrust losses, the following were analysed: transverse and longitudinal forces (jet and sea current interaction), thruster-hull interaction, the Coanda effect, thruster-thruster interaction, thruster ventilation and in-and-out water effects. For the purpose of this thesis, the effects of thruster – incoming current and thruster – thruster interaction were of particular interest.

The nonlinear constraints of the optimization tasks assume the use of optimization methods such as the SQP or GA, but the use of other significant global optimization algorithms such as pattern (direct) search algorithms (Kolda et al., 2003) is also suggested in this thesis. The three most commonly used direct search (DS) algorithms are GPS (generalized pattern search), GSS (generating set search), and MADS (mesh adaptive direct search). They all calculate a number of points approaching the optimum solution. At each step, the algorithm seeks for a set of points, i.e. the so-called mesh around the current point calculated in the previous step. If the algorithm finds a point in the mesh that improves the objective function, that point becomes the current point in the next step of the algorithm. The GPS algorithm uses the constant direction vectors in order to form the so-called pattern. The GSS algorithm is similar to a GPS algorithm with the difference that it is used in the case of linear constraints and when the current solution is close to them. The MADS algorithm uses the randomized selection of the vector to create the mesh. In order to solve the optimization tasks with nonlinear constraints, pattern search algorithms use the so-called Augmented Lagrangian Pattern Search (ALPS) algorithm (Conn et al., 1991; Kolda et al., 2006). When compared to other solutions such as application of GA, the application of pattern search algorithms takes precedence in mathematical terms because the convergence to the global minimum can be proved (Conn et al., 1997, 1991), which is not the case with the GA. Given that these optimization methods do not use gradients, the objective function does not have to be continuous nor derivable (Kolda et al., 2003), does not even have to be explicitly stated, but can be based solely on the data.

The problems of applying global optimization algorithms are usually apparent due to their complexity in the computational sense. In practical applications, the optimal thrust allocation has to be performed in an exceptionally short time interval, while generally the application of global optimization algorithms to find the optimal solution may require a very long convergence time, particularly when using GA. For this reason, the possibility of applying the parallel computing has been tested and the hybrid approach strategy in optimizing the thrust allocation has been developed, where the

complex and demanding numerical calculations were performed in an "off-line" mode of operation, while the allocation was done in an "on-line" mode of operation with a previously trained artificial neural network in the off-line mode of operation. The main purpose of such trained neural network is to determine the initial solutions of the optimization algorithms that are completely aligned with the current environmental loads and are very close to global optima. In addition to this primary purpose, such a trained network can fully or partially substitute the commonly used optimal thrust allocator (e.g. QP solver) and provide an extremely fast, accurate and reliable thrust allocation without the need for additional optimization. If the possibility of adapting the trained neural network is added, the developed model of optimal allocation is extremely robust and flexible considering the various objective functions and constraints, but also considering various environmental loads.

The research plan consisted of a number of work assignments and objectives, of which the following are outlined:

- the review of previous work has been completed with the continuous monitoring of the up to date results of the papers in this field;
- the results of the so far proposed optimization methods in the thrust allocation (pseudo-inverse, SVD, QP, mp-QP, BCQP, pQP, SQP, GA, AGA) were analysed and synthesized, and their advantages and disadvantages have been identified;
- the effects that cause thrust losses were analysed (transverse and longitudinal forces, thruster – incoming current interaction, thruster-thruster interaction, thruster-hull interaction, Coanda effect, thruster ventilation), where selected effects have been quantified and prepared for the purpose of thrust allocation;
- the possibilities of implementing the selected thrust loss effects into existing and newly suggested optimization methods and strategies were investigated;
- the mathematical, semi-empirical and empirical models (e.g. for environmental loads, ducted propellers, thrust losses, etc.) required for the optimal thrust allocation were developed;
- an approach proposal for the implementation of selected global optimization algorithms for solving the thrust allocation problem has been developed;
- the possibilities of a developed optimization approaches with and without the use of parallel computing have been tested;
- the approach for the development of a hybrid optimal thrust allocation system based on the off-line and on-line mode of operation has been elaborated and suggested;

- developed optimization structures for the thrust allocation were tested and confirmed on numerous simulations involving very different scenarios.

1.3 Problem statement

The main objective of the thesis was the development of the strategy and method for the optimal thruster (thrust) allocation of DP vessels in which it will be possible to add the quantified thrust loss effects to the optimization task. In selection of the optimization methods, some already suggested solutions (e.g. pseudo-inverse matrix, QP, SQP and GA) were used, but also a completely new approach based on the pattern (direct) search optimization algorithms has been also proposed.

The main hypothesis may be stated in the following form: "The models of the optimal thrust allocation of DP vessels developed in this thesis can significantly improve and enhance the existing dynamic positioning system capabilities, in particular the subsystem for the thrust allocation that can handle forbidden zones and thrust loss effects more efficiently."

Alongside the main hypothesis, there are also several auxiliary hypotheses:

- the optimization of the thrust allocation which takes into account the thrust loss effects allows the premises for a more robust and smoother operation of the entire DP system;
- the application of the pattern (direct) search algorithms provides a support for gradient-based algorithms in terms of finding the global solutions in non-convex and nonlinear optimization problems related to thruster interactions;
- the proposed hybrid model that combines gradient-based and derivative free optimization algorithms with artificial neural networks can be an effective alternative to the classical thrust allocation procedures in DP systems.

1.4 Organization of the thesis

According to the problem statement and defined objectives, this thesis is structured and organized into eight main chapters, after which the bibliography, the list of figures and tables, appendixes and CV are enclosed. In the Introduction, state-of-the-art with previous work has been analysed and the most important conclusions have been presented. The aim and goals, together with main contributions, are also outlined.

Chapter 2 presents an overview of dynamic positioning systems in terms of general characteristics of dynamically positioned marine vessels. However, particular accent has been given to the modelling of environmental loads, which present the input side of thrust allocation procedure, as well as to azimuth thrusters, which have been used throughout the work as the main actuators. Hence, hydrodynamic characteristics of ducted propellers are analysed in detail, particularly because due to their importance for modelling thruster interaction effects.

Considering the exceptional hydrodynamic complexity of interaction effects that can cause thrust reduction, simplified semi-empirical models have been created for handling thrust loss effects. Among various effects, emphasis is being put on the problem of incoming current with detailed analysis of thruster-thruster interaction, which was based on procedures and experimental data (Lehn, 1992, 1985, 1980). As a result, very convenient model for fast estimation of thrust loss ratio related to thruster-thruster interactions is presented in Chapter 3.

The focus of Chapter 4 is primarily oriented to thrust allocation problem and associated constraints and limitations. Thruster saturation cannot be handled directly by means of conventional QP solvers and forbidden zones are generally non-convex constraints. Thus, appropriate strategies are presented in order to handle these issues. In this chapter one can also find various general considerations about optimal thrust allocation.

Gradient-based and derivative free algorithms used in this thesis are briefly outlined in Chapter 5. This refers to Lagrangian multiplier method, quadratic programming, sequential quadratic programming, and direct search algorithms like generalized pattern search, generating set search and mesh adaptive direct search. Advantages and disadvantages of all algorithms are highlighted.

Impact of thruster-thruster interaction effects on optimal thrust allocation is analysed in Chapter 6. For this purpose, handling of thrust losses with generalized inverse matrix and associated reallocation strategy has been elaborated, and numerous examples and simulation results are provided in this section. Two approaches have been of particular interest, one that takes forbidden zones into account, and the other that neglect them, but considers thruster-thruster interaction instead.

Nonlinear optimization of thrust allocation with nonlinear objective functions, nonlinear inequality and non-convex nonlinear equality constraints is in the focus of

Chapter 7. In order to minimize the risks associated with non-convex optimization, several strategies have been proposed, i.e. from the two-step optimization procedure with sensitivity analysis, to modelling obtained results with generalized regression neural network. Created hybrid model was extensively simulated, tested and verified.

Finally, in Chapter 8, significant results and conclusions are briefly discussed, main contributions are outlined and recommendations for future work are given.

1.5 Scientific contributions

The scientific contributions of this thesis are reflected in:

- Quantifying and proposing procedures for implementing the effects of thrust losses in the optimization tasks of the thrust allocation of DP vessels, in particular regarding the interaction effects of thruster – income current, thruster – thruster interaction, and forbidden zones (Chapters 3 and 4);
- Proposing and evaluation of reallocation strategies for handling forbidden zones and thruster interaction effects by means of enhanced weighted generalized inverse matrix (Chapter 6);
- Implementing thrust interaction effects in terms of non-convex and nonlinear equality constraints in proposed two-step nonlinear optimization procedure of thrust allocation (Chapter 7);
- Proposal and deployment of the hybrid SQP/DS optimization approach with intensive sensitivity analysis in order to minimise the risk of solver convergence to local optima for non-convex optimization problems (Chapter 7);
- Deployment of generalized regression neural network as a generator of initial solutions for the online solver depending on the given environmental loads, and thus providing a much faster convergence of the optimization algorithm (Chapter 7);
- Extension of the aforementioned trained neural network in order to partially or fully cover the entire process of optimal thrust allocation and thus provide a very fast, computationally inexpensive and accurate thrust allocation procedure, without the need for additional numerical optimization in the on-line mode of operation (Chapter 7).
- Detailed analysis of computational intensity and convergence time for all proposed optimization strategies and approaches with particular emphasis on the overall power consumption (Chapters 6 and 7).

2 DYNAMIC POSITIONING SYSTEMS

2.1 General features and modelling characteristics of dynamically positioned marine vessels

Dynamic positioning system can be divided into several subsystems as shown in Figure 1 (Sørensen, 2011):

(*a*) DP operator with Human Machine Interface (HMI)
(*b*) Measurement system that includes reference systems for positioning (satellite positioning, hydro acoustics, etc.), heading (gyro compass), motion reference units, anemometers, etc.
(*c*) Signal processing and estimators
(*d*) Control units for guidance, navigation and control (GNC)
(*e*) Thrust allocation
(*f*) Thruster units with electrical power generators.

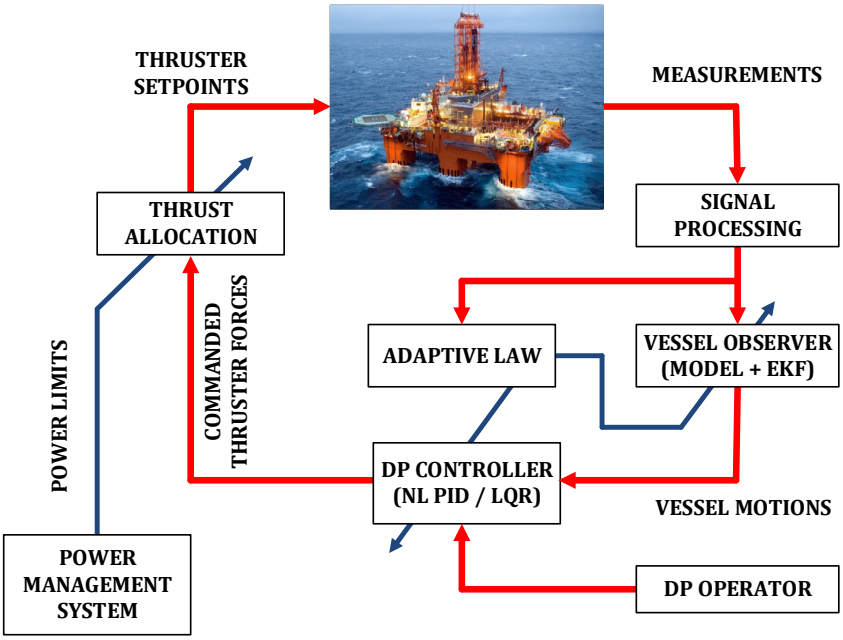

Figure 1. DP structure with associated subsystems and modules
Source: Adjusted according to (Sørensen, 2011); Photo courtesy of Seadrill

The reference and measurement systems are primarily used to collect the measurements of the vessel position and heading. However, in DP systems measurements such as wind direction and wind speed, vessel speed, vessel motions in six degrees of freedom (6DOF), measurements within the propulsion system (thruster orientation, shaft speed and/or propeller pitch), as well as the other measurements that may be of interest, are continuously conducted and logged.

All acquired measurements should pass appropriate signal analysis, processing and testing, with particular attention regarding their accuracy and reliability. The vessel's observer, in commercial DP systems most usually the extended Kalman Filter (EKF), has the function of estimating all measurements in which the process noise level is significant. Generally, when conducting the measurements on ships and other vessels, the mentioned process noise, mainly caused by the first order wave induced forces, is reflected in the form of high frequency (HF) components in measured signals, which have to be properly filtered out in order to provide smooth control as much as possible without unnecessary tear and wear of thruster equipment. It is important to point out that a vessel's observer can also estimate physical quantities that are not measured or cannot be measured (e.g. the forces and moments of the wind load, the forces and moments generated by thrusters, etc.) making it an indispensable and particularly significant component of the entire DP control system. In order for a vessel's observer to carry out its function, it is necessary to develop an appropriate mathematical model, which usually includes the models of vessel kinematics, vessel dynamics, slowly varying loads, HF components and noisy measurements.

The most common DP controller of the dynamic positioning system is the nonlinear PID regulator or the optimal linear-quadratic (LQ) regulator. Regardless of its design, its basic function is to determine the overall generalized forces and moment in the horizontal plane, which propulsion system needs to develop in order to compensate environmental loads and all other disturbances. The DP controller output is based on the tracking error between measured and demanded vessel position and heading.

The previously determined forces and moment from the DP controller are passed on to the allocator of a DP system, which has the function of their allocation by individual thrusters. As this mapping can be done in infinitely many ways, the appropriate optimization procedures are commonly used in order to ensure the minimization of the total electrical power consumption, i.e. the electrical power delivered to thruster electric motors. There could be some other objective functions as well, particularly if the exploitation profile of the vessel requires so. However, apart from the objective function, certain limitations are of particular importance to this optimization, such as thruster saturation, forbidden zones, but also the available electric power that can be delivered to a particular thruster, without endangering the entire electric power system of the vessel (blackout prevention).

After the generalized forces and moment in horizontal plane are allocated by individual thrusters based on their hydrodynamic characteristics, the reference values for each

thruster, i.e. their orientation and shaft speed or/and propeller pitch are determined, depending on the thruster type.

If the vessel is analysed as the object of control, then the modelling of her kinematics and dynamics is commonly performed in three parts. First, it is necessary to define all the required reference coordinate systems, i.e. reference frames that will be used, so the vessel kinematics could be referred to them. Vessel kinematics essentially represents the relationship between positions and Euler angles in relation to the linear and angular velocities. The modelling of the vessel dynamics is usually carried out independently of hers kinematics and, in the most general form, represents the determination of the motion equations in six degrees of freedom (6DOF). For the applications in dynamic positioning, such general models can be further simplified and reduced to three horizontal degrees of freedom in horizontal plane and linearized if necessary.

Finally, in order to develop a complete modelling environment, it is also necessary to model the appropriate environmental loads, i.e. forces and moments that act on the vessel and are caused by means of wind, sea currents, waves and other disturbances of interest like thrusters, pipes during pipe-laying operations, cables during cable-laying operations, anchor lines during position mooring, etc.

Generally, the vessel motion can be decomposed into the motion in 6DOF, i.e. on three translational and three rotational motions, as shown in Figure 2. The usual notation for forces and moments, vessel linear and angular velocities, and vessel positions and orientation (Euler angles) is listed in Table 1. The notation is adapted according to the Society of Naval Architects and Marine Engineers (SNAME, 1950).

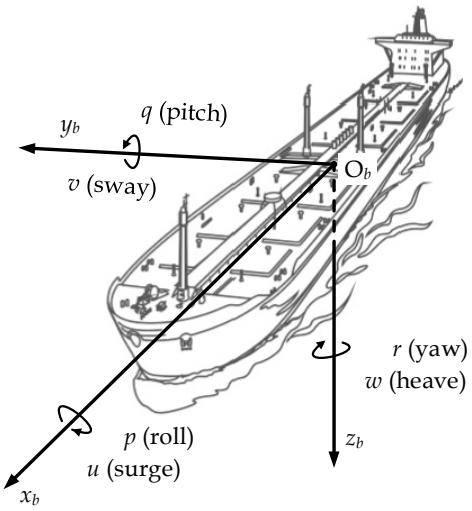

Figure 2. 6DOF with respect to the body reference frame {*b*}
Source: (Fossen, 2011)

Table 1. Notation of characteristic physical quantities with respect to the motion in 6DOF

#	Type of motion	DOF	Forces and moments	Linear and angular velocities	Positions and Euler angles
1	Translation in the x direction	Surge	X	u	x
2	Translation in the y direction	Sway	Y	v	y
3	Translation in the z direction	Heave	Z	w	z
4	Rotation about the x axis	Roll	K	p	ϕ
5	Rotation about the y axis	Pitch	M	q	θ
6	Rotation about the z axis	Yaw	N	r	ψ

Source: (SNAME, 1950)

The following coordinate systems differ in problems related to guidance, navigation and control of marine vessels (Fossen, 2011):

(*i*) ECI (Earth-Centred Inertial), i.e. {*i*}, is an inertial non-accelerating coordinate system fixed in space, with an origin in the Earth's centre. It represents an inertial coordinate system for the terrestrial navigation.

(*ii*) ECEF (Earth-Centred Earth-Fixed), i.e. {*e*}, is a coordinate system whose origin is also located in the Earth's centre, with the difference that its horizontal axes rotate around the vertical axes relative to the inertial coordinate system ECI at angular velocity of the Earth. For the vessels that are moving at relatively low velocities (e.g. station-keeping, path following, trajectory tracking), the rotation of the Earth may be neglected, i.e. ECEF can be considered as an inertial coordinate system. This does not apply to vessels that float freely.

(*iii*) NED (North-East-Down), i.e. {*n*}, is a coordinate system with an origin at some selected point, placed on a tangential plane that touches the surface of the Earth and moves together with the vessel. The coordinate system {*n*} is set relative to the Earth's reference ellipsoid WGS84, with its axis x_n oriented towards the true north (N), axis y_n towards the east (E), and axis z_n follows the normal with respect to the aforementioned tangential plane directed towards the Earth's centre (D).

(*iv*) BODY, i.e. {*b*}, is a coordinate system of a vessel with an origin at an appropriate fixed point on a vessel. For this purpose, the most commonly used points are CO, which is positioned at a point amidships in the waterline, the centre of gravity CG, the centre of floatation CF distant of CO for some length LCF in x_b direction, centre of buoyancy CB, etc.

Position (x, y, z) and Euler angles (ϕ, θ, ψ), i.e. the orientation of the vessel, are expressed relatively with regard to inertial coordinate system ({e} or {n}), while linear (u, v, w) and angular (p, q, r) velocities are commonly expressed in {b} reference frame.

2.2 Kinematics and dynamics of marine vessels

Kinematic equations of motion can be written in matrix form as (Fossen, 2011):

$$\dot{\boldsymbol{\eta}} = \mathbf{J}(\boldsymbol{\eta})\mathbf{v}, \tag{2.1}$$

where

$$\boldsymbol{\eta} = [x,\ y,\ z,\ \phi,\ \theta,\ \psi]^{\mathrm{T}} \tag{2.2}$$

is a vector of position and orientation in {e} reference frame. Derivation of position and orientation vector (2.2) is equal to

$$\dot{\boldsymbol{\eta}} = [\dot{x},\ \dot{y},\ \dot{z},\ \dot{\phi},\ \dot{\theta},\ \dot{\psi}]^{\mathrm{T}} \tag{2.3}$$

where $\dot{\boldsymbol{\eta}}$ is a vector of velocities by translational and rotational degrees of freedom and is expressed in inertial reference frame {e} or {n}.

Vector of linear and angular velocities

$$\mathbf{v} = [u,\ v,\ w,\ p,\ q,\ r]^{\mathrm{T}} \tag{2.4}$$

from (2.1) also presents velocities by translational and rotational degrees of freedom, but these ones are expressed in {b} reference frame.

Relationship between velocities $\dot{\boldsymbol{\eta}}$ and $\mathbf{v}$ expressed in {e} or {n} and {b} reference frames, respectively, is defined in (2.1) by means of transformation matrix $\mathbf{J}(\boldsymbol{\eta})$ as

$$\mathbf{J}(\boldsymbol{\eta}) = \begin{bmatrix} \mathbf{R}_b^n(\boldsymbol{\Theta}_{nb}) & 0_{3\times3} \\ 0_{3\times3} & \mathbf{T}_\Theta(\boldsymbol{\Theta}_{nb}) \end{bmatrix}, \tag{2.5}$$

where $\mathbf{R}_b^n(\boldsymbol{\Theta}_{nb})$ is rotation matrix of Euler angles expressed in terms of argument $\boldsymbol{\Theta}_{nb} = [\phi,\ \theta,\ \psi]^{\mathrm{T}}$. If complex rotational motion in space is separated according to *zyx* notation on three simple single axis rotations, matrix $\mathbf{R}_b^n(\boldsymbol{\Theta}_{nb})$ will become

$$\mathbf{R}_b^n(\boldsymbol{\Theta}_{nb}) = \mathbf{R}_{z,\psi}\mathbf{R}_{y,\theta}\mathbf{R}_{x,\phi} = \begin{bmatrix} \cos\psi & -\sin\psi & 0 \\ \sin\psi & \cos\psi & 0 \\ 0 & 0 & 1 \end{bmatrix}\begin{bmatrix} \cos\theta & 0 & \sin\theta \\ 0 & 1 & 0 \\ -\sin\theta & 0 & \cos\theta \end{bmatrix}\begin{bmatrix} 1 & 0 & 0 \\ 0 & \cos\phi & -\sin\phi \\ 0 & \sin\phi & \cos\phi \end{bmatrix}$$

$$\mathbf{R}_b^n(\boldsymbol{\Theta}_{nb}) = \begin{bmatrix} \cos\psi\cos\theta & -\sin\psi\cos\phi+\cos\psi\sin\theta\sin\phi & \sin\psi\sin\phi+\cos\psi\sin\theta\cos\phi \\ \sin\psi\cos\theta & \cos\psi\cos\phi+\sin\psi\sin\theta\sin\phi & -\cos\psi\sin\phi+\sin\psi\sin\theta\cos\phi \\ -\sin\theta & \cos\theta\sin\phi & \cos\theta\cos\phi \end{bmatrix}. \tag{2.6}$$

Transformation matrix $\mathbf{T}_{\Theta}(\mathbf{\Theta}_{nb})$ of angular velocities (p, q, r) is used for transformation of these velocities from {*b*} in {*n*} and it has the following form

$$\mathbf{T}_{\Theta}(\mathbf{\Theta}_{nb}) = \begin{bmatrix} 1 & \sin\phi\tan\theta & \cos\phi\tan\theta \\ 0 & \cos\phi & -\sin\phi \\ 0 & \sin\phi/\cos\theta & \cos\phi/\cos\theta \end{bmatrix}, \tag{2.7}$$

though it is important to emphasize that this kind of transformation is possible only for pitch angles $\theta \neq \pm 90°$.

As already mentioned, horizontal degrees of freedom (surge, sway, yaw) are of particular importance for dynamic positioning systems, so for this reason it is common to simplify the vessel's kinematics with these three instead of all six degrees of freedom. Namely, assuming ϕ and θ are relatively small (up to 10°), it can be written

$$\mathbf{R}_{b}^{n}(\mathbf{\Theta}_{nb}) = \mathbf{R}_{z,\psi}\mathbf{R}_{y,\theta}\mathbf{R}_{x,\phi} \approx \mathbf{R}_{z,\psi} = \begin{bmatrix} \cos\psi & -\sin\psi & 0 \\ \sin\psi & \cos\psi & 0 \\ 0 & 0 & 1 \end{bmatrix}, \tag{2.8}$$

$$\mathbf{T}_{\Theta}(\mathbf{\Theta}_{nb}) \approx \mathbf{I}_{3\times 3} = \begin{bmatrix} 1 & 0 & 0 \\ 0 & 1 & 0 \\ 0 & 0 & 1 \end{bmatrix}, \tag{2.9}$$

which according to (2.1) gives the matrix form of kinematic equations in 3 DOF

$$\dot{\boldsymbol{\eta}} = \mathbf{R}(\psi)\mathbf{v}, \tag{2.10}$$

where rotation matrix $\mathbf{R}(\psi)$ is now equal to

$$\mathbf{R}(\psi) = \mathbf{R}_{z,\psi} = \begin{bmatrix} \cos\psi & -\sin\psi & 0 \\ \sin\psi & \cos\psi & 0 \\ 0 & 0 & 1 \end{bmatrix}, \tag{2.11}$$

and vectors of position and velocities are redefined as

$$\boldsymbol{\eta} = [x, y, \psi]^{\mathrm{T}}, \tag{2.12}$$

$$\mathbf{v} = [u, v, r]^{\mathrm{T}}. \tag{2.13}$$

According to the following well-known property for rotational matrix

$$\mathbf{R}^{-1}(\psi) = \mathbf{R}^{\mathrm{T}}(\psi), \tag{2.14}$$

velocities $\mathbf{v}$ in {*b*}, expressed in terms of velocities $\dot{\boldsymbol{\eta}}$ in {*n*}, can be rewritten based on (2.10) and (2.11) as

$$\mathbf{v} = \mathbf{R}^{\mathrm{T}}(\psi)\dot{\boldsymbol{\eta}}. \tag{2.15}$$

On the other hand, dynamic equations of vessel motion in 6DOF can be written in matrix form according to Fossen (2011) as

$$\mathbf{M}\dot{\mathbf{v}} + \mathbf{C}(\mathbf{v})\mathbf{v} + \mathbf{D}(\mathbf{v})\mathbf{v} + \mathbf{g}(\boldsymbol{\eta}) + \mathbf{g}_0 = \boldsymbol{\tau} + \boldsymbol{\tau}_{\text{wind}} + \boldsymbol{\tau}_{\text{wave}} \tag{2.16}$$

where $\mathbf{M}$ is system inertia matrix, $\mathbf{C}$ is matrix of Coriolis and centripetal forces, $\mathbf{D}$ is damping matrix, $\mathbf{g}$ is vector of generalized gravitational and buoyancy forces, $\mathbf{g}_0$ are static recuperation forces and moments caused by acting of ballast system and other fluids in tanks, $\boldsymbol{\tau}$ is vector of generalized forces and moments in 6DOF, $\boldsymbol{\tau}_{\text{wind}}$ is vector of forces and moments of wind loads, and $\boldsymbol{\tau}_{\text{wave}}$ is vector of forces and moments of wave loads.

If one takes into account the inflow of sea current with relative current speed

$$\mathbf{v}_{rel,curr} = \mathbf{v} - \mathbf{v}_{curr}, \tag{2.17}$$

equation (2.16) can be rewritten in the following form

$$\left.\begin{aligned} &\underbrace{\mathbf{M}_{RB}\dot{\mathbf{v}} + \mathbf{C}_{RB}(\mathbf{v})\mathbf{v}}_{\text{rigid body forces}} + \underbrace{\mathbf{M}_A\dot{\mathbf{v}}_{rel,curr} + \mathbf{C}_A(\mathbf{v}_{rel,curr})\mathbf{v}_{rel,curr} + \mathbf{D}(\mathbf{v}_{rel,curr})\mathbf{v}_{rel,curr}}_{\text{hydrodynamic forces}} + \\ &+ \underbrace{\mathbf{g}(\boldsymbol{\eta}) + \mathbf{g}_0}_{\text{hydrostatic forces}} = \boldsymbol{\tau} + \boldsymbol{\tau}_{\text{wind}} + \boldsymbol{\tau}_{\text{wave}} \end{aligned}\right\} \tag{2.18}$$

where subscript *RB* is related to the part of the vessel model that can be seen as the rigid body, and subscript *A* is related to hydrodynamic part of the model in which the effect of added or virtual mass, caused by the inertia of suppressed fluid that surrounds the vessel, is analysed. Vector $\mathbf{v}_{curr}$ contains components of sea current velocity by associated axes which can be written as

$$\mathbf{v}_{curr} = [u_{curr}, v_{curr}, w_{curr}, 0, 0, 0]^{\mathrm{T}}. \tag{2.19}$$

More details on different variants of this model with respect to various applications could be found in (Fossen, 2011).

2.3 Environmental loads

Disturbances acting on the vessel are caused primarily by the action of wind, sea currents and waves, but also by other unmodelled parts of the system's dynamics. Cumulatively, they can be divided into two basic categories. The first category includes the low frequency (LF) disturbances of the second order, and the second the high frequency (HF) disturbances of the first order, also known as the first order wave induced. Usually they are referred as LF and HF motion of a vessel, while the total

motion of the vessel, illustrated in Figure 3, represents the sum of the LF and HF components. The slowly varying character can be noticed with LF motion, while the fast-oscillating character can be noticed with both HF and total motion.

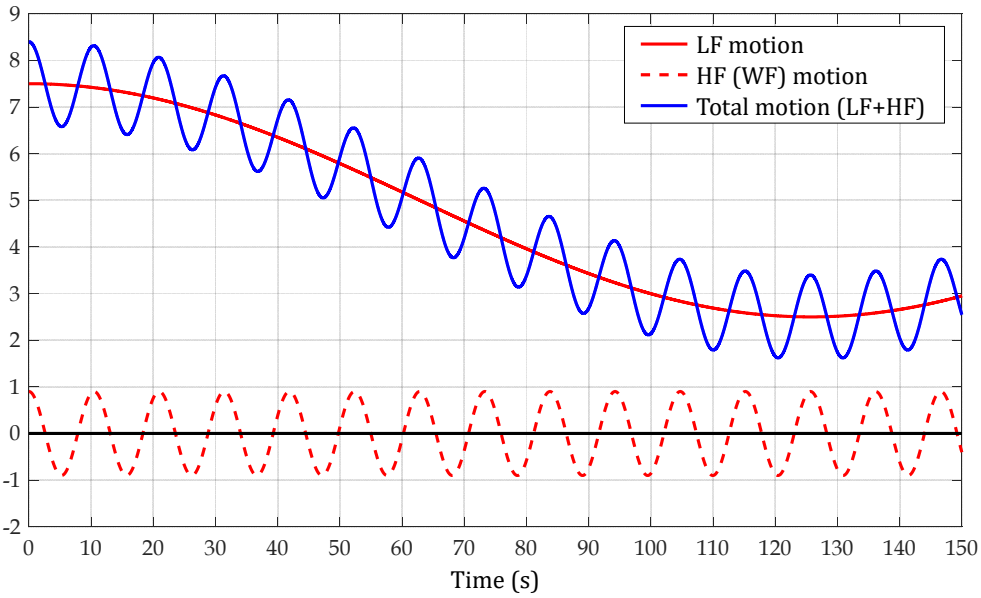

Figure 3. Total motion of a ship as a sum of LF and HF motions
Source: Adjusted according to (Sørensen, 2012)

From the vessel's dynamics in (2.18), it can be seen that external disturbances are usually located on the right-hand side of the equation. An exception are the sea currents modelled together with the damping on the left-hand side of the equation (2.18) and are taken into account with introducing the relative velocity of current inflow (2.17) to the vessel.

Environmental loads and other external disturbances can be written in the following extended form as

$$\boldsymbol{\tau}_{\text{total}} = \boldsymbol{\tau} + \boldsymbol{\tau}_{\text{wind}} + \boldsymbol{\tau}_{\text{wave}} + \boldsymbol{\tau}_{\text{anchor}} + \boldsymbol{\tau}_{\text{pipe}} + \boldsymbol{\tau}_{\text{ice}} + \ldots, \tag{2.20}$$

where $\boldsymbol{\tau}$ is vector of generalized forces and moment generated by means of the vessel's propulsion system, $\boldsymbol{\tau}_{\text{wind}}$ is vector of wind loads, $\boldsymbol{\tau}_{\text{wave}}$ is vector of wave loads, $\boldsymbol{\tau}_{\text{anchor}}$ is vector of anchor line loads during position mooring, $\boldsymbol{\tau}_{\text{pipe}}$ is vector of additional load caused by the pipe during some pipe laying operations, $\boldsymbol{\tau}_{\text{ice}}$ is vector of ice load, etc.

Vector of generalized forces and moment

$$\boldsymbol{\tau} = [F_x, F_y, M_z]^{\mathrm{T}} \tag{2.21}$$

consists of the forces F_x and F_y in surge and sway direction, respectively, and the yaw moment M_z about the vertical axis. This vector is determined by the control logic of a DP system, i.e. by the DP controller. For this reason, it is usually referred as control vector or intervention vector. Forces and moment in (2.21) should be cumulatively generated by vessel's thrusters in order to compensate environmental loads and other external disturbances.

2.3.1 Wind loads

Wind can be generally defined as the relative air motion with respect to the Earth's surface. Mathematical and empirical models of wind loads, i.e. wind forces and moments, are mostly used in marine systems in order to enhance the vessel performance and to optimize her operational profile.

If the air motion occurs above the sea surface a natural boundary layer will be formed, which means that the velocity of the wind near the surface will be close to zero, and it will gradually increase as the altitude increases. On the other hand, the local wind field generated by the ship motion will be completely homogenous, i.e. it will not have a natural boundary layer, as shown in Figure 4 (Andersen, 2013).

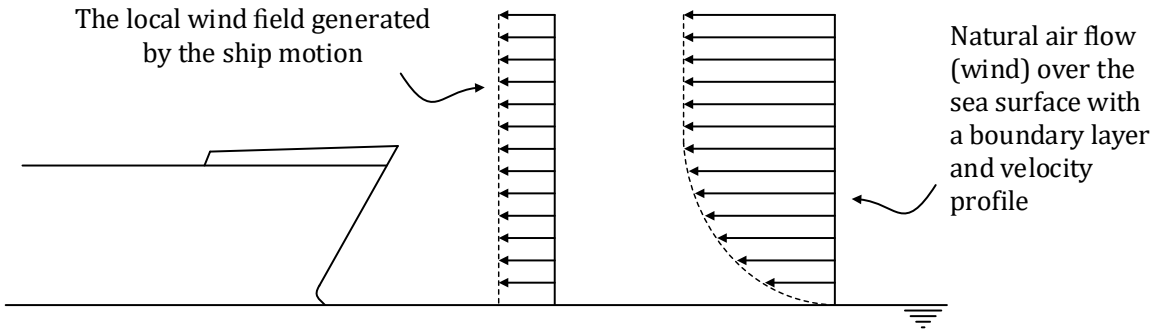

Figure 4. The local and natural wind field near the vessel

Thus, the actual, i.e. the total wind field generated both by the natural air motion and vessel motion is a combination of the wind field with a natural boundary layer and the homogenous wind field generated by the vessel motion. The relative wind direction $\gamma_{rel,wind}$ can be found using a vector sum of appropriate components of wind and vessel velocities as shown in Figure 5, where u and v represent vessel velocities in surge and sway, respectively, U is resulting speed, u_{wind} and v_{wind} are components of resulting absolute wind speed V_{wind}, respectively, and γ_{wind} is absolute wind direction.

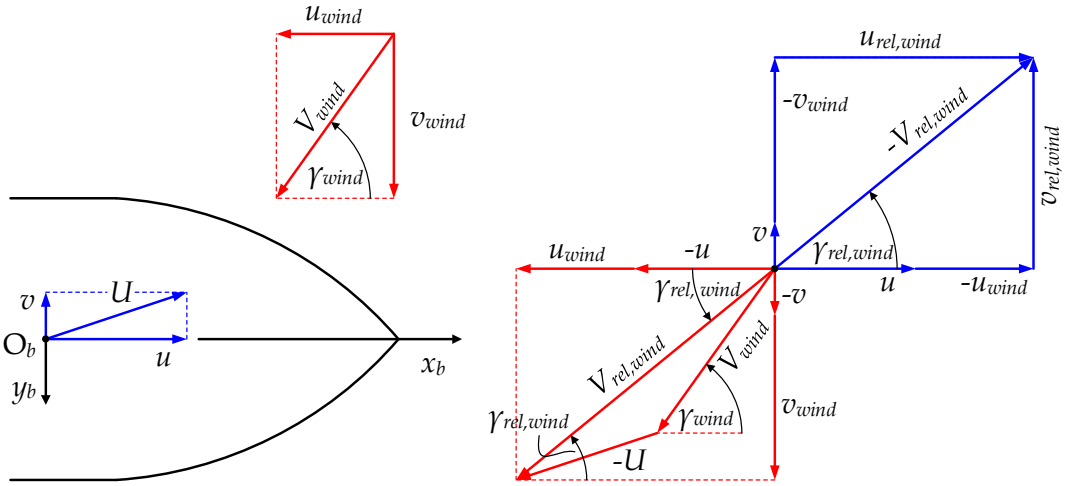

Figure 5. Relative wind speed and direction
Source: Adjusted according to (Andersen, 2013)

The relative wind speed $V_{rel,wind}$ can be found using components of the ship speed U and components of the wind speed V_{wind} according to

$$V_{rel,wind} = \sqrt{u_{rel,wind}^2 + v_{rel,wind}^2} = \sqrt{(u - u_{wind})^2 + (v - v_{wind})^2}. \tag{2.22}$$

The relative wind angle of attack $\gamma_{rel,wind}$ can be calculated using the following relation

$$\gamma_{rel,wind} = -\operatorname{atan}(v_{rel,wind} / u_{rel,wind}) = -\operatorname{atan}((v - v_{wind}) / (u - u_{wind})) \tag{2.23}$$

where atan function, whose range is $[-\pi, \pi]$, is usually calculated as

$$\operatorname{atan}(y/x) = \begin{cases} \arctan(y/x) & \text{if } x > 0, \\ \arctan(y/x) + \pi & \text{if } x < 0 \text{ and } y \geq 0, \\ \arctan(y/x) - \pi & \text{if } x < 0 \text{ and } y < 0, \\ +\pi/2 & \text{if } x = 0 \text{ and } y > 0, \\ -\pi/2 & \text{if } x = 0 \text{ and } y < 0, \\ \text{undefined}, & \text{if } x = 0 \text{ and } y = 0. \end{cases} \tag{2.24}$$

This alternative form (2.24) is particularly convenient in order to avoid singularity when $u - u_{wind} = 0$, i.e. to avoid indefinite form when $v - v_{wind} = 0$ and $u - u_{wind} = 0$.

If marine vessel is at rest $(u, v \approx 0)$, relative wind speed $V_{rel,wind}$ is equal to absolute wind speed V_{wind}, i.e.

$$V_{rel,wind} = V_{wind} = \sqrt{u_{wind}^2 + v_{wind}^2}. \tag{2.25}$$

The encounter wind angle, as indicated in Figures 5 and 6, is equal in this case to

$$\gamma_{wind} = -\operatorname{atan}(v_{wind} / u_{wind}). \tag{2.26}$$

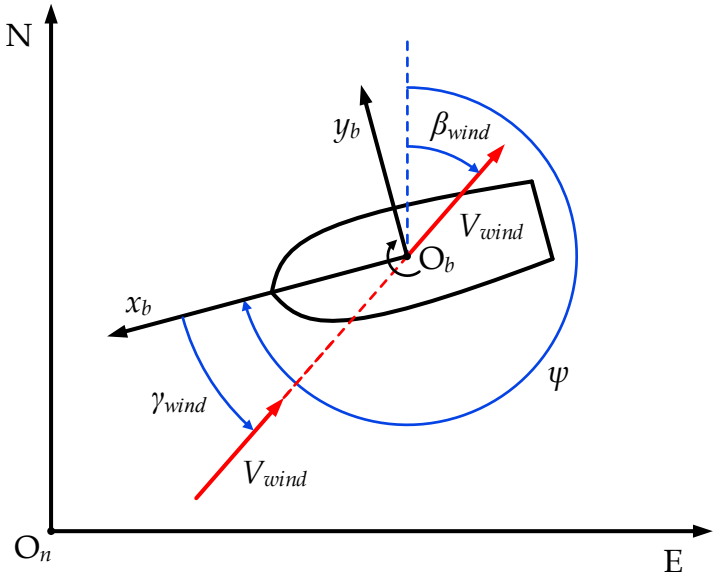

Figure 6. Notation of wind directions with respect to {b} and {n} for $u = v = 0$
Source: Adjusted according to (Fossen, 2011)

Forces and moment in the horizontal plane with respect to the wind, i.e. apparent wind if the ship is moving, are the drag force D, positive in the wind direction, and the cross force C, positive to the right when facing into the wind. Only the forces in the horizontal plane are considered. The vertical wind force and the pitching moment are unimportant for the behaviour of conventional ships, though they might be for new and special ship types (Blendermann, 1996). Due to simplicity reasons, resulting horizontal wind force is usually decomposed into two components, i.e. into longitudinal force ($F_{x,wind}$) and transverse force ($F_{y,wind}$) as shown in Figure 7.

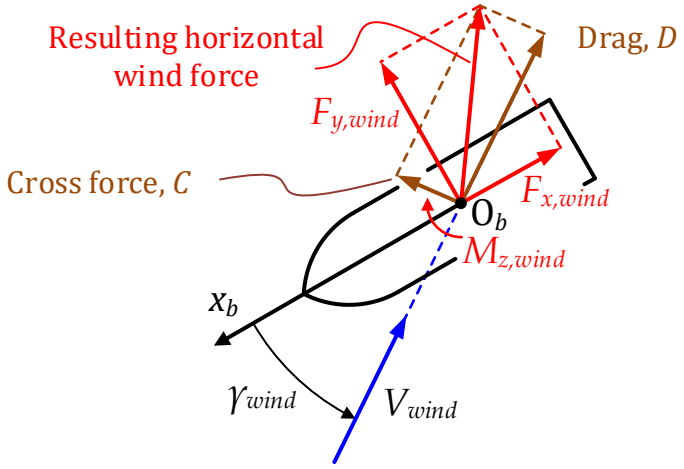

Figure 7. Wind forces and moments in the horizontal plane

For a marine vessel at rest, i.e. with zero forward speed $(u, v \approx 0)$, the vector of wind loads

$$\boldsymbol{\tau}_{wind} = [F_{x,wind} \quad F_{y,wind} \quad M_{z,wind}]^{\mathrm{T}} \tag{2.27}$$

in horizontal plane can be expressed in terms of the non-dimensional wind load coefficients $C_{X,wind}(\gamma_{wind})$, $C_{Y,wind}(\gamma_{wind})$ and $C_{N,wind}(\gamma_{wind})$ according to

$$\boldsymbol{\tau}_{wind} = \begin{bmatrix} F_{x,wind} \\ F_{y,wind} \\ M_{z,wind} \end{bmatrix} = \frac{1}{2}\rho_{air} V_{wind}^2 \begin{bmatrix} C_{X,wind}(\gamma_{wind}) A_{F,wind} \\ C_{Y,wind}(\gamma_{wind}) A_{L,wind} \\ C_{N,wind}(\gamma_{wind}) A_{L,wind} L_{oa} \end{bmatrix}, \tag{2.28}$$

where $F_{x,wind}$ and $F_{y,wind}$ are longitudinal and transverse wind forces, respectively, $M_{z,wind}$ is yawing wind moment, ρ_{air} is air density, $A_{F,wind}$ and $A_{L,wind}$ are the vessel's frontal and lateral projected areas above the water line, respectively, L_{oa} is the vessel's length overall, and γ_{wind} is wind angle of attack. It is important to emphasize that if the vessel is moving at a forward speed *U*, then (2.28) should be redefined in terms of relative wind speed and relative angle of attack (Valčić and Prpić-Oršić, 2016).

Non-dimensional wind load coefficients are usually computed numerically or can be determined experimentally in wind tunnels using appropriate scaled vessel models and other necessary equipment. Based on (2.28), they can be expressed relative to the bow as

$$\begin{bmatrix} C_{X,wind}(\gamma_{wind}) \\ C_{Y,wind}(\gamma_{wind}) \\ C_{N,wind}(\gamma_{wind}) \end{bmatrix} = \frac{2}{\rho_{air} V_{wind}^2} \begin{bmatrix} F_{x,wind} / A_{F,wind} \\ F_{y,wind} / A_{L,wind} \\ M_{z,wind} / (A_{L,wind} L_{oa}) \end{bmatrix}. \tag{2.29}$$

The non-dimensional wind coefficients $C_{X,wind}(\gamma_{wind})$, $C_{Y,wind}(\gamma_{wind})$ and $C_{N,wind}(\gamma_{wind})$ are usually computed using h = 10 m as reference height above the sea surface. To convert the non-dimensional wind coefficients to a different reference height, the ratio between the dynamic pressures at the two heights are usually used (Fossen, 2011). Except the experimental approach in wind tunnels, the values of wind load coefficients can be determined by means of various semi-empirical methods where the ones proposed by Isherwood (1972), Gould (1982), Blendermann (1996, 1995, 1994) and OCIMF (1994) are the most commonly used in industry.

2.3.2 Sea current loads

Damping forces and sea current forces that act on marine vessel in surge, sway and yaw directions are commonly expressed in terms of non-dimensional coefficients $C_{X,curr}(\gamma_{rel,curr})$, $C_{Y,curr}(\gamma_{rel,curr})$ and $C_{N,curr}(\gamma_{rel,curr})$ as

$$\boldsymbol{\tau}_{current} = \begin{bmatrix} F_{x,curr} \\ F_{y,curr} \\ M_{z,curr} \end{bmatrix} = \frac{1}{2}\rho V_{rel,curr}^2 \begin{bmatrix} C_{X,curr}(\gamma_{rel,curr})A_{F,curr} \\ C_{Y,curr}(\gamma_{rel,curr})A_{L,curr} \\ C_{N,curr}(\gamma_{rel,curr})A_{L,curr}L_{oa} \end{bmatrix}, \tag{2.30}$$

where ρ is density of (sea) water, $A_{F,curr}$ and $A_{L,curr}$ are frontal and lateral projected areas below the water line, respectively, and L_{oa} is the length overall.

Forces $F_{x,curr}$, $F_{y,curr}$ and moment $M_{z,curr}$ are expressed in terms of relative velocity of sea current with respect to the velocity of marine vessel. This relative velocity can be written in terms of velocity components in surge and sway directions as

$$V_{rel,curr} = \sqrt{(u-u_{curr})^2 + (v-v_{curr})^2}. \tag{2.31}$$

Sea current angle of attack $\gamma_{rel,curr}$ is commonly defined relatively towards the vessel bow in the counter clockwise direction, i.e. similarly like in the case of wind loads (Figure 6). It can be expressed in terms of vessel velocity components and sea current velocity components as

$$\gamma_{rel,curr} = -\text{atan}((v-v_{curr})/(u-u_{curr})). \tag{2.32}$$

If marine vessel is at rest $(u, v \approx 0)$, relative velocity of sea current is equal to absolute velocity of sea current, i.e. it yields $V_{rel,curr} = V_{curr} = \sqrt{u_{curr}^2 + v_{curr}^2}$. In this case, sea current angle of attack can be also rewritten as $\gamma_{curr} = -\text{atan}(v_{curr}/u_{curr})$.

It is important to emphasize that according to the usual notation (e.g. Blendermann, 1994), encounter angle (β_{curr}) is commonly expressed with respect to axis N, similarly like the vessel heading (ψ), while the angle of attack (γ_{curr}) is expressed relatively to the x_b axis in counter clockwise direction. This approach is used for any environmental load throughout this work.

2.3.3 Mean and slowly varying wave drift forces

Total wave load $\boldsymbol{\tau}_{wave}$ in (2.20) can be generally written as the following sum

$$\boldsymbol{\tau}_{wave} = \boldsymbol{\tau}_{wave1} + \boldsymbol{\tau}_{wave2} \tag{2.33}$$

where $\boldsymbol{\tau}_{wave1}$ presents the first order wave induced forces proportional with wave amplitude, and $\boldsymbol{\tau}_{wave2}$ presents the second order wave induced forces proportional with the square of wave amplitude.

As previously stated, the second-order wave induced forces can be observed as slowly varying components referring to the LF part of the vessel's motion. These forces make a significant contribution to the vessel's drift and therefore are of particular interest for dynamic positioning. In the commercial DP systems they are treated as slowly varying disturbances, so they are implemented in the control law in the conjunction with the estimated forces of sea currents by the means of the so-called bias $\mathbf{b}$ (Fossen, 2011).

In order to determine the values of the vectors $\boldsymbol{\tau}_{wave1}$ and $\boldsymbol{\tau}_{wave2}$ for requirements of numerical simulations, it is necessary to use methods based on the response amplitude operators (RAO) of the first and second order, whereby the wave amplitude is modelled by the corresponding wave spectra (Bretschneider, Pierson-Moskowitz, JONSWAP, etc.) with respect to the sea state defined by a significant wave height and appropriate wave period (Faltinsen, 1990; Fossen, 2011; Journée and Massie, 2001; Newman, 1977).

The wave elevation ζ in irregular sea in a point may be written as

$$\zeta(t) = \sum_{k=1}^{N} \zeta_{a,k} \cos(\omega_k t + \varepsilon_k) \tag{2.34}$$

where $\zeta_{a,k}$ is the wave amplitude, ω_k is the wave frequency, ε_k is the random phase angle of wave component k, and N is the number of harmonic components.

The square of the wave elevation in (2.34) is equal to (Pinkster, 1979)

$$\zeta^2(t) = \sum_{j=1}^{N} \sum_{k=1}^{N} \zeta_{a,j} \zeta_{a,k} \cos(\omega_k t + \varepsilon_k) \cos(\omega_j t + \varepsilon_j) \tag{2.35}$$

and the LF part of the expression (2.35) is equal to

$$\zeta_{LF}^2(t) = \sum_{j=1}^{N} \sum_{k=1}^{N} \tfrac{1}{2} \zeta_{a,j} \zeta_{a,k} \cos\{(\omega_k - \omega_j)t + (\varepsilon_k - \varepsilon_j)\}. \tag{2.36}$$

The second order wave effects can be divided into mean, slowly varying and rapidly varying wave loads (Sørensen, 2012). For the applications considered in this thesis, the effect of the rapidly varying second order wave loads is neglected. The LF second-order wave drift forces are related to the square of the wave elevation and can be determined by means of quadratic transfer functions as follows (Faltinsen, 1990; Newman, 1977; Pinkster, 1979)

$$\left.\begin{aligned}\boldsymbol{\tau}^{i}_{wave2} &= \overline{\boldsymbol{\tau}}^{i}_{wave,\,\text{mean}} + \boldsymbol{\tau}^{i}_{wave,\,\text{slowly varing}} \\ &= \sum_{j=1}^{N}\sum_{k=1}^{N}\zeta_{a,j}\zeta_{a,k}\{T^{ic}_{jk}\cos[(\omega_k-\omega_j)t+(\varepsilon_k-\varepsilon_j)]+ \\ &\qquad + T^{is}_{jk}\sin[(\omega_k-\omega_j)t+(\varepsilon_k-\varepsilon_j)]\}\end{aligned}\right\} \tag{2.37}$$

where ω_j is the wave frequency, $\zeta_{a,j}$ is the wave amplitude, ε_j is the random phase angle of wave component j, c and s superscripts denote cos and sin functions, respectively, and $i = 1,2,\ldots,6$. The quadratic transfer functions T_{jk} depend on the first and second order velocity potentials, which require a nonlinear panel methodology in order to be calculated (Pinkster, 1979; Sørensen, 2012). T^{c}_{jk} is the second-order transfer function for the part of the force which is in-phase with the LF part of the squared wave elevation and T^{s}_{jk} is the out-of-phase part of the second-order transfer function (Pinkster, 1979).

The mean value of equation (2.37) can be found by noting that the mean value over a long period of any oscillating term in (2.37) is zero. Thus, the only time independent terms occur when $j = k$, i.e. when $T^{ic}_{jk} = T^{is}_{jk} = T^{ic}_{jj}$. In this case, the slowly-varying loads could be approximated by the mean drift loads. Namely, the direct summation in (2.37) is relatively time consuming, so Newman (1974) proposed an approximate equation of (2.37) in the following form

$$\left.\begin{aligned}\boldsymbol{\tau}^{i}_{wave2} &= \overline{\boldsymbol{\tau}}^{i}_{wave,\,\text{mean}} + \boldsymbol{\tau}^{i}_{wave,\,\text{slowly varing}} \\ &= 2\left(\sum_{j=1}^{N}\zeta_{a,j}\sqrt{T^{ic}_{jj}(\omega_j,\beta_{wave}-\psi)}\cos(\omega_j t+\varepsilon_j)\right)^2\end{aligned}\right\} \tag{2.38}$$

where $T^{ic}_{jj} > 0$ is the frequency dependent wave drift function and β_{wave} is the mean wave direction with the same sign convention as for the wind and sea current (Figures 6 and 7). The equation (2.38) includes HF effects that have no specific physical meaning, but in the analysis of slow drift responses, these terms usually have no significant influence. Otherwise, they should be filtered out.

The mean value of (2.37) can be written in the following form (Faltinsen, 1990)

$$\overline{\boldsymbol{\tau}}^{i}_{wave,\,\text{mean}} = \sum_{j=1}^{N}\zeta^{2}_{a,j}T^{ic}_{jj}. \tag{2.39}$$

Expression (2.39) presents the mean wave load in direction i due to incident regular waves of amplitude $\zeta_{a,j}$ and circular wave frequency ω_j.

When the results of mean wave loads in regular waves are known, it is relatively easy to obtain results in irregular waves. If one can assume that long-crested seas can be described by a sea spectrum $S(\omega)$, than the equation for mean wave loads can be expressed in the integral form as follows (Faltinsen, 1990)

$$\overline{\boldsymbol{\tau}}^{i}_{wave,\,\mathrm{mean}} = 2\int_{0}^{\infty} S(\omega)\left(\frac{\tau^{i}_{wave,\,\mathrm{mean}}(\omega_j,\beta_{wave})}{\zeta^{2}_{a,j}}\right)\mathrm{d}\omega, \quad i=1,2,\ldots,6 \tag{2.40}$$

where $\tau^{i}_{wave,\,\mathrm{mean}}(\omega_j,\beta_{wave})$ is the *i*-th mean wave load component in regular incident waves of circular frequency ω_j, wave amplitude $\zeta_{a,j}$ and wave propagation direction β_{wave}.

The most commonly used wave spectra are Bretschneider, Pierson-Moskowitz, JONSWAP and Torsethaugen spectrum (Fossen, 2011; Ochi, 1998), although some other formulations and extensions can be used as well (Ochi, 1998). In order to represent fully as well as partially developed seas, Bretschneider (1959) developed an extension of Neumann spectrum (Neumann, 1952), as a two-parameter formulation of the following form

$$S(\omega) = 1.25\frac{\omega_0^4 H_s^2}{4}\omega^{-5}e^{-1.25(\omega_0/\omega)^4} \tag{2.41}$$

where ω_0 is the peak frequency of the spectrum and H_s is the significant wave height. This spectrum is widely used for the design of marine systems and was developed for the North Atlantic, for unidirectional seas, sufficiently large depth, without swell.

Pierson and Moskowitz (1964) spectrum also presents a two-parameter wave spectral formulation, particularly for fully developed wind-generated seas

$$S(\omega) = A\omega^{-5}e^{-B\omega^{-4}}. \tag{2.42}$$

This spectrum was developed from analysis of measured data obtained in the North Atlantic Ocean by wave recorders installed on meteorological vessels and is commonly used in various formulations with respect to different parameters A and B.

In order to predict the responses of marine vessels in open sea, the International Towing Tank Conference (ITTC, 1978) has recommended the use of a modified version of the Pierson-Moskowitz spectrum in the following form

$$A = \frac{4\pi^3 H_s^2}{T_z^4}, \quad B = \frac{16\pi^3}{T_z^4} \tag{2.43}$$

where T_z is the average zero-crossing wave period. This modification should only be used for a fully developed sea with large depth, without swell and with unlimited fetch. For non-fully developed seas the JONSWAP or Torsethaugen spectra are recommended (Fossen, 2011).

The JONSWAP spectrum is also based on extensive wave measurement campaign (Joint North Sea Wave Project) and has been adopted as an ITTC standard (ITTC, 1984) in the following form

$$S(\omega) = 155 \frac{H_s^2}{T_1^4} \omega^{-5} e^{-944\omega^{-4}/T_1^4} \gamma^Y \tag{2.44}$$

where T_1 is the average wave period. The value of the peak-shape parameter γ is commonly chosen as 3.30 (Hasselmann et al., 1973) and

$$Y = e^{-[(0.191\omega T_1 - 1)/(\sqrt{2}\sigma)]^2} \tag{2.45}$$

where

$$\sigma = \begin{cases} 0.07, & \text{for } \omega \le 5.24 / T_1 \\ 0.09, & \text{for } \omega > 5.24 / T_1. \end{cases} \tag{2.46}$$

Different spectrum formulations of (2.44) are possible with respect to various characteristic periods T_0, T_1 and T_z, based on the following relation

$$T_1 = 0.834\, T_0 = 1.073\, T_z, \tag{2.47}$$

where T_0 is the peak wave period. The JONSWAP spectrum is mostly used to describe non-fully developed seas for wind-generated waves under the assumption of finite water depth and limited fetch.

As mentioned before, the mean wave drift forces in irregular waves could be also determined using both experimental results and theoretical calculations (Nabergoj, 2013; Ström-Tejsen et al., 1973). In the first part of this approach, the wave drift forces and moment in regular waves should be determined by the action of wave-maker generated waves on a particular ship model without speed, placed at different encounter wave angles. Prior to testing, a static and dynamic calibration of the model should be made in order to ensure similarity between the model and the ship.

Under steady-state conditions, using a three-component dynamometer placed on the model, longitudinal and lateral mean wave drift forces $F_{x,wave}^{\text{model}}$ and $F_{y,wave}^{\text{model}}$ should be measured in {*b*}, together with moment of rotation $M_{z,wave}^{\text{model}}$ about the vertical axis. In

addition, the amplitude of regular wave ζ_a and the steady encounter angle θ should be recorded as well.

The measured values of $F_{x,wave}^{\text{model}}$, $F_{y,wave}^{\text{model}}$ and $M_{z,wave}^{\text{model}}$ obtained from the tests could be used for determination of non-dimensional coefficients of longitudinal ($C_{X,wave}$) and lateral ($C_{Y,wave}$) forces and yaw moment ($C_{N,wave}$) with respect to non-dimensional wavelength $\bar{\lambda}$, at various encounter angles θ, as follows (Nabergoj, 2013):

$$\begin{bmatrix} C_{X,wave}(\bar{\lambda},\theta) \\ C_{Y,wave}(\bar{\lambda},\theta) \\ C_{N,wave}(\bar{\lambda},\theta) \end{bmatrix} = \frac{1}{\rho_{water} g \zeta_a^2 L_{WL}^{\text{model}}} \begin{bmatrix} F_{x,wave}^{\text{model}} \\ F_{y,wave}^{\text{model}} \\ M_{z,wave}^{\text{model}} / L_{WL}^{\text{model}} \end{bmatrix} \tag{2.48}$$

where ρ_{water} is the water density, usually assumed to be 1000 kg/m^3 and $g = 9.81\ \text{m/s}^2$ is the gravitational acceleration. The relative wavelength $\bar{\lambda}$ is defined as

$$\bar{\lambda} = \frac{\lambda}{L_{WL}}, \tag{2.49}$$

where λ is the wavelength and L_{WL}^{model} is the length of the model at waterline.

In the short-wave region, the construction of relationships $C_{X,wave}(\bar{\lambda},\theta = \text{const.})$, $C_{Y,wave}(\bar{\lambda},\theta = \text{const.})$ and $C_{N,wave}(\bar{\lambda},\theta = \text{const.})$ based on experimental data is usually difficult due to a limited capability of the wave-maker when generating waves of very short length. In order to overcome this issue, some appropriate extrapolation of these non-dimensional characteristics should be applied.

The second part of this approach includes the calculation of mean wave drift forces in 2D irregular waves. This calculation is based on the superposition principle for the components of the wave, motion and resistance spectra as well as on the assumption of linearity of the ship's response (Ström-Tejsen et al., 1973). Thus, the added resistance in irregular waves can be expressed with superposition of the regular wave responses. Ström-Tejsen et al. (1973) showed that relation between added resistance in regular waves $R_{AW}(\omega)$, obtained with experiments, and the mean added resistance in irregular waves $\bar{R}_{AW}$ can be expressed with sufficiently good accuracy in the following form

$$\bar{R}_{AW} = 2\int_0^{\infty} \frac{R_{AW}(\omega)}{\zeta_a^2} S_{\zeta}(\omega)\,\mathrm{d}\omega, \tag{2.50}$$

where $S_\zeta(\omega)$ is the appropriate wave energy spectrum. Usually Pierson-Moskowitz or JONSWAP spectrum is used, but this is more related to geographical conditions.

One can notice that expression (2.50), similarly like (2.40), can be also used for calculation of the mean wave drift forces for full-scale ship in 2D irregular waves for associated sea states. Namely, using (2.40) and (2.50), one can express longitudinal mean wave drift force as follows

$$\overline{F}_{x,wave}(\theta) = 2\int_0^\infty \frac{F_{x,wave}}{\zeta_a^2} S_\zeta(\omega)\,\mathrm{d}\omega = 2\int_0^\infty \frac{C_{X,wave}(\omega,\theta)\rho g \zeta_a^2 L_{WL}}{\zeta_a^2} S_\zeta(\omega)\,\mathrm{d}\omega$$

$$\overline{F}_{x,wave}(\theta) = 2\rho g L_{WL}\int_0^\infty C_{X,wave}(\omega,\theta) S_\zeta(\omega)\,\mathrm{d}\omega. \tag{2.51}$$

Similarly, one can obtain

$$\overline{F}_{y,wave}(\theta) = 2\rho g L_{WL}\int_0^\infty C_{Y,wave}(\omega,\theta) S_\zeta(\omega)\,\mathrm{d}\omega, \tag{2.52}$$

$$\overline{M}_{z,wave}(\theta) = 2\rho g L_{LW}^2\int_0^\infty C_{N,wave}(\omega,\theta) S_\zeta(\omega)\,\mathrm{d}\omega, \tag{2.53}$$

and thus the mean wave loads can be rewritten in the vector form as

$$\overline{\boldsymbol{\tau}}^{i}_{wave,\,\mathrm{mean}} = \begin{bmatrix} \overline{F}_{x,wave}(\theta) \\ \overline{F}_{y,wave}(\theta) \\ \overline{M}_{z,wave}(\theta) \end{bmatrix}, \tag{2.54}$$

where $C_{X,wave}(\omega,\theta)$, $C_{Y,wave}(\omega,\theta)$ and $C_{N,wave}(\omega,\theta)$ are non-dimensional coefficients (2.48) of the longitudinal and lateral forces and drift moment, respectively, obtained from experiments in regular waves and represented with respect to the wave frequency of full-scale seas, L_{WL} is the length of full-scale ship at waterline, and $i = 1, 2, 6.$

2.4 Thrusters in dynamic positioning systems

According to classification societies, dynamically positioned vessel can be defined as the one that keeps her position and heading, i.e. fixed position or predefined path, exclusively by means of active thrusters. This can be achieved with the implementation of tunnel thrusters in combination with main propellers and rudders and/or by using azimuth thrusters that can generate thrust in any direction (DNV, 2012). This definition best describes the function and importance of thrusters in DP systems.

Although various types of thrusters can be used for the propulsion of these vessels, such as podded azimuth thruster, tunnel thruster, waterjet, classic propeller with a rudder, Voith Schneider propeller, etc., the fact remains that the azimuth ducted propeller is the most commonly used within these vessels. The reason for this is primarily in the possibilities of generating the thrust in all directions, but also in very favourable hydrodynamic properties typical for the exploitation conditions of dynamically positioned vessels that are very close to bollard pull conditions, i.e. when the advance velocity is either relatively low or almost equal to zero. Hence, knowing of all significant characteristics of the ducted propeller is crucial for modelling of propulsion systems for dynamically positioned vessels.

2.4.1 General features of azimuth thrusters

The combination of the propeller and the nozzle represents one of the most common propulsion units on the vessels with dynamic positioning systems. If such a propulsion unit can be freely rotated 360° around its vertical axis, then it comes to the so-called azimuth ducted propeller, i.e. azimuth thruster or azimuth propulsor (Figure 8).

The nozzle can be accelerating or decelerating, depending on its geometric characteristics. Marine propellers in accelerating nozzles are mainly used when the propeller is extremely loaded or when the restrictions with respect to the allowed diameter of the propeller (D) are necessary. Given that this nozzle creates a positive thrust, it also increases the efficiency of the extremely loaded propellers.

During the last 50 years, there were numerous studies and researches related to marine propellers with and without nozzle. Perhaps the best-known are those derived from Wageningen Institute MARIN (Wageningen, The Netherlands) by Oosterveld (1970) and (Kuiper, 1992). In their reports, the details of these studies can be found.

Even the theoretical calculations clearly indicate that the application of accelerating nozzle increases the efficiency of loaded propellers (Oosterveld, 1970). If the load of the propeller increases, then the nozzle length L should be longer, while at lesser loads the shorter nozzle is recommended. However, even with extreme loads, the nozzle should not have a ratio L/D greater than 1.0 (Figure 9).

The initial tests with different accelerating nozzles were conducted with the Wageningen *B*-screw series, whereof more information can be found in (Oosterveld, 1970) and (Kuiper, 1992). Due to the certain deficiencies of *B*-series ducted propellers,

e.g. cavitation, the specific K_a series of propellers were developed in former *Netherlands Ship Model Basin* (NSMB), today's *Maritime Research Institute Netherlands* (MARIN).

Figure 8. Azimuth thruster
Photo courtesy of SCHOTTEL

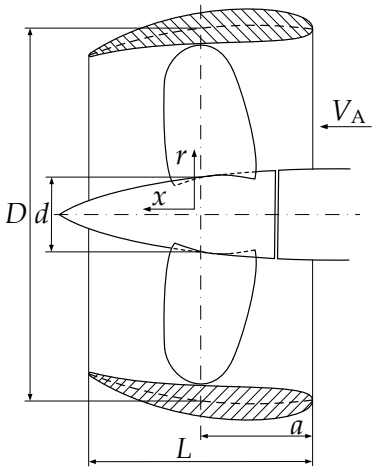

Figure 9. Ducted propeller basic dimensions
Source: (Oosterveld, 1970)

The examined propellers of particular importance are K_a 3-65, K_a 4-55, K_a 4-70 and K_a 5-75 with the diameter of $D = 2400$ mm and clearance of 1 mm in the combination with the nozzle No. 19A $(L/D = 0.5)$, and the combination of propeller K_a 4-70 in the nozzle No. 37 $(L/D = 0.5)$. The details about this series can also be found in (Oosterveld, 1970) and (Kuiper, 1992). The aforementioned nozzles No. 19A and No. 37 are also often used in practice because of their production simplicity and the possession of many desirable hydrodynamic characteristics. In this thesis, they are used because of numerous available data required for the propulsion modelling of dynamically positioned vessels in combination with the ducted propeller K_a 4-70.

The forces and the torques generated by the ducted propeller are usually expressed by the so-called non-dimensional open water characteristics which are completely general regarding specific geometric configurations of the propeller and the nozzle. These characteristics are:

(*i*) Thrust coefficient K_T

$$K_T = \frac{T}{\rho n^2 D^4} \tag{2.55}$$

(*ii*) Torque coefficient K_Q

$$K_Q = \frac{Q}{\rho n^2 D^5} \tag{2.56}$$

(*iii*) Nozzle thrust coefficient K_{TN}

$$K_{TN} = \frac{T_N}{\rho n^2 D^4} \tag{2.57}$$

(*iv*) Advance coefficient J

$$J = \frac{V_A}{nD} \tag{2.58}$$

(*v*) Open water efficiency of a propeller η_0

$$\eta_0 = \frac{J}{2\pi}\frac{K_T}{K_Q} \tag{2.59}$$

where T is the thrust (kN), Q is the torque (kNm), T_N is the nozzle thrust (kN), V_A is the speed of advance (m/s), n is the propeller revolution (s^{-1}), D is the propeller diameter (m), and ρ is the water density (t/m^3).

2.4.2 Empirical modelling of ducted propeller hydrodynamic characteristics

The test results of the propellers K_a 3-65, K_a 4-55, K_a 4-70 and K_a 5-75 in the combination with the nozzle no. 19A can be aggregated using multidimensional nonlinear polynomial regression so the coefficients of thrust (K_T, K_{TN}) and torque K_Q are expressed as polynomials in the function of the advance coefficient J and the pitch ratio P/D. Oosterveld (1970) showed that it is sufficient to choose the multivariable sixth- or at the most seventh-order polynomials, so for K_T, K_{TN} and K_Q they can be written as the regression polynomials of two variables of the following form:

$$K_T = \sum_{x=0}^{n}\sum_{y=0}^{n} A_{x,y}\left(\frac{P}{D}\right)^x J^y, \tag{2.60}$$

$$K_{TN} = \sum_{x=0}^{n}\sum_{y=0}^{n} B_{x,y}\left(\frac{P}{D}\right)^x J^y, \tag{2.61}$$

$$K_Q = \sum_{x=0}^{n}\sum_{y=0}^{n} C_{x,y}\left(\frac{P}{D}\right)^x J^y, \tag{2.62}$$

where the coefficient values $A_{x,y}$, $B_{x,y}$ and $C_{x,y}$ $(x = 0,1,...,6;\ y = 0,1,...,6)$ can be found in (Oosterveld, 1970) and (Carlton, 2007), wherein $n = 6$ for combinations {K_a 3-65 and No. 19A}, {K_a 4-70 and No. 19A} and {K_a 5-75 and No. 19A}, and $n = 7$ for combinations {K_a 4-55 and No. 19A} and {K_a 4-70 and No. 37}.

In order to avoid double-sum calculations using nested loops, and to increase the calculation speed, relations (2.60)-(2.62) are further vectorised. For this purpose, the associated matrices and vectors have been defined (Valčić and Dejhalla, 2015) as follows:

(*i*) Matrix of coefficients $A_{x,y}$

$$\mathbf{A} = \begin{bmatrix} A_{0,0} & A_{0,1} & \cdots & A_{0,n} \\ A_{1,0} & A_{1,1} & \cdots & A_{1,n} \\ \vdots & \vdots & \ddots & \vdots \\ A_{n,0} & A_{n,1} & \cdots & A_{n,n} \end{bmatrix} \tag{2.63}$$

(*ii*) Matrix of coefficients $B_{x,y}$

$$\mathbf{B} = \begin{bmatrix} B_{0,0} & B_{0,1} & \cdots & B_{0,n} \\ B_{1,0} & B_{1,1} & \cdots & B_{1,n} \\ \vdots & \vdots & \ddots & \vdots \\ B_{n,0} & B_{n,1} & \cdots & B_{n,n} \end{bmatrix} \tag{2.64}$$

(*iii*) Matrix of coefficients $C_{x,y}$

$$\mathbf{C} = \begin{bmatrix} C_{0,0} & C_{0,1} & \cdots & C_{0,n} \\ C_{1,0} & C_{1,1} & \cdots & C_{1,n} \\ \vdots & \vdots & \ddots & \vdots \\ C_{n,0} & C_{n,1} & \cdots & C_{n,n} \end{bmatrix} \tag{2.65}$$

(*vi*) Vector of pitch ratio P/D

$$\mathbf{P} = [(P/D)^0 \quad (P/D)^1 \quad \cdots \quad (P/D)^n]^{\mathrm{T}} \tag{2.66}$$

(*v*) Vector of advance coefficient J

$$\mathbf{J} = [J^0 \quad J^1 \quad \cdots \quad J^n]^{\mathrm{T}}. \tag{2.67}$$

Using matrices $\mathbf{A}$, $\mathbf{B}$, $\mathbf{C}$, $\mathbf{P}$ and $\mathbf{J}$, relations (2.60)-(2.62) can be written by means of the vectorization in the following matrix form (Valčić and Dejhalla, 2015):

$$K_T = \mathbf{J}^{\mathrm{T}}\mathbf{A}^{\mathrm{T}}\mathbf{P},$$

$$K_{TN} = \mathbf{J}^{\mathrm{T}}\mathbf{B}^{\mathrm{T}}\mathbf{P},$$

$$K_Q = \mathbf{J}^{\mathrm{T}}\mathbf{C}^{\mathrm{T}}\mathbf{P}.$$

Taking into account the well-known property of multiplied transposed matrices

$$\mathbf{X}^{\mathrm{T}}\mathbf{Y}^{\mathrm{T}} = (\mathbf{YX})^{\mathrm{T}}, \tag{2.68}$$

previous vectorised terms for K_T, K_{TN} and K_Q can be written as

$$K_T = (\mathbf{AJ})^{\mathrm{T}}\mathbf{P}, \tag{2.69}$$

$$K_{TN} = (\mathbf{BJ})^{\mathrm{T}}\mathbf{P}, \tag{2.70}$$

$$K_Q = (\mathbf{CJ})^{\mathrm{T}}\mathbf{P}. \tag{2.71}$$

Although K_T, K_{TN}, K_Q and η_0 are functions of two variables J and P/D, their visualization is usually planar, which means they are shown as curves, i.e. functions of one variable J, for the selected (constant) values of the pitch ratio P/D. The usual interval for J is $[0, J(\eta_0 = 0)]$, and the values for P/D are of the set {0.6, 0.8, 1.0, 1.2, 1.4}. An example of such a visualization of hydrodynamic characteristics K_T, K_{TN}, K_Q and η_0 for the propeller K_a 4-70 in the nozzle No. 19A is shown in Figure 10.

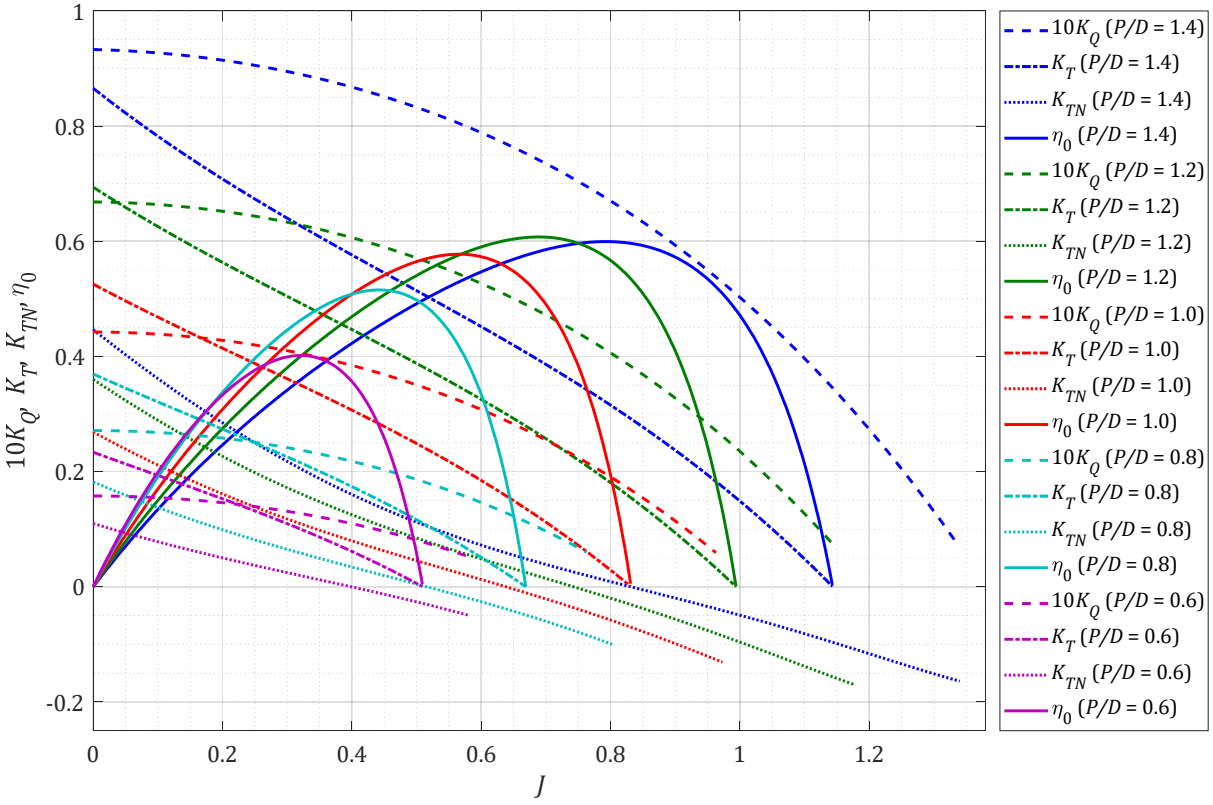

Figure 10. Open water characteristics for the propeller K_a 4-70 in the nozzle no. 19A
Source: Adjusted according to (Oosterveld, 1970)

The total thrust produced by the ducted propeller can be divided into two components (Carlton, 2007):

- the algebraic sum of the propeller thrust and the nozzle thrust,
- second-order effects caused by the mutual influence of the propeller and the nozzle.

If the first approximation is supposed, the total thrust T in (2.55) can be defined as

$$T = T_P + T_N, \tag{2.72}$$

where T_P is the propeller thrust, and T_N is the nozzle thrust. In non-dimensional form, (2.72) can be rewritten as

$$K_T = K_{TP} + K_{TN}, \tag{2.73}$$

where the factor $\rho n^2 D^4$ is the same as in (2.55).

On the other hand, the torque characteristics cannot be decomposed into two components, because the propeller fully absorbs the torque of the engine, i.e. of the prime mover (diesel engine, electric motor, etc.). Generally, the part of the thrust generated by the nozzle considering the overall thrust T is also a variable which changes depending on the advance coefficient J. In applications of azimuth thrusters in the merchant navy and offshore industry, the absolute majority of them is made with the accelerating nozzles. In such thrusters the ratio K_{TN} / K_T takes the value of 0.5 in the bollard pull conditions or generally in the conditions when $V_A \approx 0$, which is a common operation mode in dynamic positioning. In conditions of free sailing, the value of K_{TN} / K_T drops to values of 0.05 to 0.10. If the advance coefficient increases to some high critical value, the nozzle thrust will change direction, and it will begin to act as a drag. However, it should be emphasized that such a situation is almost impossible in practice.

3 MODELLING OF THRUST AND THRUSTER INTERACTION EFFECTS

3.1 Modelling of thrust in propulsion system of a dynamically positioned marine vessel

The propulsion control on the vessels with dynamic positioning is commonly based on the indirect control of the actual thrust $\mathbf{u}_a$ over the demanded (desired) thrust $\mathbf{u}_d$, which is the result of the thrust allocation. It should be noted that the demanded thrust is the vector $\mathbf{u}_d$ whose elements are the thrust magnitude and direction (polar coordinates) or the thrust components (Cartesian coordinates) of individual thrusters of the total thruster configuration. The intermediate parameter between the demanded thrust T_d and the actual thrust T_a, for an arbitrarily selected thruster, is the demanded shaft speed n_d for fixed-pitch propeller (FPP), the demanded propeller pitch ratio $(P/D)_d$ for controllable pitch propeller (CPP), or both n_d and $(P/D)_d$ for combined fixed/controllable pitch propellers (FPP-CPP).

In this thesis, only fixed-pitch propellers are of interest. Hence, the relationship between T_d and n_d (Figure 11) is defined by the following mapping (Sørensen, 2012):

$$n_d = g(T_d). \tag{3.1}$$

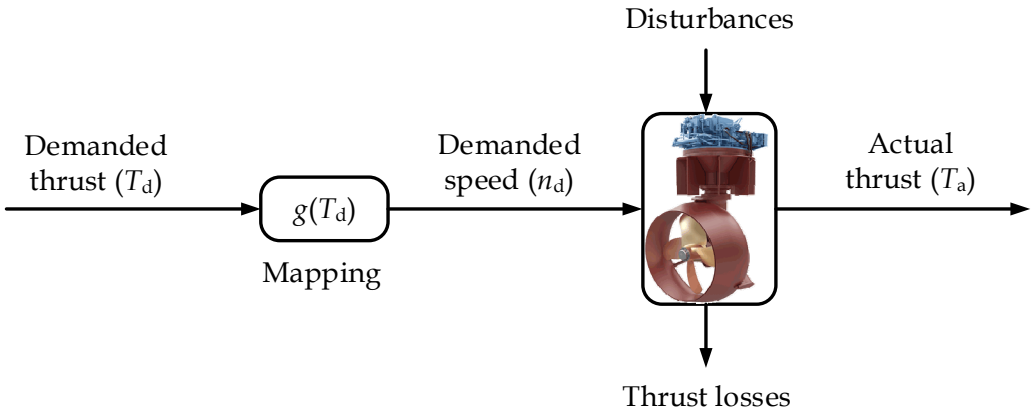

Figure 11. Thrust propagation from demanded thrust T_d to actual thrust T_a

Source: Adjusted according to (Sørensen, 2012); Photo courtesy of Rolls-Royce Marine

Since the measurements of the actual thrust T_a are generally not available on the vessels, there is no guarantee in the control systems that the demanded thrust T_d will indeed be achieved. Therefore, in the control sense the mapping $T_d \rightarrow T_a$ can be viewed as an open-loop system (Sørensen, 2012).

Usually, the demanded shaft speed n_{d} is determined based on the static $T_{\mathrm{d}} - n_{\mathrm{d}}$ characteristics which are mainly the result of model tests, bollard pull tests, as well as possible full-scale tests and sea trial tests. On the other hand, numerous tests have shown that the connection between T_{d} and T_{a} is significantly influenced by localized fluid flow near the thrusters, hull construction, control philosophy and strategy, the vessel's motion in 6DOF, waves, sea currents, etc. All these effects cause the thrust losses (Figure 11), and consequently there is always a certain difference between T_{d} and T_{a} in practice. Moreover, in the ideal conditions T_{d} and T_{a} should be the same, but in actual commercial DP systems there is usually very significant and non-negligible deviation between these two thrusts, which ultimately results in the degradation of accuracy and reliability of positioning, as well as in the prolongation of the response time (Sørensen, 2012).

According to (2.55) and (2.56), actual thrust T_{a} and actual torque Q_{a} can be written as (Carlton, 2007; Sørensen, 2012):

$$T_{\mathrm{a}} = \mathrm{sgn}(n) K_T \rho n^2 D^4, \tag{3.2}$$

$$Q_{\mathrm{a}} = \mathrm{sgn}(n) K_{\mathrm{Q}} \rho n^2 D^5, \tag{3.3}$$

where function $\mathrm{sgn}(n)$ defines the sign of thrust and torque with respect to four quadrant operation. Similarly, one can define propeller power consumption P_{a} that is delivered to the propeller

$$P_{\mathrm{a}} = Q_{\mathrm{a}} \omega = 2\pi n Q_{\mathrm{a}}, \tag{3.4}$$

which in combination with (3.3) yields

$$P_{\mathrm{a}} = \mathrm{sgn}(n) 2\pi K_{\mathrm{Q}} \rho n^3 D^5. \tag{3.5}$$

This is also one of the most important quantities regarding the optimization of the thrust allocation, particularly because the minimization of the power consumed by electric motors, which are powered by diesel-generators, is the commonly defined objective function. The losses caused by the transformation of the electric energy into the propeller torque are neglected here.

As already mentioned, thrust coefficient (2.55) and torque coefficient (2.56) for ducted propellers can be according to (2.60) and (2.62) described in general as functions of advance coefficient J and pitch ratio (P/D), but also of expanded-area ratio A_E / A_0 and number of blades Z. Thus, it can be written

$$K_T = f_1\left(J, \frac{P}{D}, \frac{A_E}{A_0}, Z\right), \tag{3.6}$$

$$K_Q = f_2\left(J, \frac{P}{D}, \frac{A_E}{A_0}, Z\right), \tag{3.7}$$

where (3.6) contains the total thrust of the propeller and the nozzle (2.72).

Given that for some selected fixed-pitch propeller variables P/D, A_E/A_0 and Z are constant, functions f_1 and f_2 can be considered as functions of one variable. On the other hand, for the purpose of the DP vessel's control, there is often a need for further simplification of the relations (3.6) and (3.7), and in such a way that they are linearized by the parameter J. Consequently, with all the appropriate assumptions, the nominal parameters are equal to the demanded parameters, so it can be written

$$T_\mathrm{d} = T_n = \mathrm{sgn}(n) K_{T0} \rho n^2 D^4, \tag{3.8}$$

$$Q_\mathrm{d} = Q_n = \mathrm{sgn}(n) K_{Q0} \rho n^2 D^5, \tag{3.9}$$

$$P_\mathrm{d} = P_n = 2\pi n Q_n = \mathrm{sgn}(n) 2\pi K_{Q0} \rho n^3 D^5, \tag{3.10}$$

where K_{T0} and K_{Q0} are nominal coefficients of thrust and torque, respectively, for sufficiently immersed propeller in case of $V_\mathrm{A} = 0$ and with all losses neglected.

As already mentioned, the output from the DP controller of the conventional DP systems is a vector $\boldsymbol{\tau}_c$ of generalized forces and moment (2.21) that must be generated by the propulsion system (Figure 12).

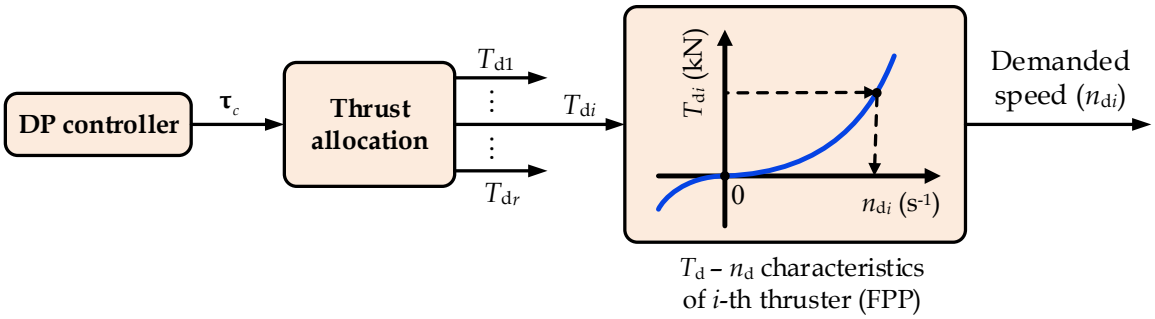

Figure 12. Thrust allocation from a DP controller ($\boldsymbol{\tau}_c$) to demanded speed n_d for FPP

Source: Adjusted according to (Sørensen, 2012)

On the other hand, the function of allocation logic of the DP system's control part is the optimal distribution of these forces by individual thrusters. Once the allocation is

completed, the demanded thrust magnitude and direction of each thruster are determined.

In order to develop the required thrust $T_{\mathrm{d}i}$ by some *i*-th fixed-pitch thruster, it is necessary to determine the shaft speed $n_{\mathrm{d}i}$ corresponding to that thrust (Figure 12). The relation (3.8) can be used for this purpose, considering that the appropriate thruster characteristics should also be known.

3.2 Thruster interaction effects and thrust reduction

Considering the exceptional hydrodynamic complexity of all interaction effects that cause the thrust reduction, the accurate analytical or numerical methods and procedures for their estimation have not yet been exhaustively developed. The existing methods are mainly based on simplified empirical expressions, which are the results of model tests carried out in the well-known hydrodynamic institutes like MARINTEK / SINTEF Ocean (Trondheim, Norway), MARIN (Wageningen, The Netherlands), KSRC (Saint Petersburg, Russia), HSVA (Hamburg, Germany), etc.

So far, several different effects, which to some extent cause the thrust reduction of dynamically positioned vessels, have been noticed. Regarding the physical nature of these particular effects, in general, one can differ:

- thrust reduction due to currents, i.e. axial and transverse current interaction,
- thrust reduction due to thruster-thruster interaction,
- thrust reduction due to thruster-hull interaction,
- thrust reduction due to ventilation and in-and-out-water-effects.

For the purpose of this work, particularly regarding the available experimental data, only the first two effects have been analysed in more detail and have been used for thrust allocation with thrust loss effects included.

3.2.1 The problem of incoming current

It is commonly known that an increase in the advance speed, i.e. in the axial velocity component of the incoming current in this case, reduces the thrust of DP vessel's thrusters which results in a degradation of the position, reduction of the DP system's accuracy, increase in power consumption, etc. (Sørensen, 2012).

In quantitative terms, thrust losses due to the effects of sea currents are roughly 10-20 % (Lehn, 1985) where almost twice as large loss has been recorded for ducted propeller (20 %) in comparison to non-ducted propeller (10 %). However, these results are based on the assumption that the pitch can be increased to compensate the reduced power, while in this work additional thrust is assumed to be generated by means of increased shaft velocity of fixed-pitch propeller.

On the other hand, transverse current interaction effect occurs when the water inflow is perpendicular to the propeller axis. This interaction effect is usually caused by ocean current, vessel speed (e.g. low-speed manoeuvring) or propeller races from other closely spaced thrusters and is commonly treated as a cross-coupling drag under the propeller-hull interaction (Lehn, 1992). It is also important to emphasize that this perpendicular water inflow will induce a force in the inflow direction due to deflection of the propeller race.

In commercial DP systems it is commonly that the control part has only one set of thruster characteristics which meet the bollard pull conditions, i.e. $J_0 = 0$ ($V_A = 0$). The values of the nominal thrust coefficient K_{T0} for $J = 0$ of the ducted propeller can be easily determined from the open water diagrams, computationally by means of regression polynomials, etc., where

$$K_{T0} = f_1(J_0) = \frac{T_0}{\rho n^2 D^4}, \tag{3.11}$$

from where $T - n$ characteristics for $V_A = 0$ follows

$$T_0 = g_1(n) = \rho D^4 K_{T0} n^2. \tag{3.12}$$

Similarly, torque Q_0 at bollard pull can be calculated

$$Q_0 = \rho n_0^2 D^5 K_{Q0} \tag{3.13}$$

as well as delivered power

$$P_0 = 2\pi n_0 Q_0. \tag{3.14}$$

However, it is quite clear that if the DP vessel moves at a certain low speed (e.g. pipe-laying vessel) or is fixedly positioned, but due to the effects of sea currents or the action of other thrusters is simply valid that $V_A \neq 0$, $T - n$ characteristics will no longer be sufficiently reliable and accurate. For the purpose of this work, the thruster mode of operation in all four quadrants will not be analysed, but only for the first quadrant where $V_A > 0$ and $n > 0$.

After the thrust T_0 of some arbitrarily fixed-pitch thruster is allocated, it is easy to determine corresponding shaft speed

$$n_0 = \sqrt{\frac{T_0}{\rho D^4 K_{T0}}}. \tag{3.15}$$

In a case when advance velocity starts to increase $(V_A > 0)$, the DP controller still demands the shaft speed n_0 in (3.15). On the other hand, and regarding the changed water inflow, it yields

$$J_{1a} = \frac{V_A}{n_{1a} D} = \frac{V_A}{n_0 D}. \tag{3.16}$$

Because of demand for allocated speed n_0, it is obvious that $n_{1a} = n_0$, so the new state $1a$ in $T-n$ diagram (Figure 13) is placed vertically below the state 0 on the following curve

$$T_{1a} = g_3(n) = \rho D^4 K_{T1a} n^2. \tag{3.17}$$

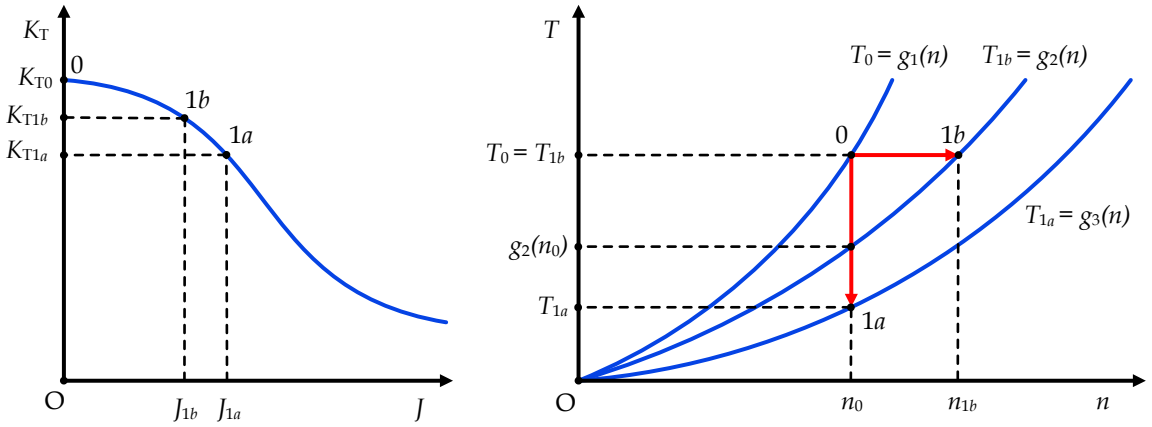

Figure 13. Thrust loss effects for $V_A > 0$

It is obvious that for increased advance velocity V_A with the same shaft speed some thrust reduction occurs. The estimation of this thrust reduction can be absolute

$$\Delta T_{1a} = T_0 - T_{1a} = \rho D^4 n_0^2 (K_{T0} - K_{T1a}), \tag{3.18}$$

or relative

$$t_{1a} = \frac{\Delta T_{1a}}{T_0} = \frac{T_0 - T_{1a}}{T_0} = \frac{K_0 - K_{1a}}{K_0}, \tag{3.19}$$

where coefficient t_{1a} presents non-dimensional thrust reduction ratio. It is required to express all the other thrust losses in a similar way.

It is easy to determine associated K_{Q1a} from (3.16), as well as the torque Q_{1a}

$$Q_{1a} = \rho D^5 K_{Q1a} n_{1a}^2, \tag{3.20}$$

and associated power

$$P_{1a} = 2\pi n_{1a} Q_{1a}, \tag{3.21}$$

that should be delivered to the propeller if the state 1*a* is the referent one. But, considering this is not a case, a part of power ΔP_{1a} is lost together with thrust reduction where

$$\Delta P_{1a} = P_0 - P_{1a}. \tag{3.22}$$

A case in which the allocated thrust T_0 should be kept constant demands the increase of shaft speed and associated delivered power (state 1*b*). One can notice that in the state 1*b* (Figure 13) is $T_{1b} = T_0$, which consequently brings the problem to the following nonlinear equation

$$K_{T1b} n_{1b}^2 = K_{T0} n_0^2, \tag{3.23}$$

with two unknowns K_{T1b} and n_{1b}.

Equation (3.23) can be solved by the fixed-point iteration method in terms of J, because $K_{T1b} = h_1(J_{1b})$ for $P/D = \text{const.}$, and $n_{1b} = V_A/(J_{1b}D) = h_2(J_{1b})$. The iteration function $\varphi(J)$ yields from (3.23), where $K_{T1b} = K_T(J)$ and $J_{1b} = J$, i.e.

$$\varphi(J) = J = \frac{V_A}{n_0 D\sqrt{K_{T0}}}\sqrt{K_T(J)} = \frac{J_{1a}}{\sqrt{K_{T0}}}\sqrt{K_T(J)}. \tag{3.24}$$

First derivation of (3.24) is equal to

$$\frac{\partial\varphi(J)}{\partial J} = \frac{V_A}{n_0 D\sqrt{K_{T0}}}\frac{1}{2\sqrt{K_T(J)}}\frac{\partial K_T(J)}{\partial J}, \tag{3.25}$$

where the first derivation of Oosterveld's regression polynomial for $K_T(J, P/D)$ is equal to

$$\frac{\partial K_T(J)}{\partial J} = \sum_{x=0}^{n}\sum_{y=1}^{n} A_{x,y}\left(\frac{P}{D}\right)^x y J^{y-1}. \tag{3.26}$$

In addition, if the matrices $\mathbf{J}_d$, $\mathbf{P}_d$ and $\mathbf{A}_d$ are defined as follows

$$\mathbf{J}_d = [J^0 \quad 2J^1 \quad 3J^2 \quad \cdots \quad nJ^{n-1}]^{\mathrm{T}},$$

$$\mathbf{P}_d = [(P/D)^0 \quad (P/D)^1 \quad (P/D)^2 \quad \cdots \quad (P/D)^n]^{\mathrm{T}},$$

$$\mathbf{A}_d = \begin{bmatrix} A_{0,1} & A_{0,2} & \cdots & A_{0,n} \\ A_{1,1} & A_{1,2} & \cdots & A_{1,n} \\ \vdots & \vdots & \ddots & \vdots \\ A_{n,1} & A_{n,2} & \cdots & A_{n,n} \end{bmatrix},$$

the derivation in (3.26) can be written in vectorised form as

$$\frac{\partial \mathbf{K_T(J)}}{\partial \mathbf{J}} = \mathbf{J}_d^{\mathrm{T}} \mathbf{A}_d^{\mathrm{T}} \mathbf{P}_d = (\mathbf{A}_d \mathbf{J}_d)^{\mathrm{T}} \mathbf{P}_d. \tag{3.27}$$

If one wants to apply the iteration method in order to solve some nonlinear equation $J = \varphi(J)$ on selected interval $[a,b]$, which contains the solution of the equation, a following condition

$$|\varphi'(J)| < 1 \tag{3.28}$$

should be fulfilled.

The algorithm of the iteration method is well known and it can be written as

$$J_m = \varphi(J_{m-1}), \quad m = 1,2,3,\ldots \tag{3.29}$$

where the accuracy ε_m of obtained solution is satisfied in *m*-th iteration, i.e. when $|J_m - J_{m-1}| < \varepsilon_m$. Considering the empirical nature of the function $K_T(J)$, and regarding the numerical approach in solving equation (3.23), it is sufficient to embed a control measure of the form

$$|\varphi'(J)| < \underbrace{\max}_{[a,b]} |\varphi'(J)| < 1 \tag{3.30}$$

for testing algorithm convergence. This control measure (3.30) should be satisfied on the entire domain of the function $K_T(J)$, i.e. on the interval $[a,b]$.

For some specific values V_A and $T_{1b} = T_0$, iteration method provides a solution in form J_{1b}, from which it is relatively easy to obtain the value of K_{T1b}. In that way, state 1*b* is unambiguously determined in $K_T - J$ diagram (Figure 13). Now, it is also very simple to calculate shaft speed n_{1b} by which the state 1*b* is unambiguously determined in $T - n$ diagram as well.

Torque coefficient K_{Q1b} yields from J_{1b}, so the torque Q_{1b} can be calculated as

$$Q_{1b} = \rho D^5 K_{Q1b} n_{1b}^2, \tag{3.31}$$

as well as the power P_{1b}

$$P_{1b} = 2\pi n_{1b} Q_{1b}, \tag{3.32}$$

which should be delivered to the propeller in order to establish required increase in the shaft speed from n_0 to n_{1b}, i.e. in order to keep the thrust constant. Associated increase of delivered power can be calculated as

$$\Delta P_{1b} = P_{1b} - P_0. \tag{3.33}$$

Relations of the states 0, 1*a* and 1*b* (Figure 13) are also interesting. First of all, it is obvious that $n_0 = n_{1a} < n_{1b}$, from which it yields

$$0 = J_0 < J_{1b} = \frac{V_A}{n_{1b} D} < \frac{V_A}{n_{1a} D} = J_{1a}. \tag{3.34}$$

Considering that $K_T(J)$ is monotonically decreasing function, it yields

$$K_{T0} > K_{T1b} > K_{T1a}. \tag{3.35}$$

With inequalities (3.34) and (3.35), position and mutual relationship of the states 0, 1*a* and 1*b* is unambiguously determined in $K_T - J$ diagram. If (3.35) is multiplied with $\rho D^4 n_0^2$, it yields

$$T_0 = T_{1b} > g_2(n_0) > T_{1a}, \tag{3.36}$$

so one can conclude that the state 1*a* always lies beneath the parabola $T_{1b} = g_2(n)$, i.e. it lies on the parabola $T_{1a} = g_3(n)$. With (3.36), position and mutual relationship of the states 0, 1*a* and 1*b* is unambiguously determined in $T - n$ diagram as well. The real relationship between the curves $T_0 = g_1(n)$ and $T_{1a} = g_3(n)$ is shown in Figure 14 for the propeller K_a 4-70 in nozzle no. 19A (P/D = 1.0) in cases when J = 0 (K_{T0} = 0.5257) and J = 0.25 (K_{T1} = 0.3877), respectively.

As already mentioned, in station-keeping or low speed manoeuvring operations, advance velocity V_A is usually caused by means of sea currents and motion of the vessel. Therefore, for some arbitrarily chosen azimuth thruster, only the axial component of relative current velocity is important, i.e.

$$V_A = V_{rel,curr} \cos\left|\alpha_i - \gamma_{rel,curr}\right|, \tag{3.37}$$

where $V_{rel,curr}$ is relative current velocity (2.31), $\gamma_{rel,curr}$ is relative current encounter angle (2.32) and α_i is azimuth direction of some *i*-th azimuth thruster and is defined

with respect to the axis x_b of $\{b\}$ in counter-clockwise direction. One should notice that (3.37) stands only for the first quadrant. This assumption is acceptable for quasi-stationary conditions when thrusters are directed towards the environmental loads, but for dynamic analysis, (3.37) should be redefined in order to meet requirements for four quadrant conditions.

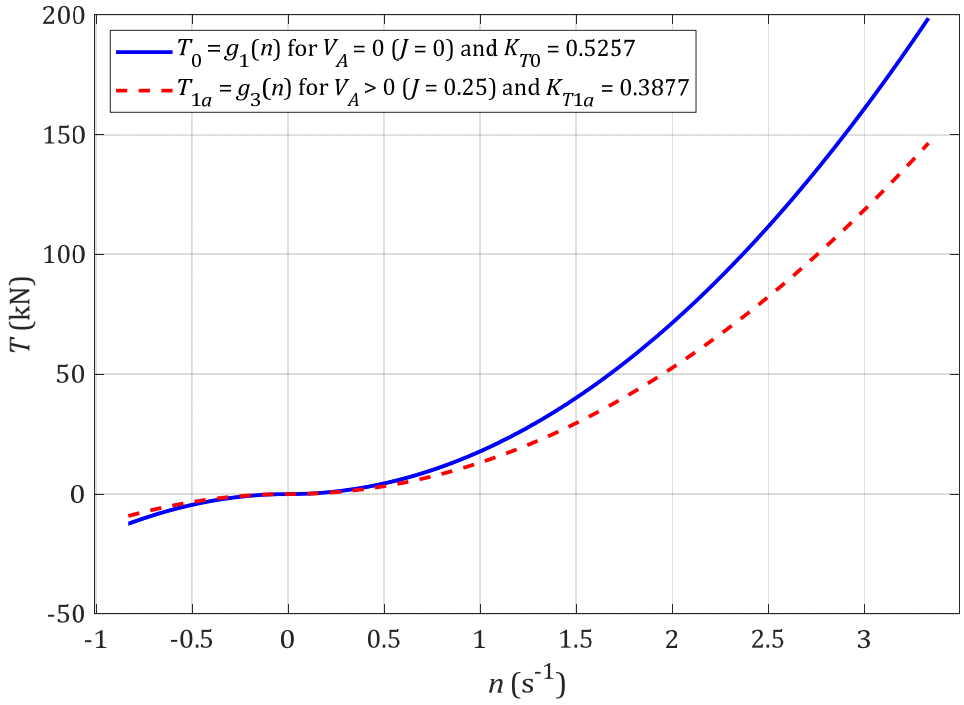

Figure 14. $T-n$ characteristics for thruster combination {K_a 4-70 and no. 19A} and P/D = 1.0 in case of $V_A = 0$ ($J = 0$) and $V_A > 0$ ($J = 0.25$)

The impact of the sea current expressed by the increase in the speed V_A should not be mixed up with the influence of the sea current on the ship's drift, because the wind, sea current and wave forces are already taken into account in the model of ship dynamics, and are certainly taken into account in the thrust allocation. In other words, when the vector of the generalized forces is determined, the vector $\boldsymbol{\tau}_c$ will contain the impact of the sea current through the bias $\mathbf{b}$ of slowly varying loads such as sea currents, second order wave induced forces, etc. This means that the allocated thrust T_0 will also contain a part of the thrust whose function is to compensate the effect of sea current. However, the same thrust will be transformed to n_0 assuming that $V_A = 0$, which again poses a problem, since the impact of the sea current on the thruster itself, i.e. the impact on the generation of the thrust, is neglected. This work does not address the control issues of the propulsion system, but it is quite clear that the estimation of the thrust losses could

be well used for control purposes, either in the form of a corresponding component of the thrust-loss feedforward control or in some other appropriate way.

3.2.2 Thruster-thruster interaction

This is one of the most significant losses caused by the slipstream impact of one thruster to another, which is located in its proximate vicinity. Several important tests of this type of interaction were conducted of which the most distinguished are the reports of Nienhuis (1992) and Lehn (1980). An excellent summary of almost all conducted tests as well as the empirical expressions for the fast estimation of losses arising from the thruster-thruster interaction can be found in (Dang and Laheij, 2004). Depending on the diameter and distance of analysed thrusters, the thrust losses resulting from their interaction can be up to 80 %, although in commercial systems and due to some other physical constraints, this loss is usually up to 40 %.

For the purpose of this analysis, the results of Lehn (1980) with some additional extensions of his results were solely used. Namely, Lehn investigated the interaction of two closely spaced identical azimuth thrusters in case of open water through three typical configurations (Figure 15):

- Configuration #1: $\delta = \phi = 0°$,
- Configuration #2: $\delta = 0°$ and $0° < \phi \leq 30°$,
- Configuration #3: $0° < \delta = \phi \leq 30°$,

where δ and T_R are the interaction angle and the thrust of the rear thruster, respectively , ϕ and T_F are the interaction angle and the thrust of the front thruster, respectively, x is the distance between rear and front thruster and D is thruster diameter. For the purpose of these experiments Lehn used ducted propeller K_a 4-70 in accelerating nozzle no. 19A with P/D = 1.0 and D = 208 mm, n_{max} = 10 s^{-1}.

In general, the reduced real thrust T of some thruster can be determined by the thrust T_0 which would be produced by that thruster in the case without losses, i.e. for open water bollard pull conditions. Thus, the thrust reduction ratio t can be determined for the thruster configuration of interest as well. Generally, for the rear thruster with reduced thrust due to the interaction effects stands

$$t = \frac{T}{T_0}, \tag{3.38}$$

though in some thrust allocation procedures opposite thrust reduction ratio t_0 could be used as well. It is defined similarly like t_{1a} in (3.19), i.e. as

$$t_0 = \frac{T_0 - T}{T_0} = 1 - \frac{T}{T_0} = 1 - t. \tag{3.39}$$

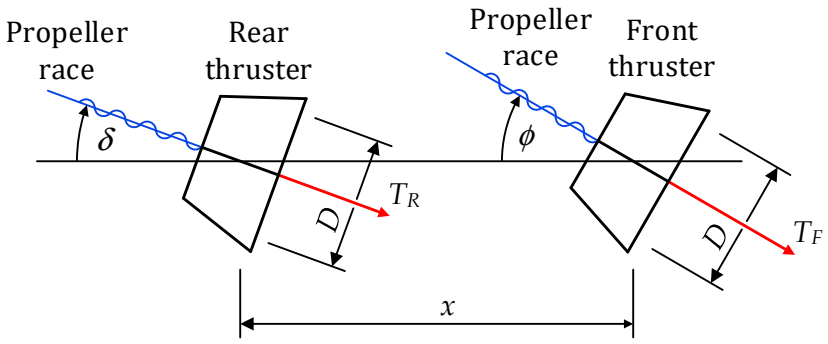

Figure 15. Interaction of two closely spaced azimuth thrusters

For the values of ϕ outside the specified interval $[-30°, 30°]$ one can consider that the losses are negligible or none, no matter on the orientation of the rear thruster.

The simplest thruster-thruster interaction case is obviously for two thrusters in so-called tandem conditions when $\delta = \phi = 0°$ (configuration #1). Experimental results are available for this configuration, both for thrusters in open water conditions (Lehn, 1980; Moberg and Hellström, 1983) and thrusters installed under a solid plate (Blaurock, 1977; Nienhuis, 1992). From the engineering point of view, Dang and Laheij (2004) suggested sufficiently accurate expression for an estimation of the thrust reduction ratio t for the rear thruster in open water conditions

$$t = \frac{T}{T_0} = 1 - 0.80^{(x/D)^{\frac{2}{3}}}, \tag{3.40}$$

where T is the thrust of the rear thruster and T_0 is the bollard pull thrust of that thruster in open water conditions. If the thrusters are installed under the flat plate, the thrust of the rear thruster will be somewhat larger in comparison with the open water conditions due to some reduction of advance water velocity. Therefore, estimation formula for these conditions is similar to (3.40), but with the following correction

$$t = \frac{T}{T_0} = 1 - 0.75^{(x/D)^{\frac{2}{3}}}. \tag{3.41}$$

In case when one wants to prevent striking the rear thruster with a jet generated by the front thruster, some steering of the front thruster is required. These conditions for

configuration #2 ($\delta = 0°,\ 0° < \phi \leq 30°$), are experimentally covered by Lehn (1980) and Nienhuis (1992) for $x/D \in \{2.0, 4.0, 8.0, 16.0\}$, while empirical formula for estimation of thrust reduction ratio based on these experimental results is suggested by Dang and Laheij (2004) as follows

$$t_\phi = t + (1-t)\frac{\phi^3}{130/t^3 + \phi^3}, \tag{3.42}$$

where ϕ is the interaction angle of the front thruster (°), t_ϕ is the thrust reduction ratio for the rear thruster at steering angle ϕ $(0° < \phi \leq 30°)$ and t is the thrust reduction ratio for $\phi = 0°$ which can be determined by using (3.40) or (3.41).

Extended configuration #4a for $0° \leq \delta \leq \phi \leq 30°$ can be obtained by interpolation, and thus one can cover the situation when $\delta < \phi$, which is of particular importance to the final thrust allocation. All other available experiments mainly cover only configurations #1 and #2 for $x/D \leq 30.0$, while configurations #2 and #3 are covered only by results of Lehn (1980), but with the constraint $x/D \leq 6.0$ (Figure 16), which is unfortunately a significant constraint for more distant thrusters, i.e. for $x/D > 6.0$, where the thrust losses still occur as a result of their interaction. Nienhuis (1992) covered x/D up to 16.0, particularly in the case of thruster-thruster interactions under a flat plate, but unfortunately, he performed his experiments just for configurations #1 and #2.

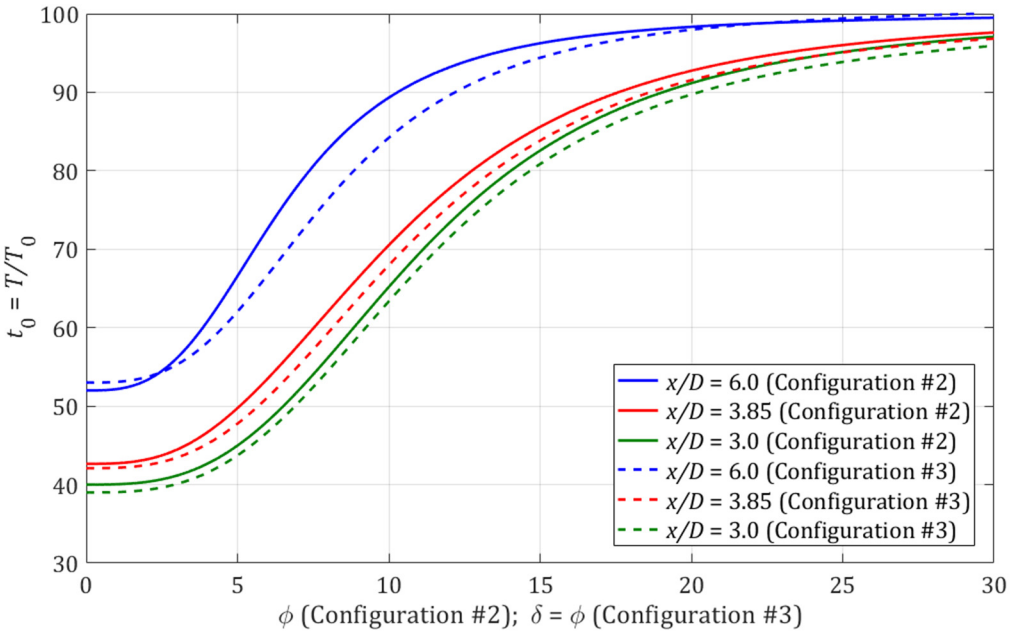

Figure 16. Thruster-thruster interactions for thruster configurations #2 and #3 and $x/D \in \{3.0, 3.85, 6.0\}$

In order to cover all configurations of interest in terms of angles δ and ϕ, it is necessary to extend existing configurations for at least two following cases, i.e. for configuration #4b ($0° \le \phi \le \delta \le 30°$) and configuration #5 ($-30° \le \delta \le 0°,\ 0 \le \phi \le 30°,\ |\delta| + \phi \le 30°$). One can notice that configurations #4a and #4b can be aggregated as one compact configuration #4 ($0 \le \delta \le 30°,\ 0 \le \phi \le 30°$). Hence, all required configurations are summarized in Table 2.

Table 2. Summary of thruster configurations in terms of interaction angles δ and ϕ

Configuration #	Characteristic ranges of interaction angles δ and ϕ
1	$\delta = \phi = 0°$
2	$\delta = 0°,\ 0° < \phi \le 30°$
3	$0° < \delta = \phi \le 30°$
4	$0° < \delta \le 30°,\ 0° < \phi \le 30°$
5	$-30° \le \delta < 0°,\ 0° < \phi \le 30°,\ \|\delta\| + \phi \le 30°$

Source: Adjusted according to (Espedal, 2015)

In order to obtain appropriate data for configurations #4b and #5 without additional experiments, some extension of Lehn's (1980) model is required (Espedal, 2015; Lehn, 1980). Originally, Lehn analysed the velocities in the propeller race based on viscous and turbulent effects. He simplified the problem by comparing the propeller race with a circular turbulent jet without swirl. Analysed velocities are shown in Figure 17. The area marked as potential core is the area behind the propeller where the flow has not been fully developed and is characterized with velocity u_0 at the nozzle outlet that can be determined by using the definition of ideal thrust at bollard pull. Potential core fade away quickly, and afterwards the flow is fully developed. The spreading of the flow is determined by the jet width b, which presents the radial distance from the centreline in a point when half of the maximum axial velocity u_m is established.

From theoretical point of view, Lehn's analysis of the propeller race is based on Reynolds equations, equation of continuity for axisymmetric, turbulent and stationary flow, Prandtl's mixing length theory and Goertler's solution for eliminating Reynolds stress (Lehn, 1985). By combining the theory with experimental results, he obtained the following expressions for centreline axial velocity u_m

$$u_m = \frac{u_0}{0.89 + 0.149\frac{x}{D}} \tag{3.43}$$

for the jet width b, i.e. the radial distance where $u = 0.5u_m$

$$b = 0.39D + 0.0875x \tag{3.44}$$

and for the centreline velocity u at some arbitrary radial distance r

$$u = \frac{u_m}{\left[1 + 0.4142\left(\frac{r}{b}\right)^2\right]^2}. \tag{3.45}$$

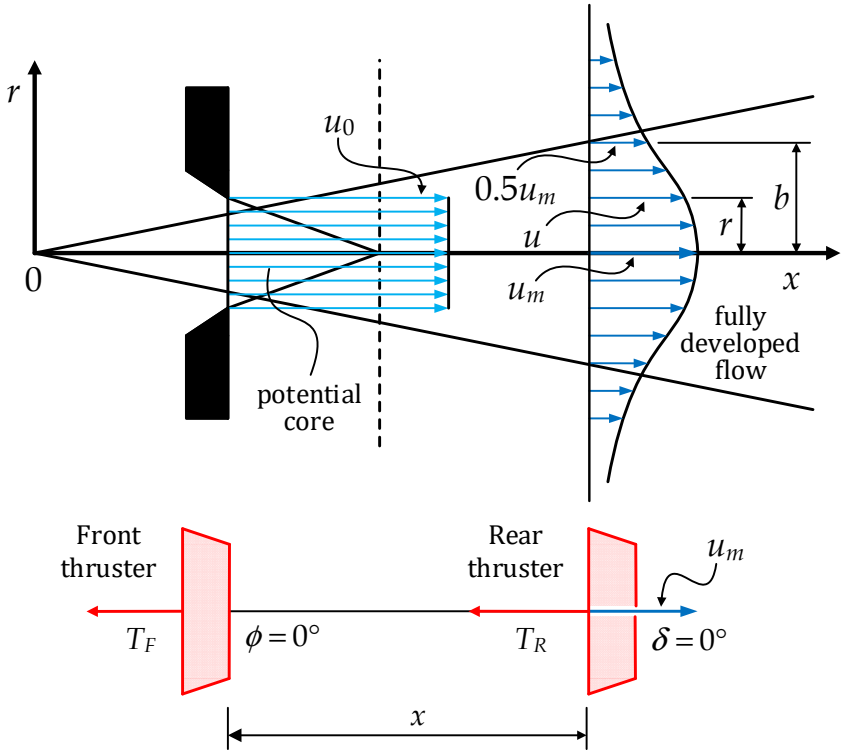

Figure 17. Circular jet and characteristic propeller race velocities

Source: Adjusted according to (Lehn, 1985)

As mentioned before, outlet velocity u_0 can be determined by using the ideal thrust at bollard pull that can be written as (Steen, 2014):

$$T_0 = \rho A u_0^2 = \rho \frac{D^2 \pi}{4} u_0^2. \tag{3.46}$$

Considering the bollard pull thrust T_0 can be also calculated from (2.55) for $J = 0$ as

$$T_0 = \rho n^2 D^4 K_{T0}, \tag{3.47}$$

the outlet velocity u_0 can be expressed based on (3.46) and (3.47) in the following form

$$u_0 = 2\sqrt{\frac{T_0}{\rho \pi D^2}}. \tag{3.48}$$

Maximum centreline axial velocity u_m of the front thruster can be taken as advance velocity of the rear thruster only for configuration #1 (Figure 17). In other words, for all other configurations it is required to properly determine the advance velocity of the rear thruster.

In configuration #2, one can notice that significant velocity for the rear thruster will be centreline velocity u at position $r = x\sin\phi$ (Figure 18). Outlet velocity u_0 can be still determined as in (3.48), but the centreline axial velocity u_m, at the distance $x\cos\phi$, should be calculated according to (3.43) as

$$u_m = \frac{u_0}{0.89 + 0.149\dfrac{x\cos\phi}{D}}. \tag{3.49}$$

Similarly, according to (3.44), the jet width b at the distance of $x\cos\phi$ is equal to

$$b = 0.39D + 0.0875x\cos\phi, \tag{3.50}$$

as well as the centreline velocity u from (3.45), at radial distance $r = x\sin\phi$

$$u = \frac{u_m}{\left[1 + 0.4142\left(\dfrac{x\sin\phi}{b}\right)^2\right]^2}. \tag{3.51}$$

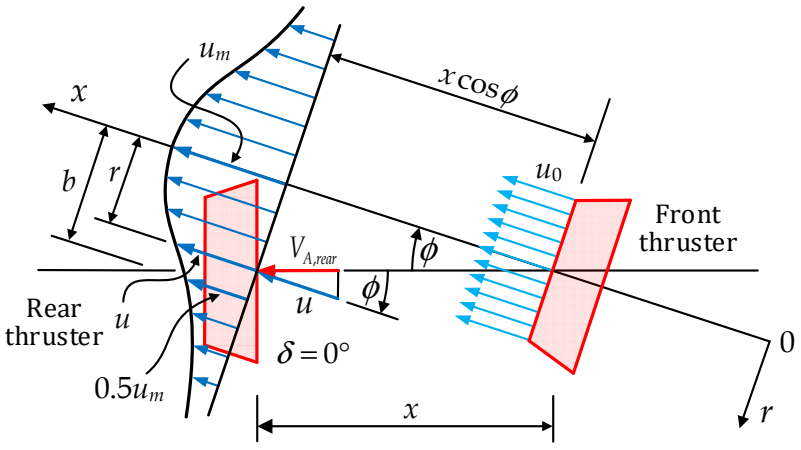

Figure 18. Geometry and distribution of velocities for configuration #2

Finally, only the axial component of centreline velocity u is relevant for the rear thruster. This axial component (Figure 18) presents the advance velocity $V_{A,rear}$ for the rear thruster and it can be easily calculated from

$$V_{A,rear} = u\cos\phi. \tag{3.52}$$

The axial velocity component (3.52), aiming the propeller centre, is assumed to be identical over the complete propeller area. In reality, it will vary slightly according to the bell-shaped surface (Figure 18). Based on this advance velocity, corresponding advance coefficient J_{rear} can be determined according to (2.58) and (3.52) as

$$J_{rear} = \frac{V_{A,rear}}{nD}, \tag{3.53}$$

as well as associated thrust coefficient $K_{T,rear} = f_1(J_{rear})$ by using (2.60) or (2.69) for selected ducted propeller. Finally, thrust reduction ratio t can be determined as

$$t = \frac{K_{T,rear}}{K_{T0,rear}}, \tag{3.54}$$

where $K_{T0,rear}$ is the thrust coefficient of the rear thruster in bollard pull conditions.

Calculation for configurations #4 and #5 is very similar to the previous one. The only difference is regarding the axial component of the inflow current, i.e. the advance velocity of the rear thruster (Figures 19 and 20). Thus, one can notice that expressions for advance velocity of the rear thruster for configurations #2, #3, #4 and #5 can be written respectively in the following compact form

$$V_{A,rear} = \begin{cases} u\cos\phi, & \text{for } \delta = 0°,\ 0° < \phi \le 30° \\ u, & \text{for } 0° < \delta = \phi \le 30° \\ u\cos|\phi - \delta|, & \text{for } 0° < \delta \le 30°,\ 0° < \phi \le 30° \\ u\cos(\phi + |\delta|), & \text{for } -30° \le \delta < 0°,\ 0° < \phi \le 30°,\ |\delta| + \phi \le 30°. \end{cases} \tag{3.55}$$

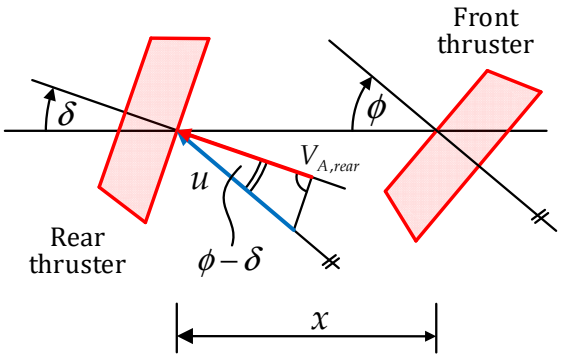

Figure 19. Geometry of velocities for configuration #4

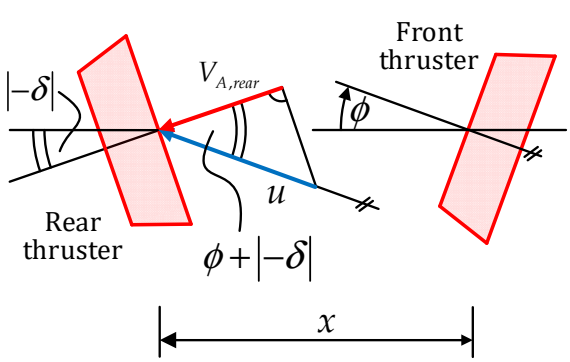

Figure 20. Geometry of velocities for configuration #5

Configuration #3 is just a special case of configuration #4, but some special cases are pointed out because of available experimental data that can be used for partial

validation of a model. Any other configuration of interest that can arise during thrust allocation procedure, i.e. when $-30° \le \phi < 0°$, can be treated as symmetrical to some corresponding configuration from Table 2, as shown in Figures 21 and 22 as an example of thrust reduction ratio for ducted propeller K_a 4-70 in the nozzle no. 19A, with $D = 208$ mm, $n = 10$ s^{-1}, $\rho = 1000$ kg/m^3, $x/D = 6$, and $-30° \le \delta, \phi < 30°$.

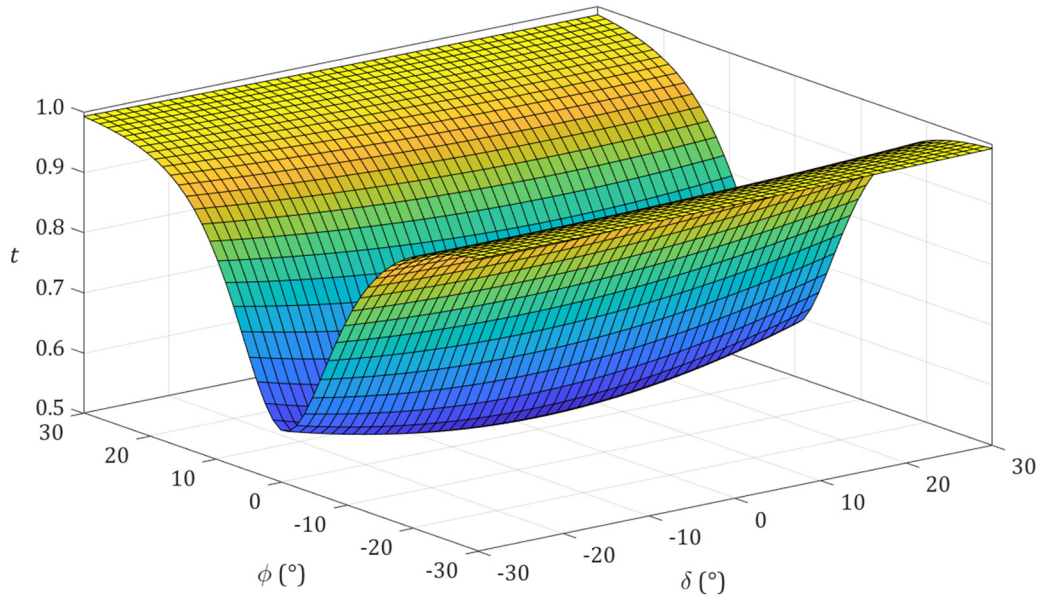

Figure 21. 3D visualization of thrust reduction ratio t for ducted propeller K_a 4-70 in nozzle no. 19A, $D = 208$ mm, $n = 10$ s^{-1}, $\rho = 1000$ kg/m^3, $x/D = 6$, $-30° \le \delta, \phi < 30°$

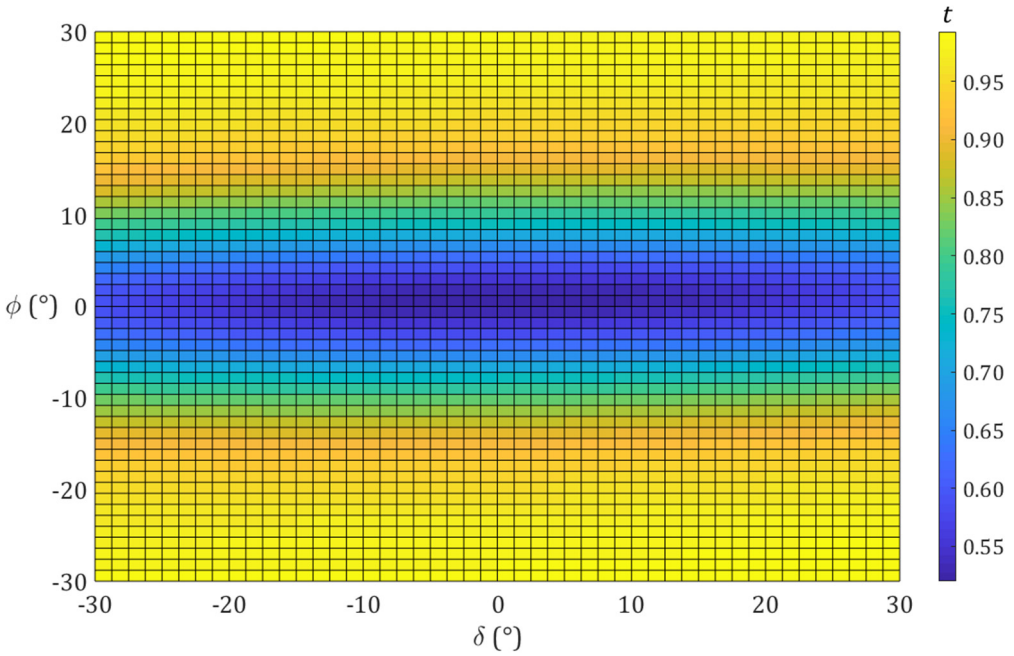

Figure 22. Top view visualization of thrust reduction ratio t for ducted propeller K_a 4-70 in nozzle no. 19A, $D = 208$ mm, $n = 10$ s^{-1}, $\rho = 1000$ kg/m^3, $x/D = 6$, $-30° \le \delta, \phi < 30°$

The afore described approach can cover any thruster-thruster configuration for any available ducted propeller with known thrust coefficient characteristic $K_T = f_1(J, P/D, A_E/A_0, Z)$, any shaft speed n and propeller diameter D, any x/D ratio, and any steering angles δ and ϕ with before mentioned constraints, like the ones defined in Table 2.

These results might be used for sufficiently accurate estimation of thrust reduction ratio (3.54) within thruster-thruster interactions until more experimental or CFD data become available in order to make it even more accurate.

3.2.3 Thruster-hull interaction and Coanda effect

The interaction between the thruster and the hull certainly belongs to the most complex interaction effects. When it comes to DP vessels, the thrust losses when the thruster race is steered to a skeg in classic DP vessels or when the thruster race of a thruster mounted on one pontoon directly collides with a vertical wall of the adjacent pontoon in semi-submersible DP vessels are of particular interest (Lehn, 1980). The thrust losses due to a friction between the slipstream and the hull are in direct dependence on the hull shape and the relative position of the thruster. In other words, if the thruster is closer to the hull the losses are higher due to smaller suction volume of the sea water.

On the other hand, significant losses can occur as a result of slipstream deflection. The so-called Coanda effect is of particular interest which occurs at rough seas when the thruster slipstream begins to follow a wavy surface of the sea and thereby further increases the losses caused by the interaction of the slipstream and the hull (Fjørtoft, 2010). However, nowadays some manufacturers already offer the so-called tilted thrusters in which the vertical deflection, i.e. the thruster pitch angle can be varied. By directing the slipstream downwards, i.e. with a deflection of 5-7°, the negative effects caused by Coanda effect can be significantly reduced up to 10-15 % (Fjørtoft, 2010). If no measures are applied, than in quantitative terms these interaction effects result in the thrust losses of 5-25 % (Lehn, 1992).

Although majority of these interactions present very complex problems in terms of the first principle hydrodynamic modelling, it seems that CFD approach could be cost-efficient and sufficiently accurate method for determination of thruster-hull

interactions as well as for other thruster interaction effects (Bulten and Stoltenkamp, 2013; Koop et al., 2017; Maciel et al., 2013).

3.2.4 Ventilation and in-and-out-of-water effects

The ventilation represents a very unstable phenomenon, which depends on the thrust intensity, thruster immersion and disturbances on the surface. It occurs with a significant thrust increase whereby the pressure on the propeller blades decreases. If this pressure drops below some critical value, the process of air suction towards the thruster will initiate, which results in almost immediate thrust reduction that can be as high as of 20-30 % in extreme cases (Lehn, 1992). This loss will be even higher if the emergence of the thruster occurs. For a tunnel thruster the combination of ventilation and out of water effects may result in thrust losses up to 40-50 % (Lehn, 1992). The ventilation and in-and-out-water-effects for DP vessels are exhaustively investigated by Smogeli (2006), Koushan et al. (2009) and Yvin et al. (2017).

4 THRUST ALLOCATION AND OPTIMALITY CONSIDERATIONS

In industrial applications, the high-level feedback and feedforward controllers in DP systems compute demanded vector $\boldsymbol{\tau}_c$ of surge and sway forces and yaw moment. The thrust allocator determines the corresponding thrust magnitude and direction for each thruster. After that, the low-level thruster controllers will control the propeller pitch and/or speed, torque, and delivered power. The thrust allocation should be performed optimally according to objectives like the total power consumption, fuel consumption, wear and tear of the thrusters, etc. (Sørensen, 2011). Moreover, the thrust allocator should take into account various constraints related to the equilibrium of forces and moment that act on the vessel, the thruster saturation, forbidden zones, thruster magnitude rate, thruster rotation rate, etc.

For the purpose of this study, $\boldsymbol{\tau}_c$ is taken into account as a vector $\boldsymbol{\tau}$

$$\boldsymbol{\tau} = [F_x, F_y, M_z]^{\mathrm{T}} \tag{4.1}$$

of environmental loads and is calculated as a sum of wind, wave and ocean current loads as explained in Chapter 2.3. If required, any other load can be easily added to $\boldsymbol{\tau}$.

4.1 Thrust allocation problem

The state of any i-th thruster in terms of Cartesian coordinate system is given by a thrust vector $T_i = \left\| (u_{ix}, u_{iy})^{\mathrm{T}} \right\|_2$, where T_i indicates the total amount of thrust generated by *i*-th thruster, while u_{ix} and u_{iy} represent the components of the thrust T_i in surge and sway directions, respectively, and $\|\cdot\|_2$ indicates ℓ^2-norm. If required, u_{ix} and u_{iy} can be easily transformed to polar form according to the terms:

$$T_i = \sqrt{u_{ix}^2 + u_{iy}^2}, \tag{4.2}$$

$$\alpha_i = \arctan(u_{iy} / u_{ix}), \tag{4.3}$$

where α_i is azimuth angle of *i*-th thruster. It should be pointed out that it is recommendable to use the alternative atan function (2.24) instead of regular arctan function (4.3) in order to avoid singularity issues when $u_{ix} \to 0$ or both $(u_{ix}, u_{iy}) \to 0$. All afore mentioned quantities together with the sign conventions are shown in Figure 23.

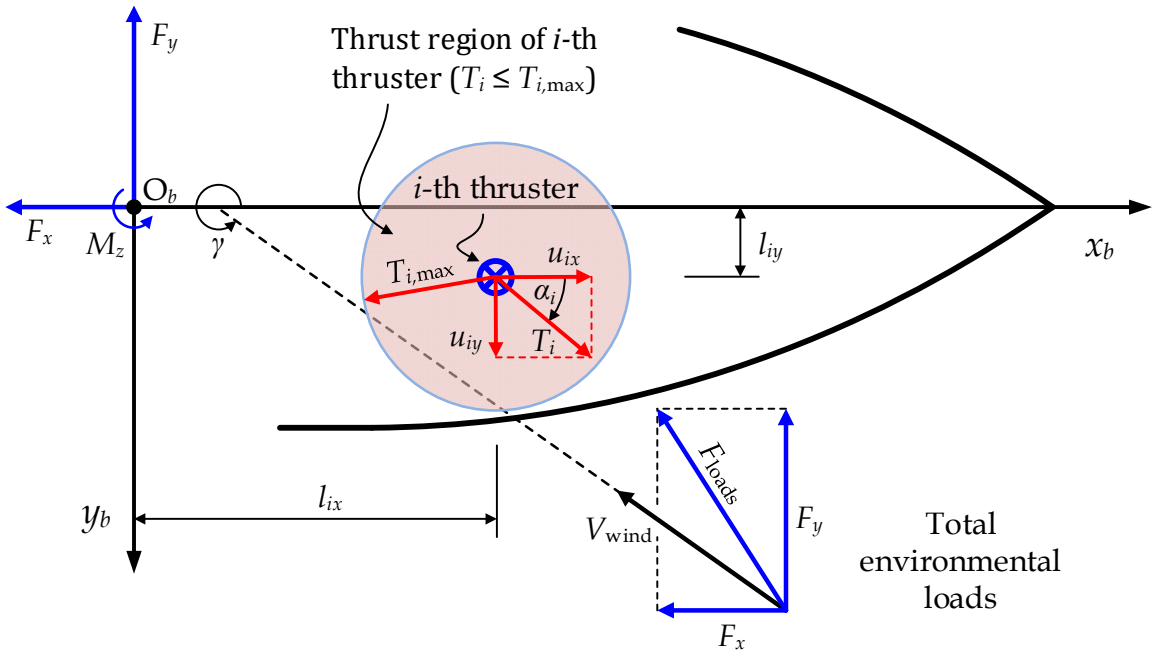

Figure 23. Characteristic thruster quantities and sign convention

If one assumes that r azimuth thrusters are available, then equilibrium equations in the horizontal plane for surge, sway and yaw axis can be written respectively as

$$F_x = \sum_{i=1}^{r} u_{ix}, \tag{4.4}$$

$$F_y = \sum_{i=1}^{r} u_{iy}, \tag{4.5}$$

$$M_z = \sum_{i=1}^{r} (-u_{ix} l_{iy} + u_{iy} l_{ix}), \tag{4.6}$$

where (l_{ix}, l_{iy}) are coordinates of the i-th thruster, $i = 1, 2, \ldots, r$, expressed in the body-fixed reference frame $\{b\}$, as shown in Figure 23.

The thrust allocation part of a DP control system presents the mapping of the demand vector $\boldsymbol{\tau} \in \mathbb{R}^3$ to the space of thruster states which is for r thrusters defined as

$$\mathbf{u} = [u_{1x}, u_{1y}, u_{2x}, u_{2y}, \ldots, u_{ix}, u_{iy}, \ldots, u_{rx}, u_{ry}]^{\mathrm{T}} \in \mathbb{R}^{2r}. \tag{4.7}$$

Considering $2r > 3$, for $r \ge 2$, there is a very large number of possible referent states of the thrusters, which consequently leads to the solution ambiguity of the allocation problem, simply because the system of equations (4.4)-(4.6) is under-determined, i.e. the system has infinitely many solutions that form a characteristic hyper-plane. In other words, the solution is not unique and hence the mapping $\boldsymbol{\tau} \rightarrow \mathbf{u}$ must be optimal in some sense.

System of equations (4.4)-(4.6) can be rewritten in the matrix form as follows

$$\boldsymbol{\tau} = \begin{bmatrix} F_x \\ F_y \\ M_z \end{bmatrix} = \sum_{i=1}^{r} \begin{bmatrix} 1 \cdot u_{ix} + 0 \cdot u_{iy} \\ 0 \cdot u_{ix} + 1 \cdot u_{iy} \\ -l_{iy} \cdot u_{ix} + l_{ix} \cdot u_{iy} \end{bmatrix},$$

$$\boldsymbol{\tau} = \begin{bmatrix} 1 & 0 & 1 & 0 & \cdots & 1 & 0 \\ 0 & 1 & 0 & 1 & \cdots & 0 & 1 \\ -l_{1y} & l_{1x} & -l_{2y} & l_{2x} & \cdots & -l_{ry} & l_{rx} \end{bmatrix} \begin{bmatrix} u_{1x} & u_{1y} & u_{2x} & u_{2y} & \cdots & u_{rx} & u_{ry} \end{bmatrix}^{\mathrm{T}},$$

i.e.

$$\boldsymbol{\tau} = \mathbf{B}\mathbf{u}, \tag{4.8}$$

where

$$\mathbf{B} = \begin{bmatrix} 1 & 0 & 1 & 0 & \cdots & 1 & 0 \\ 0 & 1 & 0 & 1 & \cdots & 0 & 1 \\ -l_{1y} & l_{1x} & -l_{2y} & l_{2x} & \cdots & -l_{ry} & l_{rx} \end{bmatrix} \in \mathbb{R}^{3\times 2r} \tag{4.9}$$

is so-called configuration matrix that consists only of thruster coordinates in {*b*}.

If positions of all thrusters on the hull are fixed, than configuration matrix ***B*** can be considered as constant and thrust allocation equation (4.8) presents linear matrix equation, i.e. linear mapping $\boldsymbol{\tau} \to \mathbf{u}$, where $\mathbf{u}$ presents the unknown vector and should be determined in some optimal sense by means of optimal thrust allocation procedures.

One can notice that there are several special cases like when $u_{ix} = T_i$ and $u_{iy} = 0$ for non-rotatable main propellers without rudders, or when $u_{iy} = T_i$ and $u_{ix} = 0$ for fixed tunnel thrusters, but these are not of interest in this analysis. Moreover, if required, configuration matrix $\mathbf{B}$ and vector of allocated thrust $\mathbf{u}$ could be rewritten in terms of polar coordinates. This approach is commonly used for dynamic allocation within control subsystem.

4.1.1 Thrust regions

Regarding the type of thruster, each of them has its own operational domain, i.e. so-called thrust region. This region, visually presented for azimuth thruster in Figure 24, presents the domain of possible values u_{ix} and u_{iy} that can be allocated by means of optimal thrust allocation procedures according to all predefined physical constraints that have to be satisfied.

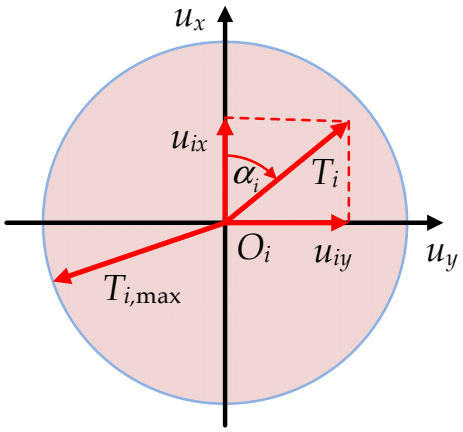

Figure 24. Circle area as the thrust region of an azimuth thruster

For some azimuth thruster, thrust region can be written in a form of the following inequality

$$u_{ix}^2 + u_{iy}^2 \leq T_{i,\max}^2 \tag{4.10}$$

which defines the area of the circle with radius $T_{i,\max}$, where $T_{i,\max}$ presents the maximum thrust that *i*-th thruster can generate. It is important to emphasize that region (4.10) presents a convex set of possible solutions which is crucial for using convex optimization algorithms. Other characteristic regions for tunnel thruster and main propeller with a rudder could be found in (Wit, 2009).

4.1.2 Constraints and limitations

Regardless of used optimization method for optimal thrust allocation, it is necessary to define a number of limitations and constraints in order to meet all physical preconditions related to thrusters and their capabilities. The most important constraints and limitations are related to thruster saturation, forbidden or spoil zones, feasible shaft speed and/or propeller pitch rate of change, feasible thrust rate of change, feasible thruster azimuth angle rate of change, etc. For quasi-static analyses, thruster saturation and forbidden zones are commonly used as main constraints, while in dynamic analyses all constraints related to the rate of change should additionally be included as well.

4.1.2.1 Thruster saturation

Thruster saturation presents a procedure that has to ensure a feasibility of obtained optimal solution for T_i, $i = 1,2,\ldots,r$, in order to allocate only the thrust that can be

produced by *i*-th thruster considering its physical limitations and capabilities. Thruster saturation constraint can be generally written in the following form

$$T_i = \sqrt{u_{ix}^2 + u_{iy}^2} \le T_{i,\max} = R_i, \tag{4.11}$$

where $R_i = T_{i,\max}$ is the radius of a circle that defines thrust region of *i*-th thruster. Relation (4.11) generally presents a non-linear constraint and can be used directly only with appropriate non-linear optimization solvers. On the other hand, commercial DP systems usually use some kind of quadratic optimization solvers and in order to be able to use them, one should take into account that all constraints have to be linear or at least linearized. Thus, constraint (4.11) should be also linearized, which is commonly done by means of so-called polygon approximation shown in Figure 25. This approach was introduced by Leavitt (2008), although much better description is provided by Wit (2009) and Rindarøy (2013).

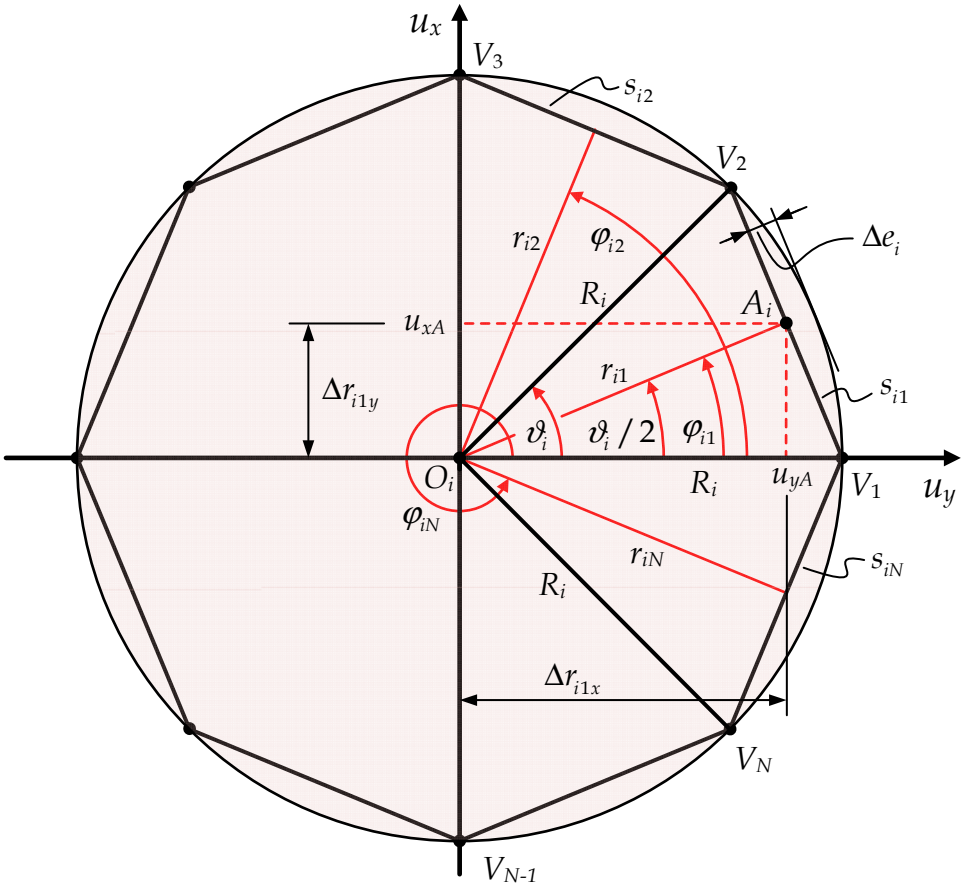

Figure 25. Circle area approximation with *N*-sided polygon

Each polygon side $s_{ij} = \overline{V_{ij}V}_{ij+1}$, where $j = 1, 2, \ldots, N_i$ and $V_{N+1} = V_1$, represents one linear inequality constraint and number of polygon sides N_i determines the

approximation accuracy for *i*-th thruster. Inner radius r_i of *i*-th azimuth thruster can be expressed as

$$r_i = R_i \cos(\vartheta_i / 2), \tag{4.12}$$

where exterior angle can be determined as $\vartheta_i = 2\pi / N_i$. A slope Δr_{i1} of the first inner radius which is perpendicular to the first polygon side s_{i1} is equal to

$$\Delta r_{i1} = \frac{\Delta r_{i1y}}{\Delta r_{i1x}} = \frac{\sin(\vartheta_i / 2)}{\cos(\vartheta_i / 2)}, \tag{4.13}$$

and thus a slope of the first line s_{i1} is equal to

$$\Delta s_{i1} = -\frac{1}{\Delta r_{i1}} = -\frac{\cos(\vartheta_i / 2)}{\sin(\vartheta_i / 2)}. \tag{4.14}$$

Intersection of s_{i1} and r_{i1}, i.e. the point $A_i(u_{yA}, u_{xA}) = s_{i1} \cap r_{i1}$ has the following coordinates

$$\begin{bmatrix} u_{yA} \\ u_{xA} \end{bmatrix} = \begin{bmatrix} \Delta r_{i1x} \\ \Delta r_{i1y} \end{bmatrix} = r_i \begin{bmatrix} \cos(\vartheta_i / 2) \\ \sin(\vartheta_i / 2) \end{bmatrix}. \tag{4.15}$$

Hence, from an equation of the line s_{i1} through the point $A_i(u_{yA}, u_{xA})$ with the slope Δs_{i1}, i.e. from

$$u_{xA} = \Delta s_{i1} u_{yA} + b_{i1}, \tag{4.16}$$

one can easily determine the intercept b_{i1} as

$$b_{i1} = r_i \sin(\vartheta_i / 2) + r_i \frac{\cos^2(\vartheta_i / 2)}{\sin(\vartheta_i / 2)}, \tag{4.17}$$

and finally using (4.14), (4.16) and (4.17), the equation of the line s_{i1} in terms of angle ϑ_i and inner radius r_i can be expressed in the implicit form as

$$u_x \sin(\vartheta_i / 2) + u_y \cos(\vartheta_i / 2) = r_i. \tag{4.18}$$

In order to approximate the circle, only the half-plane

$$u_x \sin(\vartheta_i / 2) + u_y \cos(\vartheta_i / 2) \le r_i \tag{4.19}$$

that contains origin O_i is important. In very similar way, one can easily prepare all other half-planes based on equations of lines s_{ij}, $j = 2, 3, \ldots, N_i$. Thus, all half-planes based on line equations s_{ij} expressed in terms of ϑ_i and r_i can be written as

$$\left.\begin{aligned} u_x \sin(\vartheta_i/2) + u_y \cos(\vartheta_i/2) &\le r_i \\ u_x \sin(\vartheta_i/2 + \vartheta_i) + u_y \cos(\vartheta_i/2 + \vartheta_i) &\le r_i \\ u_x \sin(\vartheta_i/2 + 2\vartheta_i) + u_y \cos(\vartheta_i/2 + 2\vartheta_i) &\le r_i \\ &\vdots \\ u_x \sin[(\vartheta_i/2 + (N_i - 1)\vartheta_i)] + u_y \cos[(\vartheta_i/2 + (N_i - 1)\vartheta_i)] &\le r_i. \end{aligned}\right\} \tag{4.20}$$

Inequality equations (4.20) represent a linearization of the circle area (4.11). Thus, non-linear constraint (4.11) can be approximated with N_i linear inequalities (4.20). If one embed $\vartheta_i = 2\pi / N_i$ in (4.20), these inequalities can be redefined in terms of number of polygon sides N_i as

$$\left.\begin{aligned} u_x \sin\left(\frac{\pi}{N_i}\right) + u_y \cos\left(\frac{\pi}{N_i}\right) &\le r_i \\ u_x \sin\left(\frac{\pi}{N_i} + \frac{2\pi}{N_i}\right) + u_y \cos\left(\frac{\pi}{N_i} + \frac{2\pi}{N_i}\right) &\le r_i \\ u_x \sin\left(\frac{\pi}{N_i} + 2\frac{2\pi}{N_i}\right) + u_y \cos\left(\frac{\pi}{N_i} + 2\frac{2\pi}{N_i}\right) &\le r_i \\ &\vdots \\ u_x \sin\left(\frac{\pi}{N_i} + (N_i - 1)\frac{2\pi}{N_i}\right) + u_y \cos\left(\frac{\pi}{N_i} + (N_i - 1)\frac{2\pi}{N_i}\right) &\le r_i \end{aligned}\right\} \tag{4.21}$$

which can be written in the following compact form

$$u_x \sin(\varphi_{ik}) + u_y \cos(\varphi_{ik}) \le r_i \tag{4.22}$$

where

$$\varphi_{ik} = \frac{\pi}{N_i} + k\frac{2\pi}{N_i}, \quad k = 0, 1, 2, \ldots, N_i - 1. \tag{4.23}$$

Similarly, (4.22) can be rewritten as

$$u_x \sin(\varphi_{ij}) + u_y \cos(\varphi_{ij}) \le r_i \tag{4.24}$$

where

$$\varphi_{ij} = j\frac{2\pi}{N_i} - \frac{\pi}{N_i}, \quad j = 1, 2, \ldots, N_i. \tag{4.25}$$

Absolute approximation error Δe_i depends on the given outer radius R_i, i.e. on chosen number of polygon sides N_i, where

$$\Delta e_i = R_i - r_i = R_i - R_i \cos(\vartheta_i / 2) = R_i[1 - \cos(\pi / N_i)]. \tag{4.26}$$

For the given relative error

$$\delta e_i = \frac{\Delta e_i}{R_i}, \tag{4.27}$$

the minimum number of polygon sides $N_{i,\min}$ can be determined according to (4.26) and (4.27) as

$$N_{i,\min} = \frac{\pi}{\arccos(1 - \delta e_i)}. \tag{4.28}$$

4.1.2.2 Forbidden zones

Considering that thrust region of an azimuth thruster is a circle, forbidden zones could be defined as appropriate circle sectors that are required to be taken out in order to prevent the thrust allocator to allocate azimuth angles and thrust magnitudes in these forbidden regions. For the purpose of this analysis, only simple pie shaped regions will be left over as forbidden zones (FZ). This kind of thrust region can be described as a circle sector bounded with two radii at angles $\varphi_{\text{start}}^{\text{FZ}_i}$ and $\varphi_{\text{end}}^{\text{FZ}_i}$, as shown in Figure 26. It should be noted that any angle of interest $\varphi \in [0, 2\pi\rangle$ should be defined from positive part of u_y axis in counter clockwise direction.

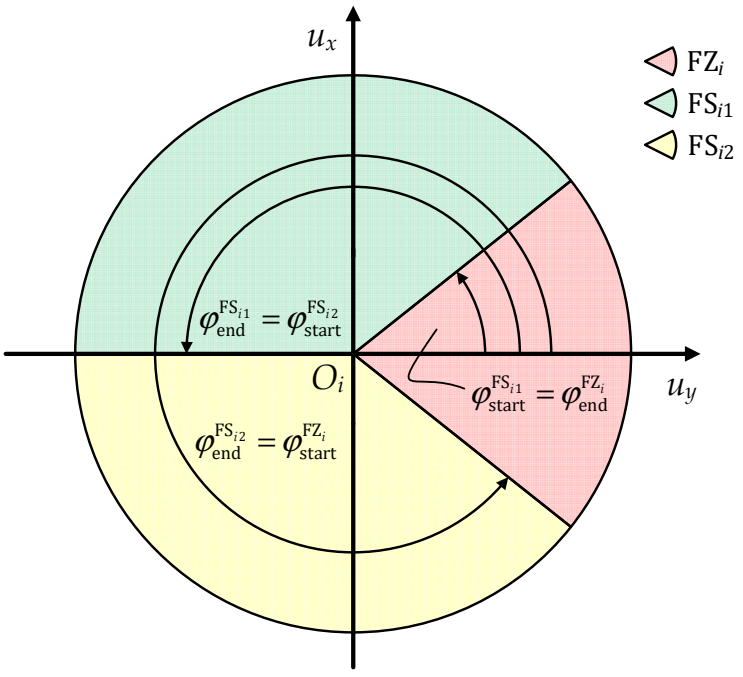

Figure 26. Thrust region divided to one forbidden zone (FZ) and two convex feasible sets (FS)

If a forbidden zone is defined as a circle sector, usually with exterior angle less than 180°, the remaining thrust region will be non-convex and it should be divided into at least two convex regions, i.e. two feasible sets of possible solutions.

After the forbidden zone is defined, remaining part of the circular thrust region should be divided into at least two feasible regions, i.e. two feasible sets (FS) of possible solutions. Due to simplicity reasons, it is sufficiently to divide this non-convex region into two symmetrical feasible regions. These regions are also circle sectors defined with two radii at angles $\varphi_{\text{start}}^{\text{FS}_{i1}}$ and $\varphi_{\text{end}}^{\text{FS}_{i1}}$, i.e. at $\varphi_{\text{start}}^{\text{FS}_{i2}}$ and $\varphi_{\text{end}}^{\text{FS}_{i2}}$, respectively. One can notice that

$$\left.\begin{aligned}\varphi_{\text{start}}^{\text{FZ}_i} &= \varphi_{\text{end}}^{\text{FS}_{i2}} \\ \varphi_{\text{end}}^{\text{FZ}_i} &= \varphi_{\text{start}}^{\text{FS}_{i1}}\end{aligned}\right\} \tag{4.29}$$

and splitting angle $\varphi_{\text{split}}^{\text{FS}_{i12}}$, which divides non-convex Pacman shaped thrust region into two convex circular sectors FS$_{i1}$ and FS$_{i2}$, can be defined in terms of predefined angles $\varphi_{\text{start}}^{\text{FZ}_i}$ and $\varphi_{\text{end}}^{\text{FZ}_i}$ as

$$\varphi_{\text{split}}^{\text{FS}_{i12}} = \frac{1}{2}(\varphi_{\text{start}}^{\text{FZ}_i} + \varphi_{\text{end}}^{\text{FZ}_i}) + k\pi, \tag{4.30}$$

where $k \in \{-1, 0, 1\}$ and $\varphi_{\text{split}}^{\text{FS}_{i12}} = \varphi_{\text{end}}^{\text{FS}_{i1}} = \varphi_{\text{start}}^{\text{FS}_{i2}}$. Value of k should be selected considering the quadrant in which characteristic angles $\varphi_{\text{start}}^{\text{FZ}_i}$ and $\varphi_{\text{end}}^{\text{FZ}_i}$ are located.

Forbidden zones can be also implemented using half-planes of interest (Figure 27). For that purpose one can determine the line equation through the following two points $S_{i1}(R_i \cos\varphi_{\text{start}}^{\text{FS}_{i1}},\ R_i \sin\varphi_{\text{start}}^{\text{FS}_{i1}})$ and $O_i(0,0)$ as

$$-u_x \cos\varphi_{\text{start}}^{\text{FS}_{i1}} + u_y \sin\varphi_{\text{start}}^{\text{FS}_{i1}} = 0. \tag{4.31}$$

Similarly, the line equation through points $S_{i12}(R_i \cos\varphi_{\text{end}}^{\text{FS}_{i1}},\ R_i \sin\varphi_{\text{end}}^{\text{FS}_{i1}})$ and $O_i(0,0)$ is of the form

$$u_x \cos\varphi_{\text{end}}^{\text{FS}_{i1}} - u_y \sin\varphi_{\text{end}}^{\text{FS}_{i1}} = 0. \tag{4.32}$$

If equations (4.31) and (4.32) are rewritten as

$$\left.\begin{aligned}-u_x \cos\varphi_{\text{start}}^{\text{FS}_{i1}} + u_y \sin\varphi_{\text{start}}^{\text{FS}_{i1}} &\le 0 \\ u_x \cos\varphi_{\text{end}}^{\text{FS}_{i1}} - u_y \sin\varphi_{\text{end}}^{\text{FS}_{i1}} &\le 0\end{aligned}\right\} \tag{4.33}$$

they form characteristic half-planes that capture the feasible set FS$_{i1}$. In order to capture the complete thrust region FS$_{i1}$, equations (4.33) that can be written in the following component-wise matrix form

$$\begin{bmatrix} -\cos\varphi_{\text{start}}^{\text{FS}_{i1}} & \sin\varphi_{\text{start}}^{\text{FS}_{i1}} \\ \cos\varphi_{\text{end}}^{\text{FS}_{i1}} & -\sin\varphi_{\text{end}}^{\text{FS}_{i1}} \end{bmatrix} \begin{bmatrix} u_x \\ u_y \end{bmatrix} \leq \begin{bmatrix} 0 \\ 0 \end{bmatrix}, \tag{4.34}$$

should be merged with thruster saturation equations as well. For instance, if QP solvers are used, one should use linearized form (4.22)-(4.23) with (4.34), and if appropriate non-linear solvers are used than thruster saturation can be handled in nonlinear form (4.11) with linear inequality constraints (4.34).

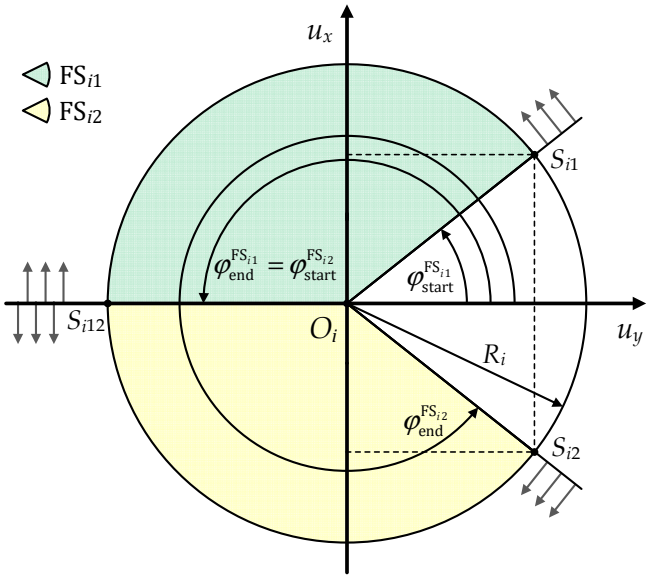

Figure 27. Determination of feasible set thrust regions

In the same way, one can determine the half-planes that are based on line equations through points $S_{i12}(R_i\cos\varphi_{\text{end}}^{\text{FS}_{i1}},\ R_i\sin\varphi_{\text{end}}^{\text{FS}_{i1}}) = S_{i12}(R_i\cos\varphi_{\text{start}}^{\text{FS}_{i2}},\ R_i\sin\varphi_{\text{start}}^{\text{FS}_{i2}})$ and $O_i(0,0)$, i.e. through $S_{i2}(R_i\cos\varphi_{\text{end}}^{\text{FS}_{i2}},\ R_i\sin\varphi_{\text{end}}^{\text{FS}_{i2}})$ and $O_i(0,0)$, respectively. These half-planes capture the feasible set FS$_{i2}$ and can be written in the component-wise matrix form as

$$\begin{bmatrix} -\cos\varphi_{\text{start}}^{\text{FS}_{i2}} & \sin\varphi_{\text{start}}^{\text{FS}_{i2}} \\ \cos\varphi_{\text{end}}^{\text{FS}_{i2}} & -\sin\varphi_{\text{end}}^{\text{FS}_{i2}} \end{bmatrix} \begin{bmatrix} u_x \\ u_y \end{bmatrix} \leq \begin{bmatrix} 0 \\ 0 \end{bmatrix}. \tag{4.35}$$

As explained afore, merging of (4.35) with thruster saturation equations is also required in order to capture only the feasible set FS$_{i12}$. Depending on selected optimization algorithm, i.e. on thruster saturation equations that are directly related to selected algorithm, one can differ linearized and nonlinear approach of thruster saturation with forbidden zones included, as shown in Figure 28.

Computational implementation of forbidden zones can be a little bit tricky. It is not possible to combine feasible sets FS$_{i1}$ and FS$_{i2}$ as one large non-convex set at the same time. Therefore, only one feasible set FS$_{i1}$ or FS$_{i2}$ can be used at a time. This selection

can be based on previously allocated azimuth angle $\alpha_i \in [\varphi_{\text{start}}^{\text{FZ}_i}, \varphi_{\text{end}}^{\text{FZ}_i}]$ of *i*-th azimuth thruster in a case of allocation without forbidden zones included. With determination of α_i, forbidden zone can be detected as well as the direction of propeller race $\alpha_i + k\pi$. This estimation of propeller race direction is based on the simple assumption of neglected propeller race deflection. However, if $\varphi_{\text{start}}^{\text{FS}_{i1}} < \alpha_i + k\pi \le \varphi_{\text{end}}^{\text{FS}_{i1}}$, feasible set FS$_{i1}$ can be selected, and if $\varphi_{\text{start}}^{\text{FS}_{i2}} < \alpha_i + k\pi < \varphi_{\text{end}}^{\text{FS}_{i2}}$, feasible set FS$_{i2}$ can be selected.

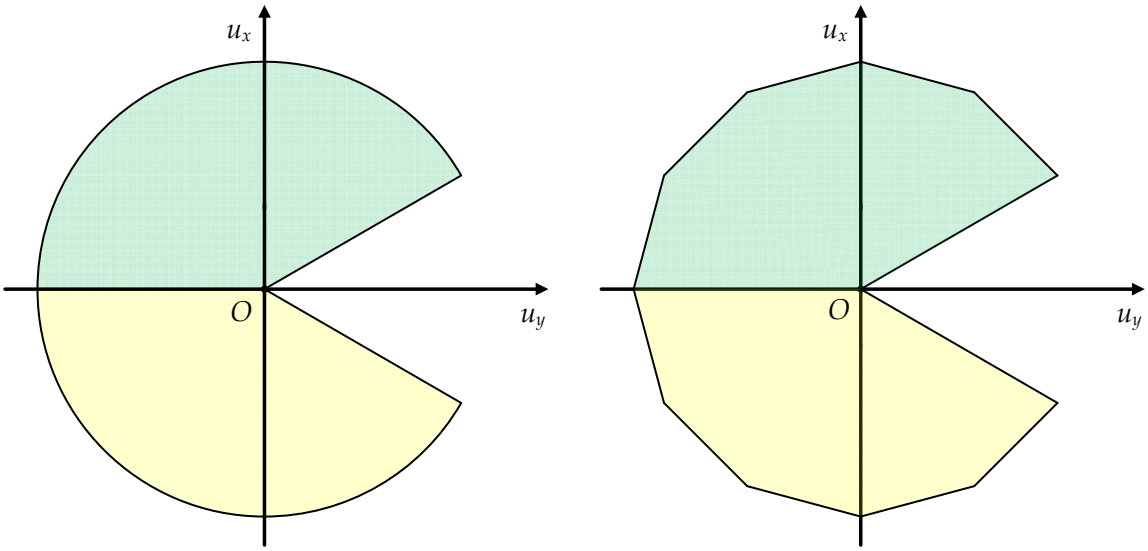

Figure 28. Nonlinear (left) and linearized (right) feasible thrust regions with thruster saturation and forbidden zone included

Other approach includes independent and dual thrust allocation with both feasible sets and afterwards selection can be made regarding the lesser total power consumption required for these two cases. Anyhow, implementation of forbidden zones will surely increase computational time required for thrust allocation and this problem can become even more significant if high accuracy of thruster saturation linearization is required. Namely, the smaller δe_i in (4.27), the larger minimum number of polygon sides $N_{i,\min}$ in (4.28) is required, and large $N_{i,\min}$ means a huge number of linear inequality constraints (4.24) as a part of appropriate optimization procedure that will become computationally very heavy.

4.1.2.3 Other constraints and limitations

In simulations with control part included, as well as in commercial DP systems, some other specific constraints and limitations are usually taken into account. These are

mostly related to the rate of change in thrust magnitude and thrust orientation. Hence, if the magnitude and orientation (T_i, α_i) of some *i*-th azimuth thruster are bounded as

$$\begin{bmatrix} T_{i,\min} \\ \alpha_{i,\min} \end{bmatrix} \leq \begin{bmatrix} T_i \\ \alpha_i \end{bmatrix} \leq \begin{bmatrix} T_{i,\max} \\ \alpha_{i,\max} \end{bmatrix}, \tag{4.36}$$

where $T_{i,\min}$ and $\alpha_{i,\min}$ are minimum, and $T_{i,\max}$ and $\alpha_{i,\max}$ are maximum thrust magnitude and orientation, respectively, then the limitation on the rate of change in thrust magnitude and orientation can be defined as

$$\begin{bmatrix} \dot{T}_{i,\min} \\ \dot{\alpha}_{i,\min} \end{bmatrix} \leq \begin{bmatrix} \dot{T}_i \\ \dot{\alpha}_i \end{bmatrix} \leq \begin{bmatrix} \dot{T}_{i,\max} \\ \dot{\alpha}_{i,\max} \end{bmatrix}, \tag{4.37}$$

where time derivation indicates the rate of change. For optimal thrust allocation solvers, constraints in (4.37) should be discretised as

$$\begin{bmatrix} \Delta T_{i,\min} \\ \Delta\alpha_{i,\min} \end{bmatrix} \leq \begin{bmatrix} \Delta T_i \\ \Delta\alpha_i \end{bmatrix} \leq \begin{bmatrix} \Delta T_{i,\max} \\ \Delta\alpha_{i,\max} \end{bmatrix}, \tag{4.38}$$

and furthermore linearized in order to be aligned with the preconditions of QP solvers.

Constraints (4.37), i.e. (4.38) cannot be handled within the quasi-static analyses. In other words, one cannot use similar approach to previously described polygon approximation in order to implement (4.38) in the optimization task. For this purpose, some kind of iterative procedure in time is required. One approach for this kind of problems can be found in (Ruth, 2008) and it should be noted that this approach can be used even for thruster saturation and forbidden zone handling. However, regarding the quasi-static approach is used in this thesis, constraints (4.38) are not taken into account.

4.2 General considerations about optimal thrust allocation

4.2.1 Objective functions

In general, application of any constrained optimization method as an effective approach for solving the thrust allocation problem (4.8) will eventually come down to defining the optimization task which consists of appropriate objective or cost function and a number of equality and/or inequality constraints that have to be met.

There are a number of possible objectives in thrust allocation like minimizing the fuel consumption, minimizing the activity of thruster units in order to prevent excessive

tear and wear of thruster equipment, maximizing vessel performance in terms of station-keeping or low speed manoeuvring characteristics, etc., though the most commonly used objective is related to the minimization of the total power consumption. It should be noted that total power consumption in this context presents only the electrical power delivered to all active thruster units at a time, i.e. not the total power consumption of the vessel, which is naturally always higher.

The power of some *i*-th azimuth thruster can be expressed according to the following relationship (Leavitt, 2008; Wit, 2009)

$$P_{i,m}(T_i) = (P_{i,\max} - P_{i,\min})\left(\frac{|T_i|}{T_{i,\max}}\right)^{m_i} + P_{\min,i}, \tag{4.39}$$

where $P_{i,\min}$ and $P_{i,\max}$ present minimal and maximal power of thruster unit (kW), respectively, $T_{i,\max}$ is the maximal thrust (kN) that can be generated by *i*-th thruster and is related to its mechanical limitations, and m_i is commonly within the range $1.3 < m_i < 1.7$. Considering only the fixed-pitch azimuth thrusters operating in the first quadrant are of interest for this work, one can notice that $P_{\min,i} = 0,\ i = 1,2,...,r,$ and $|T_i| = T_i \geq 0,\ i = 1,2,...,r.$ Thus, (4.39) can be simplified as

$$P_{i,m}(T_i) = \frac{P_{i,\max}}{(T_{i,\max})^{m_i}}(T_i)^{m_i}, \tag{4.40}$$

which can be used further in order to express the total power consumption P for r active azimuth thrusters in the following form

$$P(T_1, T_2, ..., T_r) = \sum_{i=1}^{r} \frac{P_{i,\max}}{(T_{i,\max})^{m_i}}(T_i)^{m_i}, \tag{4.41}$$

i.e. as

$$P(T_1, T_2, ..., T_r) = \sum_{i=1}^{r} w_i (T_i)^{m_i}, \tag{4.42}$$

where

$$w_i = \frac{P_{i,\max}}{(T_{i,\max})^{m_i}} \tag{4.43}$$

are the constant coefficients that could be determined using given maximal power and thrust of each *i*-th thruster, $i = 1,2,...,r.$ However, parameter m_i could be determined only by means of experiments. Considering these experiments are usually performed at bollard pull conditions, i.e. when $V_A = 0$ and $J = 0,$ one very appropriate

approximation of relationship between the delivered power and generated thrust can be obtained from the nominal power (3.10) and nominal thrust (3.8). Namely, after (3.10) is combined with (3.8) it yields the power for *i*-th thruster as

$$P_i(T_i) = \frac{2\pi K_{Q0,i}}{D_i K_{T0,i}\sqrt{\rho K_{T0,i}}} T_i^{3/2}, \tag{4.44}$$

i.e. the total power consumption for the complete thruster configuration could be approximated as

$$P(T_1, T_2, \ldots, T_r) = \sum_{i=1}^{r} \frac{2\pi K_{Q0,i}}{D_i K_{T0,i}\sqrt{\rho K_{T0,i}}} T_i^{3/2}, \tag{4.45}$$

i.e. as

$$P(T_1, T_2, \ldots, T_r) = \sum_{i=1}^{r} w_i T_i^{3/2}, \tag{4.46}$$

where

$$w_i = \frac{2\pi K_{Q0,i}}{D_i K_{T0,i}\sqrt{\rho K_{T0,i}}} \tag{4.47}$$

are constant coefficients that could be now easily determined by means of known nominal thrust and torque coefficients $K_{T0,i}$ and $K_{Q0,i}$, respectively. The drawback of this approach is related to precondition $V_A = 0$, which means that if $V_A \neq 0$, (4.45) will not be defined only in terms of generated thrusts T_i, but in that case it should be redefined also in terms of variable thrust and torque coefficients $K_{T,i}(J)$ and $K_{Q,i}(J)$, which will consequently make optimization task much more complex. The other issue is related to parameter m_i, which is in this case equal to 3/2. Therefore, (4.45) cannot be used directly as objective function in optimization tasks based on quadratic programing, particularly not in quasi-static analyses. On the other hand, one can linearize (4.45), but this will present additional approximation and the associated error could become unacceptable.

Based on results of Ruth (2008), one additional simplification of (4.45) could be presented in the following form

$$P(T_1, T_2, \ldots, T_r)_t = \sum_{i=1}^{r} \frac{2\pi K_{Q0,i}}{D_i K_{T0,i}\sqrt{\rho K_{T0,i} T_{i,t-1}}} T_{i,t}^2, \tag{4.48}$$

where t indicates the current step and $t-1$ the previous step. In this case, factor $T_i^{3/2}$ from (4.45) is defined as

$$T_i^{3/2} = \frac{1}{\sqrt{T_{i,t-1}}} T_{i,t}^2, \tag{4.49}$$

where $T_{i,t-1}$ presents the allocated thrust from the previous step $t-1$, thus $(T_{i,t-1})^{-1/2}$ is already known and could become a part of updated constant coefficient w_i in (4.47). With this approach, (4.48) becomes a QP problem. However, in quasi-static analyses this approach does not have much sense.

When it comes to commercial DP systems, the total power consumption P in terms of the generated thrusts T_1, T_2,...,T_r is commonly approximated by pure quadratic function so that some variant of quadratic programming can be used for the optimization of thrust allocation. Therefore, for $m_i = 2$, $i = 1,2,...,r$, (4.42) can be redefined as

$$P(T_1, T_2, ..., T_r) = \sum_{i=1}^{r} w_i (T_i)^2 = \sum_{i=1}^{r} w_i (u_{ix}^2 + u_{iy}^2), \tag{4.50}$$

where now

$$w_i = \frac{P_{i,\max}}{(T_{i,\max})^2}. \tag{4.51}$$

With this approximation approach, one can notice that (4.50) combined with (4.2) can be rewritten in the matrix form as follows

$$P = P(T_1, T_2, ..., T_r) = P(u_{1x}, u_{1y}, u_{2x}, u_{2y}, ..., u_{rx}, u_{ry}) = \sum_{i=1}^{r} w_i (u_{ix}^2 + u_{ix}^2)$$

$$P = \begin{bmatrix} u_{1x} & u_{1y} & \cdots & u_{rx} & u_{ry} \end{bmatrix} \begin{bmatrix} w_1 & 0 & \cdots & 0 & 0 \\ 0 & w_1 & \cdots & 0 & 0 \\ \vdots & \vdots & \ddots & \vdots & \vdots \\ 0 & 0 & \cdots & w_r & 0 \\ 0 & 0 & \cdots & 0 & w_r \end{bmatrix} \begin{bmatrix} u_{1x} \\ u_{1y} \\ \vdots \\ u_{rx} \\ u_{ry} \end{bmatrix} \tag{4.52}$$

$$P = \mathbf{u}^{\mathrm{T}} \mathbf{W} \mathbf{u} \tag{4.53}$$

where

$$\mathbf{W} = \mathrm{diag}\{w_1, w_1, w_2, w_2, ..., w_r, w_r\} \in \mathbb{R}^{2r \times 2r} \tag{4.54}$$

is so-called thrust weighting matrix that contains coefficients w_i from (4.51). Total power consumption P in matrix form (4.53) is particularly convenient form for many optimization solvers.

In general, the main advantage of objective function in the form (4.50), i.e. (4.53), is in the possibility of using appropriate QP solver that can guarantee global optimum in feasible amount of time. On the other hand, nonlinear solvers like SQP or MADS can handle highly nonlinear objective functions like (4.45) or even more general forms like (4.39) or (4.41). QP solvers can handle only linear equality and linear inequality constraints. If constraints are non-linear they should be externally linearized which can make computation more complex with additional time consumption as a consequence. Non-linear solvers like SQP or direct (pattern) search algorithms can handle even non-linear equality and non-linear inequality constraints in feasible amount of time.

Most of these techniques assumes convexity, which means that P is a convex function and U is a convex set of feasible solutions. For reduced function (4.40) of the form

$$P_{i,m}^{*}(T_i) = (T_i)^{m_i}, \tag{4.55}$$

convexity is evident for $m_i = 2,$ i.e. when the power function is quadratic, because of

$$\frac{\mathrm{d}^2 P_{i,m}^{*}(T_i)}{\mathrm{d}T_i^2} = 2 > 0. \tag{4.56}$$

However, for more general case of interest, i.e. for $1 < m_i \leq 2,$ it yields

$$\frac{\mathrm{d}^2 P_{i,m}^{*}(T_i)}{\mathrm{d}T_i^2} = m_i(m_i - 1)(T_i)^{m_i - 2} > 0, \tag{4.57}$$

for $T_i \geq 0,$ which is aligned with the assumption of this work regarding the propeller operation in the first quadrant.

If function (4.55) is convex for $1 < m_i \leq 2$ and $T_i \geq 0,$ then according to Boyd and Vandenberghe (2004), function

$$P_{i,m}(T_i) = w_i(T_i)^{m_i}, \tag{4.58}$$

is also convex for $w_i \geq 0.$ Moreover, if functions $P_{i,m}(T_i),$ $i = 1, 2, \ldots, r,$ are all convex, and $w_i \geq 0,$ $i = 1, 2, \ldots, r,$ then linear combination (4.41), i.e. (4.42), is also convex (Boyd and Vandenberghe, 2004). It should be noted that conclusion about the convexity of the function (4.58), according to Boyd and Vandenberghe (2004), should be defined as such only for $T_i > 0,$ although even for $T_i = 0,$ relation (4.57) theoretically stands due to

$$\lim_{T_i \to 0} \frac{\mathrm{d}^2 P_{i,m}^{*}(T_i)}{\mathrm{d}T_i^2} = \lim_{T_i \to 0} [m_i(m_i - 1)(T_i)^{m_i - 2}] = +\infty > 0. \tag{4.59}$$

This special case when $T_i = 0,$ i.e. when $u_{ix} = u_{iy} = 0,$ is very interesting due to already mentioned singularity issues in Chapter 4.1., relation (4.3).

4.2.2 Linear equality constraints

The most important linear equality constraint is the thrust allocation problem itself, i.e. equilibrium equations (4.4)-(4.6) in the horizontal plane written in slightly modified matrix form as

$$\mathbf{Bu} = -\boldsymbol{\tau} \tag{4.60}$$

where negative sign is added in order to properly balance left-hand and right-hand side of (4.60), because $\mathbf{Bu}$ and $\boldsymbol{\tau}$ will have opposite signs otherwise after allocation.

If thruster configuration of interest consists of azimuth thrusters only, then (4.60) presents the sole linear equality constraint. However, if there is a need to include some different thrusters like the tunnel thruster, then it is recommendable to include specific equality constraints characteristic for tunnel thrusters as well. For this purpose, let us assume that there are $r-1$ azimuth thrusters and one tunnel thruster in total thruster configuration. Without any loss of generality, one can assume that configuration submatrix of this tunnel thruster is located at (2*j*-1)-th and (2*j*)-th column of the configuration matrix $\mathbf{B}$, $j \in \{1,2,...,r\},$ i.e. it can be written

$$\mathbf{B} = \begin{bmatrix} 1 & 0 & \cdots & 0 & 0 & \cdots & 1 & 0 \\ 0 & 1 & \cdots & 0 & 1 & \cdots & 0 & 1 \\ -l_{1y} & l_{1x} & \cdots & 0 & l_{jx} & \cdots & -l_{ry} & l_{rx} \end{bmatrix} \in \mathbb{R}^{3\times 2r}. \tag{4.61}$$

Considering tunnel thruster can generate thrust only in lateral directions, it yields

$$u_{jx} = 0, \tag{4.62}$$

which presents characteristic equality constraint that should be aggregated with (4.60) in total linear equality constraint equation. For this purpose, one should define the following matrices

$$\mathbf{C}_{\text{eq}} = [0 \quad 0 \quad \cdots \quad 1 \quad 0 \quad \cdots \quad 0 \quad 0] \in \mathbb{R}^{1\times 2r}, \tag{4.63}$$

$$\mathbf{0}_{\text{eq}} = [0] \in \mathbb{R}^{1}, \tag{4.64}$$

where $\mathbf{C}_{\text{eq}}$ presents a vector of zeros with an exception at (2*j*-1)-th column where the value of the element at position $(1, 2j-1)$ is equal to 1. In that case, equality constraint (4.62) can be rewritten in matrix form as follows

$$\mathbf{C}_{\text{eq}}\mathbf{u} = \mathbf{0}_{\text{eq}}, \tag{4.65}$$

where $\mathbf{u} = [u_{1x} \quad u_{1y} \quad \dots \quad u_{jx} \quad u_{jy} \quad \dots \quad u_{rx} \quad u_{ry}]^{\mathrm{T}} \in \mathbb{R}^{2r}$. If required, similar approach can be applied for all other tunnel thrusters. However, in this case, i.e. for complete thruster configuration of $r-1$ azimuth thrusters and one tunnel thruster, linear equality constraints could be aggregated in the following form

$$\mathbf{A}_{\text{eq}}\mathbf{u} = \mathbf{b}_{\text{eq}}, \tag{4.66}$$

where

$$\mathbf{A}_{\text{eq}} = \begin{bmatrix} \mathbf{B} \\ \mathbf{C}_{\text{eq}} \end{bmatrix} \in \mathbb{R}^{4\times 2r}, \tag{4.67}$$

$$\mathbf{b}_{\text{eq}} = -\begin{bmatrix} \boldsymbol{\tau} \\ \mathbf{0}_{\text{eq}} \end{bmatrix} \in \mathbb{R}^{4}. \tag{4.68}$$

4.2.3 Linear inequality constraints

For the purpose of QP and other similar solvers that can handle only linear or linearized constraints, thruster saturation (TS) of some *i*-th thruster in linearized form (4.22)-(4.23) should be redefined in the component-wise matrix form as follows

$$\mathbf{A}_i^{\text{TS}}\mathbf{u}_i \le \mathbf{b}_i^{\text{TS}}, \tag{4.69}$$

where

$$\mathbf{A}_i^{\text{TS}} = \begin{bmatrix} \sin\varphi_{i,0} & \cos\varphi_{i,0} \\ \sin\varphi_{i,1} & \cos\varphi_{i,1} \\ \vdots & \vdots \\ \sin\varphi_{i,N-1} & \cos\varphi_{i,N-1} \end{bmatrix} \in \mathbb{R}^{N_i\times 2}, \tag{4.70}$$

$$\mathbf{u}_i = \begin{bmatrix} u_{ix} \\ u_{iy} \end{bmatrix} \in \mathbb{R}^{2}, \tag{4.71}$$

$$\mathbf{b}_i^{\text{TS}} = \begin{bmatrix} r_i \\ r_i \\ \vdots \\ r_i \end{bmatrix} = R_i \cos\left(\begin{bmatrix} \vartheta_i \\ \vartheta_i \\ \vdots \\ \vartheta_i \end{bmatrix}\right) \in \mathbb{R}^{N_i}. \tag{4.72}$$

and $\vartheta_i = 2\pi / N_{i,\min}$.

Equations of forbidden zones (4.34) and (4.35) are already written in the component-wise matrix form, but they should be also redefined as

$$\mathbf{A}_i^{\mathrm{FZ}_{ik}}\mathbf{u}_i \le \mathbf{0}_i^{\mathrm{FZ}_{ik}}, \tag{4.73}$$

where

$$\mathbf{A}_i^{\mathrm{FZ}_{ik}} = \begin{bmatrix} -\cos\varphi_{\mathrm{start}}^{\mathrm{FS}_{ik}} & \sin\varphi_{\mathrm{start}}^{\mathrm{FS}_{ik}} \\ \cos\varphi_{\mathrm{end}}^{\mathrm{FS}_{ik}} & -\sin\varphi_{\mathrm{end}}^{\mathrm{FS}_{ik}} \end{bmatrix} \in \mathbb{R}^{2\times 2}, \tag{4.74}$$

$$\mathbf{0}_i^{\mathrm{FZ}_{ik}} = \begin{bmatrix} 0 \\ 0 \end{bmatrix} \in \mathbb{R}^2, \tag{4.75}$$

and $k \in \{1,2\}$ indicates whether feasible set FS_{i1} or FS_{i2} is selected according to some predefined criteria. Any optimization programing technique in which this variation of mutually exclusive thrust (feasible) regions (4.74) for $k=1$ or $k=2$ is implemented, presents so-called disjunctive programing where by definition at least one constraint needs to be fulfilled, but certainly not all of them.

If one has to include both thruster saturation and forbidden zones, than linear inequality constraints for *i*-th thruster should be redefined in the component-wise matrix form as

$$\mathbf{A}_i\mathbf{u}_i \le \mathbf{b}_i, \tag{4.76}$$

where

$$\mathbf{A}_i = \begin{bmatrix} \mathbf{A}_i^{\mathrm{TS}} \\ \mathbf{A}_i^{\mathrm{FZ}_{ik}} \end{bmatrix} \in \mathbb{R}^{(N_i+2)\times 2}, \tag{4.77}$$

$$\mathbf{b}_i = \begin{bmatrix} \mathbf{b}_i^{\mathrm{TS}} \\ \mathbf{0}_i^{\mathrm{FZ}_{ik}} \end{bmatrix} \in \mathbb{R}^{N_i+2}. \tag{4.78}$$

For complete thruster configuration of r azimuth thrusters, linear inequality constraints could be aggregated in the following component-wise matrix form

$$\mathbf{A}_{\mathrm{ineq}}\mathbf{u} \le \mathbf{b}_{\mathrm{ineq}}, \tag{4.79}$$

where

$$\mathbf{A}_{\mathrm{ineq}} = \begin{bmatrix} \mathbf{A}_1 & \mathbf{0} & \cdots & \mathbf{0} \\ \mathbf{0} & \mathbf{A}_2 & \cdots & \mathbf{0} \\ \vdots & \vdots & \ddots & \vdots \\ \mathbf{0} & \mathbf{0} & \cdots & \mathbf{A}_r \end{bmatrix} = \mathrm{diag}\{\mathbf{A}_1, \mathbf{A}_2, ..., \mathbf{A}_r\} \in \mathbb{R}^{\sum_{i=1}^{r}\dim(\mathbf{A}_i)}, \tag{4.80}$$

$$\mathbf{u} = [\mathbf{u}_1 \quad \mathbf{u}_2 \quad \cdots \quad \mathbf{u}_r]^{\mathrm{T}} = [u_{1x} \quad u_{1y} \quad u_{2x} \quad u_{2y} \quad \ldots \quad u_{rx} \quad u_{ry}]^{\mathrm{T}} \in \mathbb{R}^{2r}, \tag{4.81}$$

$$\mathbf{b}_{\mathrm{ineq}} = [\mathbf{b}_1 \quad \mathbf{b}_2 \quad \cdots \quad \mathbf{b}_r]^{\mathrm{T}} \in \mathbb{R}^{\sum_{i=1}^{r}\dim(\mathbf{b}_i)}. \tag{4.82}$$

5 OPTIMIZATION METHODS FOR OPTIMAL THRUST ALLOCATION

5.1 Gradient-based optimization methods

From the optimization point of view, thrust allocation problem usually comes down to the minimization of total power consumption or some other appropriate objective function $f : X \to \mathbb{R}$, in terms of thrust $\mathbf{x}$. Hence, this optimization task can be defined as follows

$$\left.\begin{aligned} \mathbf{x}^* &= \arg\min_{\mathbf{x}\in\mathbb{R}^n}(f) \\ \text{s.t.} \quad & h_i(\mathbf{x}) = 0 \\ & g_j(\mathbf{x}) \le 0 \\ & \mathbf{l}_B \le \mathbf{x} \le \mathbf{u}_B \end{aligned}\right\} \tag{5.1}$$

where $\mathbf{x} \in X$ and $X = \{\mathbf{x} \in \mathbb{R}^n \mid h_i(\mathbf{x}) = 0,\ i = 1,2,...,p;\ g_j(\mathbf{x}) \le 0,\ j = 1,2,...,q\}$ presents a set of feasible thrust region that depends on equality and inequality constraints $\mathbf{h}(\mathbf{x}) = [h_1(\mathbf{x}) \quad h_2(\mathbf{x}) \quad ... \quad h_p(\mathbf{x})]^{\mathrm{T}}$, and $\mathbf{g}(\mathbf{x}) = [g_1(\mathbf{x}) \quad g_2(\mathbf{x}) \quad ... \quad g_q(\mathbf{x})]^{\mathrm{T}}$, respectively, $\mathbf{l}_B$ and $\mathbf{u}_B$ are lower and upper boundaries of $\mathbf{x}$, and power function f is commonly assumed to be twice-continuously differentiable, i.e. sufficiently smooth.

One can notice that optimal solution $\mathbf{x}^* \in X$ is global minimum of the function f if $f(\mathbf{x}^*) \le f(\mathbf{x}),\ \forall \mathbf{x} \in X$, but if $\exists \varepsilon > 0 \mid f(\mathbf{x}^*) \le f(\mathbf{x}),\ \forall \mathbf{x} \in X \cap X_L(\mathbf{x}^*, \varepsilon)$, then $\mathbf{x}^*$ is local minimum of the function f within the region X_L. However, for convex objective functions, global minimum is guaranteed.

The proper choice of selecting the appropriate optimization method is mostly based on the nature of the objective function f and associated constraints $\mathbf{h}(\mathbf{x})$ and $\mathbf{g}(\mathbf{x})$. Thus, one can differ the following commonly used optimization methods:

(*i*) Lagrangian multiplier method

In general, objective function f and constraints $\mathbf{h}(\mathbf{x})$ and $\mathbf{g}(\mathbf{x})$ could be either linear or nonlinear.

(*ii*) Linear programing (LP)

Both objective function f and associated constraints $\mathbf{h}(\mathbf{x})$ and $\mathbf{g}(\mathbf{x})$ are linear or linearized.

(*iii*) Quadratic programing (QP)

Objective function is quadratic, while constraints are linear or linearized.

(*iv*) Nonlinear programming (NLP)

Objective function f and constraints $\mathbf{h}(\mathbf{x})$ and $\mathbf{g}(\mathbf{x})$ are generally nonlinear. In NLP, one can differ gradient based (e.g. SQP) and non-gradient based optimization techniques (e.g. pattern search). Both of these approaches are used in this analysis.

5.1.1 Lagrange multiplier method

In general, for optimization problem (5.1), Lagrangian $L:\mathbb{R}^{n\times p\times q}\to\mathbb{R}$ can be defined as

$$L(\mathbf{x},\boldsymbol{\lambda},\boldsymbol{\mu})=f(\mathbf{x})+\sum_{i=1}^{p}\lambda_i h_i(\mathbf{x})+\sum_{j=1}^{q}\mu_j g_j(\mathbf{x}), \tag{5.2}$$

or in matric form as

$$L(\mathbf{x},\boldsymbol{\lambda},\boldsymbol{\mu})=f(\mathbf{x})+\boldsymbol{\lambda}^{\mathrm{T}}\mathbf{h}+\boldsymbol{\mu}^{\mathrm{T}}\mathbf{g}, \tag{5.3}$$

where λ_i is so-called Lagrange multiplier associated with *i*-th equality constraint $h_i(\mathbf{x})=0,\ \ i=1,2,\ldots,p,\ \ \mu_j$ is Lagrange multiplier associated with *j*-th inequality constraint $g_j(\mathbf{x})\le 0,\ j=1,2,\ldots,q,\ \boldsymbol{\lambda}=[\lambda_1\ \ \lambda_2\ \ldots\ \lambda_p]^{\mathrm{T}}$, and $\boldsymbol{\mu}=[\mu_1\ \ \mu_2\ \ldots\ \mu_q]^{\mathrm{T}}$.

In order to treat the optimization problem in more profound fashion, it is recommendable to substitute inequality constraints $g_j(\mathbf{x})\le 0$ with associated equality constraints that can be obtained by means of so-called slack variables $s_j\ge 0$ that should be introduced in a form such that

$$g_j(\mathbf{x})+s_j^2=0, \tag{5.4}$$

where $\mathbf{s}=[s_1\ \ s_2\ \ldots\ s_q]^{\mathrm{T}}$ is a vector of slack variables.

In that case, Lagrangian $L(\mathbf{x},\boldsymbol{\lambda},\boldsymbol{\mu})$ from (5.2) and (5.3) can be redefined as

$$L(\mathbf{x},\boldsymbol{\lambda},\boldsymbol{\mu},\mathbf{s})=f(\mathbf{x})+\sum_{i=1}^{p}\lambda_i h_i(\mathbf{x})+\sum_{j=1}^{q}\mu_j[g_j(\mathbf{x})+s_j^2], \tag{5.5}$$

i.e. as

$$L(\mathbf{x},\boldsymbol{\lambda},\boldsymbol{\mu},\mathbf{s})=f(\mathbf{x})+\boldsymbol{\lambda}^{\mathrm{T}}\mathbf{h}(\mathbf{x})+\boldsymbol{\mu}^{\mathrm{T}}(\mathbf{g}(\mathbf{x})+\mathbf{s}^2). \tag{5.6}$$

With this transformation, constrained optimization problem (5.1) with equality constraints, inequality constraints, but without bounds, can be rewritten as dual unconstrained optimization problem by means of the Lagrangian $L(\mathbf{x},\boldsymbol{\lambda},\boldsymbol{\mu},\mathbf{s})$ as

$$\mathbf{x}^*=\arg\min_{\mathbf{x}\in\mathbb{R}^n} L(\mathbf{x},\boldsymbol{\lambda},\boldsymbol{\mu},\mathbf{s}), \tag{5.7}$$

$$\mathbf{x}^* = \arg\min_{\mathbf{x}\in\mathbb{R}^n} f(\mathbf{x}) + \sum_{i=1}^{p} \lambda_i h_i(\mathbf{x}) + \sum_{j=1}^{q} \mu_j [g_j(\mathbf{x}) + s_j^2], \tag{5.8}$$

or in matrix form as

$$\mathbf{x}^* = \arg\min_{\mathbf{x}\in\mathbb{R}^n} f(\mathbf{x}) + \boldsymbol{\lambda}^{\mathrm{T}}\mathbf{h}(\mathbf{x}) + \boldsymbol{\mu}^{\mathrm{T}}(\mathbf{g}(\mathbf{x}) + \mathbf{s}^2). \tag{5.9}$$

In other words, if strong duality holds, which is mostly true for convex functions, and dual optimal solution $(\mathbf{x}, \boldsymbol{\lambda}^*, \boldsymbol{\mu}^*, \mathbf{s}^*)$ exists, then any primal optimum $\mathbf{x}^*$ is also a minimum of $L(\mathbf{x}, \boldsymbol{\lambda}^*, \boldsymbol{\mu}^*, \mathbf{s}^*)$ (Boyd and Vandenberghe, 2004).

The so-called Karush-Kuhn-Tucker (KKT) conditions have to be satisfied in order to find stationary points $(\mathbf{x}, \boldsymbol{\lambda}^*, \boldsymbol{\mu}^*, \mathbf{s}^*)$, i.e. $\mathbf{x}^*$, of the Lagrangian $L(\mathbf{x}, \boldsymbol{\lambda}^*, \boldsymbol{\mu}^*, \mathbf{s}^*)$. For objective convex function like $f(\mathbf{x})$ in (5.8) or (5.9), one can notice that if vector $\tilde{\mathbf{x}}$, multipliers $\tilde{\lambda}_i$ and $\tilde{\mu}_j$, and slack variables $\tilde{s}_j$ satisfy the following first-order KKT conditions (Boyd and Vandenberghe, 2004):

$$\left.\begin{aligned} h_i(\tilde{\mathbf{x}}) &= 0, \quad i = 1, 2, \ldots, p \\ g_j(\tilde{\mathbf{x}}) &\le 0, \quad j = 1, 2, \ldots, q \\ \tilde{\mu}_j &\ge 0, \quad j = 1, 2, \ldots, q \\ \tilde{\mu}_j g_j(\tilde{\mathbf{x}}) &= 0, \quad j = 1, 2, \ldots, q \\ \nabla f(\tilde{\mathbf{x}}) + \sum_{i=1}^{p} \tilde{\lambda}_i \nabla h_i(\tilde{\mathbf{x}}) + \sum_{j=1}^{q} \tilde{\mu}_j \nabla [g_j(\tilde{\mathbf{x}}) + \tilde{s}_j^2] &= 0, \end{aligned}\right\} \tag{5.10}$$

then $\tilde{\mathbf{x}}$ and $(\mathbf{x}, \tilde{\boldsymbol{\lambda}}, \tilde{\boldsymbol{\mu}}, \tilde{\mathbf{s}})$ are primal and dual optimal values, without duality gap, which guarantees the strong duality. Hence, $\mathbf{x}^* = \tilde{\mathbf{x}}$ is the optimal solution of (5.8), i.e. (5.9).

As can be seen from (5.10), the necessary conditions for finding the optimal solution $\mathbf{x}^*$ can be written in terms of Lagrangian gradient, i.e. Jacobian, as

$$\nabla L(\mathbf{x}, \boldsymbol{\lambda}, \boldsymbol{\mu}, \mathbf{s}) = 0, \tag{5.11}$$

which further yields

$$\nabla_{\mathbf{x}} L = 0 \quad \Rightarrow \quad \frac{\partial L}{\partial \mathbf{x}} = \frac{\partial f(\mathbf{x})}{\partial \mathbf{x}} + \boldsymbol{\lambda}^{\mathrm{T}} \frac{\partial \mathbf{h}(\mathbf{x})}{\partial \mathbf{x}} + \boldsymbol{\mu}^{\mathrm{T}} \frac{\partial \mathbf{g}(\mathbf{x})}{\partial \mathbf{x}} = \mathbf{0}, \tag{5.12}$$

$$\nabla_{\boldsymbol{\lambda}} L = 0 \quad \Rightarrow \quad \frac{\partial L}{\partial \boldsymbol{\lambda}} = \mathbf{h}(\mathbf{x}) = \mathbf{0}, \tag{5.13}$$

$$\nabla_{\boldsymbol{\mu}} L = 0 \quad \Rightarrow \quad \frac{\partial L}{\partial \boldsymbol{\mu}} = \mathbf{g}(\mathbf{x}) + \mathbf{s}^2 = \mathbf{0}, \tag{5.14}$$

$$\nabla_{\mathbf{s}} L = 0 \quad \Rightarrow \quad \frac{\partial L}{\partial \mathbf{s}} = 2\boldsymbol{\mu}^{\mathrm{T}}\mathbf{s} = 0. \tag{5.15}$$

Besides the necessary conditions, sufficient conditions also have to be met. However, if KKT conditions are fulfilled at $\mathbf{x}^*$, than the Hessian matrix of the Lagrangian L

$$\nabla^2 L = \nabla^2 f(\mathbf{x}^*) + \boldsymbol{\lambda}^{\mathrm{T}} \nabla^2 \mathbf{h}(\mathbf{x}^*) + \boldsymbol{\mu}^{\mathrm{T}} \nabla^2 \mathbf{g}(\mathbf{x}^*) \tag{5.16}$$

is positive definite within the feasible trust region X.

5.1.2 Quadratic programming

In general, the quadratic problem associated with the minimization of the objective function can be defined as

$$\left.\begin{aligned} &\min_{\mathbf{x}\in\mathbb{R}^n} \left(\tfrac{1}{2}\mathbf{x}^{\mathrm{T}}\mathbf{W}\mathbf{x} + \mathbf{x}^{\mathrm{T}}\mathbf{w}\right) \\ &\text{s.t.} \quad \mathbf{A}_{\mathrm{eq}}\mathbf{x} = \mathbf{b}_{\mathrm{eq}} \\ &\qquad \mathbf{A}_{\mathrm{ineq}}\mathbf{x} \le \mathbf{b}_{\mathrm{ineq}} \\ &\qquad \mathbf{l}_B \le \mathbf{x} \le \mathbf{u}_B \end{aligned}\right\} \tag{5.17}$$

where $\mathbf{W} \in \mathbb{R}^{n\times n}$ and $\mathbf{w} \in \mathbb{R}^n$ are weighting coefficients, matrices $\mathbf{A}_{\mathrm{eq}}$ and $\mathbf{b}_{\mathrm{eq}}$ define linear equality constraints, matrices $\mathbf{A}_{\mathrm{ineq}}$ and $\mathbf{b}_{\mathrm{ineq}}$ define linear inequality constraints, and bounds are commonly transformed into additional linear inequalities and merged with other linear inequality constraints in order to get the compact component-wise matrix form of all inequality constraints as follows

$$\tilde{\mathbf{A}}_{\mathrm{ineq}}\mathbf{x} = \begin{bmatrix} \mathbf{A}_{ineq} \\ -\mathbf{I} \\ \mathbf{I} \end{bmatrix} \mathbf{x} \le \begin{bmatrix} \mathbf{b}_{ineq} \\ -\mathbf{l}_B \\ \mathbf{u}_B \end{bmatrix} = \tilde{\mathbf{b}}_{\mathrm{ineq}}, \tag{5.18}$$

where $\mathbf{I} \in \mathbb{R}^{n\times n}$ is the unit matrix. The main property of QP solver is that it always finds a solution in a finite amount of time or shows that there is no any feasible solution. However, computational time required to find a solution is significantly dependent on objective function complexity and the number of inequality constraints (Nocedal and Wright, 2006).

Thus, quadratic problem (5.17) can be rewritten as

$$\left.\begin{aligned} &\min_{\mathbf{x}\in\mathbb{R}^n} \left(\tfrac{1}{2}\mathbf{x}^{\mathrm{T}}\mathbf{W}\mathbf{x} + \mathbf{x}^{\mathrm{T}}\mathbf{w}\right) \\ &\text{s.t.} \quad \mathbf{A}_{\mathrm{eq}}\mathbf{x} = \mathbf{b}_{\mathrm{eq}} \\ &\qquad \tilde{\mathbf{A}}_{\mathrm{ineq}}\mathbf{x} \le \tilde{\mathbf{b}}_{\mathrm{ineq}}. \end{aligned}\right\} \tag{5.19}$$

Considering optimization problem (5.19) consists both of equality and inequality constraints, it is assumed that (5.19) is a medium scaled problem and thus, for the

purpose of this work, so-called primal active-set strategy is used for solving associated QP problems (Nocedal and Wright, 2006). For simplicity reasons, when implementing QP algorithms, it is more convenient to redefine (5.19) in the following form

$$\left.\begin{aligned} &\min_{\mathbf{x}\in\mathbb{R}^n}\left(\tfrac{1}{2}\mathbf{x}^{\mathrm{T}}\mathbf{W}\mathbf{x}+\mathbf{x}^{\mathrm{T}}\mathbf{w}\right) \\ &\quad \text{s.t.} \quad \mathbf{a}_i^{\mathrm{T}}\mathbf{x}=b_i, \quad i\in E \\ &\qquad\quad \mathbf{a}_i^{\mathrm{T}}\mathbf{x}\geq b_i, \quad i\in I \end{aligned}\right\} \tag{5.20}$$

where E and I are finite sets of integers, i.e. indices of particular equality or inequality constraint, and $\mathbf{a}_i\in\mathbb{R}^n$.

The Lagrangian for the optimization task (5.20) is defined as

$$L(\mathbf{x},\boldsymbol{\lambda})=\tfrac{1}{2}\mathbf{x}^{\mathrm{T}}\mathbf{W}\mathbf{x}+\mathbf{x}^{\mathrm{T}}\mathbf{w}-\sum_{i\in E\cup I}\lambda_i(\mathbf{a}_i^{\mathrm{T}}\mathbf{x}-b_i). \tag{5.21}$$

The active set $A(\mathbf{x}^*)$ consists only of indices $i\in E\cup I$ for which applies

$$\mathbf{a}_i^{\mathrm{T}}\mathbf{x}^*=b_i, \tag{5.22}$$

i.e. one can write that $A(\mathbf{x}^*)=\{i\in E\cup I \mid \mathbf{a}_i^{\mathrm{T}}\mathbf{x}^*=b_i\}$.

It has been proven (Nocedal and Wright, 2006) that optimal solution $\mathbf{x}^*$ of the optimization task (5.20) satisfies the KKT conditions of the Lagrangian (5.21). These conditions can be expressed as

$$\left.\begin{aligned} &\mathbf{W}\mathbf{x}^*+\mathbf{w}-\sum_{i\in A(\mathbf{x}^*)}\lambda_i^*\mathbf{a}_i=\mathbf{0} \\ &\qquad \mathbf{a}_i^{\mathrm{T}}\mathbf{x}^*=b_i, \quad \forall\, i\in A(\mathbf{x}^*) \\ &\qquad \mathbf{a}_i^{\mathrm{T}}\mathbf{x}^*\geq b_i, \quad \forall\, i\in I\setminus A(\mathbf{x}^*) \\ &\qquad\quad \lambda_i^*\geq 0, \quad \forall\, i\in I\cap A(\mathbf{x}^*). \end{aligned}\right\} \tag{5.23}$$

For a convex QP problem, i.e. when $\mathbf{W}$ is positive semi-definite matrix, conditions (5.23) are sufficient for $\mathbf{x}^*$ to be global optimum.

There are commonly three active-set approaches that can be used for solving optimization problems, i.e. so-called primal, dual and primal-dual approach. The first one, which is used in this work, has very convenient property by which all generated quantities during iterative process are feasible, while objective function continuously decreases. Primal active-set approach is an iterative process in which shifting from current step to the next one is based on the solution of appropriate quadratic sub-problem that takes into account all equality and only some of inequality constraints

defined in (5.20). These selected constraints form a so-called working set $W_k \subset A(\mathbf{x}_k^*)$, where k denotes the iteration step.

At the first step, a feasible initial point $\mathbf{x}_0$ is commonly obtained by means of the following linear program (Nocedal and Wright, 2006)

$$\left.\begin{aligned} &\min_{\mathbf{x},\mathbf{z}} (\mathbf{e}^{\mathrm{T}}\mathbf{z}) \\ &\quad \text{s.t.} \quad \mathbf{a}_i^{\mathrm{T}}\mathbf{x} + \gamma_i z_i = b_i, \quad i \in E \\ &\qquad\quad \mathbf{a}_i^{\mathrm{T}}\mathbf{x} + \gamma_i z_i \geq b_i, \quad i \in I \\ &\qquad\qquad z_i \geq 0 \end{aligned}\right\} \tag{5.24}$$

where $\mathbf{e} = [1,1,\ldots,1]^{\mathrm{T}} \in \mathbb{R}^{\mathrm{card}(E)+\mathrm{card}(I)}$, and $\tilde{\mathbf{x}}$ is an estimate of initial point for

$$\gamma_i = \begin{cases} -\mathrm{sgn}(\mathbf{a}_i^{\mathrm{T}}\tilde{\mathbf{x}}_i - b_i), & \text{for } i \in E \\ 1, & \text{for } i \in I. \end{cases} \tag{5.25}$$

It is common practice to allow the end-user to choose the initial point $\tilde{\mathbf{x}}$. On the other hand, if initial point $\tilde{\mathbf{x}}$ is not provided by the user, than $\tilde{\mathbf{x}}$ is usually equal to $\mathbf{e}$, i.e. $\tilde{\mathbf{x}} = \mathbf{e}$. If lower and upper bounds are known, than one can use $\tilde{\mathbf{x}} = (\mathbf{l}_B + \mathbf{u}_B)/2$ as initial point. However, a certainly feasible initial point $\mathbf{x}_0$ can be determined according to (Nocedal and Wright, 2006)

$$\mathbf{x} = \tilde{\mathbf{x}}, \;\; z_i = \begin{cases} \left|\mathbf{a}_i^{\mathrm{T}}\tilde{\mathbf{x}} - b_i\right|, & \text{for } i \in E \\ \max(b_i - \mathbf{a}_i^{\mathrm{T}}\tilde{\mathbf{x}}, 0), & \text{for } i \in I. \end{cases} \tag{5.26}$$

The initial working set W_0 of active constraints at initial point $\mathbf{x}_0$ can be determined based on (5.22) as $W_0 = A_0 = \{i \mid \mathbf{a}_i^{\mathrm{T}}\mathbf{x}_0 = b_i\}$.

During the iteration process, at each step k, it is necessary to solve the following QP sub-problem

$$\left.\begin{aligned} &\min_{\mathbf{p}} \left(\tfrac{1}{2}\mathbf{p}^{\mathrm{T}}\mathbf{W}\mathbf{p} + (\mathbf{W}\mathbf{x}_k + \mathbf{w})^{\mathrm{T}}\mathbf{p}\right) \\ &\quad \text{s.t.} \;\; \mathbf{a}_i^{\mathrm{T}}\mathbf{p} = 0, \quad i \in W_k \end{aligned}\right\} \tag{5.27}$$

in order to determine the so-called improving direction $\mathbf{p} \in \mathbb{R}^n$ for which it stands

$$\mathbf{x}_{k+1} = \mathbf{x}_k + \mathbf{p}_k. \tag{5.28}$$

However, if $\|\mathbf{p}_k\| \neq 0$, which is the case during convergence phase, than $\mathbf{x}_{k+1}$ should be updated according to (5.28) only if $\mathbf{x}_k + \mathbf{p}_k$ is feasible for all constraints.

Otherwise, $\mathbf{x}_{k+1}$ should be updated according to

$$\mathbf{x}_{k+1} = \mathbf{x}_k + \alpha_k \mathbf{p}_k, \tag{5.29}$$

where α_k is so-called step length and is used in order to ensure feasibility.

Parameter α_k is usually chosen within the interval [0,1] in a fashion that all constraints are fulfilled. Moreover, α_k can be estimated directly according to (Nocedal and Wright, 2006)

$$\alpha_k = \min\left\{1, \min_{(i \notin W_k,\, \mathbf{a}_i^{\mathrm{T}}\mathbf{p}_k < 0)} \frac{b_i - \mathbf{a}_i^{\mathrm{T}}\mathbf{x}_k}{\mathbf{a}_i^{\mathrm{T}}\mathbf{p}_k}\right\}. \tag{5.30}$$

If $\alpha_k < 1$ occurs, which means that step in direction $\mathbf{p}_k$ is blocked by some constraint outside the working set W_k, an updated working set W_{k+1} should be made in a way that it includes at least one blocking constraint from the set of all blocking constraints J, where (Hansen and Völcker, 2007)

$$J = \arg\min_{(i \notin W_k,\, \mathbf{a}_i^{\mathrm{T}}\mathbf{p}_k < 0)} \frac{b_i - \mathbf{a}_i^{\mathrm{T}}\mathbf{x}_k}{\mathbf{a}_i^{\mathrm{T}}\mathbf{p}_k}. \tag{5.31}$$

The iteration process itself, with adding more and more constraints to the working set W_k, takes until the point $\mathbf{x}$ is reached in which the objective function is minimized on the entire current working set W_k. At this point $\mathbf{x}_k$, optimality conditions are fulfilled because $\mathbf{p} = \mathbf{0}$. Hence, from (5.23) it yields

$$\sum_{i \in W} \mathbf{a}_i \mu_i = \mathbf{W}\mathbf{x} + \mathbf{w}, \tag{5.32}$$

where μ_i are Lagrange multipliers for $i \in W_k \cap I$. One can conclude that $\mathbf{u}_k$ and μ_i satisfy first three KKT conditions in (5.23), but the forth one is dependent on the sign of multipliers μ_i. Therefore, if all the multipliers μ_i are non-negative, than the fourth KKT condition in (5.23) is also fulfilled and optimal solution $\mathbf{x}^* = \mathbf{x}_k$ is reached. Otherwise, it is necessary to exclude *j*-th negative multiplier from the working set W_k, where $j = \arg\min_{j \in W_k \cap I}(\mu_j)$, and solve updated sub-problem (5.27) in the next step.

Due to simplicity reasons, many details about the active-set methodology in QP is omitted in this work. On the other hand, complete preview of primal active-set algorithm used in this thesis for solving convex QP problems related to optimal thrust allocation is given in Appendix 1.1 in terms of pseudo-code. More details about active-

set methods and their implementation for the purpose of QP and SQP algorithms, as well as about other similar approaches like interior point methods, trust-region methods, etc., one can find in excellent references like (Nocedal and Wright, 2006), (Bonnans et al., 2006), (Hansen and Völcker, 2007) and (Luenberger and Ye, 2008).

5.1.3 Sequential quadratic programming

One could notice in the prior subchapter that nonlinear equality and nonlinear inequality constraints cannot be handled directly by means of the solvers like QP, at least not without appropriate previously applied linearization techniques that commonly entail additional problems related to the large number of supplementary inequalities caused by polygon approximation. Moreover, required computational time for convergence of QP algorithm in solving these enlarged optimization problems can easily became significant, particularly if very high accuracy of linearization is needed. Also, QP cannot minimize demanded power requirements like (4.41) or (4.45), but only their quadratic approximation like (4.50), i.e. (4.53).

If optimization requirements are strict, and problem should be solved for nonlinear objective function with nonlinear equality and inequality constraints, than one should use some appropriate nonlinear optimization technique. The current state-of-the-art in nonlinear optimization for gradient-based algorithms is surely the sequential quadratic programing (SQP). This stands both for general applications (Nocedal and Wright, 2006) as well as for specific thrust allocation problems (Johansen et al., 2004; Johansen and Fossen, 2013). In comparison with Lagrangian approach or pure QP algorithms, which are both appropriate solutions for optimization problems with linear equality and linear inequality constraints, SQP approach is superior when dealing with problems that have significant nonlinearities within their constraints. These constraints do not have to be linearized externally by the user, as SQP has implemented algorithms for the linearization purpose, which are more efficient.

As the name of the algorithm suggests, SQP can be described as a sequence of QP problems that should be solved as a part, i.e. a step, of appropriate quasi-Newton's method that is used within the SQP. For the purpose of this work, SQP is used as a line search SQP method with quasi-Newton approximation of the Hessian matrix, as described in (Nocedal and Wright, 2006) and (Bonnans et al., 2006). In order to be able to use active-set methods for solving QP problems, convexity of the objective function

is assumed, although this is not questionable for nonlinear terms of power consumption like (4.41) or (4.45).

In general, nonlinear optimization problem can be written as

$$\left.\begin{aligned} &\min_{\mathbf{x}\in\mathbb{R}^n} f(\mathbf{x}) \\ &\quad \text{s.t.} \quad \mathbf{c}_i(\mathbf{x}) = \mathbf{0}, \quad i \in E \\ &\qquad\quad \mathbf{c}_i(\mathbf{x}) \geq \mathbf{0}, \quad i \in I \end{aligned}\right\} \tag{5.33}$$

where $f(\mathbf{x}): \mathbb{R}^n \to \mathbb{R}$ is a convex nonlinear objective function, $\mathbf{c}_i(\mathbf{x}) = \mathbf{0}$ presents general nonlinear equality constraints, and $\mathbf{c}_i(\mathbf{x}) \geq \mathbf{0}$ presents general nonlinear inequality constraints. Linear equality and inequality constraints could also be a part of optimization task (5.33), but they are not particular issue considering even nonlinear constraints should be linearized, and treated likewise. Similar conclusion holds for bounds, considering they also should be included as linear inequality constraints, as described in the previous subchapter. Thus, without loss of generality, the focus is put only on nonlinear constraints in (5.33).

If nonlinear optimization problem (5.33) is considered with linear constraints only, then associated Lagrangian can be written as

$$\underset{\mathbf{x}\in\mathbb{R}^n}{L(\mathbf{x},\boldsymbol{\lambda})} = f(\mathbf{x}) - \boldsymbol{\lambda}^{\mathrm{T}}\mathbf{c}(\mathbf{x}), \tag{5.34}$$

where $\mathbf{c}(\mathbf{x}) = [\mathbf{c}_1(\mathbf{x}), \mathbf{c}_2(\mathbf{x}), \ldots, \mathbf{c}_m(\mathbf{x})]$ is a vector of equality constraints. According to necessary KKT conditions one can write

$$\nabla L(\mathbf{x},\boldsymbol{\lambda}) = \begin{bmatrix} \nabla_{\mathbf{x}} L(\mathbf{x},\boldsymbol{\lambda}) \\ \nabla_{\boldsymbol{\lambda}} L(\mathbf{x},\boldsymbol{\lambda}) \end{bmatrix} = \begin{bmatrix} \nabla f(\mathbf{x}) - \nabla \mathbf{c}(\mathbf{x})\boldsymbol{\lambda} \\ -\mathbf{c}(\mathbf{x}) \end{bmatrix} = \mathbf{0}, \tag{5.35}$$

where $\nabla L(\mathbf{x},\boldsymbol{\lambda})$ can be further expanded using second-order Taylor series about the point $(\mathbf{x}_k + \mathbf{p}_k,\ \boldsymbol{\lambda}_k + \mathbf{o}_k)$ as

$$\nabla L(\mathbf{x}_k + \mathbf{p}_k,\ \boldsymbol{\lambda}_k + \mathbf{o}_k) \approx \nabla L(\mathbf{x}_k,\ \boldsymbol{\lambda}_k) + \nabla^2 L(\mathbf{x}_k,\ \boldsymbol{\lambda}_k) \begin{bmatrix} \mathbf{p}_k \\ \mathbf{o}_k \end{bmatrix} = \mathbf{0}, \tag{5.36}$$

which yields a variation of a Newton method in the form

$$\nabla^2 L(\mathbf{x}_k,\ \boldsymbol{\lambda}_k) \begin{bmatrix} \mathbf{p}_k \\ \mathbf{o}_k \end{bmatrix} = -\nabla L(\mathbf{x}_k,\ \boldsymbol{\lambda}_k). \tag{5.37}$$

According to (5.35), one can further write

$$\nabla^2 L(\mathbf{x},\,\boldsymbol{\lambda}) = \begin{bmatrix} \nabla^2_{\mathbf{xx}} L(\mathbf{x},\,\boldsymbol{\lambda}) & -\nabla \mathbf{c}(\mathbf{x}) \\ -\nabla \mathbf{c}^{\mathrm{T}}(\mathbf{x}) & \mathbf{0} \end{bmatrix}, \tag{5.38}$$

where $\nabla^2_{\mathbf{xx}} L(\mathbf{x},\,\boldsymbol{\lambda})$ is the Hessian matrix of the Lagrangian $L(\mathbf{x},\boldsymbol{\lambda})$ in (5.34), and $\nabla \mathbf{c}(\mathbf{x}) = [\nabla \mathbf{c}_1(\mathbf{x}),\ \nabla \mathbf{c}_2(\mathbf{x}),\ldots,\nabla \mathbf{c}_m(\mathbf{x})]$ is the Jacobian of equality constraint vector $\mathbf{c}(\mathbf{x})$. Thus, by combining (5.37) with (5.38) and (5.35), it yields

$$\begin{bmatrix} \nabla^2_{\mathbf{xx}} L(\mathbf{x}_k,\,\boldsymbol{\lambda}_k) & -\nabla \mathbf{c}(\mathbf{x}_k) \\ -\nabla \mathbf{c}^{\mathrm{T}}(\mathbf{x}_k) & \mathbf{0} \end{bmatrix} \begin{bmatrix} \mathbf{p}_k \\ \mathbf{o}_k \end{bmatrix} = -\begin{bmatrix} \nabla f(\mathbf{x}_k) - \nabla \mathbf{c}(\mathbf{x}_k)\boldsymbol{\lambda}_k \\ -\mathbf{c}(\mathbf{x}_k) \end{bmatrix} \tag{5.39}$$

where $(\mathbf{p}_k, \mathbf{o}_k)$, as the solution of (5.39), is used for the next iteration within the Newton method as

$$\begin{bmatrix} \mathbf{x}_{k+1} \\ \boldsymbol{\lambda}_{k+1} \end{bmatrix} = \begin{bmatrix} \mathbf{x}_k \\ \boldsymbol{\lambda}_k \end{bmatrix} + \begin{bmatrix} \mathbf{p}_k \\ \mathbf{o}_k \end{bmatrix}. \tag{5.40}$$

If substitution $\mathbf{o}_k = \boldsymbol{\mu}_k - \boldsymbol{\lambda}_k$ is introduced in (5.39), it can be further expanded as

$$\begin{bmatrix} \nabla^2_{\mathbf{xx}} L(\mathbf{x}_k,\,\boldsymbol{\lambda}_k) & -\nabla \mathbf{c}(\mathbf{x}_k) \\ -\nabla \mathbf{c}^{\mathrm{T}}(\mathbf{x}_k) & \mathbf{0} \end{bmatrix} \begin{bmatrix} \mathbf{p}_k \\ \boldsymbol{\mu}_k \end{bmatrix} + \begin{bmatrix} \nabla \mathbf{c}(\mathbf{x}_k)\boldsymbol{\lambda}_k \\ \mathbf{0} \end{bmatrix} = \begin{bmatrix} -\nabla f(\mathbf{x}_k) \\ \mathbf{c}(\mathbf{x}_k) \end{bmatrix} + \begin{bmatrix} \nabla \mathbf{c}(\mathbf{x}_k)\boldsymbol{\lambda}_k \\ \mathbf{0} \end{bmatrix}$$

which yields

$$\begin{bmatrix} \nabla^2_{\mathbf{xx}} L(\mathbf{x}_k,\,\boldsymbol{\lambda}_k) & -\nabla \mathbf{c}(\mathbf{x}_k) \\ -\nabla \mathbf{c}^{\mathrm{T}}(\mathbf{x}_k) & \mathbf{0} \end{bmatrix} \begin{bmatrix} \mathbf{p}_k \\ \boldsymbol{\mu}_k \end{bmatrix} = \begin{bmatrix} -\nabla f(\mathbf{x}_k) \\ \mathbf{c}(\mathbf{x}_k) \end{bmatrix}. \tag{5.41}$$

Now, one should recall that for some general QP problem defined as

$$\left.\begin{array}{l} \min\limits_{\mathbf{x}\in\mathbb{R}^n} \dfrac{1}{2}\mathbf{x}^{\mathrm{T}}\mathbf{G}\mathbf{x} + \mathbf{g}^{\mathrm{T}}\mathbf{x} \\ \text{s.t.} \quad \mathbf{A}\mathbf{x} = \mathbf{b} \end{array}\right\}, \tag{5.42}$$

the Lagrangian is equal to

$$L(\mathbf{x},\boldsymbol{\lambda}) = \frac{1}{2}\mathbf{x}^{\mathrm{T}}\mathbf{G}\mathbf{x} + \mathbf{g}^{\mathrm{T}}\mathbf{x} + \boldsymbol{\lambda}^{\mathrm{T}}(\mathbf{b} - \mathbf{A}\mathbf{x}), \tag{5.43}$$

for which, based on necessary KKT conditions, it yields

$$\nabla L(\mathbf{x},\boldsymbol{\lambda}) = \begin{bmatrix} \nabla_{\mathbf{x}} L(\mathbf{x},\boldsymbol{\lambda}) \\ \nabla_{\boldsymbol{\lambda}} L(\mathbf{x},\boldsymbol{\lambda}) \end{bmatrix} = \begin{bmatrix} \mathbf{G}\mathbf{x} + \mathbf{g} - \mathbf{A}^{\mathrm{T}}\boldsymbol{\lambda} \\ \mathbf{b} - \mathbf{A}\mathbf{x} \end{bmatrix} = \begin{bmatrix} \mathbf{0} \\ \mathbf{0} \end{bmatrix}. \tag{5.44}$$

The system of equations in (5.44) can be rewritten in the matrix form as

$$\begin{bmatrix} \mathbf{G} & -\mathbf{A}^{\mathrm{T}} \\ -\mathbf{A} & \mathbf{0} \end{bmatrix} \begin{bmatrix} \mathbf{x} \\ \boldsymbol{\lambda} \end{bmatrix} = \begin{bmatrix} -\mathbf{g} \\ -\mathbf{b} \end{bmatrix}, \tag{5.45}$$

which presents an equivalent to (5.42). In this way, if (5.45) is equivalent to (5.42), than the following QP problem

$$\left.\begin{aligned} &\min_{\mathbf{p}\in\mathbb{R}^n} \frac{1}{2}\mathbf{p}_k^{\mathrm{T}}\nabla_{\mathbf{xx}}^2 L(\mathbf{x}_k, \boldsymbol{\lambda}_k)\mathbf{p}_k + \nabla f^{\mathrm{T}}(\mathbf{x}_k)\mathbf{p}_k \\ &\quad \text{s.t.} \quad \nabla \mathbf{c}^{\mathrm{T}}(\mathbf{x}_k)\mathbf{p}_k + \mathbf{c}(\mathbf{x}_k) = \mathbf{0} \end{aligned}\right\}, \tag{5.46}$$

is equivalent to (5.41). Therefore, instead of solving (5.41) iteratively, the problem should be solved as a QP problem (5.46) in each iteration of (5.40).

Equality constraint in (5.46) is just a linearized form of the equality constraint in (5.33). The same result may be obtained if Taylor expansion is applied on equality constraint in (5.33) about the current point $\mathbf{x}_k + \mathbf{p}_k$. In similar way, nonlinear inequality constraints could be also added into optimization task, like in (5.33). In that case, both equality and inequality constraints should be linearized, so the associated QP problem (5.46) will be redefined as

$$\left.\begin{aligned} &\min_{\mathbf{p}\in\mathbb{R}^n} \left(\tfrac{1}{2}\mathbf{p}_k^{\mathrm{T}}\nabla_{\mathbf{xx}}^2 L(\mathbf{x}_k, \boldsymbol{\lambda}_k)\mathbf{p}_k + \nabla f^{\mathrm{T}}(\mathbf{x}_k)\mathbf{p}_k\right) \\ &\quad \text{s.t.} \quad \nabla \mathbf{c}^{\mathrm{T}}(\mathbf{x}_k)\mathbf{p}_k + \mathbf{c}(\mathbf{x}_k) = \mathbf{0}, \quad k \in E \\ &\qquad\quad \nabla \mathbf{c}^{\mathrm{T}}(\mathbf{x}_k)\mathbf{p}_k + \mathbf{c}(\mathbf{x}_k) \geq \mathbf{0}, \quad k \in I. \end{aligned}\right\} \tag{5.47}$$

The calculation of the Hessian matrix $\nabla_{\mathbf{xx}}^2 L(\mathbf{x}_k, \boldsymbol{\lambda}_k)$ in (5.47) is usually very complicated and time consuming. Thus, instead of direct Newton method, some quasi-Newton method is usually used in order to approximate the Hessian $\nabla_{\mathbf{xx}}^2 L(\mathbf{x}_k, \boldsymbol{\lambda}_k)$. There are a number of different ways how one can perform this approximation, but it appears that BFGS algorithm, named after researchers Broyden, Fletcher, Goldfarb, and Shanno, is the most convenient and most successful (Nocedal and Wright, 2006). By the BFGS approach, the Hessian $\nabla_{\mathbf{xx}}^2 L(\mathbf{x}_k, \boldsymbol{\lambda}_k)$ is approximated with the symmetric positive definite matrix $\mathbf{B}_k \in \mathbb{R}^{n\times n} \approx \nabla_{\mathbf{xx}}^2 L(\mathbf{x}_k, \boldsymbol{\lambda}_k)$ that is updated during every iteration according to

$$\mathbf{B}_{k+1} = \mathbf{B}_k - \frac{\mathbf{B}_k \mathbf{s}_k \mathbf{s}_k^{\mathrm{T}} \mathbf{B}_k}{\mathbf{s}_k^{\mathrm{T}} \mathbf{B}_k \mathbf{s}_k} + \frac{\mathbf{y}_k \mathbf{y}_k^{\mathrm{T}}}{\mathbf{y}_k^{\mathrm{T}} \mathbf{s}_k}, \tag{5.48}$$

where step vectors $\mathbf{s}_k$ and $\mathbf{y}_k$ are equal to

$$\mathbf{s}_k = \mathbf{x}_{k+1} - \mathbf{x}_k, \tag{5.49}$$

$$\left.\begin{aligned} \mathbf{y}_k &= \nabla_{\mathbf{x}} L(\mathbf{x}_{k+1}, \boldsymbol{\lambda}_{k+1}) - \nabla_{\mathbf{x}} L(\mathbf{x}_k, \boldsymbol{\lambda}_{k+1}) = \\ &= \{\nabla f(\mathbf{x}_{k+1}) - \nabla \mathbf{c}(\mathbf{x}_{k+1})\boldsymbol{\lambda}_{k+1}\} - \{\nabla f(\mathbf{x}_k) - \nabla \mathbf{c}(\mathbf{x}_k)\boldsymbol{\lambda}_{k+1}\} \end{aligned}\right\} \tag{5.50}$$

with Lagrange multiplier $\boldsymbol{\lambda} = \boldsymbol{\lambda}_{k+1}$ considered to be constant at the current step. The issue that can arise from BFGS approximation is that matrix $\mathbf{B}_k$ is not guaranteed to be positive definite when nonlinear constraints are part of the optimization task. In order to overcome this problem, step vector $\mathbf{y}_k$ is usually modified as

$$\tilde{\mathbf{y}}_k = \theta_k \mathbf{y}_k + (1-\theta_k)\mathbf{B}_k \mathbf{s}_k, \tag{5.51}$$

where the value of $\theta_k \in [0,1]$ should be chosen as closest as possible to 1 so that condition $\tilde{\mathbf{y}}_k^{\mathrm{T}} \mathbf{s}_k \geq \sigma \mathbf{s}_k^{\mathrm{T}} \mathbf{B}_k \mathbf{s}_k$ is fulfilled for some $\sigma \in \langle 0,1 \rangle$.

One can found the following recommendation in (Nocedal and Wright, 2006) for evaluation of θ_k

$$\theta_k = \begin{cases} 1, & \text{if } \mathbf{s}_k^{\mathrm{T}} \mathbf{y}_k \geq 0.2 \mathbf{s}_k^{\mathrm{T}} \mathbf{B}_k \mathbf{s}_k \\ (0.8 \mathbf{s}_k^{\mathrm{T}} \mathbf{B}_k \mathbf{s}_k) / (\mathbf{s}_k^{\mathrm{T}} \mathbf{B}_k \mathbf{s}_k - \mathbf{s}_k^{\mathrm{T}} \mathbf{y}_k), & \text{if } \mathbf{s}_k^{\mathrm{T}} \mathbf{y}_k < 0.2 \mathbf{s}_k^{\mathrm{T}} \mathbf{B}_k \mathbf{s}_k, \end{cases} \tag{5.52}$$

and modified BFGS update of the matrix $\mathbf{B}_k$ should be redefined as

$$\mathbf{B}_{k+1} = \mathbf{B}_k - \frac{\mathbf{B}_k \mathbf{s}_k \mathbf{s}_k^{\mathrm{T}} \mathbf{B}_k}{\mathbf{s}_k^{\mathrm{T}} \mathbf{B}_k \mathbf{s}_k} + \frac{\tilde{\mathbf{y}}_k \tilde{\mathbf{y}}_k^{\mathrm{T}}}{\mathbf{s}_k^{\mathrm{T}} \tilde{\mathbf{y}}_k}. \tag{5.53}$$

Merit functions in line search SQP approach are usually used in order to determine the proper step size. Thus, for this purpose, inequality constraints in (5.33) are commonly transformed into equality constraints by means of slack variables $\mathbf{s} \geq 0$ as follows

$$\tilde{\mathbf{c}}(\mathbf{x}, \mathbf{s}) = \mathbf{c}(\mathbf{x}) - \mathbf{s} = \mathbf{0}. \tag{5.54}$$

For the objective function in (5.33), the merit function is commonly defined as

$$\phi(\mathbf{x}, \boldsymbol{\mu}) = f(\mathbf{x}) + \mu \left\| \mathbf{c}(\mathbf{x}) \right\|_1, \tag{5.55}$$

where μ is the penalty parameter, and ℓ_1- norm of constraints $\mathbf{c}(\mathbf{x})$ is defined as

$$\left\| \mathbf{c}(\mathbf{x}) \right\|_1 = \sum_{i \in E \cap I} |c_i|. \tag{5.56}$$

In this approach, a step $\mathbf{s}_k = \alpha_k \mathbf{p}_k$ will be accepted only if the following criteria for the merit function decrease is fulfilled, i.e. only if

$$\phi(\mathbf{x}_k + \alpha_k \mathbf{p}_k, \mu_k) \leq \phi(\mathbf{x}_k, \mu_k) + \eta \alpha_k D(\phi(\mathbf{x}_k, \mu_k), \mathbf{p}_k) \tag{5.57}$$

where $D(\phi(\mathbf{x}_k, \mu_k), \mathbf{p}_k)$ is directional derivative of the merit function, and $0 < \eta < 1$.

There are a number of strategies on how to choose μ_k, but the most commonly used criteria is defined as follows (Nocedal and Wright, 2006)

$$\mu_k \geq \frac{\nabla f^{\mathrm{T}}(\mathbf{x}_k)\mathbf{p}_k + \frac{1}{2}\mathbf{p}_k^{\mathrm{T}}\mathbf{B}_k\mathbf{p}_k}{(1-\rho)\left\|\mathbf{c}(\mathbf{x})\right\|_1}, \tag{5.58}$$

where $0 < \rho < 1$. In general, it is important to emphasize that both α_k and μ_k should be chosen in order to produce a sufficient decrease in merit function $\phi(\mathbf{x}, \boldsymbol{\mu})$.

Pseudo-code of the line search SQP algorithm, which is also used in this thesis for solving convex nonlinear problems related to optimal thrust allocation, is given in Appendix 1.2.

5.2 Derivative free optimization methods based on direct search algorithms

In comparison to the gradient-based optimization methods like the previously analysed Lagrangian method, QP or SQP, derivative free optimization methods usually do not need any particular information about the gradient or Hessian matrix of the objective function. Moreover, derivative free methods can be applied even for objective functions that are not continues nor differentiable, which makes them particularly convenient in cases when the objective function is not explicitly defined, when evaluation of the objective function and/or its derivatives is too much time consuming and thus not acceptable, when objective function is noisy and derivatives or finite difference approximations are not reliable nor acceptable for further analysis, etc. The field of derivative free optimization is usually extended or at least coupled with the so-called black-box optimization methods, which take into account heuristic and evolutionary inspired approaches and algorithms like genetic algorithms (GA), Nelder-Mead (NM) algorithm, particle swarm optimization (PSO), simulated annealing (SA), etc. However, for the purpose of this work, the focus is placed only on the family of the so-called direct search, or pattern search algorithms (Audet and Hare, 2017), with particular emphasis on the generating set search (GSS) algorithm and the mesh adaptive direct search (MADS) algorithm.

The main reason for this choice is that direct search algorithms are much better supported and have very detailed literature background on rigorous convergence analysis (Audet and Hare, 2017; Conn et al., 1997, 1991; Torczon, 1997). However, it should be pointed out that the gradient-based algorithms could and probably should be a better choice for optimization problems where the gradient and/or Hessian of the objective function is known or at least it can be obtained in sufficient amount of time. This will probably be true for most unconstrained optimization problems, but on the

other hand, when a large number of nonlinear constraints is added into the optimization task, and even more when the objective function is constantly changing due to some external disturbances, then the calculation of associated Lagrangian and its gradient, Hessian or Hessian approximation could be very demanding within gradient-based methods. Thus, in these cases direct search algorithms could be a good alternative.

In general, one can differ three main direct search algorithms as follows:

- generalized pattern search (GPS) algorithm,
- generating set search (GSS) algorithm,
- mesh adaptive direct search (MADS) algorithm.

All these algorithms are based on a common idea by which a sequence of points is determined with the property that in each successive point the value of objective function decreases. As already mentioned, this sequence of points, which defines directions from one point to another, is not calculated by means of function gradient, but is rather based on a set of points around the current point, in which the objective function is evaluated. These surrounding points are determined by polling and thus they create a so-called poll set that presents a mesh, i.e. all possible vector directions by which one can shift from the current point to any other point from the poll set. If some point within the poll set is found that sufficiently decreases the objective function at the current step, than that point becomes a new current point for the next iteration. Otherwise, the mesh should be redefined so the algorithm could try to find a new direction on a smaller scale.

Besides the all other significant properties, generally speaking, the main difference between GPS, GSS and MADS is the number of directions from the current point to any other point from the poll set, as well as direction geometrical characteristics. Other important properties and differences are mostly related to handling of linear and nonlinear constraints.

5.2.1 Coordinate search algorithm

From a historical point of view, the coordinate or compass search (CS) algorithm was one of the first pattern search algorithms. In many ways, CS can be considered as ancestor of nowadays pattern search algorithms.

If one consider the unconstrained optimization problem

$$\mathbf{x}^* = \arg\min_{\mathbf{x}\in\mathbb{R}^n} f(\mathbf{x}), \tag{5.59}$$

where $f:\mathbb{R}^n \to \mathbb{R}$, than for some given initial point $\mathbf{x}_0 \in \mathbb{R}^n$ and initial step length $\Delta_0 > 0$ which defines initial mesh geometry, CS creates a poll set

$$P_k = \{\mathbf{x}_k \pm \Delta_k \mathbf{e}_i \mid i = 1, 2, \ldots, n\} \tag{5.60}$$

of points for each variable, where k denotes an iteration step $(k = 0, 1, 2, \ldots)$ and $\mathbf{e}_i$ presents *i*-th unit coordinate vector in $\mathbb{R}^n$, i.e. the axis direction (Audet and Hare, 2017). For some arbitrary function of two variables, current point denoted with full circle, and surrounding points from the poll set in axes directions, denoted with open circles, are shown in Figure 29.

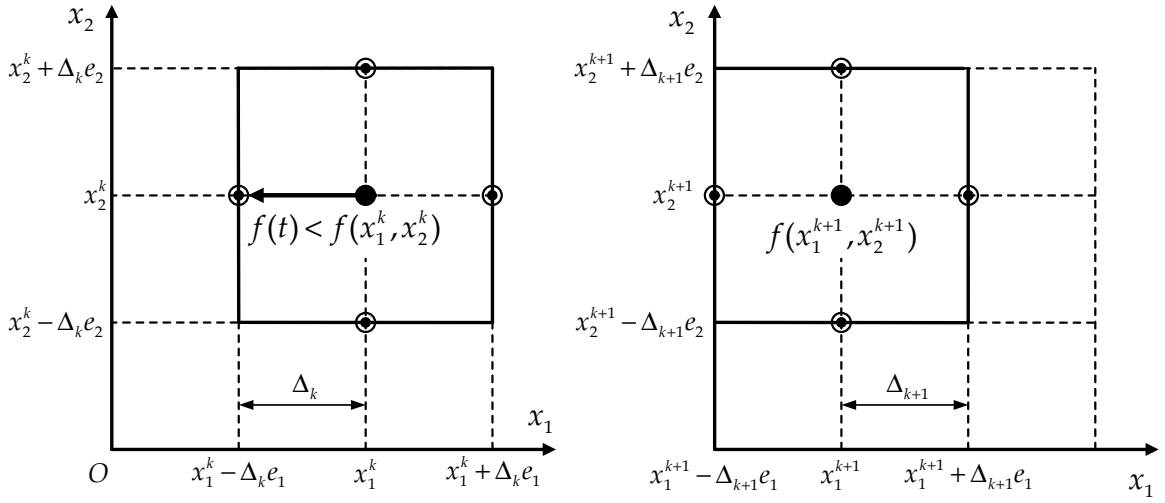

Figure 29. Visualization of successful iteration within a CS algorithm
Source: Adjusted according to (Audet and Hare, 2017)

One can notice that the points from the poll set are created based on the unit vectors $\mathbf{e}_i$, as defined in (5.60), where the set of these unit vectors presents a pattern. After the current point and points from the poll set are determined, CS performs evaluation of objective function in points $\mathbf{t} \in P_k$ from the poll set, point by point. In Figure 29, objective function evaluations are marked in parentheses. If one assumes, without the loss of generality, that in some trial poll point $(x_1^k - \Delta_k e_1, x_2^k)$ objective function decreases, i.e. if $f(x_1^k - \Delta_k e_1, x_2^k) < f(x_1^k, x_2^k)$, than this poll point $(x_1^k - \Delta_k e_1, x_2^k)$ becomes a new current point (x_1^{k+1}, x_2^{k+1}) in the next iteration, as indicated in Figure 29 (right).

On the other hand, if one assumes that in *k*-th step there is no improvement in objective function, i.e. if $f(\mathbf{t}) \geq f(x_1^k, x_2^k)$ holds for $\forall \mathbf{t} \in P_k$, then the step length Δ_k should be decreased, usually twice, in order to refine the mesh so that CS can continue with searching, as indicated in Figure 30.

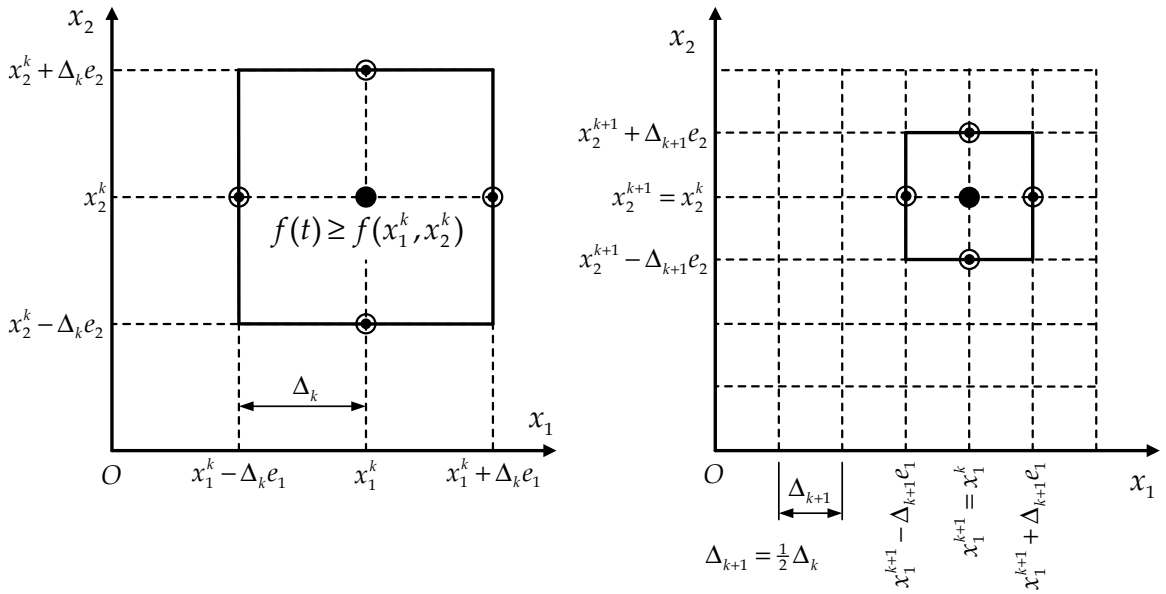

Figure 30. Visualization of unsuccessful iteration within a CS algorithm with mesh refinement
Source: Adjusted according to (Audet and Hare, 2017)

One can notice that this polling can skip some points from function evaluation, and thus these points will not be considered even if they produce better improvement. This strategy is called partial poll, while one can also take into account all points from the poll set, which will present so-called full poll. These variations could be found in all pattern search algorithms. Simplified pseudocode of CS algorithm is presented in Appendix 1.3. Although CS algorithm itself has several drawbacks, it is a convenient basis for more sophisticated algorithms like GPS or MADS. However, there are several very important differences between CS and other advanced pattern search algorithms.

5.2.2 Generalized pattern search algorithm

As could be seen in the previous subchapter, CS allows search directions only in total of $2n$ directions, i.e. in positive and negative direction aligned with coordinate axes for each of n variables. This idea was expanded with so-called positive bases (Davis, 1954) that were implemented within the GPS algorithm introduced by Lewis and Torczon (1996). According to this approach, the poll set P_k in (5.60) is substituted with more convenient and more flexible polling set at *k*-th iteration, as follows

$$P_k = \{\mathbf{x}_k + \Delta_k \mathbf{d} \mid \mathbf{d} \in \mathbb{D}_k\} \tag{5.61}$$

where $\mathbb{D}_k$ presents a finite set of poll directions.

By definition (Audet and Hare, 2017), a set $\mathbb{D}$ is a positive basis of $\mathbb{R}^n$ if and only if it is a positive spanning set of $\mathbb{R}^n$ and is positive linearly independent. In addition to that, the positive span of $\mathbb{D}$ is the set of all nonnegative linear combinations of vectors in $\mathbb{D}$, defined as

$$\text{pspan}(\mathbb{D}) = \left\{ \sum_{i=1}^{|\mathbb{D}|} \lambda_i \mathbf{d}_i \mid \lambda_i \geq 0,\ \mathbf{d}_i \in \mathbb{D} \right\} \subseteq \mathbb{R}^n, \tag{5.62}$$

where set $\mathbb{D}$ is a positive spanning set of $\mathbb{R}^n$ if and only if $\text{pspan}(\mathbb{D}) = \mathbb{R}^n$, while it is positive linearly independent if and only if $\mathbf{d} \notin \text{pspan}(\mathbb{D} \setminus \{\mathbf{d}\})$ for $\forall \mathbf{d} \in \mathbb{D}$. One should recall that a positive spanning set refers to the fact that the set has sufficient amount of information in order to reconstruct $\mathbb{R}^n$ by means of nonnegative linear combinations, while positive linear independence guarantees that there is no redundancy in vectors.

According to definitions above, it can be proven that if $\mathbb{D}$ is a positive spanning set for $\mathbb{R}^n$, then $\mathbb{D}$ contains at least $n+1$ vectors, which presents its lower bound in terms of its size. On the other hand, if $\mathbb{D}$ is a positive basis of $\mathbb{R}^n$, than $\mathbb{D}$ has at least $n+1$ vectors and at most $2n$ elements (Audet and Hare, 2017).

Thus, for the purpose of GPS, GSS and MADS algorithms, two positive basis sets are commonly used for defining a set of vectors for pattern search, i.e. in order to determine the points to search during each iteration. The first of these two positive basis sets is the so-called minimal positive basis set of $\mathbb{R}^n$ that contains $n+1$ vectors, and is usually constructed as

$$\mathbb{D}_{\min} = \left\{ \mathbf{e}_1, \mathbf{e}_2, \ldots, \mathbf{e}_n, -\sum_{i=1}^{n} \mathbf{e}_i \right\}, \tag{5.63}$$

i.e. it consists of n vectors $\mathbf{e}_i$, $i = 1, 2, \ldots, n$, and the one that is the negative of the sum of all other vectors, as indicated in (5.63). The second one is the so-called maximal positive basis set of $\mathbb{R}^n$, which contains $2n$ vectors, and this one is usually constructed as

$$\mathbb{D}_{\max} = \{\mathbf{e}_1, \mathbf{e}_2, \ldots, \mathbf{e}_n, -\mathbf{e}_1, -\mathbf{e}_2, \ldots, -\mathbf{e}_n\}, \tag{5.64}$$

i.e. it consists of n vectors $\mathbf{e}_i$, $i = 1, 2, \ldots, n$, and their n opposite vectors, as indicated in (5.64).

With GPS algorithm, selected vectors that form the pattern are commonly fixed-direction vectors that are based on a mesh that is defined for the current point $\mathbf{x}_k$ as

$$M_k = \{\mathbf{x}_k + \Delta_k \mathbf{D}\mathbf{y} \mid \mathbf{y} \in \mathbb{N}^p\}, \tag{5.65}$$

where $\mathbf{D} = \mathbf{G}\mathbf{Z}$, $\mathbf{G} \in \mathbb{R}^{n \times n}$ is invertible matrix, and matrix $\mathbf{Z} \in \mathbb{R}^{n \times p}$ is selected so that columns of $\mathbf{Z}$ form a positive spanning set of $\mathbb{R}^n$ (Audet and Hare, 2017). Example of mesh refinement in GPS algorithm during poll with selection of directions in $\mathbb{D}_k$ for trial points $\{t_1, t_2, t_3\}$, $\{t_4, t_5, t_6\}$ and $\{t_7, t_8, t_9\}$, and $n = 2$, is shown in Figure 31.

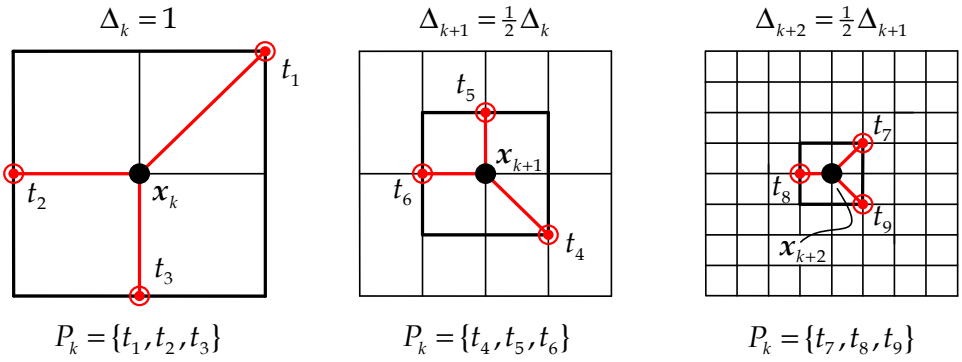

Figure 31. Example of mesh refinement in GPS algorithm during poll

Finally, simplified pseudo-code of GPS algorithm (Lewis and Torczon, 1996), in a case of unconstrained optimization, is presented in Appendix 1.4. One can notice another important difference between GPS and CS algorithm. In comparison to CS, GPS allows the step size Δ_k to be increased in the case of successful iteration, which means that algorithm allows the search radius to be increased. Moreover, besides the local poll step, a global search step is also implemented within the algorithm. The local poll guarantees convergence toward a point in which the necessary first order optimality conditions will be satisfied, while the global search enables the user to implement additional information about the model or to use surrogate functions.

5.2.3 Generating set search algorithm with augmented Lagrangian

The generating set search (GSS) algorithm is very similar to GPS, particularly for the problems of unconstrained optimization in which their patterns are identical. The main difference between GPS and GSS is related to constrained optimization problems. GSS, as an extension of GPS, is well suited for bounds and linear constraints, where directions in $\mathbb{D}$ are determined using the nearby active constraints from the working

set (Kolda et al., 2006, 2003). In other words, GSS is more efficient in comparison with GPS for linearly constrained optimization problems.

When it comes to nonlinear constraints, GPS is not well suited, but with implementation of augmented Lagrangian within the GSS algorithm, which was introduced by Kolda et al. (2006), GSS can handle optimization problems with both linear and nonlinear constraints. However, this approach has been analysed under the assumption that the objective function and constraints should be twice continuously differentiable, which is a typical required property for gradient-based methods.

The augmented Lagrangian pattern search (ALPS) algorithm is primarily used for solving optimization problems with nonlinear equality and inequality constraints, which means that bounds and linear constraints are handled differently, usually with nearby active constraints strategy (Kolda et al., 2006, 2003). For some general optimization problem with nonlinear equality and inequality constraints of the following form

$$\left.\begin{aligned} &\min_{\mathbf{x}\in\mathbb{R}^n} f(\mathbf{x}) \\ &\quad \text{s.t.} \quad c_i(\mathbf{x}) = 0, \quad i \in E \\ &\qquad\quad c_i(\mathbf{x}) \geq 0, \quad i \in I \end{aligned}\right\}, \tag{5.66}$$

which is considered to be solved by some pattern search algorithm, the associated sub-problem based on augmented Lagrangian should be formed as follows

$$L(\mathbf{x},\boldsymbol{\lambda},\mathbf{s},\boldsymbol{\rho}) = f(\mathbf{x}) - \sum_{i\in I} \lambda_i s_i \log(s_i + c_i(\mathbf{x})) + \sum_{i\in E} \lambda_i c_i(\mathbf{x}) + \frac{\rho}{2}\sum_{i\in E} c_i^2(\mathbf{x}), \tag{5.67}$$

where $\lambda_i \geq 0$ are Lagrangian multipliers, $s_i \geq 0$ are slack variables, and ρ is positive penalty parameter. One should notice that each sub-problem (5.67) presents one iterative step, which makes this approach with nonlinear constraints highly computationally expensive. During each iteration, values of λ_i, s_i and ρ are kept constant, until the sub-problem (5.67) is minimized, whereupon are all updated. Otherwise, the penalty parameter ρ is increased and a new sub-problem is formed. These steps are repeated until the termination, which is based on some predefined stopping criteria.

In comparison with other Lagrangian formulations used in Chapter 5.1, augmented Lagrangian is characterised with two properties. First, for inequality constraints slacking, so-called shifted logarithmic barrier function is used, and second, the additional quadratic penalty function for equality constraints is applied. According to

results of (Conn et al., 1997, 1991), it should be outlined that it seems that this approach is superior and more convenient than other similar alternatives. However, considering the complexity of the background of that approach, further discussion is omitted here, but all the theoretical details, as well as practical implementation guidelines, could be found in fundamental references of Conn et al. (1991), Conn et al. (1997), Kolda et al. (2003) and Kolda et al. (2006).

5.2.4 Mesh adaptive direct search algorithm

The MADS algorithm, which was introduced by Audet and Dennis (2006), primarily as direct search algorithm for solving constrained optimization problems of the general form

$$\min_{\mathbf{x}\in\Omega} f(\mathbf{x}) \tag{5.68}$$

does not require any assumptions related to the smoothness of objective function nor to constraints that could be either linear, or nonlinear, or both. If $\Omega = \mathbb{R}$ in (5.68), than the previous optimization problem becomes unconstrained.

The MADS algorithm can be considered as generalization of GPS with some enhanced properties. First, instead of mesh size parameter Δ_k in GPS, in MADS the so-called frame size parameter Θ_k is introduced in order to define in which frame polling should be performed, where $0 < \Delta_k \leq \Theta_k$. According to definition (Audet and Hare, 2017), the frame of the size Θ_k, centred at the current point $\mathbf{x}_k \in \mathbb{R}^n$, is defined as

$$F_k = \left\{ \mathbf{x} \in M_k \mid \left\| \mathbf{x} - \mathbf{x}_k \right\|_\infty \leq \Theta_k b \right\}, \tag{5.69}$$

where $b = \max\left\{ \left\| \mathbf{d}' \right\|_\infty \mid \mathbf{d}' \in \mathbb{D} \right\}$, $\left\| \cdot \right\|_\infty$ presents ℓ_∞ - norm with property $\left\| \mathbf{x} \right\|_\infty = \max_i \left| x_i \right|$.

In this way, the poll set in MADS is created with mesh points within the frame F_k. Moreover, faster decreasing of the mesh size parameter Δ_k with respect to the frame size parameter Θ_k allows the opportunity to construct even larger set of poll directions. It should be pointed out that with comparison to GPS or GSS, in MADS the vectors from the pattern are chosen randomly.

General constraints with MADS algorithm are usually handled by the so-called extreme barrier strategy (Audet and Hare, 2017), which is based on extreme barrier function $f_\Omega : \mathbb{R}^n \to \mathbb{R} \cup \{\infty\}$ defined as

$$f_{\Omega} = \begin{cases} f(\mathbf{x}), & \text{if } \mathbf{x} \in \Omega \\ \infty, & \text{if } \mathbf{x} \notin \Omega. \end{cases} \tag{5.70}$$

The associated principle is very simple and is based on the fact that optimization is performed using the barrier function $f_{\Omega}(\mathbf{x})$ as the objective, rather than $f(\mathbf{x})$. More advanced approaches can take into account two-phase extreme barrier strategy, filter methods (Audet and Dennis, 2004; Dennis Jr. et al., 2004), progressive barrier strategy (Audet and Dennis, 2009; Le Digabel, 2011) or mixture between extreme barrier and progressive barrier called progressive-to-extreme barrier strategy (Audet et al., 2010).

However, the MADS algorithm is primarily orientated to inequality constraints with bounds, which means that equality constraints could be challenging. For this purpose, one can substitute one equality constraint with two equivalent inequality constraints, although this approach could be cumbersome in some optimization problems and algorithm efficiency could be questionable or even not acceptable. This issue is also related to the complexity of equality constraints and to the selection of initial point $\mathbf{x}_0$.

Possible alternatives for handling this issues could be closely related to approaches introduced with GPS and GSS algorithms, i.e. to equality constraint handling by means of the nearby active constraints or augmented Lagrangian method (Kolda et al., 2006, 2003). Recent research directions are also aimed towards the combining of gradient-based methods, like sequential quadratic programing, and derivative free optimization with equality constraints (Tröltzsch, 2016).

Simplified pseudocode of MADS algorithm, with assumption of relatively simple parameter updating in the form of $\Delta_k = \min\{\Theta_k, \Theta_k^2\}$, is presented in Appendix 1.5. It should be noted that the mesh M_k is created similarly like with GPS algorithm in (5.65), where Δ_k is still the mesh size parameter. The matrix $\mathbf{D} \in \mathbb{R}^{n \times p}$ represents a fixed finite set of p mesh directions, and it is commonly defined as $\mathbf{D} \in [\mathbf{I} \quad -\mathbf{I}] \in \mathbb{R}^{n \times (2n)}$, where $\mathbf{I} \in \mathbb{R}^{n \times n}$.

In relation to the chosen poll method, additional poll size parameter Θ_k^p can be used in the termination step, as well as in the mesh refinement during polling. The value of the poll size parameter can be determined according to the following criteria

$$\Theta_k^p = \begin{cases} n\sqrt{\Delta_k}, & \text{for positive basis } (n+1) \text{ poll} \\ \sqrt{\Delta_k}, & \text{for positive basis } (2n) \text{ poll,} \end{cases} \tag{5.71}$$

where Δ_k is the mesh size parameter. As an illustration of the mesh refinement for $n+1$ positive basis poll, mesh adaptiveness is presented in Figure 32 for $\tau = \frac{1}{2}$ and $n = 2$. Thinner lines represent the mesh of the size $\Delta_k = \min\{\Theta_k, \Theta_k^2\}$, while thicker lines present a set of points that are distant from $\mathbf{x}_k$ (blue) for Δ_k^p in ℓ_∞- norm. Trial points (red) from the poll set are chosen randomly.

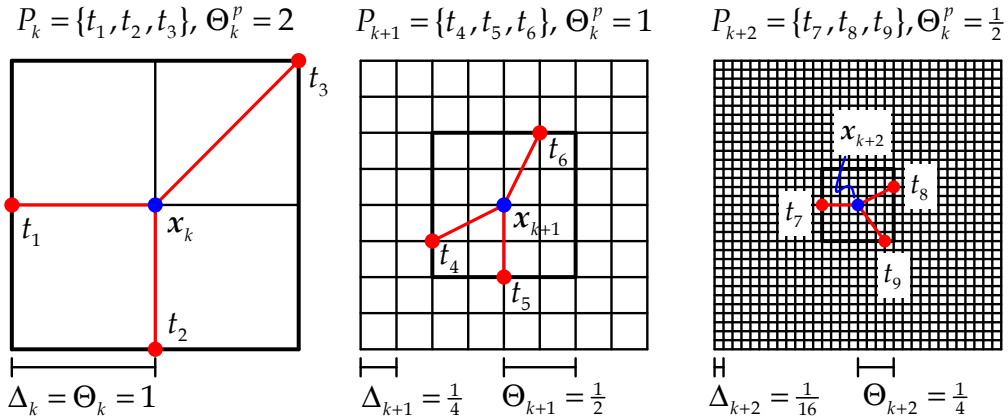

Figure 32. An illustration of the mesh refinement for $n+1$ positive basis poll in a case of unsuccessful polls

Source: Adjusted according to (Le Digabel, 2011)

All emphasized advantages of GPS, GSS and MADS, particularly in comparison with CS algorithm, provide much wider flexibility with respect to programing implementation and solving capabilities, and also provide significantly better convergence characteristics with more accurate results. However, very important issues related to optimality conditions for unconstrained and constrained optimization problems, constraints handling, as well as to convergence of these algorithms are out of the scope for this work, but all the details about these topics could be found in remarkable references produced by Audet and Hare (2017), Audet and Dennis (2006), Kolda et al. (2006, 2003), Torczon (1997), Conn et al. (1997, 1991).

Straight applications of direct search algorithms in optimal thrust allocation do not require any additional transformation of optimization tasks. In other words, optimization tasks like (7.12) or (7.13), which are defined in the forthcoming Chapter 7.2.1, are fully prepared in order to be solved by means of pattern search algorithms, which is very convenient, particularly if one wants to perform appropriate comparisons between these algorithms and any other algorithm that could be of interest, like QP, SQP, etc.

6 IMPACT OF THRUSTER-THRUSTER INTERACTION EFFECTS ON OPTIMAL THRUST ALLOCATION

6.1 Setup for numerical simulations and examples

In order to perform appropriate optimal thrust allocation procedure, some prerequisites should be introduced prior the optimization itself. This particularly applies to selected reference vessel and her most important characteristics from the main vessel particulars to the thruster configuration that defines thruster technical features and their position on the hull of the vessel. Estimation of environmental loads is another important prerequisite that should be defined and constructed before the thrust allocation procedure. From the computational point of view, all optimal thrust allocation procedures were performed using MATLAB R2018b software (The MathWorks, 2018) on Windows 10 (x64), i5-7500 CPU @ 3.40 GHz with 16 GB RAM.

6.1.1 Characteristics of the reference vessel

Analyses related to optimal thrust allocation in chapters 6 and 7 are closely related to the chosen reference vessel. For this purpose, the heavy lift dynamically positioned vessel is selected, as shown in Figure 33. She has the length overall of $L_{oa} = 162$ m, beam $B = 38$ m, displacement $\Delta = 24000$ t, and is equipped with seven thrusters, one of which is a bow tunnel thruster and the rest are azimuth thrusters. Their approximate positions on the hull regarding the body reference frame {*b*} are shown in Figure 34. The same figure also specifies the convention of the thrust T_i and the azimuth α_i of each thruster, as well as the total environmental loads with respect to specific wind angle of attack γ_{wind}. This notation is in accordance with Figure 23.

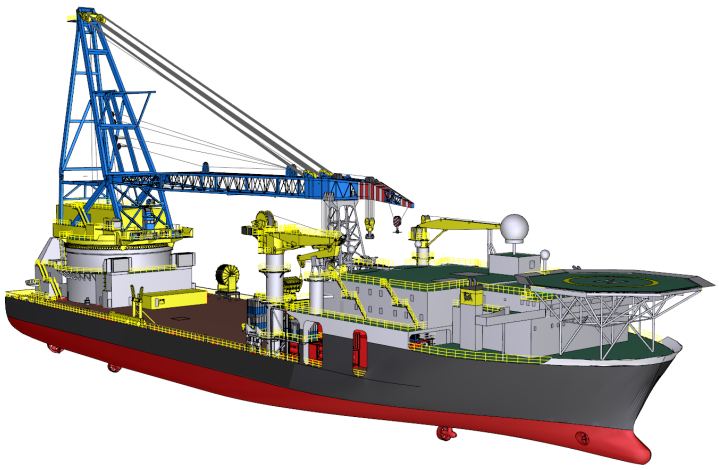

Figure 33. Heavy lift DP vessel as a reference vessel

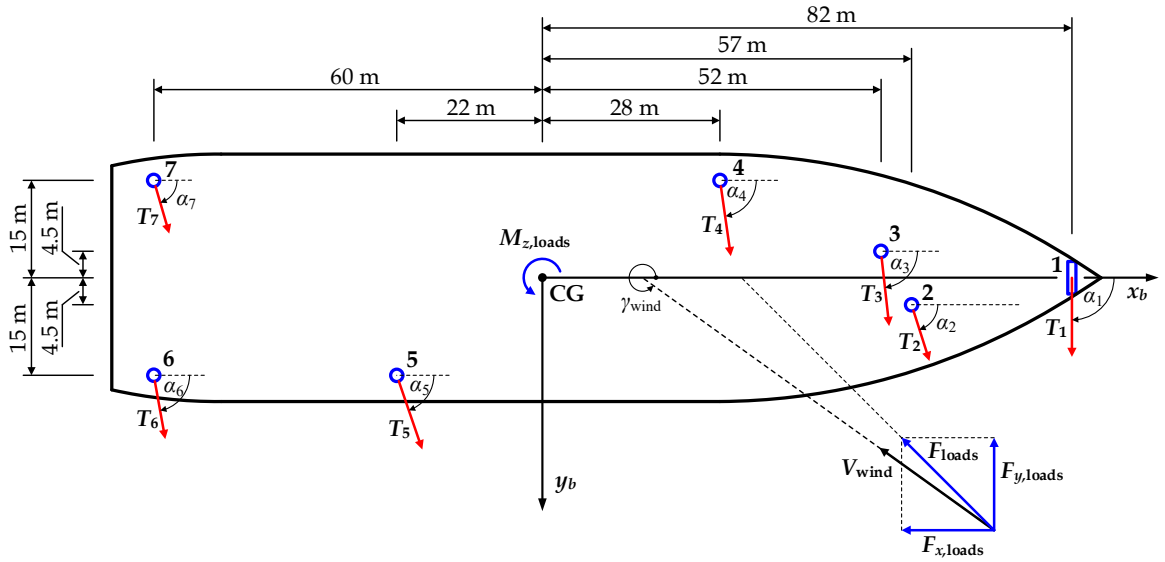

Figure 34. Approximate thruster configuration of the reference vessel

The main thruster characteristics, including the thruster coordinates l_{ix} (m) and l_{iy} (m) in $\{b\}$, maximum thrusts $T_{i,\max}$ (kN), maximum delivered powers $P_{i,\max}$ (kW), etc. are presented in Table 3, where $i = 1, 2, \ldots, 7$. The thruster coordinates l_{ix} and l_{iy} serve as a basis of the configuration matrix $\mathbf{B}$, defined as (4.9), i.e. (4.61).

Table 3. Main thruster characteristics installed on the reference vessel

i	Thruster	l_{ix} (m)	l_{iy} (m)	D_i (m)	P_i / D_i	N_i (min^{-1})	$T_{i,\max}$ (kN)	$T_{i,\min}$ (kN)	$P_{i,\max}$ (kW)
1	Tunnel	82	0	2	1.2	330	165	-165	1200
2	Azimuth	57	4.5	2.5	1.2	900	390	0	2400
3	Azimuth	52	-4.5	2.5	1.2	900	390	0	2400
4	Azimuth	28	-15	2.5	1.2	900	390	0	2400
5	Azimuth	-22	15	2.5	1.2	900	390	0	2400
6	Azimuth	-60	15	3.6	1.2	630	760	0	4500
7	Azimuth	-60	-15	3.6	1.2	630	760	0	4500

6.1.2 Environmental load modelling for the reference vessel

Environmental loads for numerical simulations performed in this work are calculated quasi-statically and are based on the model tests for the reference vessel according to usual design recommendations, as explained in Chapter 2.3. Station keeping conditions $(u = v = 0)$ are only taken into account.

Wind loads $\boldsymbol{\tau}_{wind}$ are calculated according to (2.28), with air density $\rho_{air} = 1.226$ kg/m^3 and $A_{F,wind} = 810$ m^2 and $A_{L,wind} = 2410$ m^2, as areas of vessel's frontal and lateral projections above the water line, respectively. Non-dimensional wind load coefficients $C_{X,wind}(\gamma_{wind})$, $C_{Y,wind}(\gamma_{wind})$ and $C_{N,wind}(\gamma_{wind})$ for the reference vessel have been obtained in a wind tunnel during model tests and are shown graphically in Figure 35. In this analysis, waves have been correlated with wind according to the IMCA recommendations (IMCA, 2000). Therefore, values of wind speed V_{wind} (m/s) were limited to interval $[0, 35]$. Notation of the encounter wind angle γ_{wind} is in accordance with Figures 6, 7, 23 and 34.

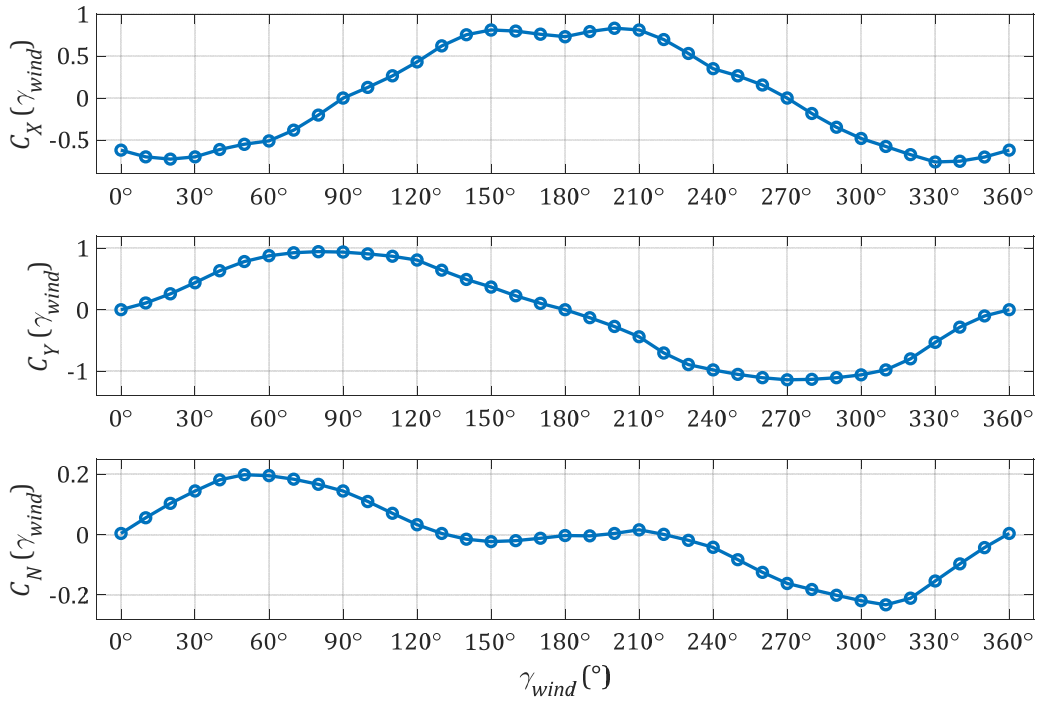

Figure 35. Non-dimensional wind load coefficients for the reference vessel

Vector $\overline{\boldsymbol{\tau}}^{i}_{wave,\,\mathrm{mean}}$ of mean wave drift forces and moment (2.54) is calculated according to (2.51)-(2.53), with water density $\rho = 1025$ kg/m^3, gravitational acceleration $g = 9.81$ m/s^2, and length of the vessel at the waterline $L_{WL} = 151.3$ m. Non-dimensional wave load coefficients $C_{X,wave}(\omega,\theta)$, $C_{Y,wave}(\omega,\theta)$ and $C_{N,wave}(\omega,\theta)$ for the reference vessel have been obtained during model tests and are shown graphically in Figure 36 for the case $\omega = 1.05$ s^{-1} $(T_0 = 6$ s$)$, and in Appendix 2 for the cases $\omega = 0.63$ s^{-1} $(T_0 = 10$ s$)$ and $\omega = 0.42$ s^{-1} $(T_0 = 15$ s$)$, where ω and T_0 indicate wave frequency and wave peak period, respectively.

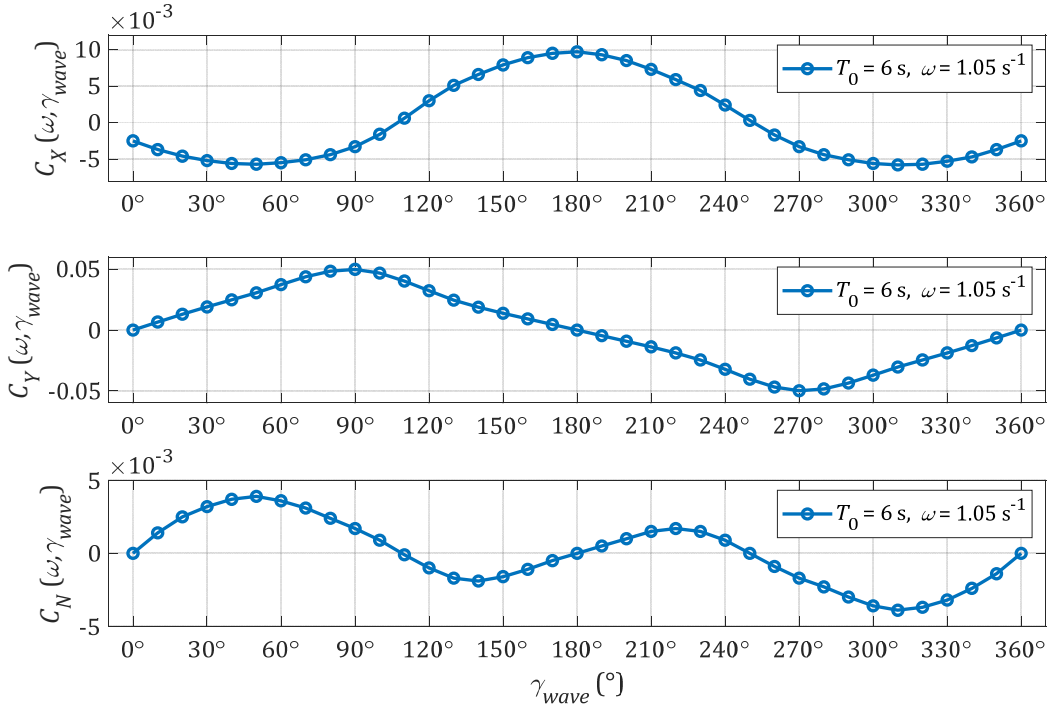

Figure 36. Non-dimensional wave load coefficients ($T_0 = 6$ s, $\omega = 1.05$ s^{-1}) for the reference vessel

Based on these model test results, a semi-empirical model for wave load estimation has been developed in order to cover the wave encounter angle $\theta \in [0°, 360°]$ and the wave frequency range of $\omega \in [0, 3]$, which is significant for practical applications. For integration purposes in (2.51)-(2.53), the JONSWAP spectrum (2.44) was used with the peak-shape parameter $\gamma = 3.3$. In addition, DNV conversion factor from (DNV, 2007) has been taken into account as well. As mentioned afore, in this thesis waves have been correlated with wind according to the IMCA recommendations (IMCA, 2000). Hence, significant wave height H_s and wave peak period T_0 for JONSWAP spectrum were determined in relation with wind speed V_{wind} using the wind-wave correlation data presented in Table 4 (IMCA, 2000). This wind-wave correlation applies one more additional assumption by which $\theta = \gamma_{waves} = \gamma_{wind}$. Notation of the wave encounter angle γ_{waves} is equal to the one of the wind encounter angle γ_{wind}.

Sea current loads $\boldsymbol{\tau}_{current}$ are calculated according to (2.30), with water density $\rho = 1025$ kg/m^3, length between perpendiculars $L_{pp} = 152.62$ m, beam $B = 38$ m and summer draft $T = 6$ m. Frontal and lateral projected areas below the water line are calculated as $A_{F,curr} = BT$ and $A_{L,curr} = L_{pp}T$.

Table 4. Relationship between mean wind speed V_{wind} (m/s), significant wave height H_s (m), wave peak period T_p (s) and wave peak frequency ω_0 (s^{-1})

V_{wind} (m/s)	H_s (m)	T_p (s)	ω_0 (s^{-1})	V_{wind} (m/s)	H_s (m)	T_p (s)	ω_0 (s^{-1})
0	0	0	3	20	7.26	12.64	0.50
2.5	1.28	5.30	1.19	22.5	8.47	13.65	0.46
5	1.78	6.26	1	25	9.75	14.65	0.43
7.5	2.44	7.32	0.86	27.5	11.09	15.62	0.40
10	3.21	8.41	0.75	30	12.50	16.58	0.38
12.5	4.09	9.49	0.66	32.5	13.97	17.53	0.36
15	5.07	10.56	0.59	35	15.49	18.46	0.34
17.5	6.12	11.61	0.54				

Source: Adjusted according to (IMCA, 2000)

For the purpose of this calculation, length overall (L_{oa}) in (2.30) is replaced with length between perpendiculars (L_{pp}). Non-dimensional current load coefficients $C_{X,curr}(\gamma_{curr})$, $C_{Y,curr}(\gamma_{curr})$ and $C_{N,curr}(\gamma_{curr})$ for the reference vessel have been obtained during model tests and are shown in Figure 37.

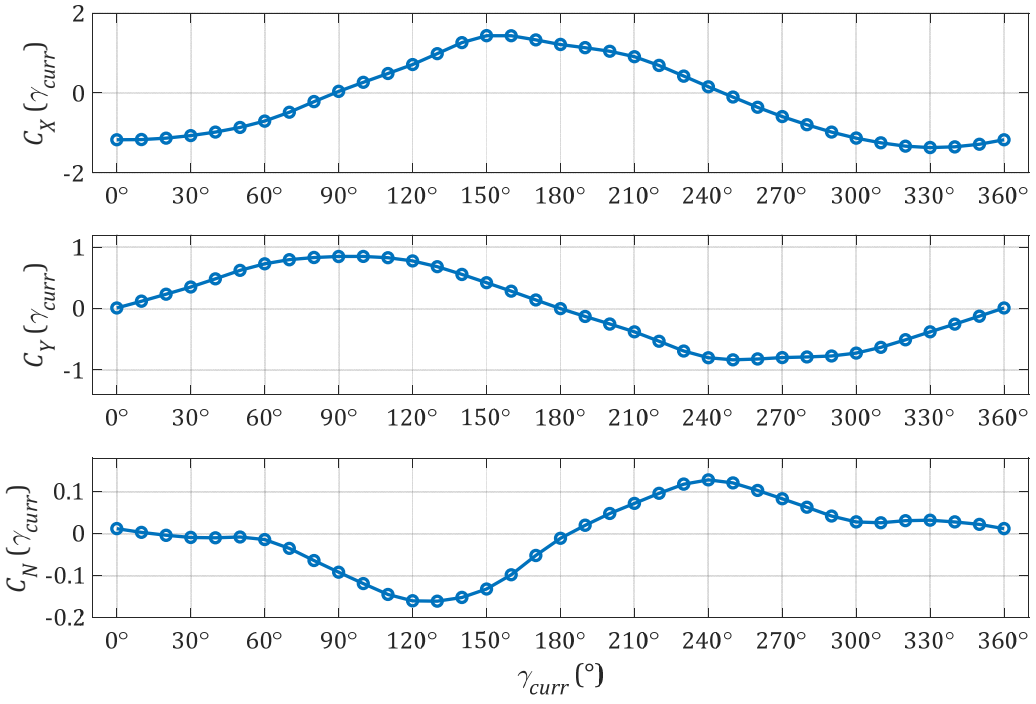

Figure 37. Non-dimensional sea current load coefficients for the reference vessel

If included as a part of environmental loads, values of the sea current speed V_{curr} (m/s) were chosen from the limited set $\{0, 0.5, 1, 1.5, 2\}$ and notation of the encounter sea current angle γ_{curr} is also equal to the one of the wind encounter angle γ_{wind}. The commonly accepted assumption $\gamma_{wind} = \gamma_{waves} = \gamma_{curr}$ was used throughout the thesis, considering it represents the worst-case scenario in terms of environmental loads.

Finally, the vector of environmental loads $\boldsymbol{\tau}$ consists of wind, wave and sea current loads, and according to (2.28), (2.54) and (2.30) is defined as follows

$$\boldsymbol{\tau} = \boldsymbol{\tau}_{wind} + \overline{\boldsymbol{\tau}}^{i}_{wave,\,\mathrm{mean}} + \boldsymbol{\tau}_{current}. \tag{6.1}$$

In this way, it represents the total environmental load for some wind angle of attack γ_{wind}, with general assumption related to wind-wave IMCA correlation $(\gamma_{waves} = \gamma_{wind})$, i.e. in the presence of sea currents with even more general assumption according to which $\gamma_{current} = \gamma_{waves} = \gamma_{wind}$, if not stated otherwise.

Vector $\boldsymbol{\tau}$ in (6.1) presents a crucial part for optimal thrust allocation. It is important to note that due to the nature of environmental loads, the angle of attack of the resulting force F_{loads} differs from the angle of attack γ_{wind}, as can be seen in Figure 34. This is significant because the allocated thrust of each thruster will strive towards this angle, and not towards the angle γ_{wind}, by which the optimal thrust allocation is implemented.

In industrial DP systems, vector $\boldsymbol{\tau}$ is not determined as defined in (6.1), but is usually calculated by means of a DP controller using some appropriate control law (e.g. nonlinear MIMO PID, optimal control, etc.). On the other hand, and since only quasi-statically approach is used in this work, calculation of vector $\boldsymbol{\tau}$, as in (6.1), can be considered appropriate for further optimal thrust allocation analyses.

6.1.3 Considerations about thruster-thruster interaction effects for the reference vessel

In order to emphasize and quantify the impact of thruster-thruster interactions on optimal thrust allocation, focus is put on the two nearest azimuth thruster 2 and 3, as indicated in Figure 34, where $x/D = 3.85$. Their asymmetric position on the hull makes the interaction even more interesting. It is worth to note that for all other thruster combinations it yields $x/D > 6$, which may be interpreted in a way that other thruster pairs are not of a great significance, although they can be covered with the

approach presented in Chapter 3.2.2. This could be of an importance due to some thrust losses that will still occur because of their interaction, although they are quite distant from each other. However, for the purpose of this work, only interaction between thrusters 2 and 3 is analysed in detail.

After implementing the optimal thrust allocation for some environmental load scenario, the thrust T_i and azimuth α_i of each thruster are obtained. Depending on the values of the obtained angles α_2 and α_3, the additional analysis should be performed of whether or not it is necessary to include the effects of thruster 2 vs. thruster 3 interaction. In fact, according to the results of Lehn (1980), the losses arising from this interaction are of interest if $\delta, \phi \in [-30°, 30°]$.

Since the optimal thrust allocation is conducted and analysed for $\gamma_{wind} \in [0°, 360°]$, and with regard to the specific position of thrusters 2 and 3 on the hull, there are two cases of the thruster 2 - thruster 3 interaction that should be taken into account (Figure 34):

- $\alpha_2 \in [30°, 90°]$

  In this case, thruster 2 is the front thruster and thruster 3 is the rear thruster. The interaction is analysed if $\alpha_3 \in [30°, 90°]$.

- $\alpha_3 \in [210°, 270°]$

  This is the reverse case, i.e. thruster 3 is now the front thruster and thruster 2 is the rear thruster. The interaction is analysed if $\alpha_2 \in [210°, 270°]$.

6.2. Direct solution approach for thruster-thruster interactions

The basic idea behind the direct solution of optimal thrust allocation is in combining the most important equality constraint (4.8) with objective function P (4.50) by means of the so-called Lagrangian duality (Boyd and Vandenberghe, 2004) in order to get equivalent optimization problem, but unconstrained in comparison with e.g. (5.1).

Direct solution of optimal thrust allocation problem is related to the minimization of quadratic power function (4.53) with including the thrust allocation equation (4.8) as the main, but only constraint. This optimization task can be written as follows

$$\left.\begin{aligned} \mathbf{u}^* &= \arg\min_{\mathbf{u}\in\mathbb{R}^{2r}}(P) \\ \text{s.t.} \quad \boldsymbol{\tau} &= \mathbf{B}\mathbf{u} \end{aligned}\right\} \tag{6.2}$$

or in equivalent form

$$\left.\begin{aligned} &\min_{\mathbf{u}\in\mathbb{R}^{2r}}(\mathbf{u}^{\mathrm{T}}\mathbf{W}\mathbf{u}) \\ &\quad \text{s.t.} \quad -\mathbf{B}\mathbf{u}+\boldsymbol{\tau}=\mathbf{0}. \end{aligned}\right\} \tag{6.3}$$

6.2.1 Moore-Penrose pseudo-inverse and generalized inverse matrix

By using (5.3) and (5.7), Lagrangian for the above optimization task (6.3) can be rewritten as

$$L(\mathbf{u},\boldsymbol{\lambda})=\mathbf{u}^{\mathrm{T}}\mathbf{W}\mathbf{u}+\boldsymbol{\lambda}^{\mathrm{T}}(-\mathbf{B}\mathbf{u}+\boldsymbol{\tau}), \tag{6.4}$$

while the dual problem of (6.3), according to (6.4), can be defined as

$$\mathbf{u}^{*}=\arg\min_{\mathbf{u}\in\mathbb{R}^{2r}}(\mathbf{u}^{\mathrm{T}}\mathbf{W}\mathbf{u}+\boldsymbol{\lambda}^{\mathrm{T}}(-\mathbf{B}\mathbf{u}+\boldsymbol{\tau})). \tag{6.5}$$

If KKT conditions (5.12) and (5.13) are applied for (6.4) and (6.5), it yields

$$\nabla_{\mathbf{u}}L=0 \quad \Rightarrow \quad \frac{\partial L}{\partial \mathbf{u}}=\frac{\partial(\mathbf{u}^{\mathrm{T}}\mathbf{W}\mathbf{u})}{\partial \mathbf{u}}+\boldsymbol{\lambda}^{\mathrm{T}}\frac{\partial(-\mathbf{B}\mathbf{u}+\boldsymbol{\tau})}{\partial \mathbf{u}}=\mathbf{0}, \tag{6.6}$$

$$\nabla_{\boldsymbol{\lambda}}L=0 \quad \Rightarrow \quad \frac{\partial L}{\partial \boldsymbol{\lambda}}=-\mathbf{B}\mathbf{u}+\boldsymbol{\tau}=\mathbf{0}. \tag{6.7}$$

Considering

$$\frac{\partial(\mathbf{u}^{\mathrm{T}}\mathbf{W}\mathbf{u})}{\partial \mathbf{u}}=(\mathbf{W}+\mathbf{W}^{\mathrm{T}})\mathbf{u}=2\mathbf{W}\mathbf{u}, \tag{6.8}$$

from (6.6) one can redefine $\mathbf{u}$ as

$$\mathbf{u}=\frac{1}{2}\mathbf{W}^{-1}\mathbf{B}^{\mathrm{T}}\boldsymbol{\lambda}, \tag{6.9}$$

which in combination with (6.7), and with assumption that $\mathbf{B}\mathbf{W}^{-1}\mathbf{B}^{\mathrm{T}}$ is not a singular matrix, yields

$$\boldsymbol{\lambda}=2(\mathbf{B}\mathbf{W}^{-1}\mathbf{B}^{\mathrm{T}})^{-1}\boldsymbol{\tau}. \tag{6.10}$$

If (6.10) is combined with (6.9), the direct solution of (6.3) follows as

$$\mathbf{u}=\mathbf{W}^{-1}\mathbf{B}^{\mathrm{T}}(\mathbf{B}\mathbf{W}^{-1}\mathbf{B}^{\mathrm{T}})^{-1}\boldsymbol{\tau}. \tag{6.11}$$

The matrix $\mathbf{B}_{w}^{\dagger}$ of the form

$$\mathbf{B}_{w}^{\dagger}=\mathbf{W}^{-1}\mathbf{B}^{\mathrm{T}}(\mathbf{B}\mathbf{W}^{-1}\mathbf{B}^{\mathrm{T}})^{-1} \tag{6.12}$$

is commonly identified as the so-called generalized inverse matrix (Ben-Israel and Greville, 2003), because the following condition is satisfied

$$\mathbf{B}\mathbf{B}_w^{\dagger}\mathbf{B} = \mathbf{B}\mathbf{W}^{-1}\mathbf{B}^{\mathrm{T}}(\mathbf{B}\mathbf{W}^{-1}\mathbf{B}^{\mathrm{T}})^{-1}\mathbf{B} = \mathbf{I}\mathbf{B} = \mathbf{B}, \tag{6.13}$$

where $\mathbf{I} \in \mathbb{R}^{2r\times 2r}$ is the unit matrix.

Thus, direct solution can be rewritten as

$$\mathbf{u} = \mathbf{B}_w^{\dagger}\boldsymbol{\tau}. \tag{6.14}$$

One can notice that for $\mathbf{W} = \mathbf{I}$, where $\mathbf{I} \in \mathbb{R}^{2r\times 2r}$ is the unit matrix, $\mathbf{B}_w^{\dagger}$ becomes the so-called Moore-Penrose pseudo-inverse matrix $\mathbf{B}^{\dagger}$ of the form

$$\mathbf{B}^{\dagger} = \mathbf{B}^{\mathrm{T}}(\mathbf{B}\mathbf{B}^{\mathrm{T}})^{-1}, \tag{6.15}$$

which was introduced by Moore (1920), and Penrose and Todd (1956). Usually, the matrix $\mathbf{B}^{\dagger}$ is calculated numerically by means of the so-called singular value decomposition (SVD) factorisation. Detailed analysis on how to calculate (6.15) by using SVD can be found in a large number of references (Ben-Israel and Greville, 2003; Barata and Hussein, 2012), thus this part will be omitted here.

In this case, if (6.14) is redefined in terms of Moore-Penrose pseudo-inverse matrix for $\mathbf{W} = \mathbf{I}$, direct solution is of the form

$$\mathbf{u} = \mathbf{B}^{\dagger}\boldsymbol{\tau}, \tag{6.16}$$

with equally weighted thrust components of $\mathbf{u}$, which presents a minimal Frobenius norm solution that is optimal in a sense of the smallest norm which minimizes $\|\mathbf{u}\|$ (Golub and Van Loan, 2013).

If required, the optimization task (6.3) can be extended with inequality constraints and additional equality constraints, as described in Chapter 5.1.1. However, this approach will lead to computationally and timely more expensive problem that is commonly avoided (Wit, 2009). As alternative, some appropriate programming technique should be rather used.

6.2.2 Thruster saturation with pseudo and generalized inverse matrix approach

If one does not embed inequality constraints in Lagrangian (6.4) as mentioned in afore chapter, thruster saturation constraints (4.11) cannot be integrated straightforwardly in (6.11). Hence, some iteration procedure is required in combination with thrust reallocation. For the purpose of this work, procedure of thrust saturation consists of three parts: initial part for initialization of required variables, thrust allocation without thruster saturation included, and finally thruster saturation checking with saturation

of saturated thruster and appropriate thrust reallocation for all other unsaturated thrusters so the equilibrium (4.8) is kept satisfied. This procedure can be described in simplified form as follows:

Step 1.1 Define maximum thrust for each thruster

Step 1.2 Define configuration matrix $\mathbf{B}$

Step 1.3 Define environmental conditions (e.g. V_{wind}, γ_{wind}, etc.)

Step 2.1 Calculate environmental load vector $\boldsymbol{\tau} = [F_{x,loads}, F_{y,loads}, M_{z,loads}]^{\mathrm{T}}$

Step 2.2 Calculate design vector $\mathbf{u}$ by means of pseudo-inverse matrix (6.14)

Step 2.3 Verify that equilibrium $\mathbf{u} = \mathbf{B}_w^{\dagger}\boldsymbol{\tau}$ is satisfied

Step 3.1 Check for each thruster whether saturation occurs

Step 3.2 Identify all saturated thrusters, if there are any

Step 3.3 Exclude saturated thrusters in terms of $\mathbf{u}$ and $\mathbf{B}$

Step 3.4 Reduce load vector $\boldsymbol{\tau}$ for saturated thrusters $(\boldsymbol{\tau}_{red})$

Step 3.5 Repeat thrust allocation by means of $\mathbf{B}^{\dagger}$ or $\mathbf{B}_w^{\dagger}$ for reduced load vector $\boldsymbol{\tau}_{red}$ and remaining unsaturated thrusters

Step 3.6 Verify that equilibrium equation is satisfied

Step 3.7 Repeat steps 3.1-3.6 until all required thrusters are saturated

Step 3.8 Compare initial and final allocated solution.

6.2.3 Further applications of the weighting matrix

As defined in (6.12), generalized inverse matrix $\mathbf{B}_w^{\dagger}$ is based on the extension of pseudo inverse matrix (6.15) and is characterised with the weighting matrix $\mathbf{W}$, which can be used for various reasons. The most common application of this matrix is related to implementation of thruster constants w_i (4.51). If one uses this approach, i.e. if one relies on (6.11), instead on (6.16), solution that is more realistic can be expected because at least some information about thrusters is taken into account in this way. Some additional and very useful applications of the weighting matrix $\mathbf{W}$ could also be found in (Millan, 2008).

In this work, further applications are referred to implementation of various thruster interaction effects, primarily thruster-thruster interactions. For this reason, extended

weighting matrix can be written in a more general way, i.e. as a product of weighting matrices. In other words, extended weighting matrix can be defined as

$$\mathbf{W} = \prod_{j=0}^{m-1} \mathbf{W}_j = \prod_{j=0}^{m-1} \operatorname{diag}\{w_1^{(j)}, w_1^{(j)}, w_2^{(j)}, w_2^{(j)}, \ldots, w_r^{(j)}, w_r^{(j)}\} \in \mathbb{R}^{2r \times 2r}, \tag{6.17}$$

where m indicates a number of weighting matrices that are used, and r is the number of thrusters. Thus, matrix $\mathbf{W}_0$ is reserved for thruster constants w_i from (4.51), while the matrices $\mathbf{W}_j$, $j = 1, 2, \ldots, m-1$, can be used for implementation of all other thruster properties or constraints. In this part of research, matrix $\mathbf{W}_1$ was used for excluding of tunnel thruster when required, and matrix $\mathbf{W}_2$ was used for implementation of thrust reduction ratios (3.38), i.e. (3.54). Therefore, matrix $\mathbf{W}_1$ for the thruster configuration shown in Figure 34 can be defined as

$$\mathbf{W}_1 = \operatorname{diag}\{w_1^{(1)}\mathbf{I}_{2\times 2}, \mathbf{I}_{12\times 12}\} \in \mathbb{R}^{14\times 14}, \tag{6.18}$$

where $w_1^{(1)}$ should be chosen sufficiently large in order to exclude contribution of tunnel thruster during optimal thrust allocation based on (6.11). If tunnel thruster is included in thrust allocation, then $\mathbf{W}_1 = \mathbf{I} \in \mathbb{R}^{14\times 14}$, where $\mathbf{I}$ is the unit matrix. For additional tunnel thrusters, (6.18) should be updated in order to cover all tunnel thrusters with associated weights $w^{(1)}\mathbf{I}_{2\times 2}$. Elements in matrix $\mathbf{W}$ should correspond to thruster configuration in $\mathbf{B}$. The same applies for any other weighting matrix $\mathbf{W}_j$.

As already described in chapter 6.1.3, thruster-thruster interactions are analysed only for thrusters 2 and 3, as two separate cases. Hence, one can differ also two cases, (*a*) and (*b*), for associated weighting matrices. When $\alpha_2 \in [30°, 90°]$ and $\alpha_3 \in [30°, 90°]$, i.e. when thruster 2 is the front one and thruster 3 is the rear one, weighting matrix $\mathbf{W}_2$ will have the following form in the case (*a*)

$$\mathbf{W}_2^{(a)} = \operatorname{diag}\{\mathbf{I}_{4\times 4}, w_3^{(2)}, w_3^{(2)}, \mathbf{I}_{8\times 8}\} \in \mathbb{R}^{14\times 14}, \tag{6.19}$$

and when $\alpha_2 \in [210°, 270°]$ and $\alpha_3 \in [210°, 270°]$, i.e. in the case (*b*) when thruster 3 is the front one and thruster 2 is the rear one, weighting matrix $\mathbf{W}_2$ can be expressed as

$$\mathbf{W}_2^{(b)} = \operatorname{diag}\{\mathbf{I}_{2\times 2}, w_2^{(2)}, w_2^{(2)}, \mathbf{I}_{10\times 10}\} \in \mathbb{R}^{14\times 14}, \tag{6.20}$$

where $w_2^{(2)}$ and $w_3^{(2)}$ are associated thrust reduction ratios (t) defined as (3.38) and calculated as in (3.54) after interaction angles ϕ and δ have been determined (Figures 15 and 21), for appropriate cases (*a*) or (*b*).

Application of the weighting matrix $\mathbf{W}_2$ withdraws the penalization of the rear thruster, which means that this reduced thrust should be compensated with other thrusters with keeping thruster saturation in mind. Thus, some reallocation strategy, similar to the one presented in the previous chapter, should be introduced as well.

Relations (6.19) and (6.20) are prepared only for the analysed case of thrusters 2 and 3 of the reference vessel. However, if more thruster-thruster interactions are of interest, they can easily be added in $\mathbf{W}_2$ using the same analogy. Moreover, in very similar way, all other thruster properties, constraints or interactions can be embedded in optimal thrust allocation procedure based on this "direct solution" approach. The application of pseudo inverse matrix ensures the singularity avoidance by itself, and considering nonlinear equality constraint (3.38) presents non-convex thrust region for the rear thruster, this approach effectively eliminates all issues that usually arise in non-convex optimization.

6.2.4 Handling of thrust losses with generalized inverse matrix approach

The impact of the thruster-thruster interactions on the optimal thrust allocation is conducted through the following three steps:

(1) *Optimal thrust allocation without thrust losses due to interaction effects*

The optimal thrust allocation is conducted for the given environmental load vector $\boldsymbol{\tau}$, design vector $\mathbf{u}_1$ is calculated using (6.11), but without taking into account any interaction effect and other constraints such as thrust saturation, forbidden zones, etc. In this step, weighting matrix is equal to $\mathbf{W} = \mathbf{W}_0\mathbf{W}_1$. Since this allocation is performed quasi-statically, it is clear that in this first step the interaction effects cannot be taken into account because the thruster azimuths, i.e. interaction angles are still unknown. On the other hand, in the dynamic allocation, the allocated thruster azimuths from the previous step, i.e. from the last conducted allocation, can be taken into account for initial thrust loss estimation.

(2) *Thrust loss analysis due to interaction effects*

After the implementation of the optimal thrust allocation, allocated azimuth angles are analysed. In this research, the angles α_2 and α_3 are of particular interest. If they reach the values from the previously mentioned intervals, the thruster-thruster interaction effect is analysed and the thrust loss of the rear thruster is validated according the

(3.38), i.e. (3.54). The real state of design vector is equal to $\mathbf{u}_2 = \mathbf{W}_2 \mathbf{u}_1$. Equilibrium (4.8) is not satisfied due to the thrust loss that occurs with the rear thruster. Consequence of this real state $\mathbf{u}_2$ in industrial DP systems is degradation of vessels position and heading, which is usually compensated by means of the slowly varying bias $\mathbf{b}$, as a part of unmodelled dynamics. This clearly indicates the possible application of this thrust loss handling approach in control part of a DP system in terms of thrust loss feedforward control.

(3) *Optimal thrust reallocation with interaction effects and thrust losses included*

Once the thrust loss of the rear thruster is estimated, the optimal thrust reallocation of all thrusters is performed, reallocated design vector $\mathbf{u}_3$ is calculated using (6.11), but now with weighting matrix $\mathbf{W} = \mathbf{W}_0 \mathbf{W}_1 \mathbf{W}_2$ that takes into account thrust losses of the rear thruster. Equilibrium (4.8) is now satisfied due to included thrust losses. This reallocation will now increase previously penalized allocated thrust of the rear thruster above the level from the step *(i)*. Thrust and azimuth angle variations in all other thrusters will not be significant, so any larger increase in power consumption should be expected only for the rear thruster. However, this is more than acceptable if degradation of vessel position and heading is minimised. At the same time, knowing any possible increase of electrical power demand in advance can be beneficiary for power management system, particularly in cases of blackout prevention and other similar problems.

Finally, if the thrust reduction ratio t is significantly varied during the implementation of losses due to the thruster-thruster interaction, then it is necessary to perform this procedure iteratively. In this research, that part is omitted due to simplicity and quasi-static approach to optimal thrust allocation.

6.2.5 Numerical example on implementation and analysis of thruster-thruster interaction

In order to illustrate the problem, representative example is provided for three environmental conditions as follows

(*a*) $V_{wind} = 5$ m/s, $H_s = 1.78$ m, $T_p = 6.26$ s, $\omega_0 = 1$ s^{-1}, $V_{curr} = 0.5$ m/s,

(*b*) $V_{wind} = 10$ m/s, $H_s = 3.21$ m, $T_p = 8.41$ s, $\omega_0 = 0.75$ s^{-1}, $V_{curr} = 0.5$ m/s,

(*c*) $V_{wind} = 15$ m/s, $H_s = 5.07$ m, $T_p = 10.56$ s, $\omega_0 = 0.59$ s^{-1}, $V_{curr} = 0.5$ m/s.

Wind-wave correlation is based on IMCA recommendations (IMCA, 2000) and associated environmental loads are calculated as described in Chapter 6.1.2. Sea current is added independently of wind and waves, although the angle of attack was the same for all disturbances at any time and was varied from $\gamma_{wind} = 0°$ to $360°$ with the rate of $5°$. Tunnel thruster was excluded in order to emphasize interactions between thrusters 2 and 3.

The thrust visualization for environmental conditions (*a*), (*b*) and (*c*) with respect to the wind angle of attack γ_{wind}, for thrusters 2 and 3, is shown in Figures 38, 39 and 40, respectively. The blue line with circle marker symbols represents the optimal thrust allocation without the interaction effects included, as described in step (1) in Chapter 6.2.4. The red line with square marker symbols represents the actual state that occurs after the interaction effects reduce the thrust of rear thruster, as described in step (2) in Chapter 6.2.4. Finally, the black line with diamond marker symbols represents the final reallocated state that takes into account thrust losses of the rear thruster, as described in step (3) in Chapter 6.2.4.

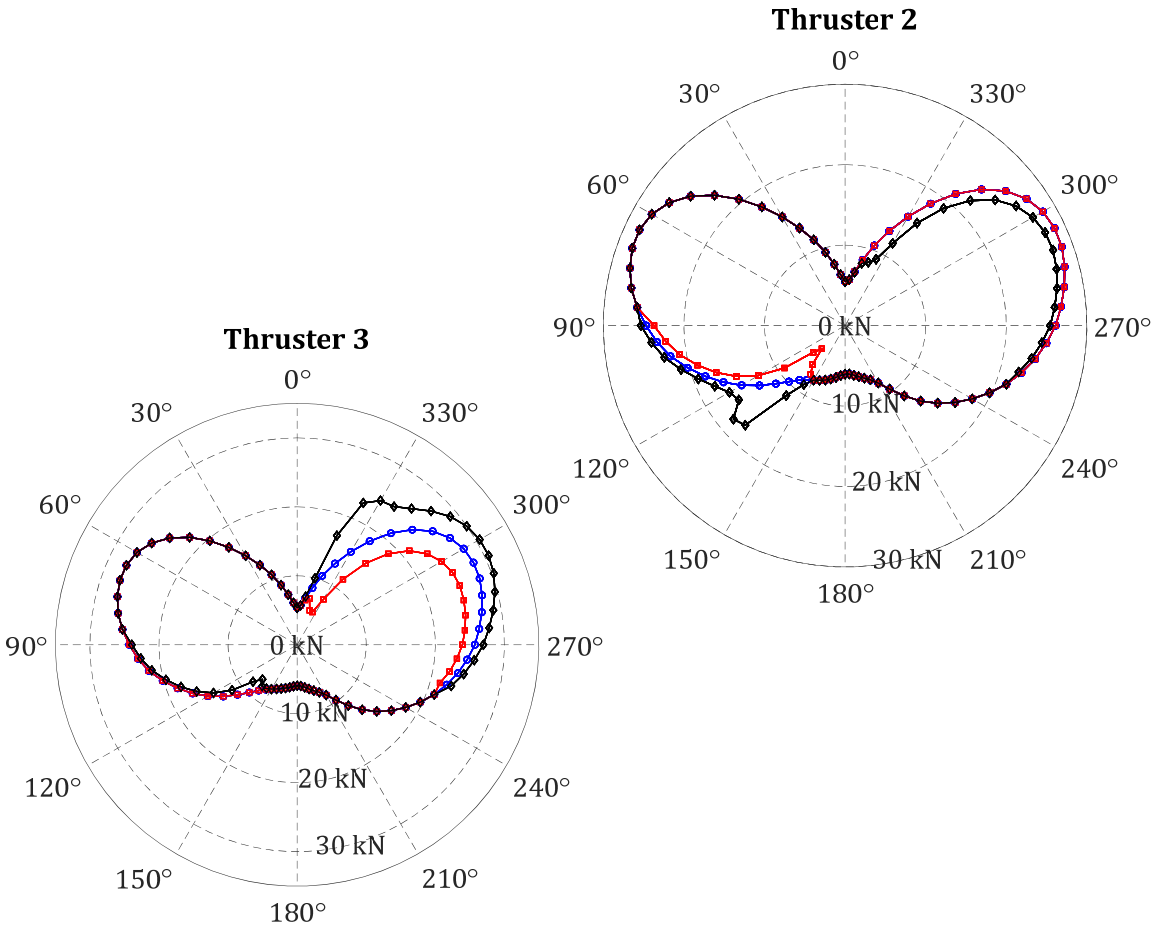

Figure 38. Polar thrust distribution of azimuth thrusters 2 and 3 with respect to the wind angle of attack γ_{wind} and for $V_{wind} = 5$ m/s, $H_s = 1.78$ m, $T_p = 6.26$ s, $V_{curr} = 0.5$ m/s

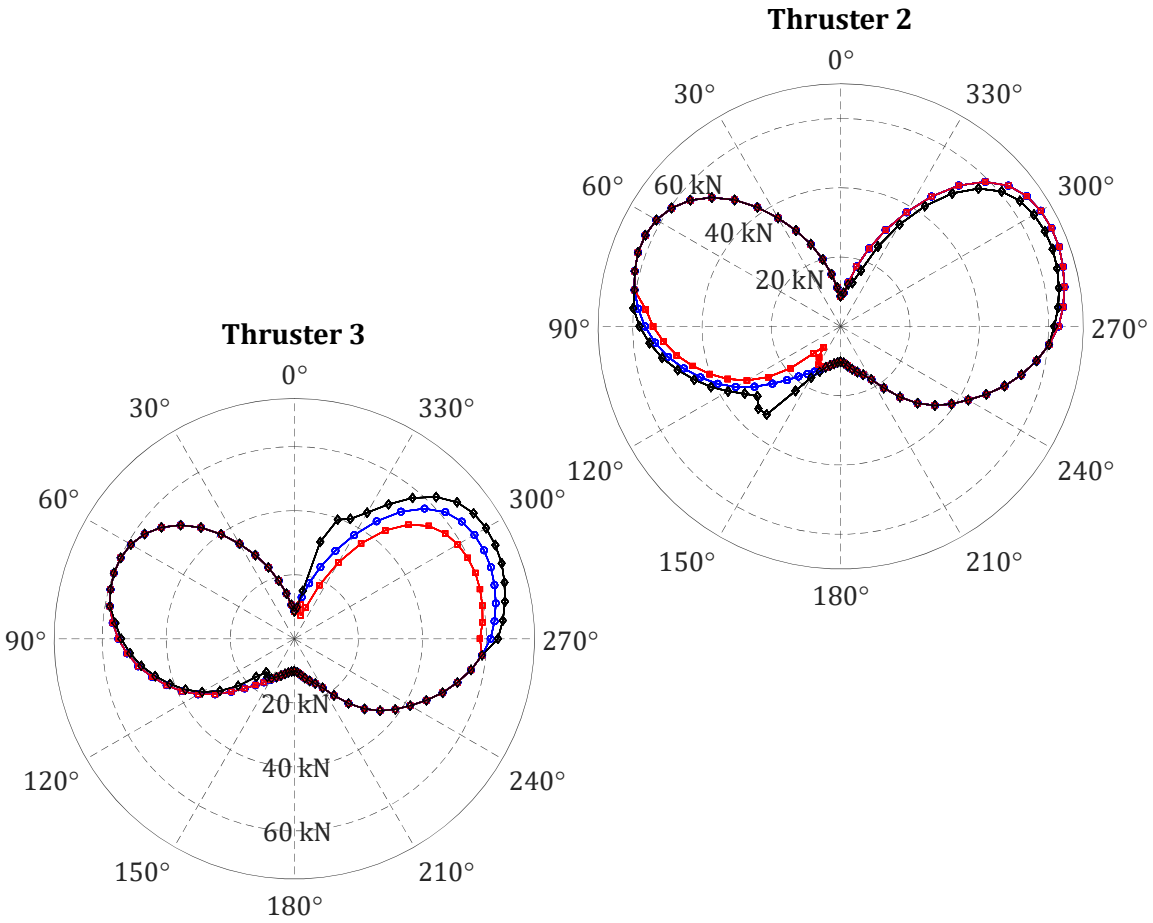

Figure 39. Polar thrust distribution of azimuth thrusters 2 and 3 with respect to the wind angle of attack γ_{wind} and for $V_{wind} = 10$ m/s, $H_s = 3.21$ m, $T_p = 8.41$ s, $V_{curr} = 0.5$ m/s

After the thrust loss estimation had been assessed, the optimal reallocation is performed, which results in an increase in the thrust of the rear thruster in order to compensate its thrust loss. At the same time, thrust of the front thruster slightly decreases. This also applies to all other thrusters, as can be seen in Appendixes 3.1-3.3.

It is important to note that an increase in the thrust to compensate losses is optimally distributed on all available thrusters during the optimal reallocation, i.e. not only with increasing the thrust of the rear thruster. However, one can notice that in the case when thruster 2 is the front one, envelope of thrust losses in terms of γ_{wind} is much wider than in the opposite case. As environmental loads increase, this envelope gradually shrinks, but still covers approximately encounter angles $\gamma_{wind} \in [270°, 360°]$. On the other hand, i.e. in the case when thruster 3 is the front one, this envelope is narrower, with relative exceptions during lower environmental loads. In a case of larger environmental loads, this envelope covers significant wind encounter angles $\gamma_{wind} \in [120°, 150°]$.

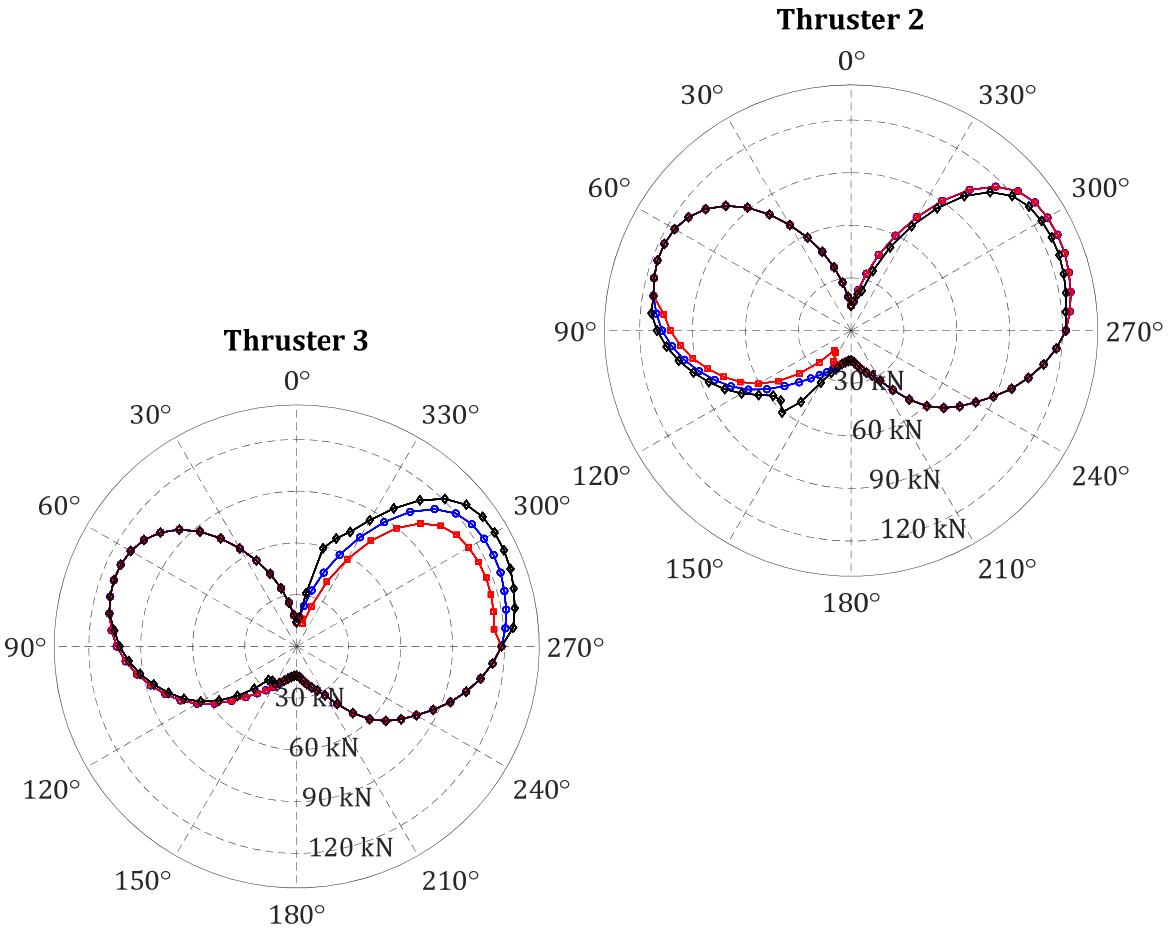

Figure 40. Polar thrust distribution of azimuth thrusters 2 and 3 with respect to the wind angle of attack γ_{wind} and for $V_{wind} = 15$ m/s, $H_s = 5.07$ m, $T_p = 10.56$ s, $V_{curr} = 0.5$ m/s

The reason for this imparity lies in relatively close vicinity of thruster 4, which significantly, but differently contributes to the overall thrust, depending whether thruster 2 or thruster 3 is the front one. Final reallocated state is in equilibrium with environmental loads.

At last, one should notice that this strategy of implementing the trust loss effects within the objective function could be very effective if there is a flexibility regarding the rear thruster, i.e. if it is acceptable to change thrust state of the rear thruster. In many cases, better approach could be in fixing the rear thruster as it is, according the thruster interaction angles and associated thrust loss ratio. On the other hand, as it can be seen in the following sections, this approach withdraws a new issue related to handling of nonlinear and non-convex constraints, which cannot be directly solved by using pseudo inverse, generalized inverse or quadratic programming approaches. In other words, some more advanced nonlinear optimization method should be introduced for handling these issues.

6.3 Forbidden zone handling in optimal thrust allocation

Forbidden zones are usually used in order to avoid or reduce thrust losses due to thruster-thruster or thruster-hull interactions. On the other hand, by defining a forbidden zone for an azimuth thruster, a Pacman like thrust region shape is left over which can consequently cause the significant deviations in allocated thruster azimuth angles and increase the time required for thrust and azimuth allocation. The optimal thrust allocation procedure is usually performed only with forbidden zones included, i.e. without the implementation of thruster-thruster interaction effects. In the next section, a comparative analysis of these two approaches is performed and advantages of optimal thrust allocation without forbidden zones but with implemented thrust loss effects are highlighted.

6.3.1 Generalized inverse matrix approach

The approach presented in Chapter 6.2 results in the two-phase thrust penalization and recuperation of the rear thruster, as well as in optimal redistribution of reallocated thrusts throughout remaining thrusters needed for the compensation of the inevitable losses. Actually, this eliminates the necessity for the implementation of forbidden zones, which consequently could provide smoother allocation without significant fluctuations in azimuth changes of affected thrusters.

With that being said, generalized inverse matrix approach in this section is used as described in Chapter 6.2, i.e. it serves as a method that takes into account thrust losses due to thruster-thruster interactions, but it does not include forbidden zones, as defined in Chapter 4.1.2.2.

6.3.2 Quadratic programming with thruster saturation and forbidden zones included

The quadratic problem that is comparable with the approach from the Chapter 6.2 is based on the QP problem (5.17), and can be modified as follows

$$\left.\begin{aligned} &\min_{\mathbf{u}\in\mathbb{R}^{2r}} \mathbf{u}^{\mathrm{T}}\mathbf{W}\mathbf{u} \\ &\text{s.t.} \quad \mathbf{B}\mathbf{u}-\boldsymbol{\tau}=\mathbf{0} \\ &\qquad \mathbf{C}_{\mathrm{eq}}\mathbf{u}=\mathbf{0} \\ &\qquad \mathbf{A}_i^{\mathrm{TS}}\mathbf{u}_i-\mathbf{b}_i^{\mathrm{TS}}\le\mathbf{0} \\ &\qquad \mathbf{A}_i^{\mathrm{FZ}_{ik}}\mathbf{u}_i-\mathbf{0}_i^{\mathrm{FZ}_{ik}}\le\mathbf{0} \end{aligned}\right\}, \tag{6.21}$$

where $\mathbf{u}^{\mathrm{T}}\mathbf{W}\mathbf{u}$ is the objective function by which one wants to minimize the total power consumption (4.53), i.e. (4.40), with assumption $m_i = 2$, $i = 1, 2, \ldots, r$. Equality constraints $\mathbf{B}\mathbf{u} - \boldsymbol{\tau} = \mathbf{0}$ and $\mathbf{C}_{\mathrm{eq}}\mathbf{u} = \mathbf{0}$ are considered in order to satisfy the equilibrium equation (4.8) and for handling of tunnel thrusters (4.62)-(4.65), respectively. Inequality constraints $\mathbf{A}_i^{\mathrm{TS}}\mathbf{u}_i - \mathbf{b}_i^{\mathrm{TS}} \leq \mathbf{0}$ and $\mathbf{A}_i^{\mathrm{FZ}_{ik}}\mathbf{u}_i - \mathbf{0}_i^{\mathrm{FZ}_{ik}} \leq \mathbf{0}$ are taken into account for handling thruster saturation (4.69)-(4.72) and forbidden zones (4.73)-(4.75).

One can notice that inequality constraints in (6.21) are used in linearized form in order to implement thruster saturation and forbidden zones with QP solver. Analytical terms for description of thrust saturation and thrust region with excluded forbidden zones are highly nonlinear. Moreover, when some portion of the thrust region is taken out one can easily notice that a Pacman like thrust region shape will be left over. Because this shape is in general non-convex, it has to be split up into multiple convex thrust regions and disjunctive programming techniques should be used in order to solve the optimization problem properly. For the purpose of this work, polygon approximation approach described in Chapters 4.1.2.1 and 4.1.2.2 was used and non-convex thrust regions were split into two symmetrical convex regions, as shown in Figure 26, i.e. in Figure 28 (right). Thruster saturation was handled with appropriate linearization technique, as described in Chapter 4.1.2.1.

Thruster saturation can be implemented as a self-standing constraint, but forbidden zones should be implemented in combination with thruster saturation, at least with the (minor or major) arc part of the circular that closes the thrust region of interest, i.e. a sector of a circle related to this constraint.

Thrust loss effects are implemented in the generalized inverse matrix approach by means of the thrust reduction ratio t (3.38), i.e. (3.54). After interaction angles φ and δ are estimated, t is calculated according the model described in Chapter 3.2.2. This means that reduced thrust T from (3.38) can now be easily calculated as

$$T = t\,T_0\,, \tag{6.22}$$

where T_0 is the thrust that would be generated in the case without losses. Equation (6.22) seems to be very simple, but if one wants to convert T in terms of design variables of optimization problem (6.21), relation (6.22) should be transformed in terms of thrust components, which yields

$$u_{ix}^2 + u_{iy}^2 = (t_i\,T_{i0})^2 \tag{6.23}$$

for some *i*-th rear thruster.

Because the right-hand side of (6.23) can be considered constant at some time step, equation (6.23) presents very nonlinear equality, but also non-convex constraint in terms of circular that (6.23) geometrically represents. It is obvious that in this form, (6.23) cannot be a part of optimization problem (6.21). Moreover, it cannot be implemented even with linearization described in Chapter 4.1.2.1. There are two reasons for this. Linearization from Chapter 4.1.2.1 works well for circles, because a circle as a convex thrust region is substituted with N-sided regular polygon, which still preserves convexity. On the other hand, circular is non-convex at the beginning, as well as a geometric shape formed with the set of polygon sides. Even if one tries to implement this linearization approach, a system of dependant linear equations will be formed, which does not make much sense from the optimization point of view. Hence, QP solver is not convenient approach for handling thrust loss effects in form (6.23), and some other nonlinear global optimization solver should be used instead. This is further analysed in Chapter 7.

6.3.3 Numerical example with comparative analysis

As already mentioned, it is a common practice in industrial DP systems to implement the forbidden zones in order to prevent the allocation of azimuth angles that will lead to thruster-thruster interactions. Thus, in this example, QP solver takes into account forbidden zones, while approach based on generalized inverse matrix takes into account thrust losses due to thruster-thruster interactions without forbidden zones.

For the purpose of this example, only azimuth thrusters were used for DP analysis, while the bow thruster was excluded from the thrust allocation. With this approach, results are easily comparable with results from the Chapter 6.2. If required, tunnel thruster(s) can be easily taken into account.

Considering the estimation of thrust losses is previously performed only for thrusters 2 and 3, forbidden zones were implemented only for these two thrusters as well (Figure 34). In Chapter 6.1.3, two cases for thruster 2 - thruster 3 interactions are pointed out, i.e. for azimuth angles $\alpha_2, \alpha_3 \in [30°, 90°]$ and $\alpha_2, \alpha_3 \in [210°, 270°]$. These two intervals also present forbidden zones that are shown in simple form in Figure 41.

In order to implement forbidden zones for thrusters 2 and 3 in a convex manner, splitting of zones was done symmetrically, which yielded with associated starting and ending angles $\varphi_{\text{start}}^{\text{FS}_{ik}}$ and $\varphi_{\text{end}}^{\text{FS}_{ik}}$ (4.74) for feasible sets FS_{ik}, $k = \{1, 2\}$, and for forbidden zones FZ_i, $i = \{2, 3\}$, as follows

(a) For $\alpha_2 \in [30°, 60°]$ $\Rightarrow$ $\varphi_{\text{start}}^{\text{FS}_{21}} = \varphi_{\text{end}}^{\text{FZ}_2} = 60°$ and $\varphi_{\text{end}}^{\text{FS}_{21}} = \varphi_{\text{start}}^{\text{FS}_{22}} = 210°$,

(b) For $\alpha_2 \in [60°, 90°]$ $\Rightarrow$ $\varphi_{\text{start}}^{\text{FS}_{22}} = \varphi_{\text{end}}^{\text{FS}_{21}} = 210°$ and $\varphi_{\text{end}}^{\text{FS}_{22}} = \varphi_{\text{start}}^{\text{FZ}_2} = 360°$,

(c) For $\alpha_3 \in [210°, 240°]$ $\Rightarrow$ $\varphi_{\text{start}}^{\text{FS}_{31}} = \varphi_{\text{end}}^{\text{FZ}_3} = 240°$ and $\varphi_{\text{end}}^{\text{FS}_{31}} = \varphi_{\text{start}}^{\text{FS}_{32}} = 30°$,

(d) For $\alpha_3 \in [240°, 270°]$ $\Rightarrow$ $\varphi_{\text{start}}^{\text{FS}_{32}} = \varphi_{\text{end}}^{\text{FS}_{31}} = 30°$ and $\varphi_{\text{end}}^{\text{FS}_{32}} = \varphi_{\text{start}}^{\text{FZ}_3} = 180°$.

Illustrative example of selection of starting and ending angles $\varphi_{\text{start}}^{\text{FS}_{2k}}$ and $\varphi_{\text{end}}^{\text{FS}_{2k}}$ for the thruster 2, $k = \{1, 2\}$, is shown in Figure 42.

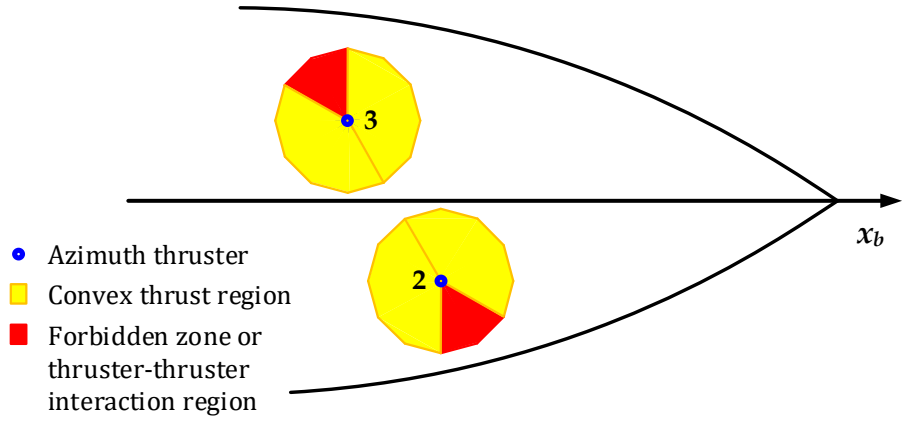

Figure 41. Polygon approximation of thrust regions with forbidden zones for thrusters 2 and 3

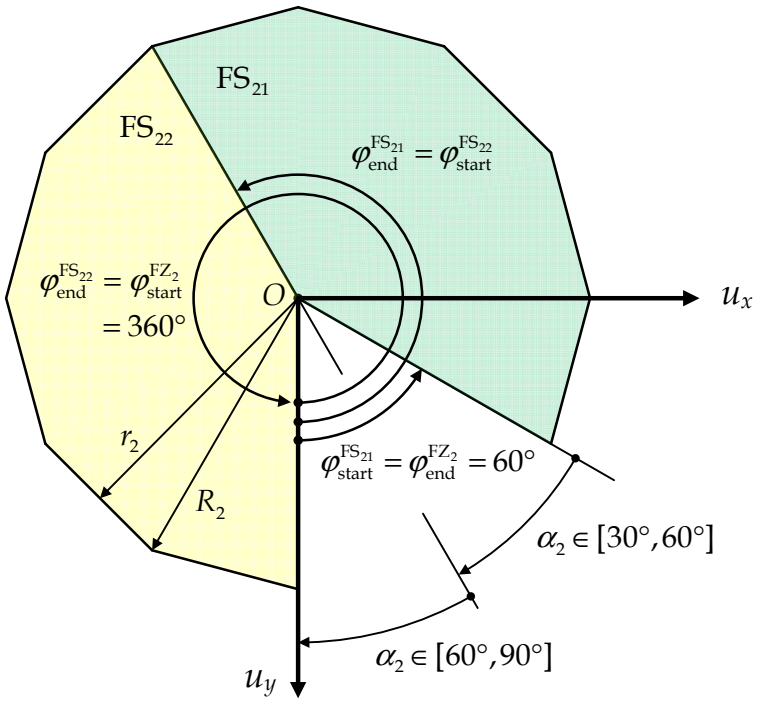

Figure 42. Selection of starting and ending angles $\varphi_{\text{start}}^{\text{FS}_{2k}}$ and $\varphi_{\text{end}}^{\text{FS}_{2k}}$ for thruster 2

Thruster saturation was calibrated in accordance with absolute approximation error Δe_i (4.26) of 1 kN and thruster data from Table 3, so associated minimum number of polygon sides $N_{i,\min}$, $i=2,3,\ldots,7$, was determined as $N_{i,\min}=44$ for $R_i=T_{i,\max}=390$ kN and $i\in\{2,3,4,5\}$, i.e. as $N_{i,\min}=62$ for $R_i=T_{i,\max}=760$ kN and $i\in\{6,7\}$. Thruster weights (4.43) were calculated based on thruster data provided in Table 3.

The effects of forbidden zone handling with quadratic programming approach were analysed for the same cases as for thruster-thruster interactions, i.e. for the same three environmental scenarios defined in Chapter 6.2.5. Analysis in very rough seas and DP capability analysis in extreme cases were omitted in this work because the emphasis was placed on the normal operating conditions up to approximately $H_s=5$ m. As usual, the angle of attack was the same for all disturbances at any time ($\gamma_{wind}=\gamma_{waves}=\gamma_{curr}$) and was varied from $\gamma_{wind}=0°$ to $360°$ with the rate of $1°$.

After all the optimizations were performed, resulting thrusts and azimuth angles showed very similar trends. Some differences are related to thrust magnitudes and interval ranges of cumulative angle of attack but these are dependent on the nature of applied environmental loads. Three optimization approaches were analysed for the same initial conditions. The first one was the generalized inverse matrix (GIM) approach without including any of thrust losses or forbidden zones. The second one was additionally weighted generalized inverse matrix (WGIM) approach in which thrust losses due to thruster 2 – thruster 3 interactions were included, but without taking forbidden zones into account. In this approach, previously described reallocation was implemented as well. Finally, the third one was the quadratic programing (QP) approach with included forbidden zones and thruster saturation, but without thruster-thruster interactions.

Resulting thrusts and azimuth angles for environmental conditions (*a*) and (*c*), as defined in Chapter 6.2.5, are presented in Appendixes 4.1 and 4.2, respectively, while the sample of resulting thrusts and thruster angles for the case (*b*) is shown in Figure 43. Trust variations are presented with solid lines and azimuth angles with dashed lines. Blue lines are related to GIM approach, red lines are related to WGIM approach, but without reallocation, black lines are also related to WGIM approach, but with reallocation, and green lines are related to QP approach without thruster interactions, but with thruster saturation and forbidden zones included. One can notice that there is no evident difference between blue (GIM) and green (QP) lines, with exception around switching from one forbidden zone boundary to another.

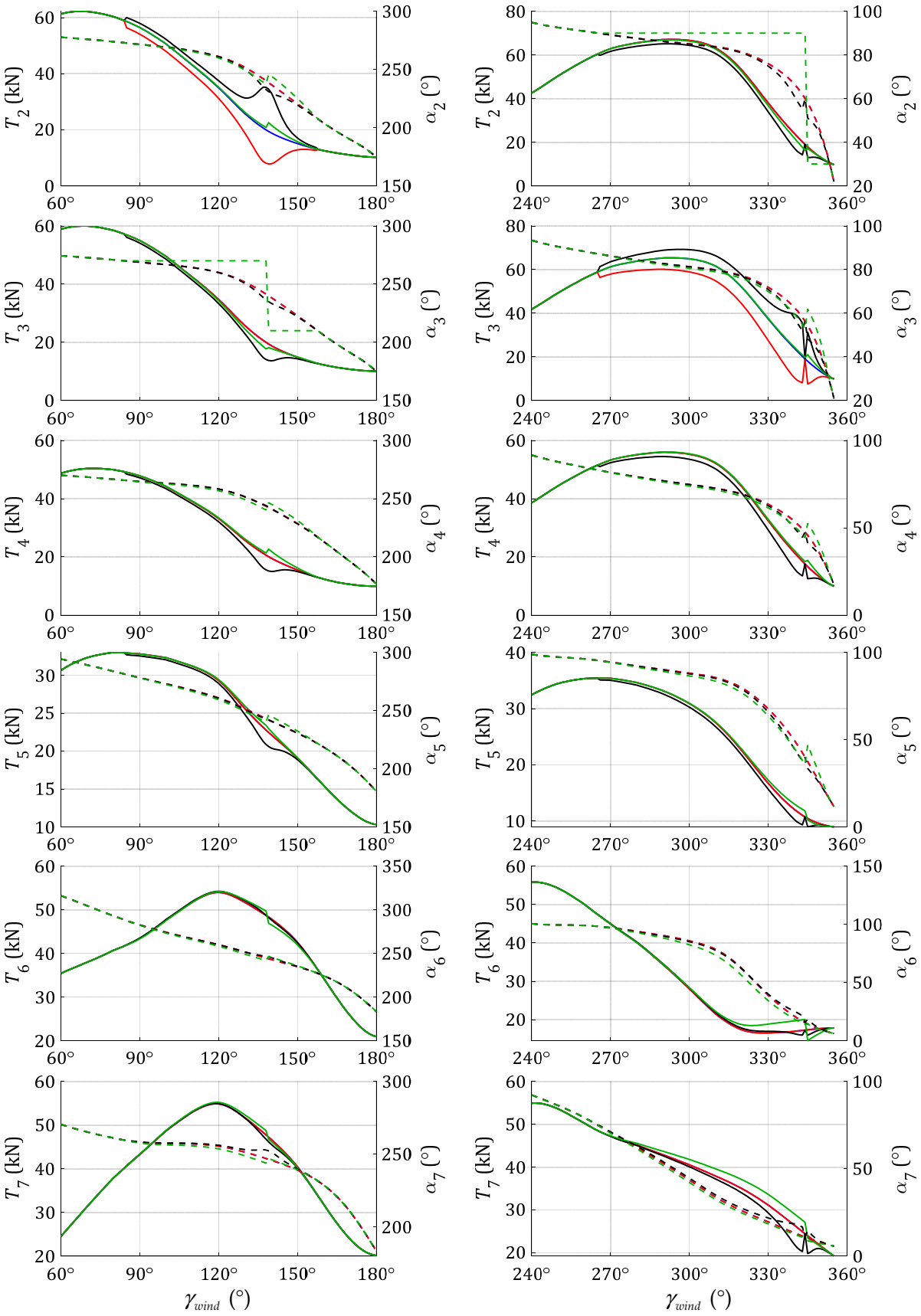

Figure 43. Resulting thrusts and azimuth angles with respect to γ_{wind} for all azimuth thrusters in environmental conditions $V_{wind} = 10$ m/s, $H_s = 3.21$ m, $T_p = 8.41$ s, $V_{curr} = 0.5$ m/s

In Figure 43, as well as in Appendixes 4.1 and 4.2, one can notice interesting anomalies that occur at some critical encounter angle. For instance, in Figure 43 this is particularly related to thruster 3 when $\gamma_{wind} = 344°$, i.e. when thruster 3 is the rear thruster. This thrust variation reflects to other thrusters during optimal thrust reallocation, although in practical applications all these anomalies should be filtered out. On the other hand, it is interesting to notice that this anomaly cannot be seen in associated Figure 39 because in that case encounter angle γ_{wind} was varied with the rate of $5°$, and thus anomaly could not be captured.

Updated overview of results from Figure 39, with added results of QP approach, is shown in Figure 44. Similarly like in the previous Figure 43, blue lines denotes GIM approach, red lines WGIM approach without reallocation, black lines WGIM approach with reallocation, and green lines QP approach without thruster interactions, but with thruster saturation and forbidden zones included.

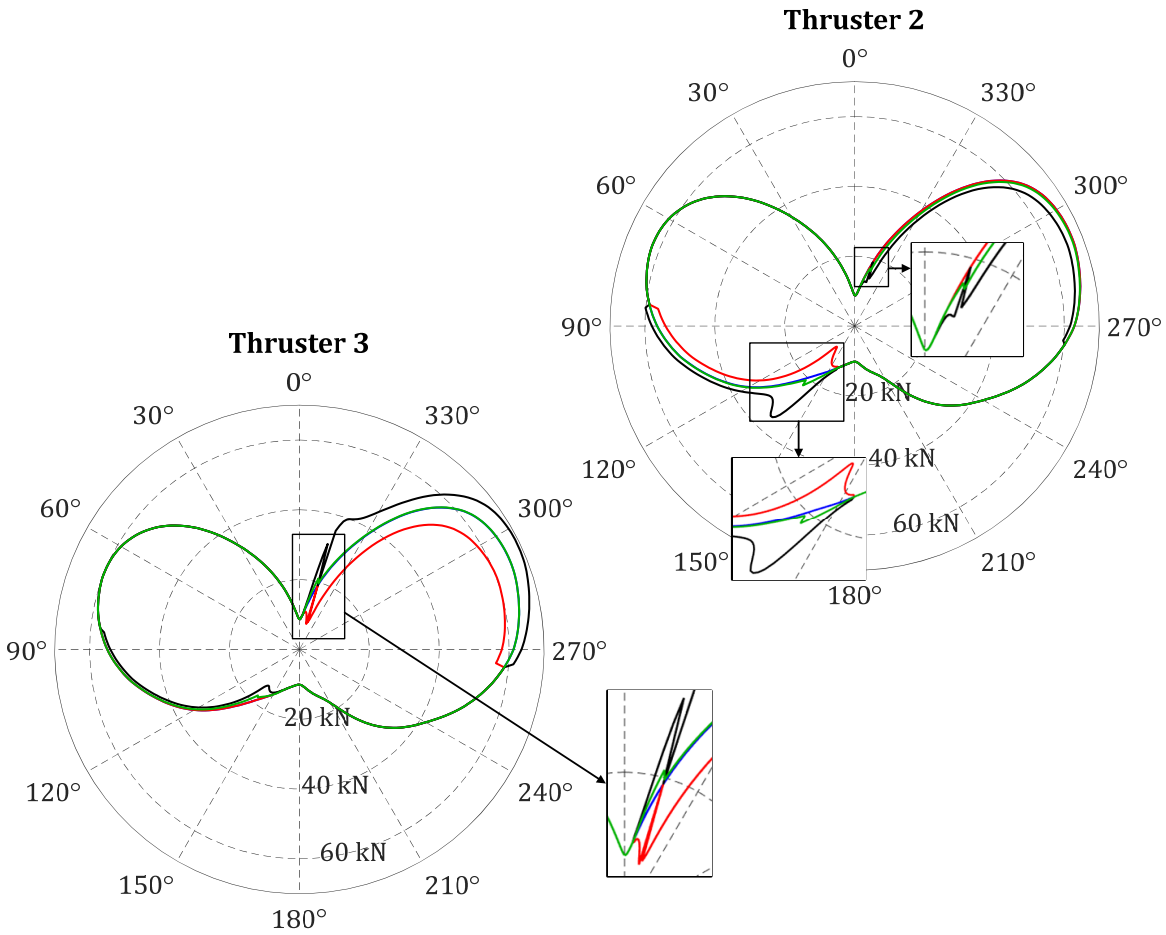

Figure 44. Polar thrust distribution of azimuth thrusters 2 and 3 with respect to the wind angle of attack γ_{wind} and for $V_{wind} = 10$ m/s, $H_s = 3.21$ m, $T_p = 8.41$ s, $V_{curr} = 0.5$ m/s

As additional comments for Figure 43 and Appendixes 4.1 and 4.2, one can notice that GIM approach without thrust losses results with the smoothest curves, both for thrusts (blue solid line) and azimuth angles (blue dashed line), which is completely reasonable because this approach did not take any constraints into account. Thus, this approach can serve as a referent optimization approach for comparison of the other two.

If one analyse the results obtained for $\gamma_{wind} = [0°, 360°]$, it can be noticed that the azimuth angles of both front and rear thrusters change quite smoothly during the thruster-thruster interactions (black dashed line), which will ensure minimum tear and wear. On the other hand, the azimuth angles of the same thrusters within the forbidden zones (green dashed line) have angle saturations α_3 at $210°$ and $270°$, i.e. α_2 at $30°$ and $90°$. At the same time, the thrust magnitudes of front thrusters decrease and the thrust magnitudes of rear thrusters increase, both with thrust losses implemented (black solid line) and forbidden zones included (green solid line).

Although it seems that the thrust magnitude increase/decrease is much larger in a case of thruster-thruster interactions, this should be analysed with additional precaution. Namely, azimuth thruster #2 with forbidden zones included can switch from $\alpha_2 = 30°$ to $\alpha_2 = 90°$, or vice versa, only by rotation of $300°$ in the opposite direction. No matter what the yaw rate of the thruster 2 is, the time required for that rotation will be 5 times longer with respect to the case without forbidden zones included. During that rotation, thruster will be far away from the optimum performance and therefore the optimization solver should exclude that thruster from the thrust allocation. When this occurs, decreased thrust of the thruster 2 should be compensated with increased generated thrust of other thrusters in a way similar to the reallocation procedure with thruster-thruster interactions (Valčić et al., 2014). These large deviations in thrust magnitudes and azimuth angles will significantly increase the wear and tear of the thruster 2, which is in contradiction with the basic goals of a DP system design philosophy. Very similar conclusions can be applied for other cases, as well as when the thrusters 2 and 3 change their roles of front and rear thruster. All other thrusters are adjusted to thrusters 2 and 3 in order to compensate the total environmental loads.

The effect of forbidden zones and thruster-thruster interactions on total demanded power for the analysed reference vessel is closely related to intensity of environmental loads. A sample of total demanded minimum power for GIM approach without thrust

losses included (P_{GIM}), for the WGIM approach with thrust reallocation (P_{WGIM}), and for the QP approach with forbidden zones included (P_{QP}), is shown in Figure 45.

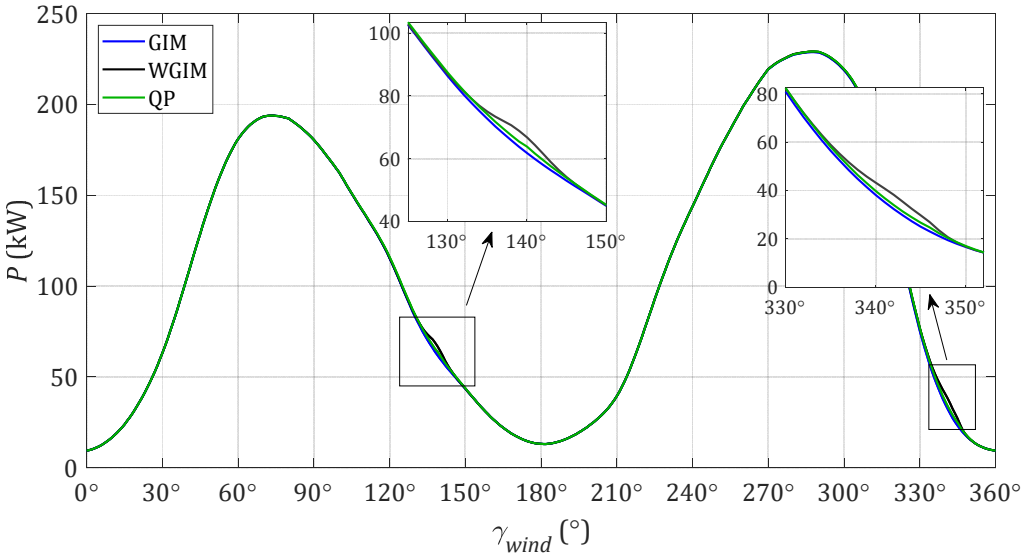

Figure 45. Total demanded minimum power for all azimuth thrusters with respect to the wind angle of attack γ_{wind} and for $V_{wind} = 10$ m/s, $H_s = 3.21$ m, $T_p = 8.41$ s, $V_{curr} = 0.5$ m/s

The only observable deviations in power consumption are around before mentioned regions of forbidden and thruster-thruster interaction zones. In order to present these deviations in more quantitative manner, characteristic ranges of the wind encounter angle γ_{wind} are identified and presented with intervals $[\gamma_{wind,\min}(\delta P), \gamma_{wind,\max}(\delta P)]$. Boundaries of these intervals are determined according to the relative deviations δP of demanded power values P_{WGIM} and P_{QP} with respect to the referent power demand P_{GIM}. Thus, these intervals are of interest only for values of wind encounter angle γ_{wind} that meet the following criteria

$$\left.\begin{aligned} \delta P_{\mathrm{WGIM}}(\gamma_{wind}) &= (P_{\mathrm{WGIM}} - P_{\mathrm{GIM}}) / P_{\mathrm{GIM}} > \varepsilon \\ \delta P_{\mathrm{QP}}(\gamma_{wind}) &= (P_{\mathrm{QP}} - P_{\mathrm{GIM}}) / P_{\mathrm{GIM}} > \varepsilon \end{aligned}\right\} \tag{6.24}$$

where the threshold value of $\varepsilon = 10^{-3}$ (0.1 %) was selected arbitrarily. If required, value of ε can be easily changed or tuned in order to meet any particular criteria.

However, in this way, only the most meaningful deviations in power demand are taken into account in order to investigate the differences between analysed optimization approaches. Calculated quantitative indicators for all three cases (*a*), (*b*) and (*c*), as defined in Chapter 6.2.5, are presented in Table 5, both when thruster 2 is the front one, and when thruster 3 is the front one. Power mean values $\mu(P)$ and power

standard deviations $\sigma(P)$ are calculated within the intervals determined according to (6.24). Relative deviations (6.24) of total demanded minimum power δP_{WGIM} and δP_{QP} for all azimuth thrusters with respect to wind encounter angle γ_{wind} and different optimization approaches are shown in Figure 46. Previously detected anomalies, like those in e.g. Figures 43 and 44, have been filtered out for the purpose of power demand calculation and analysis.

Table 5. Quantitative indicators of demanded power for analysed cases (*a*)-(*c*) obtained with WGIM and QP optimization approaches for thrusters 2 and 3

Optimization	Key variables	Front thruster	Case (*a*)	Case (*b*)	Case (*c*)
WGIM approach	$[\gamma_{wind,\min}(\delta P), \gamma_{wind,\max}(\delta P)]$	2	[276°, 347°]	[283°, 351°]	[287°, 353°]
		3	[116°, 143°]	[117°, 151°]	[116°, 155°]
	$\gamma_{wind,\text{peak}}$	2	335°	342°	345°
		3	133°	139°	141°
	$\delta P_{\text{peak}}(\gamma_{wind,\text{peak}})$	2	0.1641	0.1893	0.1952
		3	0.0530	0.0802	0.0956
	$\mu(P)$	2	0.0313	0.0298	0.0285
		3	0.0175	0.0211	0.0236
	$\sigma(P)$	2	0.0490	0.0529	0.0531
		3	0.0187	0.0261	0.0301
QP approach	$[\gamma_{wind,\min}(\delta P), \gamma_{wind,\max}(\delta P)]$	2	[269°, 349°]	[285°, 352°]	[295°, 353°]
		3	[103°, 146°]	[102°, 154°]	[101°, 158°]
	$\gamma_{wind,\text{peak}}$	2	337°	345°	347°
		3	135°	139°	142°
	$\delta P_{\text{peak}}(\gamma_{wind,\text{peak}})$	2	0.0724	0.0716	0.0762
		3	0.0187	0.0330	0.0384
	$\mu(P)$	2	0.0168	0.0160	0.0163
		3	0.0067	0.0100	0.0119
	$\sigma(P)$	2	0.0172	0.0185	0.0192
		3	0.0051	0.0085	0.0105

One can notice that the peak encounter angle $\gamma_{wind,\text{peak}}$ increases when environmental loads increase. At the same time, the regions expressed in terms of γ_{wind} and defined according to (6.24) becomes narrower and shifted more to the right, which means that peaks in power demand will be related to some narrow margin and will correspond to

smaller wind encounter angles as environmental loads become larger. Peak power deviations (δP_{peak}) also increase with increased environmental loads, but the maximum and other significant adjacent values corresponds only to some narrow interval of wind encounter angles that can be easily avoided by means of penalization, if required. Although these conclusions can be applied only to the reference vessel analysed in this work, and are valid only for analysed cases, they present a very convenient guidelines for defining more appropriate strategies in position and heading control, particularly in case of weathervaning or near weathervaning mode when $\gamma_{wind} \to 0°$.

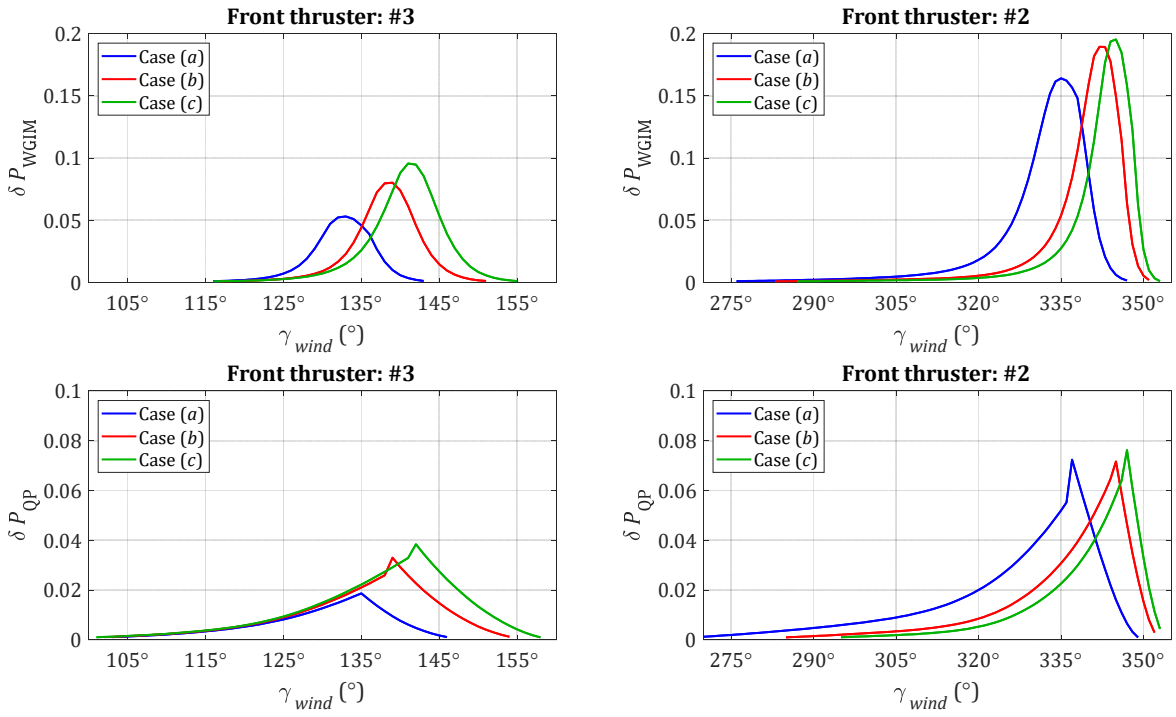

Figure 46. Relative deviations of total demanded minimum power for thrusters 2 and 3 regarding different optimization approaches

Finally, it is important to point out that results related to QP approach with forbidden zones included are presented in a way as the thruster can switch from one saturated azimuth angle to another instantly, which is of course not possible. Therefore, these results should be considered with caution and keeping in mind that the real power consumption will be more increased in real applications when forbidden zones are included.

7 NONLINEAR OPTIMIZATION OF THRUST ALLOCATION

7.1 Considerations about nonlinear optimal thrust allocation

In terms of objective functions, nonlinear optimization provides a much wider commodity in modelling of power-thrust relationship, which is particularly important when assumption of quadratic or linear relation between demanded power and generated thrust is neither sufficient nor acceptable. The same applies for numerous nonlinear or even non-convex constraints that one has within the thrust allocation problem.

7.1.1 Compatibilities and disparities of gradient based and derivative free optimization algorithms

As already mentioned in Chapter 5, gradient-based optimization algorithms like SQP have a prerequisite on the objective function to be smooth and twice-continuously differentiable. Power consumption as a function of generated thrust (4.39) is exactly that, convex, smooth and twice-continuously differentiable. However, this stands as long as propeller operates in the first quadrant, which is one of assumptions taken into account in this work. In other words, if one model the relationship between power and thrust like in (4.39), gradient-based SQP algorithm will have significant advantage in comparison with direct search algorithms like GSS or MADS, particularly in terms of computational time and convergence speed. This is completely reasonable considering SQP is widely acknowledged as the most successful algorithm available for solving smooth nonlinear programming problems. However, one should notice that SQP is not a single algorithm, but rather a conceptual method from which numerous specific algorithms have evolved (Boggs and Tolle, 1995). On the other hand, the main advantage of direct search algorithms in terms of objective functions is related to the fact that power-thrust relationship does not necessarily have to be explicitly defined, smooth, twice-continuously differentiable or convex. Although this is a great advantage, this aspect was not analysed in this work considering the real nature of power-thrust relationship.

SQP is generally classified in literature as a local optimization method, but one should notice that whilst the complete optimization problem is defined as convex, SQP would converge to local minimum, which is also a global minimum for that convex optimization problem. In general, it is very hard to guarantee the global optimum,

unless the problem is convex, as already emphasized. This is particularly problematic when adding thruster interaction effects in terms of (6.23), which present relatively simple, but still highly nonlinear and generally non-convex constraints. Consequently, the complete optimization problem now becomes non-convex and local optimizers like SQP cannot guarantee the global optimum anymore. When this kind of problem occurs, global optimization algorithms like direct search algorithms can be used in order to find global optimum with higher probability in comparison with local optimizers that can stuck in some local optimum instead.

Convergence speed of optimization algorithms is of a great importance for industrial DP systems, i.e. for real time applications. For that matter, direct search algorithms are generally less favourable in comparison with SQP, particularly if the problem is convex. For non-convex optimization, which is important in this work for implementing thruster interaction effects, direct search algorithms can provide global optimum, but generally in unacceptably long time. Therefore, they are mainly used in this work as a support for local optimizers in finding global minimum for any environmental state. In order to realise this concept, appropriate hybrid approach is proposed.

No matter which algorithm is selected for solving a problem of optimal thrust allocation, preparation of objective functions with associated constraints and boundaries is practically the same for both gradient-based and direct search algorithms. This is very important from the computational implementation point of view; because once objective function and constraints are prepared, they can be used in the same form for any of the mentioned algorithms. In this chapter, optimal thrust allocation was also performed using MATLAB R2018b (The MathWorks, 2018).

7.1.2 Power consumption as a nonlinear objective function

In the case of optimal thrust allocation, nonlinear objective function is the power consumption that can be defined based on (4.2), (4.39), (4.40) and (4.42) as

$$P(\mathbf{u}) = \sum_{i=1}^{r} w_i (u_{ix}^2 + u_{iy}^2)^{\frac{m_i}{2}}, \tag{7.1}$$

where thrust weighting coefficients w_i are defined as in (4.43). So far assumptions where that $m_i = 2,\ i = 1, 2, \ldots, r,$ in order to ensure objective function to be quadratic. However, this assumption is in contradiction with usual values of m_i, which are usually from the interval $1.3 < m_i < 1.7$ (Leavitt, 2008; Wit, 2009).

If one assumes that $m_i = 3/2,\ i = 1,2,\ldots,r,$ which presents the usual assumption for nonlinear power-thrust relationship (Leavitt, 2008; Wit, 2009), than (7.1) can be rewritten as

$$P(\mathbf{u}) = \sum_{i=1}^{r} w_i (u_{ix}^2 + u_{iy}^2)^{\frac{3}{4}}, \tag{7.2}$$

and associated weights w_i become

$$w_i = \frac{P_{i,\max}}{(T_{i,\max})^{3/2}}. \tag{7.3}$$

where maximum power values $P_{i,\max}$ and maximum thrust values $T_{i,\max}$ are predefined, as in e.g. Table 3.

Alternative approach to (7.1) or (7.2) can be based on (4.45), i.e. (4.46). In this case, objective function will remain as in (4.46), but with the thrust weighting coefficients in the form as defined in (4.47).

Assumptions $m_i = 2$ for QP solvers and $m_i = 3/2$ for SQP/DS algorithms have significantly different impact on the overall power-thrust relationship, as well as on further analyses and conclusions. This is best seen from the Figure 47, in which one can easily notice the difference ΔP in amount of power P (kW) required for some arbitrarily chosen thrust T (kN) in cases $m_i = 2$, i.e. $m_i = 3/2$. Larger exponent m_i withdraws lesser power consumption, which could be very inconvenient in control of power management system (PMS).

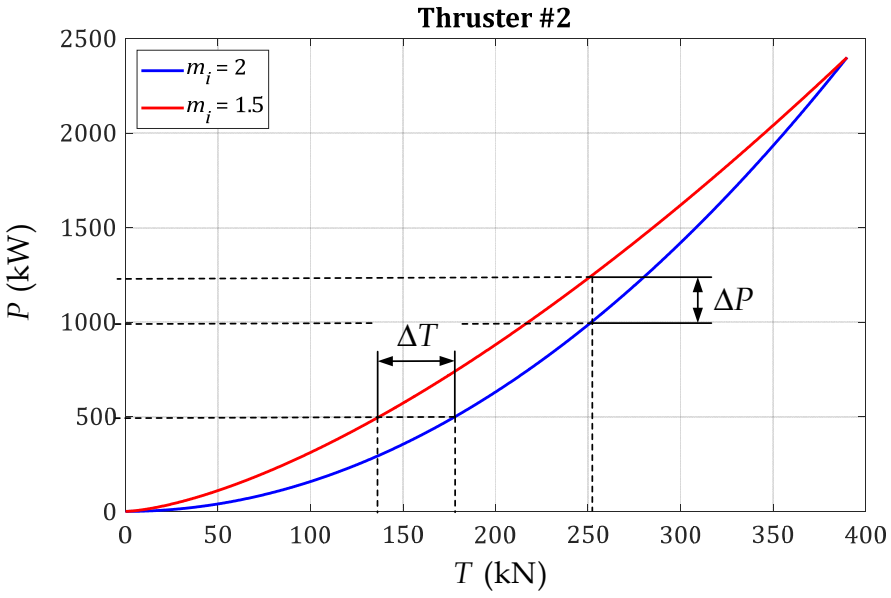

Figure 47. Illustration of power-thrust relationship for thruster 2 (Table 3)

Analogous conclusions can be drawn for the difference ΔT in amount of generated thrust T (kN) for some equally delivered power in cases $m_i = 2$ and $m_i = 3/2$. In this instance, larger exponent m_i withdraws generation of larger thrust, which should be kept in mind during power distribution.

In comparison with the previous chapter, equality and inequality constraints are mixed up in nonlinear optimization. Thus, they could be divided into nonlinear and linear inequality constraints cumulatively related to thruster saturation and forbidden zones, nonlinear and non-convex equality constraints related to implementation of thruster interaction effects, and linear equality constraints related to equilibrium equation and handling of tunnel thrusters. It is important to emphasize that no additional linearization is required for these constraints. Bounds may be included, but with thruster saturation, they might be unnecessary.

7.1.3 Nonlinear inequality constraints for thruster saturation and handling of forbidden zones

In nonlinear optimization, there is no need for additional linearization of thrust circular shapes by means of polygonal approximations. In other words, thruster saturation can be embedded directly (Figure 24) in terms of nonlinear inequality (4.11) as

$$u_{ix}^2 + u_{iy}^2 \leq T_{i,\max}^2, \tag{7.4}$$

where maximum thrusts $T_{i,\max}$ are known in advance (Table 3). On the other hand, forbidden zones should be combined with appropriate half planes in order to cut out appropriate circle sectors that define forbidden zone or feasible sets FS_{ik} (Figure 26). This means that forbidden zones in nonlinear optimization should be implemented both with nonlinear constraint (7.4) and with appropriate linear inequality constraints (4.35) of the following form

$$\begin{bmatrix} -\cos\varphi_{\text{start}}^{\mathrm{FS}_{ik}} & \sin\varphi_{\text{start}}^{\mathrm{FS}_{ik}} \\ \cos\varphi_{\text{end}}^{\mathrm{FS}_{ik}} & -\sin\varphi_{\text{end}}^{\mathrm{FS}_{ik}} \end{bmatrix} \begin{bmatrix} u_{ix} \\ u_{iy} \end{bmatrix} \leq \begin{bmatrix} 0 \\ 0 \end{bmatrix} \tag{7.5}$$

where $k = \{1, 2\}$, if one has two disjunctive convex feasible sets FS_{i1} and FS_{i2}.

In this way, feasible thrust region looks like in Figure 28 (left), rather than linearized thrust region shown in Figure 28 (right). Moreover, with this approach there is no any approximation error like (4.26) or (4.27), because complete thrust region is now taken into account, without negligence of small circle segments.

In computational sense, there is a significant difference when implementing nonlinear constraints in comparison with linear constraints. Namely, for linear constraints, it is sufficient to rewrite all of them in one compact matrix form, and for nonlinear constraints, one should write appropriate function that will be called by the solver at each time step. That being said, linear inequality constraints (7.5) should be prepared in matrix form, while nonlinear inequality constraints (7.4) should be prepared separately in a form of additional function. In case of MATLAB implementation, this function is called as anonymous one. Implementations in other software packages could have slightly different approach, but all of them are very similar in practice.

7.1.4 Nonlinear and non-convex equality constraints for handling of thruster interaction effects

Disjunctive programming approach is practically two-step optimization in which at first step optimization is performed without considering forbidden zones, and after the necessity for implementation of forbidden zones is validated, they are taken into account in terms of associated feasible sets FS_{i1} or FS_{i2}. Similar two-step optimization should be applied when one wants to implement thrust interaction effects in terms of thrust reduction ratios (3.38).

At the first step, optimization should be performed without considering thruster interaction effects, and after possible interaction is confirmed, based on estimated thrust interaction angles ϕ and δ, thrust reduction ratio t can be easily calculated, as well as the thrust

$$T_{i0} = \sqrt{u_{i0x}^2 + u_{i0y}^2}\,, \tag{7.6}$$

of the rear thruster in conditions without forbidden zones and interaction effects included, where u_{i0x} and u_{i0y} denote thrust components of the rear thruster in that case. In the intermediate step, reduced thrust T of the rear thruster can be easily calculated according to (3.38), (3.54) and (7.6) as

$$T_i = t_i\, T_{i0} = t_i \sqrt{u_{i0x}^2 + u_{i0y}^2}\,. \tag{7.7}$$

However, equation (7.7), i.e. the resultant thrust of the rear thruster, is not sufficient in order to obtain overall optimal solution in the second step. The reason for this lies in a fact that thrust components u_{ix} and u_{iy} of the thrust T_i are still not known, and azimuth

angle based on these components could be different in comparison with the one based on components u_{i0x} and u_{i0y}. For this reason, one should transform (7.7) as

$$u_{ix}^2 + u_{iy}^2 = (t_i T_{i0})^2 = t_i^2 (u_{i0x}^2 + u_{i0y}^2) \tag{7.8}$$

and handle (7.8) as nonlinear equality constraint in the second step of optimization procedure. The right-hand side of (7.8) is unknown in the first optimization step, but it is known and it is constant in the second step. However, variables u_{ix} and u_{iy} on the left-hand side of (7.8) are part of design vector $\mathbf{u} = [u_{1x}, u_{1y}, \ldots, u_{ix}, u_{iy}, \ldots, u_{rx}, u_{ry}] \in \mathbb{R}^{2r}$, and besides being included in the objective function, these variables should also be passed as input arguments to the appropriate function that handles nonlinear constraints during computational conduction of optimization procedure. If thruster interaction angles significantly differ after reallocation in the second step, some appropriate iteration procedure could be implemented as well.

In this 2-step optimization, one should also take into account what thruster is the front one and which one is the rear one. However, this can be easily determined using thruster azimuth angles calculated at the first step of optimization.

Linearization of (7.8) in terms of polygon approximation does not have much sense in this case, mostly because with this approach one nonlinear equality constraint (7.8) will be just transformed to one large linear system of mutually dependent equations, which will consequently supress and prevent the solver in converging towards the optimum solution.

In the WGIM approach (Chapter 6.2.3), thrust interaction effects were implemented by means of enhanced weighting matrix $\mathbf{W}$. Hence, implementation was conducted through the appropriate modification of the objective function. As result of this approach, optimal reallocation increased the thrust of the rear thruster, while other thrusters were negligible varied, as can be seen in Figures 38-40.

With previously presented approach of implementing thrust interactions by means of nonlinear equality constraint, i.e. almost independently of the objective function, rear thruster will be penalized according to the thruster interaction angles and associated thrust reduction ratio. All other thrusters will be optimally reallocated in order to compensate current environmental loads. One can conclude that this approach is more reasonable than the WGIM, mostly because it does not put additional strain on the rear thruster, which already operates in not so favourable conditions of the front thruster slipstream.

7.1.5 Linear equality and inequality constraints

Similarly like in Chapter 6.3.2, i.e. for the implementation with QP solver, linear equality constraints $\mathbf{Bu}-\boldsymbol{\tau}=\mathbf{0}$ and $\mathbf{C}_{\text{eq}}\mathbf{u}=\mathbf{0}$ are also considered in this section in order to satisfy the equilibrium equation (4.8) and for handling of tunnel thrusters (4.62)-(4.65), respectively. Linear inequality constraints (7.5) for partial handling of forbidden zones have been already discussed in Chapter 7.1.3, as they are inextricably connected with nonlinear thruster saturation (7.4).

7.2 Nonlinear optimal thrust allocation

7.2.1 Problem definition and two-step solution approach

In general, nonlinear optimization problem of thrust allocation can be rewritten according to (5.1) as

$$\left.\begin{aligned}\mathbf{u}^{*} &= \arg\min_{\mathbf{u}\in\mathbb{R}^{2r}}(P)\\ \text{s.t.}\quad h_i(\mathbf{u}) &= 0\\ g_j(\mathbf{u}) &\le 0\\ \mathbf{l}_B \le \mathbf{u} &\le \mathbf{u}_B\end{aligned}\right\} \tag{7.9}$$

where $\mathbf{u}\in U$ and $U=\{\mathbf{u}\in\mathbb{R}^{2r}\,|\,h_i(\mathbf{u})=0,\ i=1,2,...,p;\ g_j(\mathbf{u})\le 0,\ j=1,2,...,q\}$ presents a set of feasible thrust region that depends both on equality and inequality constraints $\mathbf{h}(\mathbf{u})=[h_1(\mathbf{u})\quad h_2(\mathbf{u})\ ...\ h_p(\mathbf{u})]^{\mathrm{T}}$ and $\mathbf{g}(\mathbf{u})=[g_1(\mathbf{u})\quad g_2(\mathbf{u})\ ...\ g_q(\mathbf{u})]^{\mathrm{T}}$, respectively, $\mathbf{l}_B$ and $\mathbf{u}_B$ are lower and upper boundaries of $\mathbf{u}$, P is twice-continuously differentiable power function, $\mathbf{u}=[u_{1x},u_{1y},...,u_{ix},u_{iy},...,u_{rx},u_{ry}]^{\mathrm{T}}\in\mathbb{R}^{2r}$ is a design vector of thrust components expressed in Cartesian coordinates, and $\mathbf{u}^{*}$ presents an optimal solution in terms of design vector $\mathbf{u}$.

Considering optimal thrust allocation with implemented forbidden zones or thruster interaction effects should be conducted as previously described 2-step optimization procedure, one should differ separable optimization tasks for each step. The first step is always the same, and it takes into account only nonlinear constraint related to thruster saturation. Hence, for some objective power function $P(\mathbf{u})$ of the form (7.2), with associated nonlinear inequality constraints (7.4), and with linear equality

constraints related to equilibrium equation (4.8) and tunnel thrusters (4.62)-(4.65), one can redefine (7.9) for $m_i = 1.5$ as

$$\left.\begin{aligned} \mathbf{u}^* = \arg\min_{\mathbf{u}\in\mathbb{R}^{2r}} & \left(\sum_{i=1}^{r} w_i (u_{ix}^2 + u_{iy}^2)^{\frac{3}{4}} \right) \\ \text{s.t.} \quad & \mathbf{B}\mathbf{u} - \boldsymbol{\tau} = \mathbf{0} \\ & \mathbf{C}_{\text{eq}}\mathbf{u} = \mathbf{0} \\ & u_{ix}^2 + u_{iy}^2 \le T_{i,\max}^2 \end{aligned}\right\} \tag{7.10}$$

where $i = 1, 2, \ldots, r$. This first optimization step is also the same regardless of whether one uses gradient based (SQP) or direct search algorithms (GPS/GSS/MADS) for finding the optimal solution.

Alternative approach based on (4.45), in which the relationship between delivered power and generated thrust is based on thrust and torque coefficients, is very similar to (7.10). The only difference is in the form of objective function, while all constraints are the same. In this case, nonlinear optimization problem can be defined as

$$\left.\begin{aligned} \mathbf{u}^* = \arg\min_{\mathbf{u}\in\mathbb{R}^{2r}} & \left(\sum_{i=1}^{r} \frac{2\pi K_{Q0,i}}{D_i K_{T0,i} \sqrt{\rho K_{T0,i}}} (u_{ix}^2 + u_{iy}^2)^{\frac{3}{4}} \right) \\ \text{s.t.} \quad & \mathbf{B}\mathbf{u} - \boldsymbol{\tau} = \mathbf{0} \\ & \mathbf{C}_{\text{eq}}\mathbf{u} = \mathbf{0} \\ & u_{ix}^2 + u_{iy}^2 \le T_{i,\max}^2 \end{aligned}\right\} \tag{7.11}$$

where $K_{T0,i}$ and $K_{Q0,i}$ are the thrust and torque coefficients at bollard pull conditions, D_i is the propeller diameter, ρ is the water density, and $i = 1, 2, \ldots, r$.

After (7.10) or (7.11) had been evaluated, it is easy to perform analysis of feasible sets FS_{ik}, $k \in \{1, 2\}$, in order to obtain feasible set boundary angles $\varphi_{\text{start}}^{\mathrm{FS}_{ik}}$ and $\varphi_{\text{start}}^{\mathrm{FS}_{ik}}$. The same applies to analysis of thruster interaction effects that are related to thruster azimuth angles α_i calculated in the first step of optimization procedure, and which are essential for determination of thruster interaction angles ϕ and δ. Any of these requirements can be added into optimization tasks. However, depending on what is of particular interest to be implemented, one should differ two independent second step constraints. The first one is related to forbidden zone half-planes (4.73), and the second one is related to thrust interaction effects expressed in terms of thrust reduction ratio (7.6)-(7.8). With that being said, the second step of optimization procedure, with two disjunctive second step constraints, can be rewritten as an enhancement of (7.10) in the following form

$$
\left.
\begin{aligned}
\mathbf{u}^{*} = \underset{\mathbf{u}\in\mathbb{R}^{2r}}{\arg\min} & \left(\sum_{i=1}^{r} w_i (u_{ix}^2 + u_{iy}^2)^{\frac{3}{4}} \right) \\
\text{s.t.} \quad & \mathbf{b}_{\text{eq}} - \mathbf{A}_{\text{eq}}\mathbf{u} = \mathbf{0} \\
& \mathbf{A}_i^{\text{FZ}_{ik}} \mathbf{u}_i \le \mathbf{0}_i^{\text{FZ}_{ik}} \quad \text{or} \quad u_{ix}^2 + u_{iy}^2 = (t_i\, T_{i0})^2 \\
& u_{ix}^2 + u_{iy}^2 \le T_{i,\max}^2
\end{aligned}
\right\} \tag{7.12}
$$

where $\mathbf{A}_{\text{eq}}$ and $\mathbf{b}_{\text{eq}}$ are defined as (4.67) and (4.68), respectively, $\mathbf{A}_i^{\text{FZ}_{ik}}$ and $\mathbf{0}_i^{\text{FZ}_{ik}}$ are defined as (4.74) and (4.75), respectively, thrust reduction ratio t_i and thrust T_{i0} (7.6) of the i-th rear thruster are calculated in the intermediate step, as shown in Figure 48.

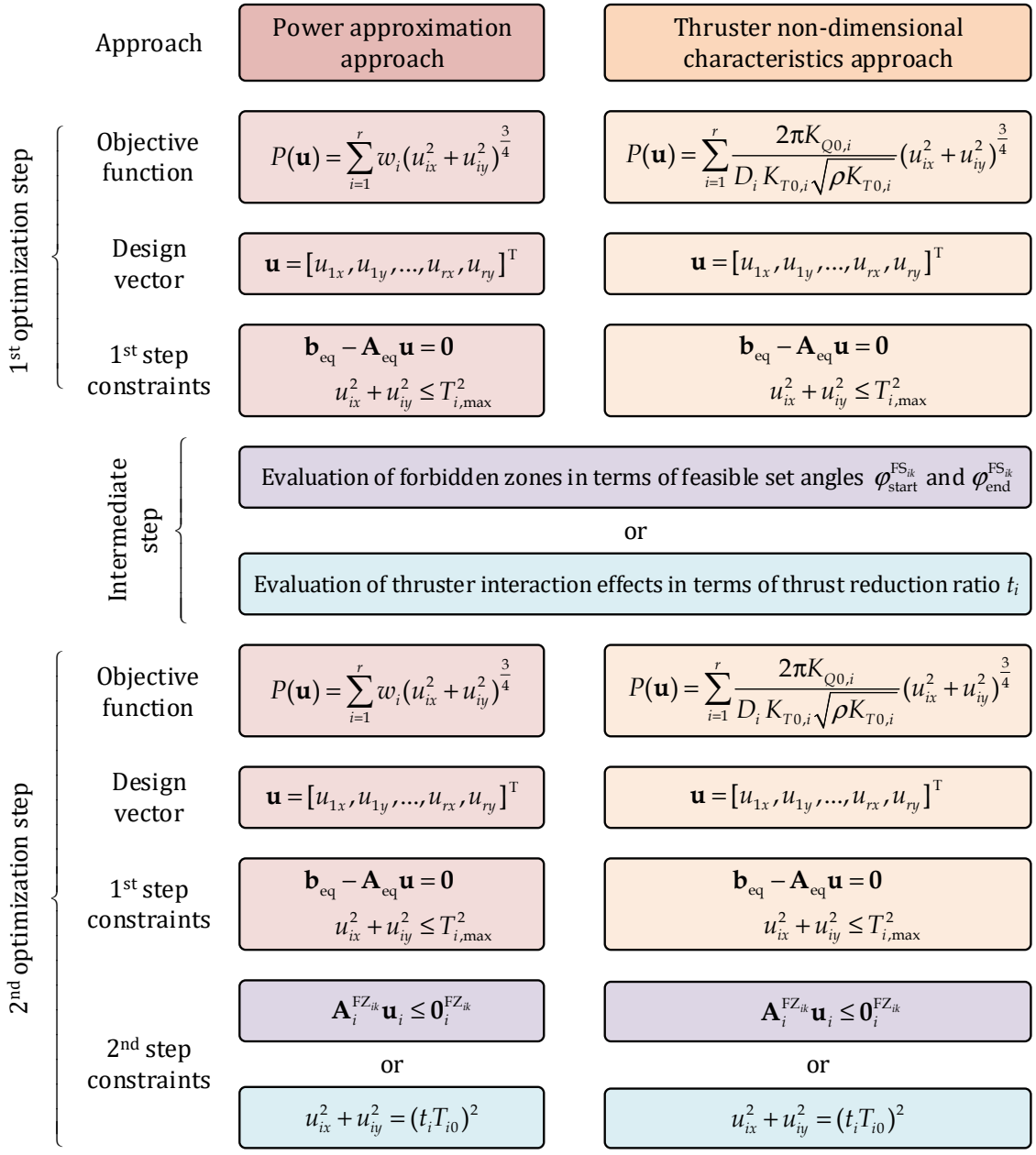

Figure 48. Workflow of proposed two-step nonlinear optimization procedure with implementation of forbidden zones or thruster interaction effects

Second step of alternative approach (7.11) can be analogously rewritten as

$$\left.\begin{aligned} \mathbf{u}^{*} = \underset{\mathbf{u}\in\mathbb{R}^{2r}}{\arg\min} & \left(\sum_{i=1}^{r} \frac{2\pi K_{Q0,i}}{D_i\, K_{T0,i}\sqrt{\rho K_{T0,i}}} \left(u_{ix}^2 + u_{iy}^2\right)^{\frac{3}{4}} \right) \\ \text{s.t.} \quad & \mathbf{b}_{\text{eq}} - \mathbf{A}_{\text{eq}}\mathbf{u} = \mathbf{0} \\ & \mathbf{A}_i^{\text{FZ}_{ik}}\mathbf{u}_i \le \mathbf{0}_i^{\text{FZ}_{ik}} \quad \text{or} \quad u_{ix}^2 + u_{iy}^2 = \left(t_i\, T_{i0}\right)^2 \\ & u_{ix}^2 + u_{iy}^2 \le T_{i,\max}^2. \end{aligned}\right\} \tag{7.13}$$

Finally, if thruster azimuth angles α_i, calculated in the first step of optimization procedure, clearly indicate that there is no need for implementation of forbidden zones or thruster interactions effects, than this first step is sufficient and the second one can be neglected (Figure 48).

7.2.2 Numerical examples and discussion of results

Enclosed examples in this section follow the routine from Chapter 6. This means that analysis has been performed for the same reference vessel (Chapter 6.1.1), and under the same environmental conditions (*a*), (*b*) and (*c*), as defined in Chapter 6.2.5. On the other hand, the main difference is in nonlinear approach to optimal thrust allocation, as described in Chapter 7.2.1.

Handling of thruster saturation and forbidden zones for the reference vessel is practically identical to procedures presented in Chapter 6.3.3. This particularly applies for angles that define feasible sets and forbidden zones. However, important exception is related to nonlinear handling of thrust regions, as emphasized in Chapter 7.1.3. Implementation of thruster interaction effects is again implemented only for thrusters 2 and 3, as described in Chapter 3.2.2, but this time in terms of nonlinear equality constraints (7.8).

Similarly as in Chapter 6.3.3, resulting thrusts and azimuth angles for environmental conditions (*a*) and (*c*), as defined in Chapter 6.2.5, are presented in Appendixes 5.1 and 5.2, respectively, while the sample of resulting thrusts and thruster angles for the case (*b*) is shown in Figure 49. Thrust variations are presented again with solid lines and azimuth angles with dashed lines. Blue lines correspond to results of SQP/DS optimization without any interactions, red lines are related to SQP/DS optimization with thruster saturation and forbidden zones included, and black lines are related to SQP/DS optimization with thruster saturation and thruster interaction effects included.

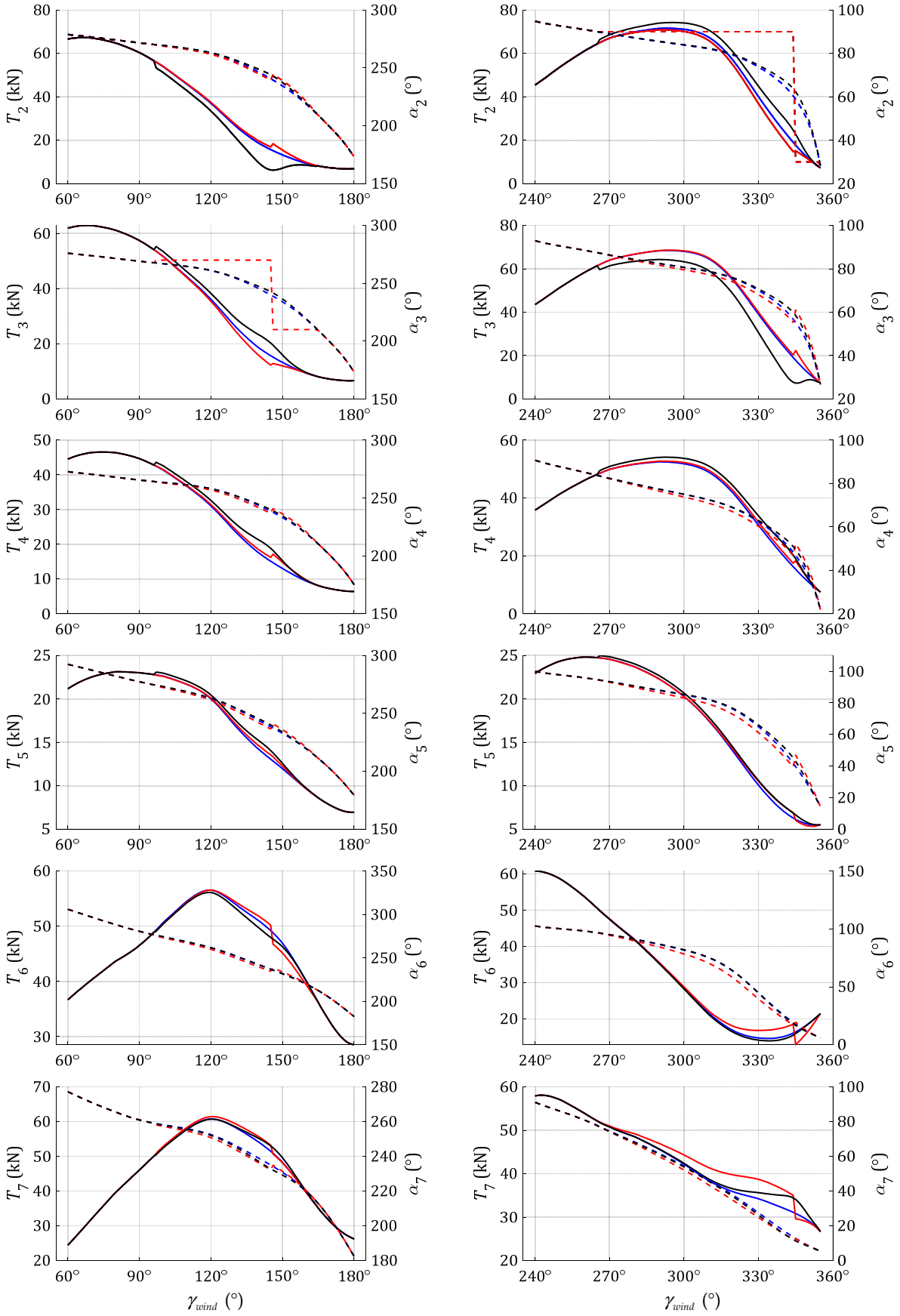

Figure 49. Resulting thrusts and azimuth angles with respect to γ_{wind} for all azimuth thrusters in environmental conditions $V_{wind} = 10$ m/s, $H_s = 3.21$ m, $T_p = 8.41$ s, $V_{curr} = 0.5$ m/s

As already mentioned, and as it can be noticed from Figure 49 and Appendixes 5.1 and 5.2, the main difference of this approach in comparison with WGIM approach (Chapter 6.2.5) can be seen in fixing the amount of thrust that rear thruster can generate regarding the predetermined thrust reduction ratio. In order to compensate this thrust loss, reallocation clearly indicates some increase of thrust with most of other thrusters, though similar effect can be noticed for approach with forbidden zones.

The implications on total demanded power that arise from this thruster-thruster interaction (TTI) strategy are of particular interest, especially in comparison with forbidden zone (FZ) strategy. It is reasonable to expect similar trends in power demand regarding the intensity of environmental loads, like presented in Chapter 6.3.3. However, considering another strategy for implementing thruster interactions was applied, some important differences can be noticed. A sample of total demanded minimum power for SQP/DS approach without any thruster interactions ($P_{\mathrm{SQP/DS}}$), for the SQP/DS approach with forbidden zones included ($P_{\mathrm{SQP/DS,FZ}}$), and for the SQP/DS approach with thruster-thruster interaction included ($P_{\mathrm{SQP/DS,TTI}}$), is shown in Figure 50. One can easily notice significantly lower power demand in comparison with results presented in Figure 45 for the same environmental conditions, but this discrepancy is just related to different objective functions used in these optimizations. On the other hand, it is much more important to notice that variations in power demand are relatively small for any of proposed strategies, which stands even around regions of forbidden and thruster-thruster interaction zones. Associated relative deviations δP of demanded power values $P_{\mathrm{SQP/DS,FZ}}$ and $P_{\mathrm{SQP/DS,TTI}}$ with respect to the referent power demand $P_{\mathrm{SQP/DS}}$, defined analogously as (6.24) with $\varepsilon = 10^{-3}$, are shown in Figure 51.

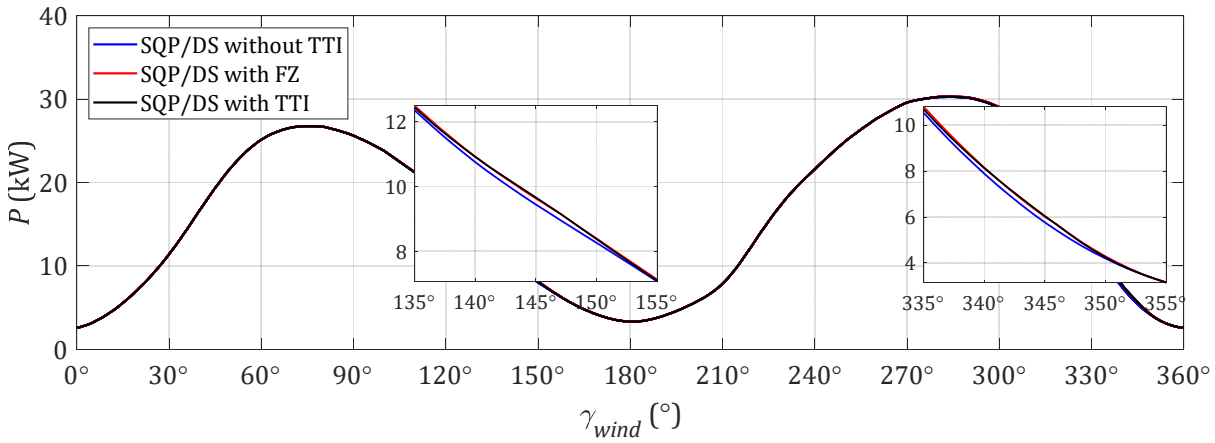

Figure 50. Total demanded minimum power for all azimuth thrusters with respect to the wind angle of attack γ_{wind} and for $V_{wind} = 10$ m/s, $H_s = 3.21$ m, $T_p = 8.41$ s, $V_{curr} = 0.5$ m/s

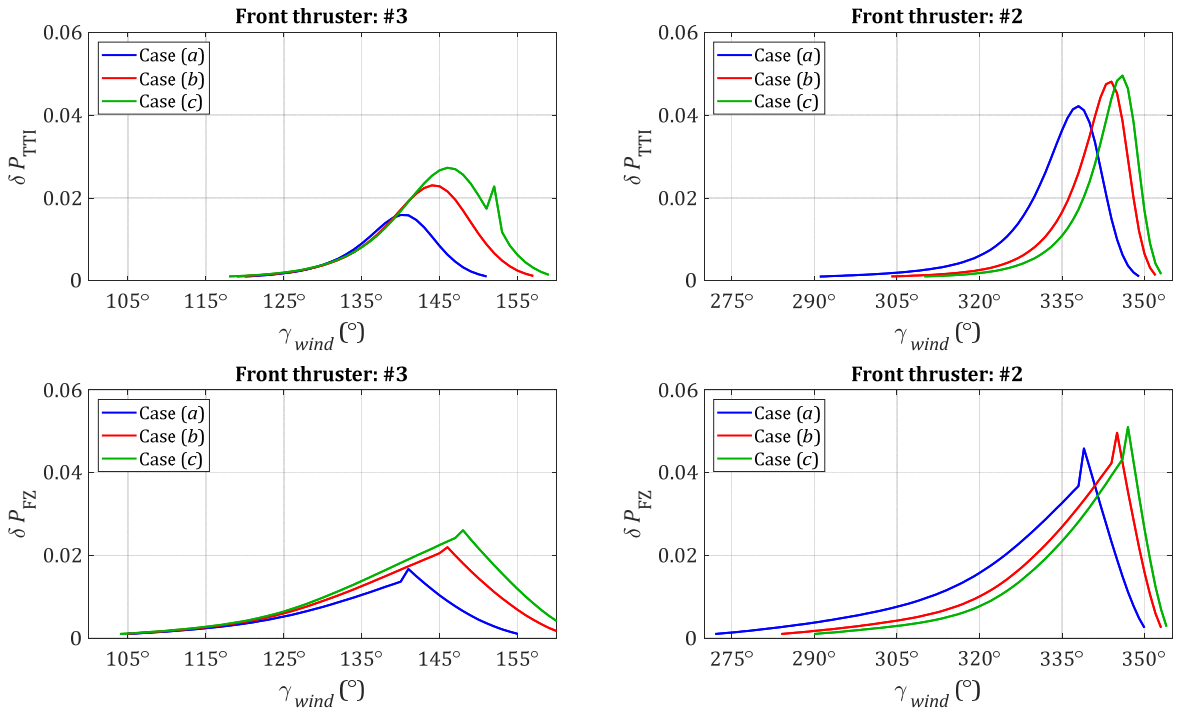

Figure 51. Relative deviations of total demanded minimum power for thrusters 2 and 3 regarding different nonlinear optimization approaches

Calculated quantitative indicators for all three cases (*a*), (*b*) and (*c*), as defined in Chapter 6.2.5, are presented in Appendix 6, both when thruster 2 is the front one and when thruster 3 is the front one. In comparison with associated results of WGIM and QP approaches (Table 5, Figure 46), and based on results in Figure 51 and Appendix 6, one can notice that in this case there is no significant difference in relative deviations δP_{TTI} and δP_{FZ} for TTI and FZ approach, respectively. Namely, during FZ implementations, front thruster does not operate in optimal, but in suboptimal manner with thruster azimuth angle saturated to the associated boundary of forbidden zone. This means that other thrusters in reallocation should compensate this, similarly like in TTI strategy. Although power consumption for thrusters 4 and 5 is slightly higher with TTI included, in comparison with FZ approach, this is opposite for thrusters 6 and 7, as can be seen in Figure 49 and Appendixes 5.1 and 5.2. On the other hand, regardless of these thrust and power fluctuations by individual thrusters, the total power consumption is practically the same (Figure 50), which consequently means that power consumption as a possible criterion does not favour any of these two strategies. However, the smoothness of azimuth angles with TTI approach that minimizes wear and tear on thrusters could be decisive indicator in decision making of which approach should be more favourable.

7.3 Hybrid approach to nonlinear optimal thrust allocation

One should notice that optimization tasks (7.10) and (7.11) are always convex, and therefore global optimum is guaranteed. This also applies to optimization task (7.12) and (7.13), but only in cases of implementing forbidden zones, where convexity is still preserved. On the other side, in cases of implementing thruster interaction effects, optimization tasks (7.12) and (7.13) are generally non-convex due to nonlinear non-convex equality constraint (7.8).

All results presented in Figures 48 and 49, as well as in Appendixes 5.1 and 5.2, are smooth and without noticeable outliers, and thus it seems they present global optima. However, it is important to point out that all obtained optimal solutions related to thruster interaction effects should be still taken into account with additional caution. The reason for this is more than obvious, considering any solver can easily stuck in some local optimum of non-convex optimization problem. In order to significantly reduce risk associated with this issue, appropriate hybrid approach that combines local and global optimizers with intensive sensitivity analysis is proposed in the following sections.

7.3.1 Convergence and computational cost issues

Convergence to global optimum is the most important issue of the global optimization field. Besides the direct search algorithms used in this work, the same applies for any other global optimization algorithm or method like genetic algorithm, particle swarm optimization, simulated annealing, etc. In general, for non-convex optimization problems there is no guarantee that any determined local optimum is the global one, at the same time. For this reason, there is no general approach that can be applied directly for any optimization task, and thus suitable strategy for specific problem should be introduced instead. It should also be noted that any of proposed strategies are more empirically and data-driven oriented, so there is usually a lack of strong theoretical background.

At first, intensive sensitivity analysis is applied in terms of initial solutions or any other initial parameters that could be of interest within selected algorithm. The idea behind this approach is similar to Monte Carlo method by which a large number of randomly chosen initial parameters is selected for performing optimization. In the case of optimization applications, random number generation for sensitivity analysis is usually based on uniform distribution, but if required, it can be easily adopted to any

other probability distribution. If sufficiently large number of optimal solutions obtained for different initial conditions coincide, than one could consider that optimal solution as the global optimum. In order to additionally minimize the possibility of obtained solution being stuck in some local optimum, specific measures and criteria based on convex optimization results should be introduced. These are directly related to whether some optimal solution obtained in non-convex optimization will be adopted as global or not.

In addition to afore described sensitivity analysis of used optimization algorithms in terms of various initial solutions, one can extend this approach to other algorithm properties as well. For DS algorithms, this could be applied particularly for tolerance on constraints, maximum number of objective function evaluations, maximum number of iterations, polling and search strategy, etc.

However, both sensitivity analysis and refinement of algorithm structure could significantly increase computational costs that arise from this exhaustive approach. This also refers to convergence time required to reach optimal solution. On the other hand, finding some optimal structure of direct search algorithm does not have much sense for thrust allocation problem, because even in the modest sparse form, any DS algorithm would have slower convergence in comparison with gradient-based SQP algorithm, particularly for real-time applications in industrial DP systems. This difference would additionally increase with adding more complex, i.e. non-convex equality constraints in optimization task. The usage of multi-core parallel computing could also be applied in order to decrease convergence time of DS algorithms, but one should not expect significant improvements on small-scaled optimization problems. Nevertheless, DS algorithm can be of great advantage for finding and adopting possible global optima in offline mode, while appropriate SQP or neural network based approach could be applied in online mode.

7.3.2 Hybrid optimization with sensitivity analysis

For the purpose of sensitivity analysis, optimization itself should be repeated M_0 times in terms of initial solution

$$\mathbf{u}_0 = [u_{01x}, u_{01y}, \ldots, u_{0ix}, u_{0iy}, \ldots, u_{0rx}, u_{0ry}]^{\mathrm{T}} \in \mathbb{R}^{2r}, \tag{7.14}$$

which had been randomly selected M_0 times as well, where M_0 is in general sufficiently large number. Random number generation is based on uniform probability

distribution, and thus each thrust component could have been chosen randomly from the interval $[0, T_{i,\max}]$, where $T_{i,\max}$ denotes the maximum thrust of *i*-th thruster.

For any of M_0 randomly chosen initial solutions $\mathbf{u}_{0j}$, $j = 1, 2, ..., M_0$, optimal thrust allocation is performed using both local (SQP) and global (DS) optimization methods. At this point, one should refer to Figure 48 and differentiate two featured classes of optimization problems. As already discussed, the first one is related to nonlinear implementation of forbidden zones, and the other one is related to nonlinear and non-convex implementation of thruster interaction effects.

Although first class presents convex optimization class of problems, and optimal solutions obtained with different algorithms should be equal, this actually does not stand due to numerical inconsistencies. In other words, even though different algorithms converge to global optimum, there is always a difference between optimal solutions $\mathbf{u}_{\mathrm{SQP}}$ and $\mathbf{u}_{\mathrm{DS}}$ from the numerical point of view. This difference is particularly noticeable if one predefines the characteristics of DS algorithms in very relaxed and sparse way, which peculiarly applies to features like tolerance on constraints, maximum number of objective function evaluations, maximum number of iterations, mesh size tolerance, initial and maximum mesh size, etc. Hence, in order to compensate this issue in numerical sense, obtained corresponding optimal solutions $\mathbf{u}_{\mathrm{SQP}}$ and $\mathbf{u}_{\mathrm{DS}}$ are compared in terms of Euclidean distance, i.e. ℓ^2-norm, defined as

$$d(\mathbf{u}_{\mathrm{SQP}}, \mathbf{u}_{\mathrm{DS}}) = \left\| \mathbf{u}_{\mathrm{SQP}} - \mathbf{u}_{\mathrm{DS}} \right\|_2 = \sqrt{(\mathbf{u}_{\mathrm{SQP}} - \mathbf{u}_{\mathrm{DS}})^{\mathrm{T}} (\mathbf{u}_{\mathrm{SQP}} - \mathbf{u}_{\mathrm{DS}})}, \tag{7.15}$$

where distance $d(\mathbf{u}_{\mathrm{SQP}}, \mathbf{u}_{\mathrm{DS}})$ presents a measure of how distant these two vectors are.

Distance measure $d(\mathbf{u}_{\mathrm{SQP}}, \mathbf{u}_{\mathrm{DS}})$ in (7.15) can be further used for defining a distance-based similarity measure $s(\mathbf{u}_{\mathrm{SQP}}, \mathbf{u}_{\mathrm{DS}})$ as follows

$$s(\mathbf{u}_{\mathrm{SQP}}, \mathbf{u}_{\mathrm{DS}}) = \frac{1}{1 + d(\mathbf{u}_{\mathrm{SQP}}, \mathbf{u}_{\mathrm{DS}})}. \tag{7.16}$$

When $d(\mathbf{u}_{\mathrm{SQP}}, \mathbf{u}_{\mathrm{DS}}) = 0$, which means that optimal solutions $\mathbf{u}_{\mathrm{SQP}}$ and $\mathbf{u}_{\mathrm{DS}}$ are equal, it yields $s(\mathbf{u}_{\mathrm{SQP}}, \mathbf{u}_{\mathrm{DS}}) = 1$, and when $d(\mathbf{u}_{\mathrm{SQP}}, \mathbf{u}_{\mathrm{DS}}) \to \infty$, it yields $s(\mathbf{u}_{\mathrm{SQP}}, \mathbf{u}_{\mathrm{DS}}) \to 0$. Thus, one can notice that $0 < s(\mathbf{u}_{\mathrm{SQP}}, \mathbf{u}_{\mathrm{DS}}) \leq 1$, where values of $s(\mathbf{u}_{\mathrm{SQP}}, \mathbf{u}_{\mathrm{DS}})$ closer to one indicate higher similarity of optimal solutions $\mathbf{u}_{\mathrm{SQP}}$ and $\mathbf{u}_{\mathrm{DS}}$, while $s(\mathbf{u}_{\mathrm{SQP}}, \mathbf{u}_{\mathrm{DS}}) = 1$ indicates that solutions $\mathbf{u}_{\mathrm{SQP}}$ and $\mathbf{u}_{\mathrm{DS}}$ are completely identical.

For M_0 randomly chosen initial solutions $\mathbf{u}_{0j}$, $j=1,2,...,M_0$, one can assume that there could also be M_0 different optimal solutions $\mathbf{u}_{j,\mathrm{SQP}}$ and $\mathbf{u}_{j,\mathrm{DS}}$ for the first class of convex optimization problems. However, it is quite simple to evaluate their associated similarity measures $s_j(\mathbf{u}_{\mathrm{SQP}},\mathbf{u}_{\mathrm{DS}})$, $j=1,2,...,M_0$, and to determine the critical tolerance value $s_{tol}(\mathbf{u}_{\mathrm{SQP}},\mathbf{u}_{\mathrm{DS}})$ as

$$s_{tol}(\mathbf{u}_{\mathrm{SQP}},\mathbf{u}_{\mathrm{DS}})=\min[s_j(\mathbf{u}_{\mathrm{SQP}},\mathbf{u}_{\mathrm{DS}})],\ j=1,2,...,M_0. \tag{7.17}$$

This tolerance value (7.17) is of utmost importance for analysing optimal solutions obtained in afore mentioned second class of nonlinear and non-convex optimization problems related to thruster interaction effects. During convergence phase, any of selected algorithms can stuck in some local optimum in this class of problems, instead of convergence to the global optimum. In order to significantly lower the risk of this scenario, the tolerance value (7.17) is used as a threshold value within the following criterion

$$s_k(\mathbf{u}_{\mathrm{SQP}},\mathbf{u}_{\mathrm{DS}})\geq s_{tol}(\mathbf{u}_{\mathrm{SQP}},\mathbf{u}_{\mathrm{DS}}),\ k=1,2,...,M_0, \tag{7.18}$$

where $s_k(\mathbf{u}_{\mathrm{SQP}},\mathbf{u}_{\mathrm{DS}})$ in (7.18) is defined analogously as (7.16), but for the second class of optimization problems. Hence, in order to consider optimal solutions $\mathbf{u}_{\mathrm{SQP}}$ and $\mathbf{u}_{\mathrm{DS}}$ sufficiently similar in numerical sense, and thus global, the criterion (7.18) should have been satisfied for any obtained solution regardless of randomly chosen initial solution. However, measure (7.17) is highly dependent on initial conditions of optimization algorithm structure. Thus, if one changes any of optimization algorithm properties, than (7.17) should be updated and adapted to these changes as well.

Final optimal solutions $\mathbf{u}_{\mathrm{SQP}}$ and $\mathbf{u}_{\mathrm{DS}}$ for the first class of optimization problems are obtained as the mean values of optimal solutions $\mathbf{u}_{j,\mathrm{SQP}}$ and $\mathbf{u}_{j,\mathrm{DS}}$, respectively. Analogous approach is applied also for the second class of optimization problems, but with taking into account only solutions that satisfy the criterion (7.18). Complete workflow of this hybrid optimization part is illustrated in Figure 52 (left).

After obtained optimal solutions have been determined and adopted for both first and second class of optimization problems, they are further used as a basis for deploying associated generalized regression neural network (GRNN), which is one of the most commonly used networks for approximation of multivariate continuous functions (Specht, 1991). The GRNN is a one-pass learning algorithm with a highly parallel structure that makes it extremely fast, both in training and application phase. It can be

used efficiently even with sparse data and can provide smooth transitions from one observed value to another (Specht, 1991; Valčić and Prpić-Oršić, 2016). More details about GRNN structure can be found in (Beale et al., 2017) and (Specht, 1991). As can been seen in Figure 52 (right), first and second class GRNN are created, where the first class is related to FZ approach, and the second one is related to TTI approach.

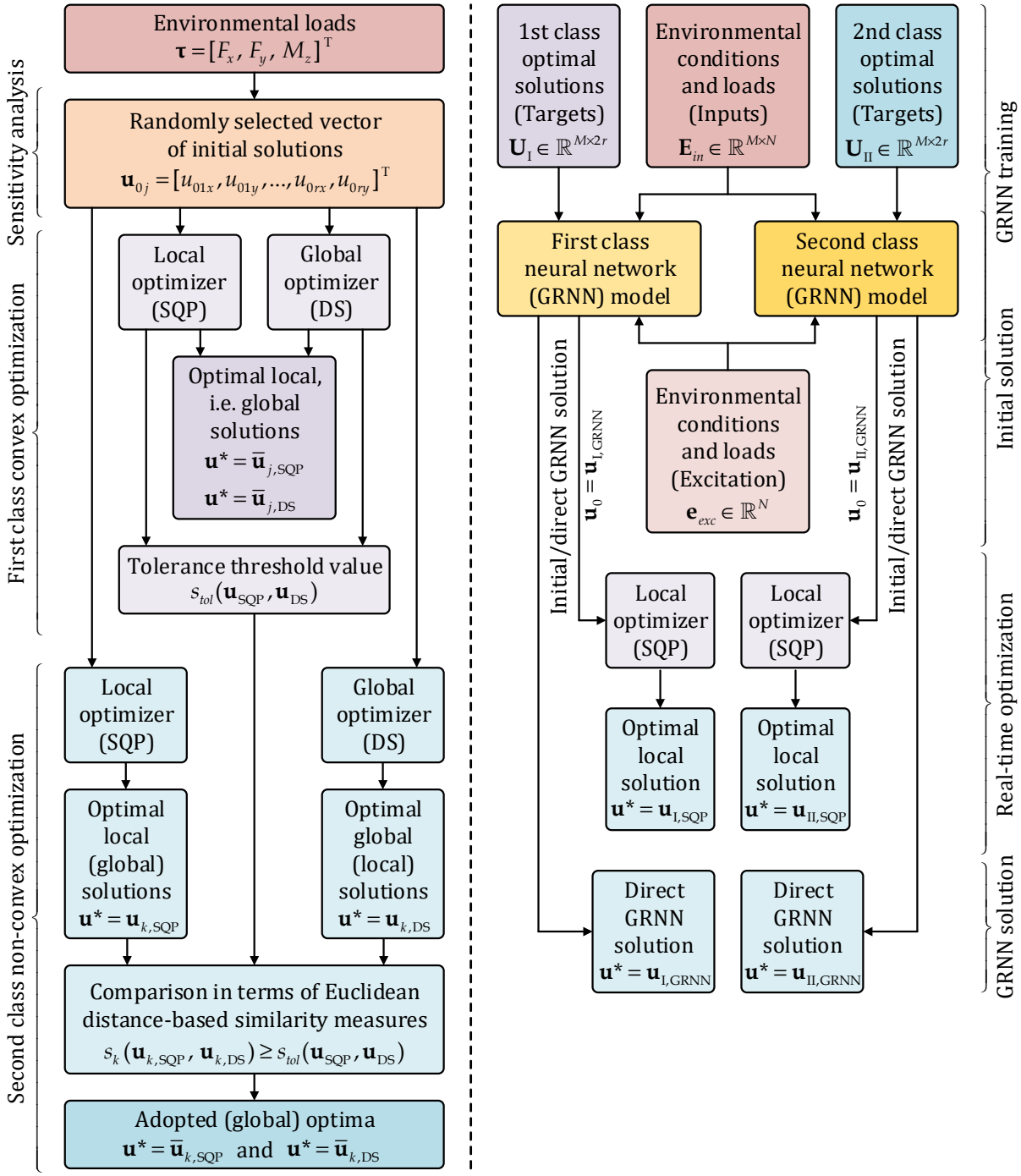

Figure 52. Workflow of the proposed hybrid optimization approach with sensitivity analysis (left) and GRNN as a generator of initial or direct solutions (right)

Both networks are trained with environmental loads and conditions in terms of input matrix $\mathbf{E}_{in}$ of the following form

$$\mathbf{E}_{in} = [\mathbf{F}_x \;\; \mathbf{F}_y \;\; \mathbf{M}_z \;\; \mathbf{V}_{wind} \;\; \boldsymbol{\gamma}_{wind} \;\; \mathbf{H}_s \;\; \mathbf{T}_0 \;\; \mathbf{V}_{curr}] \in \mathbb{R}^{M \times N}, \tag{7.19}$$

where $\mathbf{F}_x \in \mathbb{R}^M$, $\mathbf{F}_y \in \mathbb{R}^M$ and $\mathbf{M}_z \in \mathbb{R}^M$ are vectors of associated environmental loads, i.e. forces and moment in the horizontal plane. $\mathbf{V}_{wind} \in \mathbb{R}^M$, $\boldsymbol{\gamma}_{wind} \in \mathbb{R}^M$, $\mathbf{H}_s \in \mathbb{R}^M$, $\mathbf{T}_0 \in \mathbb{R}^M$ and $\mathbf{V}_{curr} \in \mathbb{R}^M$ are vectors of associated environmental conditions expressed in terms of V_{wind}, γ_{wind}, H_s, T_0 and V_{curr}, respectively. M is the number of optimal solution vectors used for this training, and $N = 8$ in this case, but the number of inputs, i.e. input variables, can be reduced to environmental loads only, or to environmental conditions only, depending on what data are available.

Targets for this training are adopted optimal solutions rearranged in a matrix form as

$$\mathbf{U}_k = [\mathbf{u}_{1x}^{(k)} \;\; \mathbf{u}_{1y}^{(k)} \;\; \mathbf{u}_{2x}^{(k)} \;\; \mathbf{u}_{2y}^{(k)} \;\; \ldots \;\; \mathbf{u}_{rx}^{(k)} \;\; \mathbf{u}_{ry}^{(k)}] \in \mathbb{R}^{M \times 2r}, \tag{7.20}$$

where $k \in \{\mathrm{I}, \mathrm{II}\}$ denotes first (I) or second (II) class of optimal solutions, $\mathbf{u}_{ix}^{(k)} \in \mathbb{R}^M$ and $\mathbf{u}_{iy}^{(k)} \in \mathbb{R}^M$ denote vectors of optimal thrust component values $u_{ix}^{(k)}$ and $u_{iy}^{(k)}$ for i-th thruster, $i = 1, 2, \ldots, r$, and k-th class.

When the GRNN is trained, it can provide during the online optimization a response vector $\mathbf{u}_0 = \mathbf{u}_{k,\mathrm{GRNN}} \in \mathbb{R}^{2r}$ for any excitation vector $\mathbf{e}_{exc} \in \mathbb{R}^N$, which is defined in accordance with input matrix $\mathbf{E}_{in}$. This response $\mathbf{u}_0$ can be used as an initial solution for a local online solver like SQP, or even as a direct solution of the thrust allocation problem. The latter option may consequently discard the necessity for the online optimal thrust allocation after all. Initial solution $\mathbf{u}_0$ determined in this way is already very close to global optimum, thus convergence time will be even lesser for the used online solver, and the risk of converging to some other (local) optimum is minimised.

7.3.3 Numerical examples and analysis of results

The approach presented in the previous section additionally confirmed that all optimum solutions of associated non-convex problems analysed in Chapter 7.2.2 present global optima. In order to further investigate and analyse this concept, additional set of environmental conditions and associated loads have been determined. For this purpose, environmental loads were determined in accordance with wind

speed $V_{wind} = \{1, 2, \ldots, 30\}$ (m/s) and wind angle of attack $\gamma_{wind} = \{0°, 5°, \ldots, 360°\}$. Associated values related to waves were determined according the IMCA recommendations (Table 4), and sea current load was added for sea current speed of $V_{curr} = 0.5$ m/s. The same assumption ($\gamma_{wind} = \gamma_{waves} = \gamma_{curr}$), as in previous sections, was applied here as well. However, this means that in this case $M = 30 \cdot 73 = 2190.$

Sensitivity analyses during the first and second class optimizations (Figure 52, left) were conducted as described in the previous chapter, using $M_0 = 100.$ First class optimization is the convex one, so it was applied in case without FZ or TTI approach, as well as in case with FZ approach. Obtained results served both for finding tolerance threshold value (7.17), and as first class target vectors of target matrix $\mathbf{U}_{\mathrm{I}}$, used for the training of the first class GRNN model. Optimal solutions of the second-class non-convex optimization, related to TTI approach, were selected in accordance with criterion (7.18). These adopted solutions were further used as the second class target vectors of target matrix $\mathbf{U}_{\mathrm{II}}$, used for training of the second class GRNN model.

The aim of the GRNN used in this concept is not an extrapolation or forecasting, but an overall approximation of multivariable function that presents a mapping of large input space of environmental loads and conditions to another large space of predetermined optimal thrust solutions expressed in terms of Cartesian coordinates. Thus, the analysis of extrapolation or interpolation possibilities of GRNN for the addressed problem is not investigated in this thesis. However, it is important to point out that for any other environmental state GRNN can be easily retrained in off-line (non-real-time) mode, and used again afterwards in online mode. The very short (re)training time makes GRNN ideal tool when one has adaptive approximation requirements.

A total number of conducted optimizations for cases without FZ/TTI approach, with FZ and TTI approaches, was 6570, and obtained results are cumulatively presented in Tables 6 and 7 in terms of mean values (μ), standard deviations (σ) and other performance measures. SQP was applied in standard form, while DS was implemented with changing polling strategy accordingly and type of search between GSS and MADS.

According to obtained results, SQP outperformed all other DS algorithms, and as a local solver, it presents an excellent solution for online optimization, i.e. for real-time applications. Results for DS algorithms with TTI approach clearly indicate that they have some problems in terms of solution feasibility and convergence time. This is particularly related with how these algorithms handle these kind of constraints. In

comparison with MADS, GSS can be coupled with ALPS, and in that way, these issues can be resolved. However, even with this approach, in order to ensure the feasibility of solution, one often needs to allow much larger number of objective function evaluations (N_{eval}) than is usually required. Consequently, DS will eventually converge, hopefully to global optimum, but with the high price of large N_{eval} and long convergence time $t_{elapsed}$.

Table 6. Quantitative indicators of optimization results based on initial solution $\mathbf{u}_0 = \mathbf{0} \in \mathbb{R}^{2r}$ in three different cases, with associated GRNN performance

Method	Performance	Indicator	Without FZ/TTI	With FZ	With TTI
SQP optimization	Elapsed time (s)	$\mu(t_{elapsed})$	0.043	0.041	0.042
		$\sigma(t_{elapsed})$	0.007	0.007	0.0076
	Number of iterations	$\mu(N_{iter})$	68.52	67.48	71.114
		$\sigma(N_{iter})$	11.03	9.96	11.0814
	Number of objective function evaluations	$\mu(N_{eval})$	1060.01	1029.11	1094.26
		$\sigma(N_{eval})$	161.38	153.17	205.856
DS optimization	Elapsed time (s)	$\mu(t_{elapsed})$	1.5186	5.7795	25.0172
		$\sigma(t_{elapsed})$	1.3533	27.5075	36.5012
	Number of iterations	$\mu(N_{iter})$	5.48	7.2202	6.8765
		$\sigma(N_{iter})$	1.22	1.021	0.5564
	Number of objective function evaluations	$\mu(N_{eval})$	13963.34	51734.39	288360.31
		$\sigma(N_{eval})$	12493.24	21721.67	442046.36
Comparison of optimal solutions (SQP vs. DS)	Euclidean distance $d(\mathbf{u}_{SQP}, \mathbf{u}_{DS})$	$\mu(d)$	0.0435	1.2420	0.8816
		$\sigma(d)$	0.6714	14.7659	4.0280
		$\max(d)$	19.5176	359.3676	22.3534
		$\min(d)$	0.0006	0.0007	0.0012
	Similarity index $s(\mathbf{u}_{SQP}, \mathbf{u}_{DS})$	$\mu(s)$	0.9934	0.9806	0.9521
		$\sigma(s)$	0.0618	0.1217	0.2051
		$\min(s)$	0.0487	0.0028	0.0428
		$\max(s)$	0.9994	0.9993	0.9988
GRNN performance	Euclidean distance	$d(\mathbf{U}, \hat{\mathbf{U}})$	0.0342	0.0866	0.0341
	Similarity index	$s(\mathbf{U}, \hat{\mathbf{U}})$	0.9670	0.9203	0.9670
	Mean Squared Error	$\mathrm{MSE}(\mathbf{U}, \hat{\mathbf{U}})$	$9.547 \cdot 10^{-9}$	$5.829 \cdot 10^{-9}$	$9.692 \cdot 10^{-9}$
	Elapsed time (s)	t_{train}	0.6628	0.9252	0.0999
	Response time of trained GRNN (s)	$\mu(t_{resp})$	0.0168	0.0153	0.0159
		$\sigma(t_{resp})$	0.0015	0.000727	0.000779

Table 7. Quantitative indicators of optimization results based on GRNN generated initial solutions for three different cases

Method	Performance	Indicator	Without FZ/TTI	With FZ	With TTI
SQP optimization	Elapsed time (s)	$\mu(t_{elapsed})$	0.0036	0.004	0.0156
		$\sigma(t_{elapsed})$	0.0001	0.0011	0.0150
	Number of iterations	$\mu(N_{iter})$	1.13	1.1016	22.08
		$\sigma(N_{iter})$	1.13	0.9915	25.67
	Number of objective function evaluations	$\mu(N_{eval})$	29.38	28.94	346.74
		$\sigma(N_{eval})$	19.03	16.55	338.84
DS optimization	Elapsed time (s)	$\mu(t_{elapsed})$	0.2349	1.0586	1.8104
		$\sigma(t_{elapsed})$	0.1146	0.6683	2.7652
	Number of iterations	$\mu(N_{iter})$	6	7.33	6.857
		$\sigma(N_{iter})$	0	0.97	0.6423
	Number of objective function evaluations	$\mu(N_{eval})$	2655.02	10440.05	21621.30
		$\sigma(N_{eval})$	937.72	6383.18	32103.37

This is best seen with larger standard deviations than the mean values of $t_{elapsed}$ and N_{eval} for DS optimization with TTI included, even when GRNN is used for determination of initial solutions. Although this means that DS algorithms will not be the most suitable for real-time optimization, the fact by which they present a great support in the off-line part of presented hybrid optimization workflow, still stands.

One should notice that results presented in Table 6 were all based on the same initial solutions $\mathbf{u}_0 = \mathbf{0} \in \mathbb{R}^{2r}$, while optimization results presented in Table 7 were all based on initial solutions determined by means of pre-trained GRNN. It is easy to conclude that by using this strategy, GRNN can additionally lower the risk of convergence in any possible local optimum and can significantly speed up convergence time for both SQP and DS algorithms.

Moreover, according to obtained results (Table 6), one can identify the possibility of GRNN as an adequate alterative to the online solvers, not only from the point of view of accuracy, but also from the point of view of response time. Finally, one should emphasize that extremely short time required for training or retraining the GRNN, makes it an excellent choice as a part of control strategy in which proven adaptiveness of GRNN can be of a great importance for guidance and control of DP vessels.

8 CONCLUSIONS AND RECOMMENDATIONS

8.1 Conclusions

Thruster-thruster interactions can consequently cause significant thrust reduction for rear thrusters of DP vessels. In order to avoid these losses, forbidden zones are usually implemented into the optimal thrust allocation, as one of possible strategies. However, forbidden zone for some azimuth thruster generally presents a non-convex thrust region that consequently can cause significant deviations in allocated thruster azimuth angles. In addition, time required for thrust and azimuth allocation is increased as well. On the other side, with appropriate reallocation strategy that considers thrust losses, it is possible to achieve smoother thrust control without using forbidden zones at all. The comparison between the strategy that excludes forbidden zones, but considers thruster-thruster interactions and the strategy that includes forbidden zones without considering thrust losses is performed with numerous simulations.

Thrust loss effects are defined in terms of thrust reduction ratios and are implemented using two approaches. The first approach is related to proposed reallocation strategy that is based on the weighted generalised inverse matrix. In this approach, thrust losses are implemented through objective function. Consequently, optimal thrust reallocation compensates thrust losses by increasing the thrust of the rear thruster with non-significant reallocation of other thrusters. Results obtained with implemented thrust losses indicate very smooth transients of azimuth angles for thrusters that operate within the forbidden zones with very small total power increase. This approach can ensure minimum wear and tear of the thrusters. On the other hand, the time required for the thruster rotation from one boundary of forbidden zone region to another can be several times longer than in the case without forbidden zones included. During that rotation, thruster will be far away from the optimum performance and other thrusters should compensate this. The consequent large deviations in thrust magnitudes and azimuth angles will significantly increase the wear and tear of the thruster, which does not comply with a DP system design philosophy, and will additionally increase total power consumption and response time.

The second approach defines thruster interaction effects as nonlinear equality constraints and thus appropriate nonlinear optimization method should be applied for solving this problem. Moreover, thruster interaction effect defined in this way presents a non-convex thrust region, which makes complete optimization problem non-convex. In order to resolve this issue, a detailed structure of hybrid optimization approach is

outlined. This second approach consists of two main parts. In the first part, local (SQP) and global (DS) solvers are used together in other to determine required tolerance threshold value and to prepare optimal solutions for training the generalized regression neural network. This tolerance threshold value is used in non-convex optimization so the risk of accepting local optimum as global one is minimised. In comparison with the first approach that is based on the weighted generalized inverse matrix, this approach will fix generated thrust of the rear thruster as it is, according to estimated current thrust loss. At the same time, required thrust for compensating this loss is reallocated using other thrusters. It is important to note that no evident increase in total power consumption was identified within this approach in comparison with strategy based on forbidden zones. One can conclude that this approach is more reasonable than the one with the weighted generalized inverse matrix, mostly because it does not put additional strain on the rear thruster, which already operates in not so favourable conditions of the front thruster slipstream. It is important to point out that results related to the strategy with forbidden zones included are presented statically, i.e. in a way as the thruster can switch from one saturated azimuth angle to another instantly, which is of course not possible. Hence, these results should be considered with caution and keeping in mind that the real power consumption will be even more increased in real applications when forbidden zones are included, which additionally favours approach with flexible thruster azimuth allocation proposed in this thesis.

Detailed analysis of computational intensity and convergence time for all proposed optimization strategies with particular emphasis on the overall power consumption is provided in Chapters 6 and 7. In comparison with the state-of-the-art algorithm like SQP, results of optimal thrust allocation obtained with direct search algorithms are more than satisfactory, although it should be pointed out that the gradient-based algorithms (SQP) could and probably should be a better choice for optimization problems. This particularly applies where the gradient and/or Hessian of the objective function is known or at least it can be obtained in sufficient amount of time. Possible issues related to non-convexity can be resolved with the proposed hybrid approach.

Numerous simulations and optimizations were performed in order to evaluate proposed approaches of optimal thrust allocation. These included scenarios without forbidden zones or thruster-thruster interactions, with forbidden zones included only and with thruster-thruster interactions included only. The second approach with thruster-thruster interactions included as a nonlinear equality constraint obviously presented the biggest challenge, both for SQP and DS algorithms. This is naturally

related to non-convexity issues, but even more with how these algorithms handle these kind of constraints. It is well known that MADS cannot handle equality constraints adequately, and its primary application is for solving problems with nonlinear objective functions and nonlinear inequality constraints. Even reformulation of the nonlinear equality constraint in terms of two equivalent nonlinear inequality constraints cannot be of much help. On the other hand, GSS can be combined with ALPS, and thus this inconvenient constraint can be handled in terms of augmented Lagrangian. However, even in this way, results clearly indicate that DS algorithms have much difficulty with convergence when dealing with these kind of problems. On the other hand, SQP can easily converge to some local optima in non-convex optimization. Thus, the proposed synergy between SQP and DS algorithms in finding global optima is even more important.

Associated generalized regression neural network (GRNN), used as a generator of initial solutions in the second part of this approach, additionally accelerated the convergence time of both SQP and DS, with significant reduction of number of objective function evaluations. Namely, pre-trained GRNN can determine initial solution that is by far closer to the optimal one, particularly in comparison with any stochastic approach generally used in global optimization. Moreover, one should highlight that according to obtained results, the GRNN can present an adequate alterative to the online solvers, both from the points of view of accuracy and response time. Extremely short time required for training or retraining of the GRNN makes it particularly convenient as an adaptive approximation tool.

According to everything stated so far, one can highlight the most important scientific contributions of this thesis as follows:

- In Chapters 3 and 4, quantification of selected thrust interaction effects were conducted. This particularly applies to thruster-income current interaction, thruster-thruster interaction and forbidden zones. Procedures on how to implement these interactions in terms of thrust reduction ratios are also given.
- In Chapter 6, proposition and evaluation of appropriate reallocation strategies for handling forbidden zones and thruster interaction effects by means of enhanced weighted generalized inverse matrix are provided. With this approach, thrust is reallocated in order to increase the thrust of the rear thruster in accordance with the previously determined thrust loss.
- In Chapter 7, thruster interaction effects are implemented in terms of non-convex and nonlinear equality constraints in newly proposed two-step nonlinear

optimization procedure of thrust allocation. This hybrid SQP/DS optimization approach is proposed and deployed with intensive sensitivity analysis in order to minimise the risk of solver convergence to any of possible local optima for non-convex optimization problems that include thruster interactions. With this approach, thrust is reallocated in order to fix generated thrust of the rear thruster in accordance with the previously determined thrust loss. All other thrusters are optimally reallocated in order to compensate current environmental loads, but with no significant increase in total power consumption, compared to the strategy based on forbidden zones.

- In Chapter 7, a generalized regression neural network is deployed with the main aim of generating initial solutions for the online solvers depending on the given environmental loads. In this way, a much faster convergence of the optimization algorithm is achieved, both for SQP and DS algorithms. Generalized regression neural network trained as described may partially or fully cover the entire process of optimal thrust allocation and thus provide a very fast, computationally inexpensive and accurate thrust allocation tool, without the need for additional numerical optimization in the on-line (real-time) mode of operation.

8.2 Recommendations for future work

The future work should be focused on two main research avenues. The first one is directly related to the proposed hybrid optimization approach, i.e. in particular to direct search optimization methods for which is of utmost importance to find optimal structure in terms of convergence time and number of objective function evaluations. In addition to that, independent research should be also aimed on how to implement local gradient-based nonlinear optimization algorithms like SQP for solving the problems of non-convex and nonlinear equality constraints without using global optimization algorithms as direct support.

The second research avenue is oriented towards the control part of a DP system, which was not taken into account in this research. Namely, it is very important to embed optimization strategies and approaches proposed in this thesis with various control laws and to investigate their impact on control performance and power management system of DP vessels. In this form, proposed optimization strategy could be used in terms of thrust-loss feedforward control, and thus additionally contribute to the overall reliability and accuracy of a DP system.

BIBLIOGRAPHY

[1] Andersen, I.M.V., 2013. Wind loads on post-panamax container ship. Ocean Eng. 58, 115–134. https://doi.org/10.1016/j.oceaneng.2012.10.008

[2] Audet, C., Dennis, J.E., 2009. A Progressive Barrier for Derivative-Free Nonlinear Programming. SIAM J. Optim. 20, 445–472. https://doi.org/10.1137/070692662

[3] Audet, C., Dennis, J.E., 2006. Mesh Adaptive Direct Search Algorithms for Constrained Optimization. SIAM J. Optim. 17, 188–217. https://doi.org/10.1137/040603371

[4] Audet, C., Dennis, J.E., 2004. A Pattern Search Filter Method for Nonlinear Programming without Derivatives. SIAM J. Optim. 14, 980–1010. https://doi.org/10.1137/S105262340138983X

[5] Audet, C., Dennis, J.E., Le Digabel, S., 2010. Globalization strategies for Mesh Adaptive Direct Search. Comput. Optim. Appl. 46, 193–215. https://doi.org/10.1007/s10589-009-9266-1

[6] Audet, C., Hare, W., 2017. Derivative-Free and Blackbox Optimization, Springer Series in Operations Research and Financial Engineering. Springer International Publishing, Cham. https://doi.org/10.1007/978-3-319-68913-5

[7] Barata, J.C.A., Hussein, M.S., 2012. The Moore–Penrose Pseudoinverse: A Tutorial Review of the Theory. Brazilian J. Phys. 42, 146–165. https://doi.org/10.1007/s13538-011-0052-z

[8] Beale, M.H., Hagan, M.T., Demuth, H.B., 2017. Neural Network Toolbox: User's Guide. The MathWorks, Inc., Natick, MA, USA.

[9] Ben-Israel, A., Greville, T.N.E., 2003. Generalized inverses: Theory and applications. 2nd ed., Springer, New York, NY, USA.

[10] Blaurock, J., 1977. Gegenseitige Beeinflussung von zwei unter einem Schwimmkörper arbeitenden Schottel- Ruderpropeller. HSVA – Bericht PS 2/77, Hamburg, Germany.

[11] Blendermann, W., 1996. Wind Loading of Ships - Collected Data from Wind Tunnel Tests in Uniform Flow. Report No. 574, Institut für Schiffbau der Universität Hamburg, Hamburg, Germany.

[12] Blendermann, W., 1995. Estimation of wind loads on ships in wind with a strong gradient, in: Proceedings of the 14th International Conference on Offshore Mechanics and Arctic Engineering (OMAE), New York. pp. 271–277.

[13] Blendermann, W., 1994. Parameter identification of wind loads on ships. J. Wind Eng. Ind. Aerodyn. 51, 339–351. https://doi.org/10.1016/0167-6105(94)90067-1

[14] Boggs, P.T., Tolle, J.W., 1995. Sequential Quadratic Programming. Acta Numer. 4, 1–51. https://doi.org/10.1017/S0962492900002518

[15] Bonnans, J.F., Gilbert, J.C., Lemarechal, C., Sagastizábal, C.A., 2006. Numerical Optimization: Theoretical and Practical Aspects. 2nd Ed., Springer, Berlin Heidelberg, Germany.

[16] Boyd, S., Vandenberghe, L., 2004. Convex Optimization. Cambridge University Press, New York, NY.

[17] Brandner, P., Renilson, M., 1998. Interaction between two closely spaced azimuthing thrusters. J. Sh. Res. 42, 15–32.

[18] Bretschneider, C.L., 1959. Wave Variability and Wave Spectra for Wind Generated Gravity Waves. Wave Variability and Wave Spectra for Wind Generated Gravity Waves Technical Report, Beach Erosion Board, Corps. of Engineers, Technical memorandum no. 118.

[19] Bulten, N., Stoltenkamp, P., 2013. Full Scale Thruster-Hull Interaction Improvement Revealed with CFD Analysis, in: Proceedings of the ASME 2013 32nd International Conference on Ocean, Offshore and Arctic Engineering (OMAE 2013), Nantes, France.

[20] Carlton, J.S., 2007. Marine Propellers and Propulsion. 2nd Ed., Butterworth-Heinemann, Elsevier.

[21] Conn, A.R., Gould, N.I.M., Toint, P., 1991. A Globally Convergent Augmented Lagrangian Algorithm for Optimization with General Constraints and Simple Bounds. SIAM J. Numer. Anal. 28, 545–572. https://doi.org/10.1137/0728030

[22] Conn, A.R., Gould, N.I.M., Toint, P.L., 1997. A Globally Convergent Augmented Lagrangian Barrier Algorithm for Optimization with General Inequality Constraints and Simple Bounds. Math. Comput. 66, 261–288.

[23] Cozijn, J.L., Buchner, B., van Dijk, R.R.T., 1999. Hydrodynamic Research Topics for DP Semi Submersibles, in: Proceedings of the 31st Offshore Technology Conference (OTC 1999), Houston, TX, USA. https://doi.org/10.4043/10955-MS

[24] Dang, J., Laheij, H., 2004. Hydrodynamic Aspects of Steerable Thrusters, in: Proceedings of the Dynamic Positioning Conference, Houston, TX, USA.

[25] Davis, C., 1954. Theory of Positive Linear Dependence. Am. J. Math. 76, 733. https://doi.org/10.2307/2372648

[26] Dennis Jr., J.E., Price, C.J., Coope, I.D., 2004. Direct Search Methods for Nonlinearly Constrained Optimization Using Filters and Frames. Optim. Eng. 5, 123–144. https://doi.org/10.1023/B:OPTE.0000033371.04406.e0

[27] DNV, 2012. Dynamic Positioning Vessel Design Philosophy Guidelines. DNV-RP-E306, Det Norske Veritas AS, Høvik, Norway.

[28] DNV, 2007. Environmental conditions and environmental loads. DNV-RP-C205, April 2007. Det Norske Veritas AS, Høvik, Norway.

[29] Ekstrom, L., Brown, D.T., 2002. Interactions between thrusters attached to a vessel hull, in: Proceedings of the 21st International Conference on Offshore Mechanics and Artic Engineering (OMAE'02), Oslo, Norway.

[30] Espedal, M.H., 2015. Thruster-thruster interactions. Project Thesis, Norwegian University of Science and Technology, Department of Marine Technology, Trondheim, Norway. (unpublished work).

[31] Faltinsen, O.M., 1990. Sea Loads on Ships and Offshore Structures. Cambridge University Press, Cambridge, UK.

[32] Fjørtoft, H., 2010. Thrust loss on azimuthing thrusters due to Coanda effect. M.Sc. Thesis. Norwegian University of Science and Technology, Faculty of Engineering Science and Technology, Department of Marine Technology, Trondheim, Norway.

[33] Fossen, T.I., 2011. Handbook of Marine Craft Hydrodynamics and Motion Control. John Wiley & Sons Ltd, Chichester, UK.

[34] Gierusz, W., Tomera, M., 2006. Logic thrust allocation applied to multivariable control of the training ship. Control Eng. Pract. 14, 511–524.

[35] Golub, G.H., Van Loan, C.F., 2013. Matrix Computations. 4th Ed., The Johns Hopkins University Press, Baltimore, MD, USA.

[36] Gould, R.W.F., 1982. The estimation of wind loads on ship superstructures. The Royal Institution of Naval Architects, Report RINA-MTM-8, No. 8, pp. 1-34.

[37] Hansen, E.L., Völcker, C., 2007. Numerical algorithms for sequential quadratic optimization. M.Sc. Thesis. Informatics and Mathematical Modelling, Technical University of Denmark, DTU, Kongens Lyngby, Denmark.

[38] Hasselmann, K., Barnett, T.P., Bouws, E., Carlson, H., Cartwright, D.E., Enke, K., Ewing, J.A., Gienapp, H., Hasselmann, D.E., Kruseman, P., Meerburg, A., Müller, P., Olbers, D.J., Richter, K., Sell, W., Walden, H., 1973. Measurements of Wind-Wave Growth and Swell Decay during the Joint North Sea Wave Project (JONSWAP). Deutschen Hydrografischen Zeitschrift, Reihe A(8), Nr. 12, Hamburg, Germany.

[39] IMCA, 2000. Specification for DP Capability Plots. Report IMCA M 140 Rev. 1, June 2000. The International Marine Contractors Association.

[40] Isherwood, R.M., 1972. Wind resistance of merchant ships. Transcr. R. Inst. Nav. Archit. 115, 327–338.

[41] ITTC, 1984. Report of the Seakeeping Committee, in: Proceedings of the 17th International Towing Tank Conference, The Hague, Netherlands. pp. 531–534.

[42] ITTC, 1978. Report of the Seakeeping Committee., in: Proceedings of the 15th International Towing Tank Conference, The Hague, Netherlands. pp. 55–70.

[43] Jenssen, N.A., 1980. Estimation and Control in Dynamic Positioning of Vessels. PhD thesis. The Norwegian Institute of Technology, ITK report 80-90-W, Trondheim, Norway.

[44] Jenssen, N.A., Realfsen, B., 2006. Power Optimal Thruster Allocation, in: Proceedings of the Dynamic Positioning Conference, Houston, TX, USA.

[45] Johansen, T.A., Fossen, T.I., 2013. Control allocation - A survey. Automatica 49, 1087–1103. https://doi.org/10.1016/j.automatica.2013.01.035

[46] Johansen, T.A., Fossen, T.I., Berge, S.P., 2004. Constrained Nonlinear Control Allocation With Singularity Avoidance Using Sequential Quadratic Programming. IEEE Trans. Control Syst. Technol. 12, 211–216. https://doi.org/10.1109/TCST.2003.821952

[47] Johansen, T.A., Fossen, T.I., Tøndel, P., 2005. Efficient Optimal Constrained Control Allocation via Multiparametric Programming. J. Guid. Control. Dyn. 28, 506–515. https://doi.org/10.2514/1.10780

[48] Journée, J.M.J., Massie, W.W., 2001. Offshore hydromechanics. Delft University of Technology, Delft, The Netherlands.

[49] Kolda, T.G., Lewis, R.M., Torczon, V., 2006. A generating set direct search augmented Lagrangian algorithm for optimization with a combination of general and linear constraints. SANDIA REPORT SAND2006-5315, Sandia National Laboratories, Albuquerque, New Mexico, California, USA.

[50] Kolda, T.G., Lewis, R.M., Torczon, V., 2003. Optimization by Direct Search: New Perspectives on Some Classical and Modern Methods. SIAM Rev. 45, 385–482. https://doi.org/10.1137/S003614450242889

[51] Koop, A., Cozijn, H., Schrijvers, P., Vaz, G., 2017. Determining thruster-hull interaction for a drill-ship using CFD, in: Proceedings of the ASME 2017 36th International Conference on Ocean, Offshore and Arctic Engineering (OMAE 2017), Trondheim, Norway.

[52] Koushan, K., Spence, S., Byron, J., Hamstad, T.S., 2009. Experimental Investigation of the Effect of Waves and Ventilation on Thruster Loadings, in: Proceedings of the First International Symposium on Marine Propulsors Smp'09, Trondheim, Norway.

[53] Kuiper, G., 1992. The Wageningen Propeller Series. MARIN Publication 92-001, Maritime Research Institute Netherlands (MARIN), Wageningen, The Netherlands.

[54] Le Digabel, S., 2011. Algorithm 909. ACM Trans. Math. Softw. 37, 1–15. https://doi.org/10.1145/1916461.1916468

[55] Leavitt, J.A., 2008. Optimal Thrust Allocation in a Dynamic Positioning System. SNAME Trans. 116, 153–165.

[56] Lehn, E., 1992. Practical methods for estimation of thrust losses. FPS-2000 mooring and positioning, Summary Report Part 1.6, Dynamic positioning – Thruster efficiency. Technical Report 513003.00.06. Marintek, SINTEF, Trondheim, Norway.

[57] Lehn, E., 1985. On the propeller race interactions effects. Technical Report P-01.85. Marintek, The Sintef Group, Trondheim, Norway.

[58] Lehn, E., 1980. Thruster interaction effects. NSFI Report R-102.80, The Ship Research Institute of Norway, Marine Technology Center, Trondheim, Norway.

[59] Lewis, R.M., Torczon, V., 1996. Rank ordering and positive bases in pattern search algorithms. Technical Report No. 96-71, ICASE, NASA Langley Research Center, Hampton, VA, USA. 1996.

[60] Liang, C.C., Cheng, W.H., 2004. The optimum control of thruster system for dynamically positioned vessels. Ocean Eng. 31, 97–110. https://doi.org/10.1016/S0029-8018(03)00016-7

[61] Lindfors, I., 1993. Thrust allocation method for the dynamic positioning system, in: Proceedings of the 10th International Ship Control Systems Symposium (SCSS'93), Ottawa, Canada. p. 3.93-3.106.

[62] Luenberger, D.G., Ye, Y., 2008. Linear and nonlinear programming. 3rd Ed., Springer, New York, NY, USA.

[63] Maciel, P., Koop, A., Vaz, G., 2013. Modelling thruster-hull interaction with CFD, in: Proceedings of the ASME 2013 32nd International Conference on Ocean, Offshore and Arctic Engineering (OMAE 2013), Nantes, France.

[64] Millan, J., 2008. Thrust allocation techniques for dynamically positioned vessels. Report No LM-2008-04. National Research Council, Institute for Ocean Technology, Canada. https://doi.org/https://doi.org/10.4224/8894957

[65] Moberg, S., Hellström, S.A., 1983. Dynamic Positioning of a Four-Column Semi-Submersible - Model Tests of Interaction Forces and A Philosophy about Optimum Strategy when Operating the thrusters, in: Proceedings of the Second International Symposium on Ocean Engineering and Ship Handling, Gothenburg, Sweden. pp. 443–480.

[66] Moore, E.H., 1920. On the Reciprocal of the General Algebraic Matrix. Bull. Am. Math. Soc. 26, 394–395.

[67] Nabergoj, R., 2013. Pipelaying vessel Maxita - DP Basic Performance Analysis. Internal Report, Trieste, Italy. (Confidential).

[68] Neumann, G., 1952. On Wind-Generated Ocean Waves with Special Reference to the Problem of Wave Forecasting. New York University, College of Engineering Research Division, Department of Meteorology and Oceanography. New York, NY, USA.

[69] Newman, J.N., 1977. Marine Hydrodynamics. The MIT Press, Cambridge, MA, USA.

[70] Newman, J.N., 1974. Second-order, slowly-varying forces on vessels in irregular waves, in: Proceedings of the International Symposium on the Dynamics of Marine Vehicles and Structures in Waves, Mechanical Engineering Publications Ltd., University College, London, UK.

[71] Nienhuis, U., 1992. Analysis of thruster effectivity for dynamic positioning and low speed manoeuvring. Ph.D. Thesis. Delft University of Technology, Delft, The Netherlands.

[72] Nocedal, J., Wright, S.J., 2006. Numerical Optimization, 2nd ed. Springer Science+Business Media, LLC., New York, NY.

[73] Nordtveit, R., Nygård, B., Jullumstrø, E., 2007. Thrust Degradation in DP Operations, in: Proceedings of the Dynamic Positioning Conference, Houston, TX, USA.

[74] Ochi, M.K., 1998. Ocean Waves. Cambridge University Press, Cambridge. https://doi.org/10.1017/CBO9780511529559

[75] OCIMF, 1994. Prediction of wind loads and current loads on VLCCs. 2nd ed., Witherby and Co., London, UK.

[76] Oosterveld, M.W.C., 1970. Wake Adapted Ducted Propellers. Publication No. 345, Netherlands Ship Model Basin (NSMB), Wageningen, The Netherlands.

[77] Penrose, R., Todd, J.A., 1956. On best approximate solutions of linear matrix equations. Math. Proc. Cambridge Philos. Soc. 52, 17. https://doi.org/10.1017/S0305004100030929

[78] Pierson, W.J., Moskowitz, L., 1964. A proposed spectral form for fully developed wind seas based on the similarity theory of S. A. Kitaigorodskii. J. Geophys. Res. 69, 5181–5190. https://doi.org/10.1029/JZ069i024p05181

[79] Pinkster, J.A., 1979. Mean and low frequency wave drifting forces on floating structures. Ocean Eng. 6, 593–615. https://doi.org/10.1016/0029-8018(79)90010-6

[80] Rindarøy, M., 2013. Fuel Optimal Thrust Allocation In Dynamic Positioning. M.Sc. Thesis. Norwegian University of Science and Technology, Department of Engineering Cybernetics, Trondheim, Norway.

[81] Ruth, E., 2008. Propulsion control and thrust allocation on marine vessels. Ph.D. Thesis, NTNU, Department of Marine Technology, Trondheim, Norway.

[82] Ruth, E., Smogeli, O.N., Perez, T., Sorensen, A.J., 2009. Antispin Thrust Allocation for Marine Vessels. IEEE Trans. Control Syst. Technol. 17, 1257–1269. https://doi.org/10.1109/TCST.2008.2006187

[83] Shi, X., Wei, Y., Ning, J., Fu, M., Zhao, D., 2011. Optimizing Adaptive Thrust Allocation Based on Group Biasing Method for Ship Dynamic Positioning, in: Proceeding of the IEEE International Conference on Automation and Logistics, Chongqing, China. pp. 394–398.

[84] Smogeli, Ø.N., 2006. Control of Marine Propellers - From Normal to Extreme Conditions. Ph.D. Thesis, NTNU, Department of Marine Technology, Trondheim, Norway.

[85] SNAME, 1950. Nomenclature for treating the motion of a submerged body through a fluid. Tech. Res. Bull. 1–5, 1–15.

[86] Snijders, J.G., 2005. Wave Filtering and Thruster Allocation for Dynamic Positioned Ships. M.Sc. Thesis. Delft University of Technology, Delft, The Netherlands.

[87] Sørdalen, O.J., 1997. Optimal thrust allocation for marine vessels. Control Eng. Pract. 5, 1223–1231. https://doi.org/10.1016/S0967-0661(97)84361-4

[88] Sørensen, A.J., 2012. Marine Control Systems - Propulsion and Motion Control of Ships and Ocean Structures. Lecture Notes (Report UK-12-76). Department of Marine Technology, NTNU, Trondheim, Norway.

[89] Sørensen, A.J., 2011. A survey of dynamic positioning control systems. Annu. Rev. Control 35, 123–136. https://doi.org/10.1016/j.arcontrol.2011.03.008

[90] Specht, D.F., 1991. A general regression neural network. IEEE Trans. Neural Networks 2, 568–576. https://doi.org/10.1109/72.97934

[91] Spjøtvold, J., Johansen, T.A., 2009. Fault tolerant control allocation for a thruster-controlled floating platform using parametric programming, in: Proceedings of the 48th IEEE Conference on Decision and Control, Shanghai, China.

[92] Steen, S., 2014. Naval Hydrodynamics: Foil and Propeller Theory. Lecture Notes TMR4220. Department of Marine Technology, NTNU, Trondheim, Norway.

[93] Ström-Tejsen, J., Yeh, H.Y.H., Moran, D.D., 1973. Added Resistance in Waves. Trans. SNAME 81, 109–143.

[94] The MathWorks, 2018. MATLAB R2018b. Software package. The MathWorks, Inc., Natick, MA, USA.

[95] Torczon, V., 1997. On the Convergence of Pattern Search Algorithms. SIAM J. Optim. 7, 1–25. https://doi.org/10.1137/S1052623493250780

[96] Tröltzsch, A., 2016. A sequential quadratic programming algorithm for equality-constrained optimization without derivatives. Optim. Lett. 10, 383–399. https://doi.org/10.1007/s11590-014-0830-y

[97] Valčić, M., Dejhalla, R., 2015. Neural Network Prediction of Open Water Characteristics of Ducted Propeller. Pomor. Zb. - J. Marit. Transp. Sci. 49–50, 101–115.

[98] Valčić, M., Prpić-Oršić, J., 2017. Forbidden zone handling in optimal thrust allocation of DP vessels, in: Proceedings of the 17th International Congress of the International Maritime Association of the Mediterranean IMAM 2017 - Maritime Transportation and Harvesting of Sea Resources, Lisbon, Portugal. pp. 1043–1050.

[99] Valčić, M., Prpić-Oršić, J., 2016. Hybrid method for estimating wind loads on ships based on elliptic Fourier analysis and radial basis neural networks. Ocean Eng. 122, 227–240. https://doi.org/10.1016/j.oceaneng.2016.06.031

[100] Valčić, M., Prpić-Oršić, J., Nabergoj, R., 2014. Impact of Thruster Interaction Effects on Optimal Thrust Allocation in Dynamic Positioning Systems, in: Proceedings of the 21st Symposium on Theory and Practice of Shipbuilding, In Memoriam Prof. Leopold Sorta - Sorta 2014, Baška, the Island of Krk, Croatia. pp. 347–356.

[101] Van Dijk, R.R.T., Aalbers, A.B., 2001. "What Happens in Water" - The use of Hydrodynamics to Improve DP, in: Proceedings of the Dynamic Positioning Conference, Houston, TX, USA.

[102] Vartdal, L., Garen, R., 2001. A Thruster System which Improves Positioning Power by Reducing Interaction Losses, in: Proceedings of the Dynamic Positioning Conference, Houston, TX, USA.

[103] Wichers, J., Bultema, S., Matten, R., 1998. Hydrodynamic Research on and Optimizing Dynamic Positioning System of a Deep Water Drilling Vessel, in: Proceedings of the 30th Offshore Technology Conference (OTC 1998), Houston, TX, USA.

[104] Wit, C. de, 2009. Optimal Thrust Allocation Methods for Dynamic Positioning of Ships. M.Sc. Thesis. Delft University of Technology, Faculty of Electrical Engineering, Mathematics and Computer Science, Delft Institute of Applied Mathematics, Delft, The Netherlands.

[105] Yang, S.-Z., Wang, L., S., Z., 2011a. Optimal Thrust Allocation Based on Fuel-efficiency for Dynamic Positioning System. J. Sh. Mech. 15, 217–226.

[106] Yang, S.-Z., Wang, L., Sun, P., 2011b. Optimal thrust allocation logic design of dynamic positioning with pseudo-inverse method. J. Shanghai Jiaotong Univ. 16, 118–123.

[107] Yvin, C., Muller, P., Koushan, K., 2017. Numerical Study of Propeller Ventilation, in: Proceedings of the Fifth International Symposium on Marine Propulsors Smp'17, Espoo, Finland.

[108] Zhao, D.-W., Ding, F.-G., Tan, J.-F., Liu, Y.-Q., Bian, X.-Q., 2010. Optimal Thrust Allocation based GA for Dynamic Positioning Ship, in: Proceedings of the 2010 IEEE International Conference on Mechatronics and Automation, Xi'an, China. pp. 1254–1258.

List of figures

#	Caption	Page
1	DP structure with associated subsystems and modules	12
2	6DOF with respect to the body reference frame {*b*}	14
3	Total motion of a ship as a sum of LF and HF motions	19
4	The local and natural wind field near the vessel	20
5	Relative wind speed and direction	21
6	Notation of wind directions with respect to {*b*} and {*n*} for $u = v = 0$	22
7	Wind forces and moments in the horizontal plane	22
8	Azimuth thruster	32
9	Ducted propeller basic dimensions	32
10	Open water characteristics for the propeller K_a 4-70 in the nozzle no. 19A	35
11	Thrust propagation from demanded thrust T_d to actual thrust T_a	37
12	Thrust allocation from a DP controller $(\boldsymbol{\tau}_c)$ to demanded speed n_d for FPP	39
13	Thrust loss effects for $V_A > 0$	42
14	$T - n$ characteristics for thruster combination {K_a 4-70 and no. 19A} and $P/D = 1.0$ in case of $V_A = 0$ $(J = 0)$ and $V_A > 0$ $(J = 0.25)$	46
15	Interaction of two closely spaced azimuth thrusters	48
16	Thruster-thruster interactions for thruster configurations #2 and #3 and $x/D \in \{3.0, 3.85, 6.0\}$	49
17	Circular jet and characteristic propeller race velocities	51
18	Geometry and distribution of velocities for configuration #2	52
19	Geometry of velocities for configuration #4	53
20	Geometry of velocities for configuration #5	53
21	3D visualization of thrust reduction ratio t for ducted propeller K_a 4-70 in nozzle no. 19A, $D = 208$ mm, $n = 10$ s^{-1}, $\rho = 1000$ kg/m^3, $x/D = 6$, $-30° \le \delta, \phi < 30°$	54
22	Top view visualization of thrust reduction ratio t for ducted propeller K_a 4-70 in nozzle no. 19A, $D = 208$ mm, $n = 10$ s^{-1}, $\rho = 1000$ kg/m^3, $x/D = 6$, $-30° \le \delta, \phi < 30°$	54
23	Characteristic thruster quantities and sign convention	58
24	Circle area as the thrust region of an azimuth thruster	60
25	Circle area approximation with *N*-sided polygon	61
26	Thrust region divided to one forbidden zone (FZ) and two convex feasible sets (FS)	64
27	Determination of feasible set thrust regions	66
28	Nonlinear (left) and linearized (right) feasible thrust regions with thruster saturation and forbidden zone included	67

29 Visualization of successful iteration within a CS algorithm 90

30 Visualization of unsuccessful iteration within a CS algorithm with mesh refinement 91

31 Example of mesh refinement in GPS algorithm during poll 93

32 An illustration of the mesh refinement for $n+1$ positive basis poll in a case of unsuccessful polls 97

33 Heavy lift DP vessel as a reference vessel 98

34 Approximate thruster configuration of the reference vessel 99

35 Non-dimensional wind load coefficients for the reference vessel 100

36 Non-dimensional wave load coefficients ($T_0 = 6$ s, $\omega = 1.05$ s^{-1}) for the reference vessel 101

37 Non-dimensional sea current load coefficients for the reference vessel 102

38 Polar thrust distribution of azimuth thrusters 2 and 3 with respect to the wind angle of attack γ_{wind} and for $V_{wind} = 5$ m/s, $H_s = 1.78$ m, $T_p = 6.26$ s, $V_{curr} = 0.5$ m/s 111

39 Polar thrust distribution of azimuth thrusters 2 and 3 with respect to the wind angle of attack γ_{wind} and for $V_{wind} = 10$ m/s, $H_s = 3.21$ m, $T_p = 8.41$ s, $V_{curr} = 0.5$ m/s 112

40 Polar thrust distribution of azimuth thrusters 2 and 3 with respect to the wind angle of attack γ_{wind} and for $V_{wind} = 15$ m/s, $H_s = 5.07$ m, $T_p = 10.56$ s, $V_{curr} = 0.5$ m/s 113

41 Polygon approximation of thrust regions with forbidden zones for thrusters 2 and 3 117

42 Selection of starting and ending angles $\varphi_{\text{start}}^{\text{FS}_{2k}}$ and $\varphi_{\text{end}}^{\text{FS}_{2k}}$ for thruster 2 117

43 Resulting thrusts and azimuth angles with respect to γ_{wind} for all azimuth thrusters in environmental conditions $V_{wind} = 10$ m/s, $H_s = 3.21$ m, $T_p = 8.41$ s, $V_{curr} = 0.5$ m/s 119

44 Polar thrust distribution of azimuth thrusters 2 and 3 with respect to the wind angle of attack γ_{wind} and for $V_{wind} = 10$ m/s, $H_s = 3.21$ m, $T_p = 8.41$ s, $V_{curr} = 0.5$ m/s 120

45 Total demanded minimum power for all azimuth thrusters with respect to the wind angle of attack γ_{wind} and for $V_{wind} = 10$ m/s, $H_s = 3.21$ m, $T_p = 8.41$ s, $V_{curr} = 0.5$ m/s 122

46 Relative deviations of total demanded minimum power for thrusters 2 and 3 regarding different optimization approaches 124

47 Illustration of power-thrust relationship for thruster 2 (Table 3) 127

48 Workflow of proposed two-step nonlinear optimization procedure with implementation of forbidden zones or thruster interaction effects 133

49 Resulting thrusts and azimuth angles with respect to γ_{wind} for all azimuth thrusters in environmental conditions $V_{wind} = 10$ m/s, $H_s = 3.21$ m, $T_p = 8.41$ s, $V_{curr} = 0.5$ m/s 135

50 Total demanded minimum power for all azimuth thrusters with respect to the wind angle of attack γ_{wind} and for $V_{wind} = 10$ m/s, $H_s = 3.21$ m, $T_p = 8.41$ s, $V_{curr} = 0.5$ m/s 136

51 Relative deviations of total demanded minimum power for thrusters 2 and 3 regarding different nonlinear optimization approaches 137

52 Workflow of the proposed hybrid optimization approach with sensitivity analysis (left) and GRNN as a generator of initial or direct solutions (right) 142

List of tables

#	Caption	Page
1	Notation of characteristic physical quantities with respect to the motion in 6DOF	15
2	Summary of thruster configurations in terms of interaction angles δ and ϕ	50
3	Main thruster characteristics installed on the reference vessel	99
4	Relationship between mean wind speed V_{wind} (m/s), significant wave height H_s (m), wave peak period T_p (s) and wave peak frequency ω_0 (s^{-1})	102
5	Quantitative indicators of demanded power for analysed cases (*a*)-(*c*) obtained with WGIM and QP optimization approaches for thrusters 2 and 3	123
6	Quantitative indicators of optimization results based on initial solution $\mathbf{u}_0 = \mathbf{0} \in \mathbb{R}^{2r}$ in three different cases, with associated GRNN performance	145
7	Quantitative indicators of optimization results based on GRNN generated initial solutions for three different cases	146

APPENDIXES

Appendix 1 Pseudo-code of optimization algorithms

In Appendix 1, the pseudo-code for selected optimization algorithms used in this thesis is presented, as follows:

- Appendix 1.1 Pseudo-code of active-set algorithm for convex QP problems
- Appendix 1.2 Pseudo-code of line search SQP algorithm
- Appendix 1.3 Pseudo-code of coordinate search (CS) algorithm
- Appendix 1.4. Pseudo-code of the generalised pattern search (GPS) algorithm
- Appendix 1.5 Pseudo-code of the mesh adaptive direct search (MADS) algorithm

Appendix 1.1 Pseudo-code of active-set algorithm for convex QP problems

Step 1 Determine a feasible initial point $\mathbf{x}_0$ by means of linear programing

Step 2 Set an initial working subset W_0 of active constraints at initial point $\mathbf{x}_0$ where $W_0 = A_0 = \{i \mid \mathbf{a}_i^{\mathrm{T}}\mathbf{x}_0 = b_i\}$

Step 3 Start iterative process (loop)

for $k = 0,1,2,\ldots$

Solve the following QP sub-problem

$$\min_{\mathbf{p}} \left(\tfrac{1}{2}\mathbf{p}^{\mathrm{T}}\mathbf{W}\mathbf{p} + (\mathbf{W}\mathbf{x}_k + \mathbf{w})^{\mathrm{T}}\mathbf{p}\right)$$
$$\text{s.t. } \mathbf{a}_i^{\mathrm{T}}\mathbf{p} = 0, \quad i \in W_k$$

in order to find improving (optimal) direction $\mathbf{p}^* = \mathbf{p}_k$

if $\|\mathbf{p}_k\| = 0$

Compute Lagrange multipliers μ_i, $i \in W_k$, from

$$\sum_{i \in W} \mathbf{a}_i \mu_i = \mathbf{W}\mathbf{x} + \mathbf{w}$$

if $\mu_i \geq 0, \ \forall i \in W_k \cap I$

stop – optimal solution found, $\mathbf{x}^* = \mathbf{x}_k$

else

Remove *j*-th constraint from the working set W_k

$$j = \arg\min_{j \in W_k \cap I}(\mu_j)$$
$$\mathbf{x}_{k+1} = \mathbf{x}_k$$
$$W_{k+1} = W_k \setminus \{j\}$$

end

else

Compute the step length α_k from

$$\alpha_k = \min\left\{1, \min_{(i \notin W_k,\ \mathbf{a}_i^{\mathrm{T}}\mathbf{p}_k < 0)} \frac{b_i - \mathbf{a}_i^{\mathrm{T}}\mathbf{x}_k}{\mathbf{a}_i^{\mathrm{T}}\mathbf{p}_k}\right\}$$

Update $\mathbf{x}_k$ according to

$$\mathbf{x}_{k+1} = \mathbf{x}_k + \alpha_k \mathbf{p}_k$$

Determine the set of blocking constraints J

$$J = \arg\min_{(i \notin W_k,\ \mathbf{a}_i^{\mathrm{T}}\mathbf{p}_k < 0)} \frac{b_i - \mathbf{a}_i^{\mathrm{T}}\mathbf{x}_k}{\mathbf{a}_i^{\mathrm{T}}\mathbf{p}_k}$$

if $\alpha_k < 1$

Add one of the blocking constraints to $\mathbf{W}_k$

$$W_{k+1} = W_k \cup \{j\}, \ j \in J$$

else

$$W_{k+1} = W_k$$

end

end

end

Source: Adjusted according to (Nocedal and Wright, 2006)

Appendix 1.2 Pseudo-code of line search SQP algorithm

Step 1 Initialization

- Choose parameters $0 < \eta < 0.5,\ 0 < \rho < 1$ and $0 < \tau < 1$
- Determine a feasible initial point $(\mathbf{x}_0, \boldsymbol{\lambda}_0)$ by means of linear programing
- Evaluate $f(\mathbf{x}_0),\ \nabla f(\mathbf{x}_0),\ \mathbf{c}(\mathbf{x}_0)$ and $\nabla \mathbf{c}(\mathbf{x}_0)$
- Choose initial Hessian approximation $\mathbf{B}_0$ (e.g. $\mathbf{B}_0 = \mathbf{I} \in \mathbb{R}^{n \times n}$)

Step 2 Start iterative process (loop)

repeat (until a convergence criteria is fulfilled)

if (convergence criteria is fulfilled)

stop – optimal solution found

end

Solve the following QP sub-problem

$$\min_{\mathbf{p} \in \mathbb{R}^n} \left(\tfrac{1}{2} \mathbf{p}_k^{\mathrm{T}} \nabla_{\mathbf{xx}}^2 L(\mathbf{x}_k, \boldsymbol{\lambda}_k) \mathbf{p}_k + \nabla f^{\mathrm{T}}(\mathbf{x}_k) \mathbf{p}_k \right)$$

$$\text{s.t.} \quad \nabla \mathbf{c}^{\mathrm{T}}(\mathbf{x}_k) \mathbf{p}_k + \mathbf{c}(\mathbf{x}_k) = \mathbf{0}, \quad i \in E$$

$$\nabla \mathbf{c}^{\mathrm{T}}(\mathbf{x}_k) \mathbf{p}_k + \mathbf{c}(\mathbf{x}_k) \geq \mathbf{0}, \quad i \in I$$

in order to find step $\mathbf{p}_k$, i.e. the solution of KKT conditions

$$\begin{bmatrix} \nabla_{\mathbf{xx}}^2 L(\mathbf{x}_k, \boldsymbol{\lambda}_k) & -\nabla \mathbf{c}(\mathbf{x}_k) \\ -\nabla \mathbf{c}^{\mathrm{T}}(\mathbf{x}_k) & \mathbf{0} \end{bmatrix} \begin{bmatrix} \mathbf{p}_k \\ \mathbf{o}_k \end{bmatrix} = - \begin{bmatrix} \nabla f(\mathbf{x}_k) - \nabla \mathbf{c}(\mathbf{x}_k) \boldsymbol{\lambda}_k \\ -\mathbf{c}(\mathbf{x}_k) \end{bmatrix}.$$

Choose μ_k and α_k so that $\mathbf{p}_k$ defines a descent direction for the merit function $\phi(\mathbf{x}_k)$, i.e. μ_k should fulfil the following criteria

$$\mu_k \geq \frac{\nabla f^{\mathrm{T}}(\mathbf{x}_k) \mathbf{p}_k + \frac{1}{2} \mathbf{p}_k^{\mathrm{T}} \mathbf{B}_k \mathbf{p}_k}{(1 - \rho) \left\| \mathbf{c}(\mathbf{x}) \right\|_1}$$

and α_k should be evaluated according to

$\alpha_k = 1$

while $\phi(\mathbf{x}_k + \alpha_k \mathbf{p}_k, \mu_k) > \phi(\mathbf{x}_k, \mu_k) + \eta \alpha_k D(\phi(\mathbf{x}_k, \mu_k), \mathbf{p}_k)$

$\alpha_k = \tau_\alpha \alpha_k,\ 0 < \tau_\alpha < \tau$

end

Set: $\mathbf{x}_{k+1} = \mathbf{x}_k + \alpha_k \mathbf{p}_k,\ \boldsymbol{\lambda}_{k+1} = \boldsymbol{\lambda}_k + \alpha_k \mathbf{o}_k$

Evaluate: $f(\mathbf{x}_{k+1}),\ \nabla f(\mathbf{x}_{k+1}),\ \mathbf{c}(\mathbf{x}_{k+1})$ and $\nabla \mathbf{c}(\mathbf{x}_{k+1})$

Set: $\mathbf{s}_k = \alpha_k \mathbf{p}_k,\ \mathbf{y}_k = \nabla_{\mathbf{x}} L(\mathbf{x}_{k+1}, \boldsymbol{\lambda}_{k+1}) - \nabla_{\mathbf{x}} L(\mathbf{x}_k, \boldsymbol{\lambda}_{k+1})$

Obtain $\boldsymbol{\theta}_k$: **if** $\mathbf{s}_k^{\mathrm{T}} \mathbf{y}_k \geq 0.2 \mathbf{s}_k^{\mathrm{T}} \mathbf{B}_k \mathbf{s}_k$

$\theta_k = 1$

else

$\theta_k = (0.8 \mathbf{s}_k^{\mathrm{T}} \mathbf{B}_k \mathbf{s}_k) / (\mathbf{s}_k^{\mathrm{T}} \mathbf{B}_k \mathbf{s}_k - \mathbf{s}_k^{\mathrm{T}} \mathbf{y}_k)$

end

Evaluate: $\tilde{\mathbf{y}}_k = \theta_k \mathbf{y}_k + (1 - \theta_k) \mathbf{B}_k \mathbf{s}_k$

Update $\mathbf{B}_k$ according the BFGS quasi-Newton approximation

$$\mathbf{B}_{k+1} = \mathbf{B}_k - \frac{\mathbf{B}_k \mathbf{s}_k \mathbf{s}_k^{\mathrm{T}} \mathbf{B}_k}{\mathbf{s}_k^{\mathrm{T}} \mathbf{B}_k \mathbf{s}_k} + \frac{\tilde{\mathbf{y}}_k \tilde{\mathbf{y}}_k^{\mathrm{T}}}{\mathbf{s}_k^{\mathrm{T}} \tilde{\mathbf{y}}_k}$$

end

Source: Adjusted according to (Nocedal and Wright, 2006)

Appendix 1.3 Pseudo-code of coordinate search (CS) algorithm

Step 1 Initialization

- Choose initial step length, i.e. initial mesh size $\Delta_0 \in \langle 0, +\infty \rangle$
- Define stopping tolerance $\varepsilon_{\text{stop}} \in [0, +\infty\rangle$
- Initialize iteration counter $k = 0$
- Define initial point $\mathbf{x}_0 \in \mathbb{R}^n$ such that $f(\mathbf{x}_0) < \infty$

Step 2 Poll

if $f(\mathbf{t}) < f(\mathbf{x}_k)$ for some $\mathbf{t} \in P_k = \{\mathbf{x}_k \pm \Delta_k \mathbf{e}_i \mid i = 1, 2, \ldots, n\}$

$\mathbf{x}_{k+1} = \mathbf{t}$

$\Delta_{k+1} = \Delta_k$

else

$\mathbf{x}_{k+1} = \mathbf{x}_k$

$\Delta_{k+1} = \frac{1}{2}\Delta_k$

end

Step 3 Termination

if $\Delta_{k+1} \geq \varepsilon_{\text{stop}}$

$k = k + 1$

go to *Step 2* (Poll)

else

stop

end

Source: Adjusted according to (Audet and Hare, 2017)

Appendix 1.4. Pseudo-code of the generalised pattern search (GPS) algorithm

Step 1 Initialization

- Define initial point $\mathbf{x}_0 \in \mathbb{R}^n$ such that $f(\mathbf{x}_0) < \infty$
- Choose initial step length, i.e. initial mesh size $\Delta_0 \in \langle 0, +\infty \rangle$
- Determine the positive spanning set of directions in terms of matrix $\mathbf{D} = \mathbf{GZ}$
- Define parameter $\tau \in \langle 0, 1 \rangle$ for the adjustment of the mesh size
- Define stopping tolerance $\varepsilon_{\text{stop}} \in [0, +\infty \rangle$
- Initialize iteration counter $k = 0$

Step 2 Search

if $f(\mathbf{t}) < f(\mathbf{x}_k)$ for some $\mathbf{t} \in S_k \subseteq M_k$

$\mathbf{x}_{k+1} = \mathbf{t}$

$\Delta_{k+1} = \tau^{-1} \Delta_k$

go to *Step 4* (Termination)

else

go to *Step 3* (Poll)

end

Step 3 Poll

Select a positive spanning set $\mathbb{D}_k \subseteq \mathbb{D}$

if $f(\mathbf{t}) < f(\mathbf{x}_k)$ for some $\mathbf{t} \in P_k = \{\mathbf{x}_k + \Delta_k \mathbf{d} \mid \mathbf{d} \in \mathbb{D}_k\}$

$\mathbf{x}_{k+1} = \mathbf{t}$

$\Delta_{k+1} = \tau^{-1} \Delta_k$

else

$\mathbf{x}_k$ is a mesh local optimizer

$\mathbf{x}_{k+1} = \mathbf{x}_k$

$\Delta_{k+1} = \tau \Delta_k$

end

Step 4 Termination

if $\Delta_{k+1} \geq \varepsilon_{\text{stop}}$

$k = k + 1$

go to *Step 2* (Search)

else

stop

end

Source: Adjusted according to (Audet and Hare, 2017)

Appendix 1.5 Pseudo-code of the mesh adaptive direct search (MADS) algorithm

Step 1 Initialization

- Define initial point $\mathbf{x}_0 \in \Omega$ and barrier function $f_\Omega(\mathbf{x})$
- Choose initial step length, i.e. initial frame size $\Theta_0 \in \langle 0, +\infty \rangle$
- Determine the positive spanning set of directions in terms of the matrix $\mathbf{D} = \mathbf{GZ}$
- Define parameter $\tau \in \langle 0, 1 \rangle$ for the adjustment of the mesh size
- Define stopping tolerance $\varepsilon_{\text{stop}} \in [0, +\infty \rangle$
- Initialize iteration counter $k = 0$

Step 2 Parameter update

Set the mesh size parameter

$$\Delta_k = \min\{\Theta_k, \Theta_k^2\}$$

Step 3 Search

if $f_\Omega(\mathbf{t}) < f_\Omega(\mathbf{x}_k)$ for some $\mathbf{t} \in S_k \subseteq M_k$

$\mathbf{x}_{k+1} = \mathbf{t}$

$\Theta_{k+1} = \tau^{-1}\Theta_k$

go to *Step 5* (Termination)

else

go to *Step 4* (Poll)

end

Step 4 Poll

Select a positive spanning set $\mathbb{D}_k$ such that $P_k = \{\mathbf{x}_k + \Delta_k \mathbf{d} \mid \mathbf{d} \in \mathbb{D}_k\} \subseteq F_k$

if $f_\Omega(\mathbf{t}) < f_\Omega(\mathbf{x}_k)$ for some $\mathbf{t} \in P_k \subseteq F_k$

$\mathbf{x}_{k+1} = \mathbf{t}$

$\Theta_{k+1} = \tau^{-1}\Theta_k$

else

$\mathbf{x}_{k+1} = \mathbf{x}_k$

$\Theta_{k+1} = \tau\Theta_k$

end

Step 5 Termination

if $\Theta_{k+1} \geq \varepsilon_{\text{stop}}$

$k = k + 1$

go to *Step 2* (Parameter update)

else

stop

end

Source: Adjusted according to (Audet and Hare, 2017)

Appendix 2 Non-dimensional wave load coefficients for the reference vessel

In Appendix 2, the non-dimensional wave load coefficients are presented in the following figures for the reference vessel in cases $\omega = 0.63$ s^{-1} (upper figure) and $\omega = 0.42$ s^{-1} (lower figure).

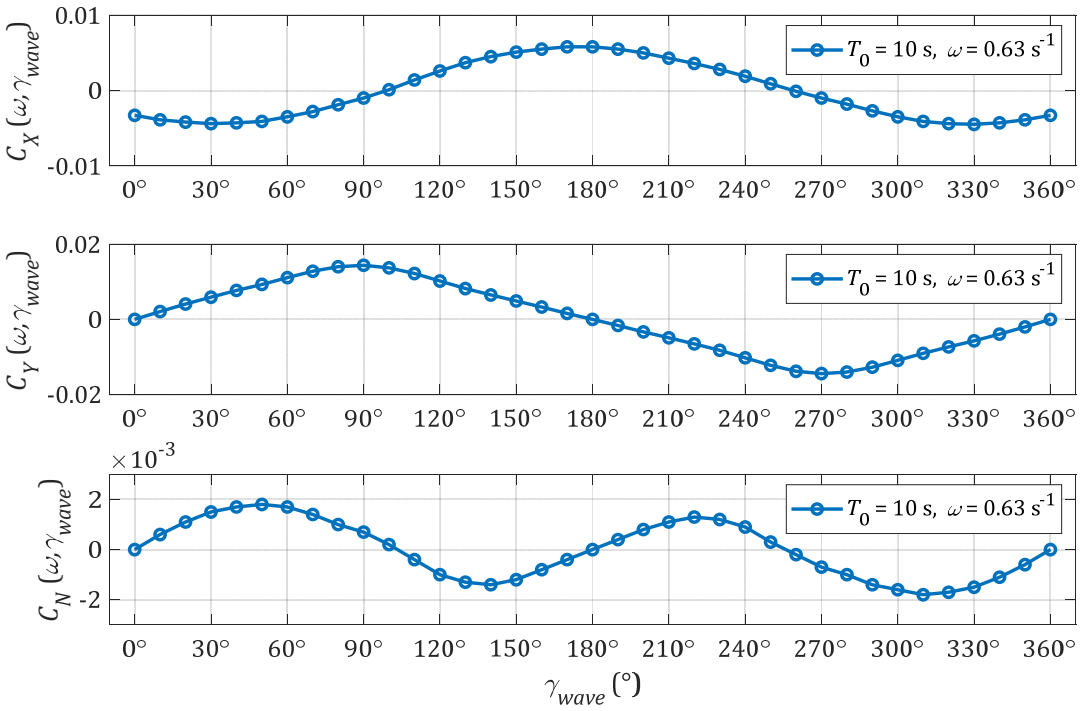

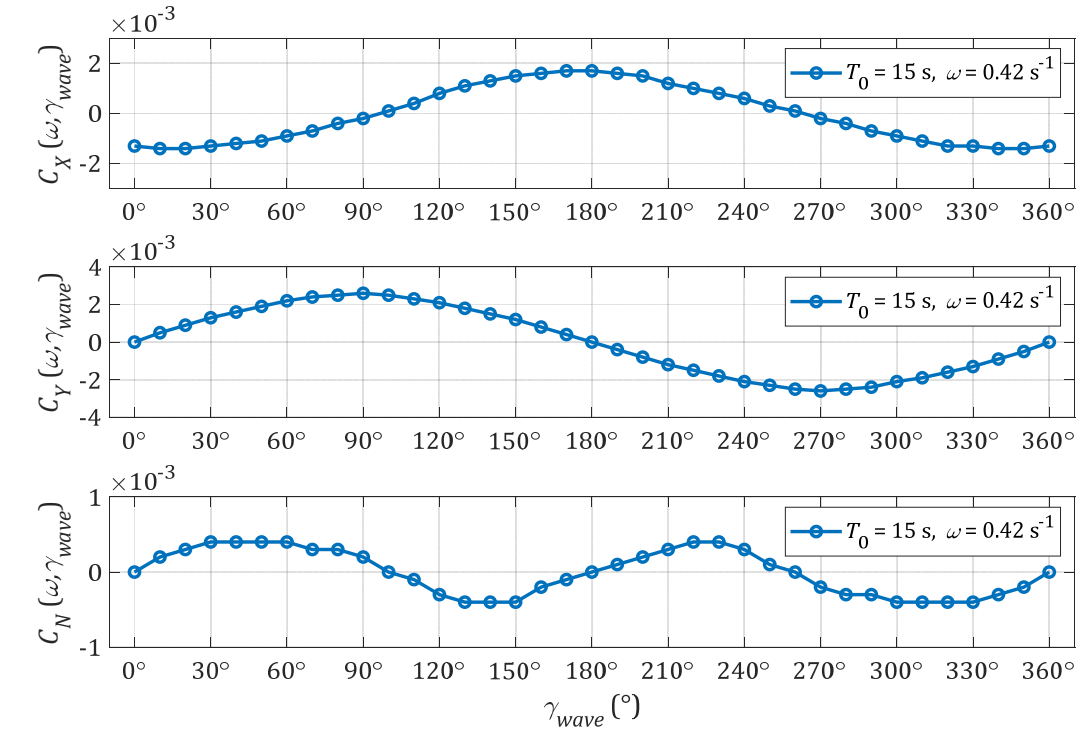

Appendix 3 Polar thrust distribution of azimuth thrusters with respect to the wind angle of attack and various environmental conditions

In Appendix 3, polar thrust distributions of analysed azimuth thrusters are graphically presented with respect to the wind angle of attack and various environmental conditions, as follows:

- Appendix 3.1 Polar thrust distribution of azimuth thrusters with respect to the wind angle of attack γ_{wind} and for $V_{wind} = 5$ m/s, $H_s = 1.78$ m, $T_p = 6.26$ s, $V_{curr} = 0.5$ m/s, Case (*a*) in Chapter 6.2.5
- Appendix 3.2 Polar thrust distribution of azimuth thrusters with respect to the wind angle of attack γ_{wind} and for $V_{wind} = 10$ m/s, $H_s = 3.21$ m, $T_p = 8.41$ s, $V_{curr} = 0.5$ m/s, Case (*b*) in Chapter 6.2.5
- Appendix 3.3 Polar thrust distribution of azimuth thrusters with respect to the wind angle of attack γ_{wind} and for $V_{wind} = 15$ m/s, $H_s = 5.07$ m, $T_p = 10.56$ s, m/s, Case (*c*) in Chapter 6.2.5

In the following figures (Appendixes 3.1-3.3), one should notice that the blue line with circle marker symbols represents the optimal thrust allocation without the interaction effects included, as described in step (1) in Chapter 6.2.4. On the other hand, the red line with square marker symbols represents the actual state that occurs after the interaction effects reduce the thrust of rear thruster, as described in step (2) in Chapter 6.2.4. Finally, the black line with diamond marker symbols represents the final reallocated state that takes into account thrust losses of the rear thruster, as described in step (3) in Chapter 6.2.4.

Appendix 3.1 Polar thrust distribution of azimuth thrusters with respect to the wind angle of attack γ_{wind} and for $V_{wind} = 5$ m/s, $H_s = 1.78$ m, $T_p = 6.26$ s, $V_{curr} = 0.5$ m/s Case (a) in Chapter 6.2.5

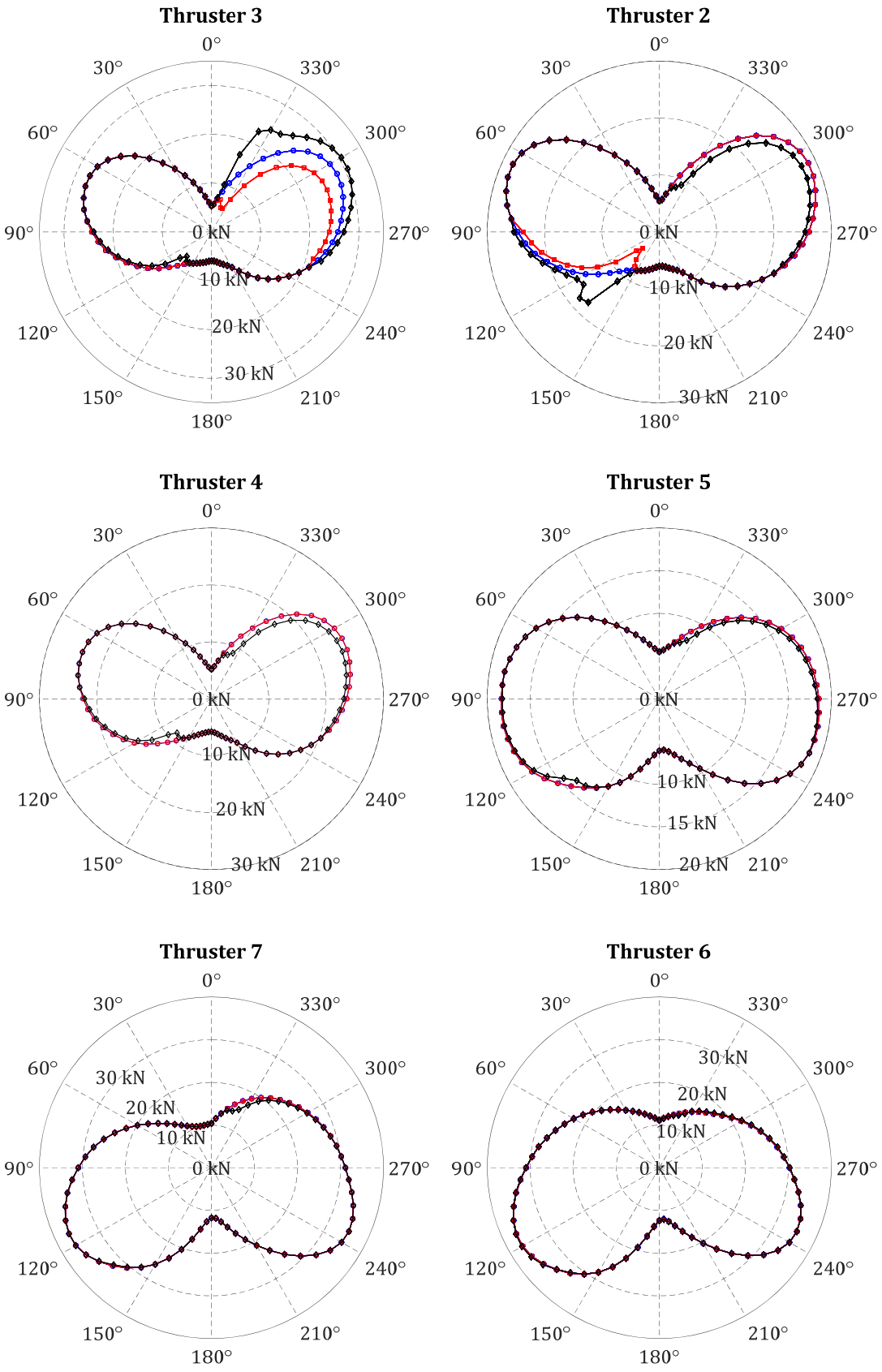

Appendix 3.2 Polar thrust distribution of azimuth thrusters with respect to the wind angle of attack γ_{wind} and for $V_{wind} = 10$ m/s, $H_s = 3.21$ m, $T_p = 8.41$ s, $V_{curr} = 0.5$ m/s Case (*b*) in Chapter 6.2.5

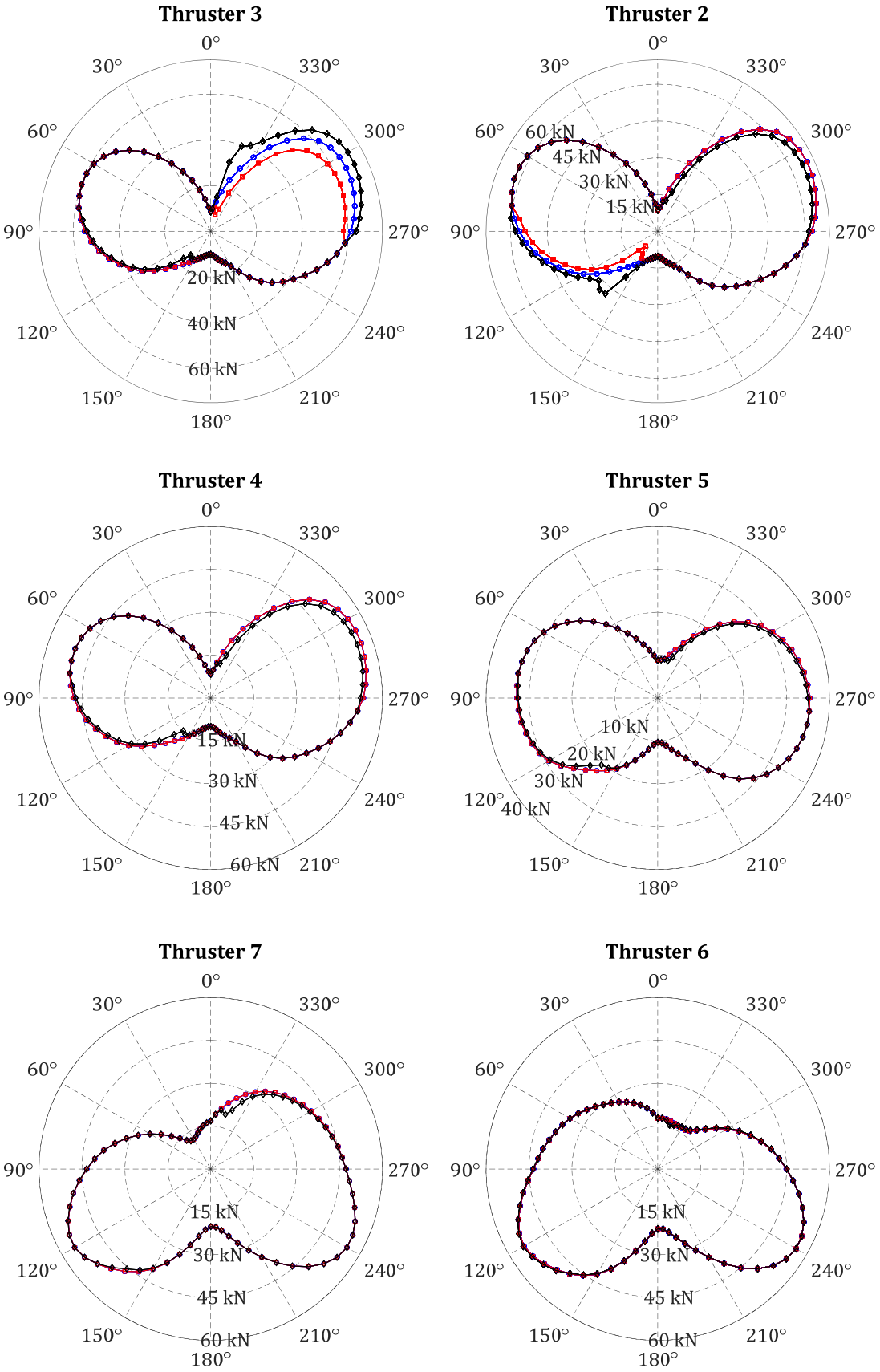

Appendix 3.3 Polar thrust distribution of azimuth thrusters with respect to the wind angle of attack γ_{wind} and for $V_{wind} = 15$ m/s, $H_s = 5.07$ m, $T_p = 10.56$ s, $V_{curr} = 0.5$ m/s Case (*c*) in Chapter 6.2.5

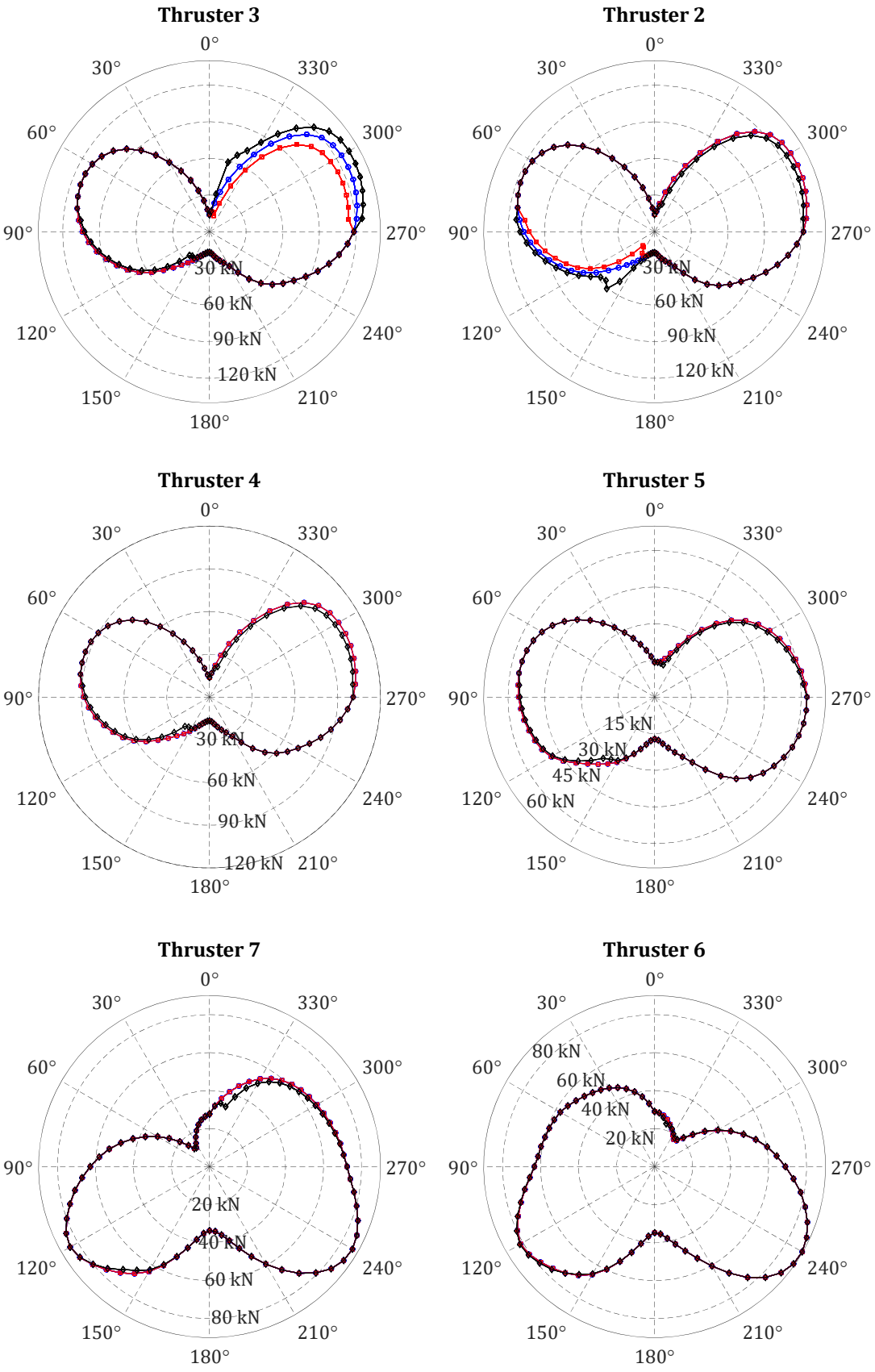

Appendix 4 Resulting thrusts and azimuth angles with respect to the wind angle of attack for all azimuth thrusters under specific environmental conditions (WGIM/QP approach)

In Appendix 4, resulting thrusts and azimuth angles are graphically presented for all azimuth thrusters with respect to the wind angle of attack and under specific environmental conditions. Presented results are associated with:

- the generalized inverse matrix (GIM) approach, without including any of thrust losses or forbidden zones,
- the weighted generalized inverse matrix (WGIM) approach, in which thrust losses due to thruster 2 – thruster 3 interactions were included, but without taking forbidden zones into account, and
- the quadratic programing (QP) approach with included forbidden zones and thruster saturation, but without thruster-thruster interactions.

The resulting thrusts and azimuth angles for environmental conditions (*a*) and (*c*), as defined in Chapter 6.2.5, are presented as two appendixes, i.e. as

- Appendix 4.1 Resulting thrusts and azimuth angles with respect to γ_{wind} for all azimuth thrusters with environmental conditions $V_{wind} = 5$ m/s, $H_s = 1.78$ m, $T_p = 6.26$ s, $\omega_0 = 1$ s^{-1}, $V_{curr} = 0.5$ m/s
- Appendix 4.2 Resulting thrusts and azimuth angles with respect to γ_{wind} for all azimuth thrusters with environmental conditions $V_{wind} = 15$ m/s, $H_s = 5.07$ m, $T_p = 10.56$ s, $\omega_0 = 0.59$ s^{-1}, $V_{curr} = 0.5$ m/s.

One should notice that trust variations are presented with solid lines and azimuth angles with dashed lines. Blue lines are related to GIM approach, red lines are related to WGIM approach, but without reallocation, black lines are also related to WGIM approach, but with reallocation, and green lines are related to QP approach without thruster interactions, but with thruster saturation and forbidden zones included.

Appendix 4.1 Resulting thrusts and azimuth angles with respect to γ_{wind} for all azimuth thrusters in environmental conditions $V_{wind} = 5$ m/s, $H_s = 1.78$ m, $V_{curr} = 0.5$ m/s

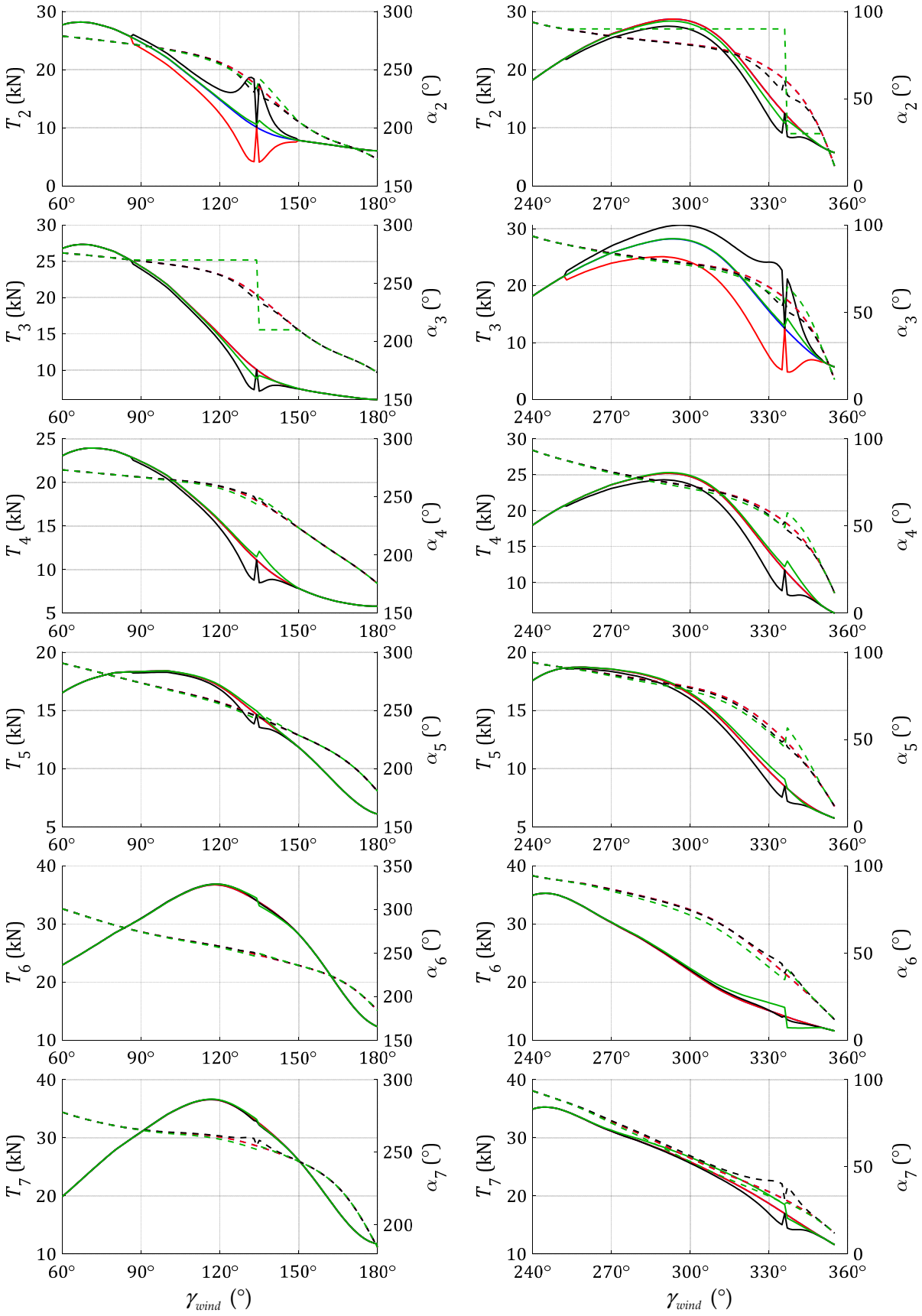

Appendix 4.2 Resulting thrusts and azimuth angles with respect to γ_{wind} for all azimuth thrusters in environmental conditions $V_{wind} = 15$ m/s, $H_s = 5.07$ m, $V_{curr} = 0.5$ m/s

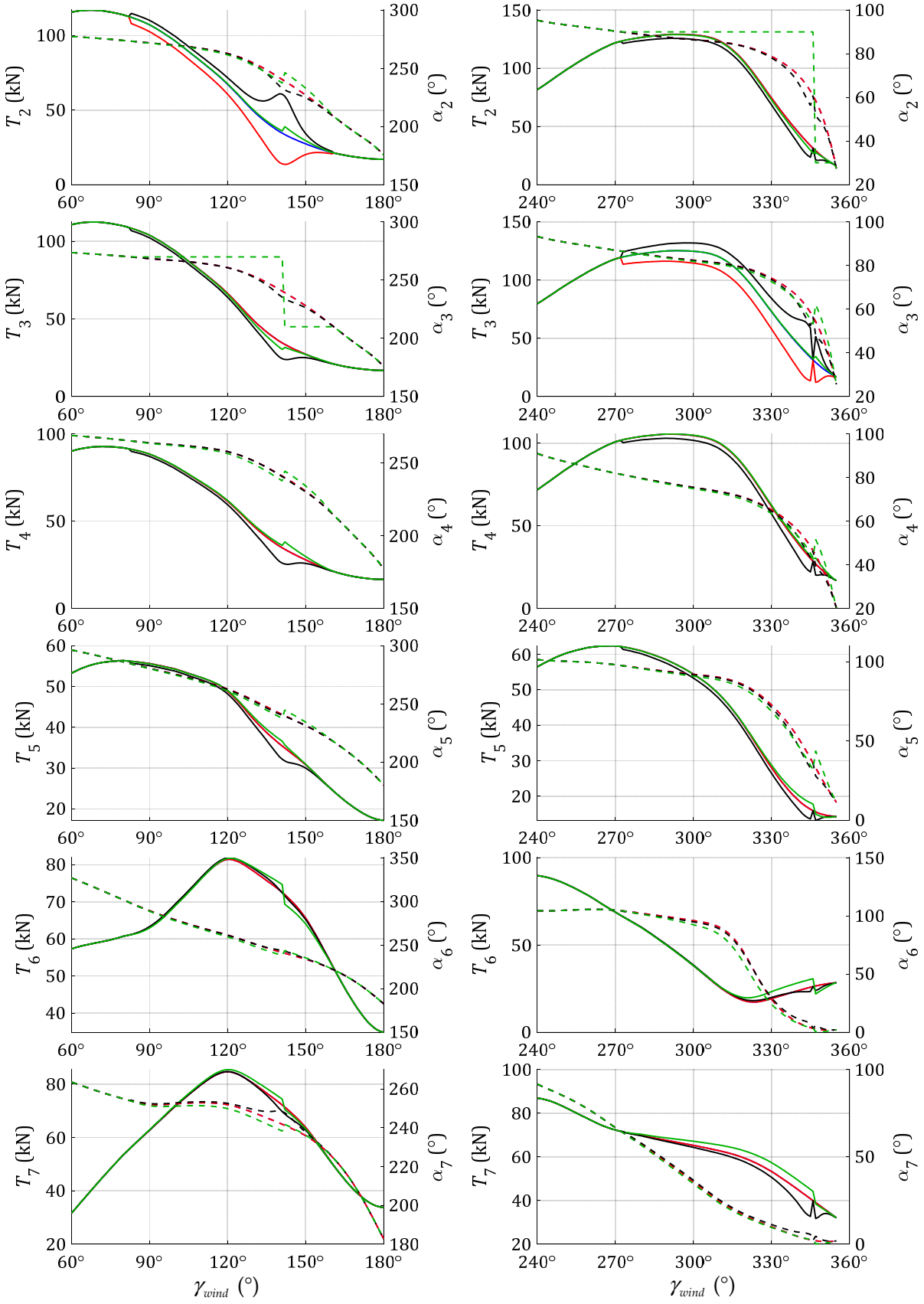

Appendix 5 Resulting thrusts and azimuth angles with respect to the wind angle of attack for all azimuth thrusters under specific environmental conditions (SQP/DS approach)

In Appendix 5, resulting thrusts and azimuth angles are graphically presented for all azimuth thrusters with respect to the wind angle of attack and under specific environmental conditions (*a*) and (*c*), as defined in Chapter 6.2.5. Obtained results are associated with sequential quadratic programming (SQP) and/or direct search (DS) optimization approach, and are presented as two appendixes, i.e. as

- Appendix 5.1 Resulting thrusts and azimuth angles with respect to γ_{wind} for all azimuth thrusters with environmental conditions $V_{wind} = 5$ m/s, $H_s = 1.78$ m, $T_p = 6.26$ s, $\omega_0 = 1$ s^{-1}, $V_{curr} = 0.5$ m/s
- Appendix 5.2 Resulting thrusts and azimuth angles with respect to γ_{wind} for all azimuth thrusters with environmental conditions $V_{wind} = 15$ m/s, $H_s = 5.07$ m, $T_p = 10.56$ s, $\omega_0 = 0.59$ s^{-1}, $V_{curr} = 0.5$ m/s.

Trust variations are again presented with solid lines and azimuth angles with dashed lines. Blue lines correspond to results of SQP/DS optimization without any interactions, red lines are related to SQP/DS optimization with thruster saturation and forbidden zones included, and black lines are related to SQP/DS optimization with thruster saturation and thruster interaction effects included.

Appendix 5.1 Resulting thrusts and azimuth angles with respect to γ_{wind} for all azimuth thrusters in environmental conditions $V_{wind} = 5$ m/s, $H_s = 1.78$ m, $V_{curr} = 0.5$ m/s

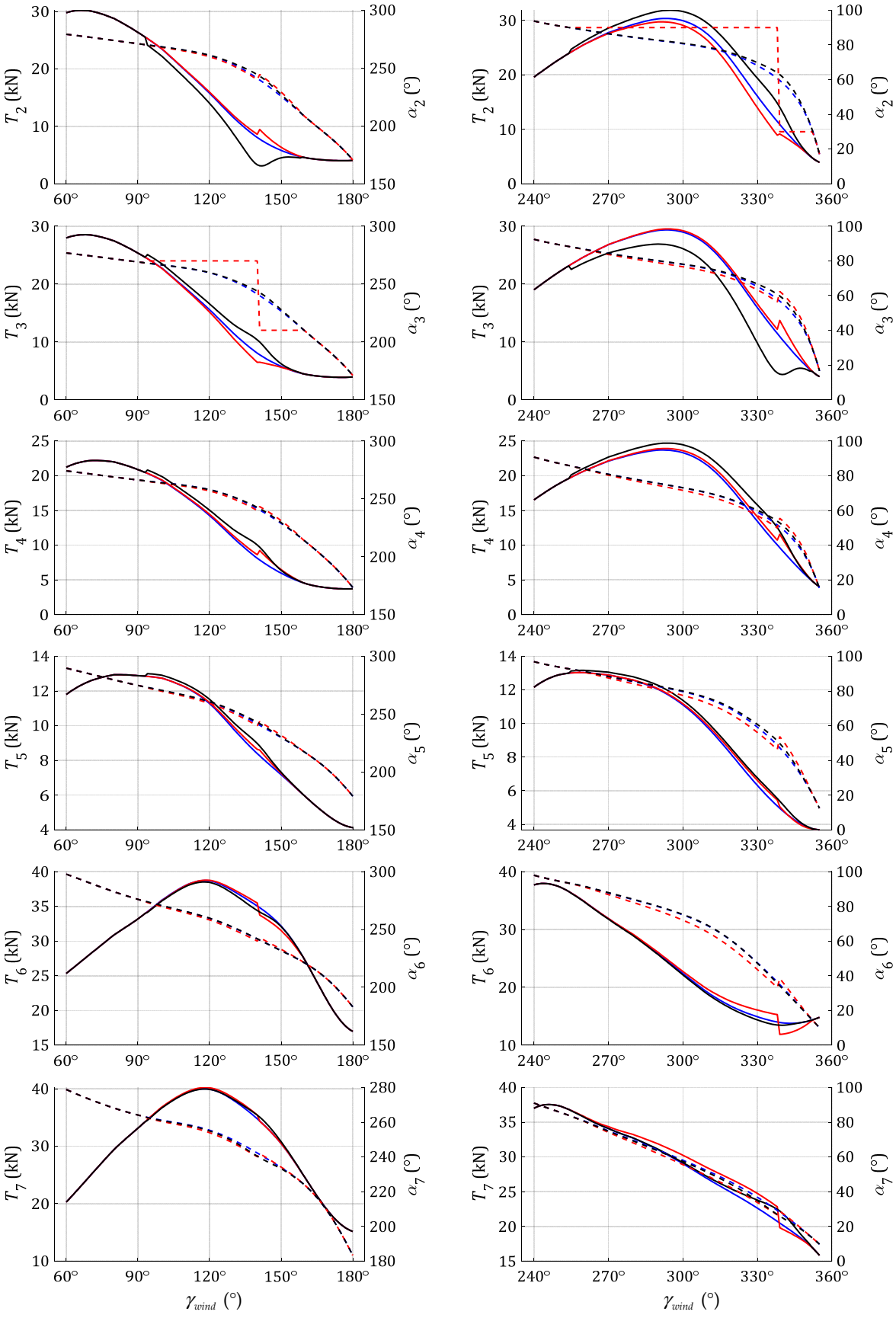

Appendix 5.2 Resulting thrusts and azimuth angles with respect to γ_{wind} for all azimuth thrusters in environmental conditions $V_{wind} = 15$ m/s, $H_s = 5.07$ m, $V_{curr} = 0.5$ m/s

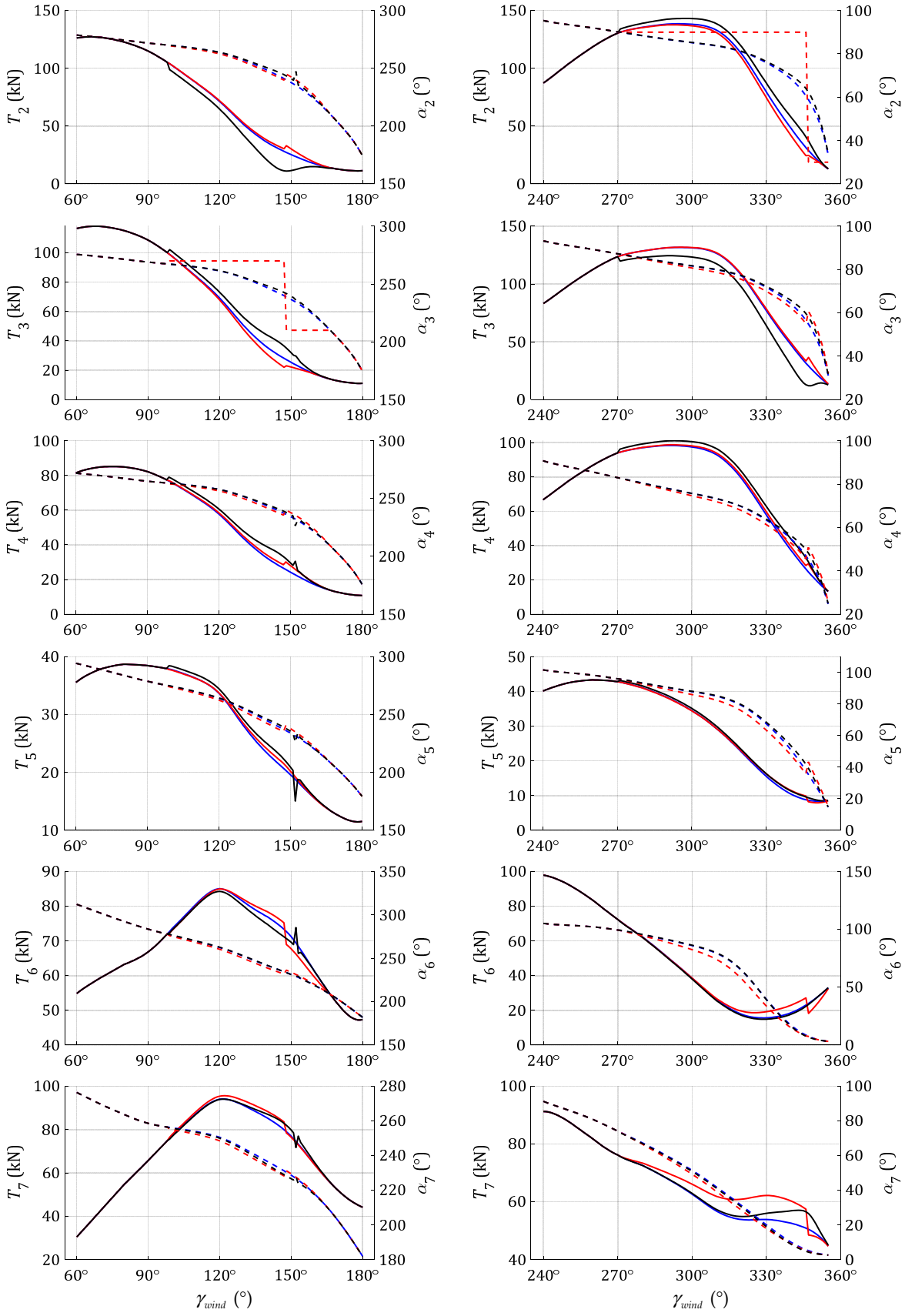

Appendix 6 Quantitative indicators of demanded power for analysed cases obtained with FZ and TTI optimization approaches for analysed thrusters

In Appendix 6, quantitative indicators of demanded power for analysed cases (*a*)-(*c*), as defined in Chapter 6.2.5., obtained with forbidden zones (FZ) and thruster-thruster interaction (TTI) optimization approaches for thrusters 2 and 3, are shown in the following table:

Optimization	Key variables	Front thruster	Case (*a*)	Case (*b*)	Case (*c*)
FZ approach	$[\gamma_{wind,\min}(\delta P), \gamma_{wind,\max}(\delta P)]$	2	[272°, 350°]	[284°, 353°]	[290°, 354°]
		3	[105°, 155°]	[105°, 161°]	[104°, 163°]
	$\gamma_{wind,\text{peak}}$	2	339°	345°	347°
		3	141°	146°	148°
	$\delta P_{\text{peak}}(\gamma_{wind,\text{peak}})$	2	0.0459	0.0496	0.0511
		3	0.0167	0.0220	0.0261
	$\mu(P)$	2	0.0131	0.0136	0.0138
		3	0.0060	0.0085	0.0099
	$\sigma(P)$	2	0.0115	0.0130	0.0134
		3	0.0043	0.0063	0.0076
TTI approach	$[\gamma_{wind,\min}(\delta P), \gamma_{wind,\max}(\delta P)]$	2	[291°, 349°]	[304°, 352°]	[310°, 353°]
		3	[120°, 151°]	[119°, 157°]	[118°, 159°]
	$\gamma_{wind,\text{peak}}$	2	338°	344°	346°
		3	140°	144°	146°
	$\delta P_{\text{peak}}(\gamma_{wind,\text{peak}})$	2	0.0422	0.0481	0.0496
		3	0.0159	0.0231	0.0273
	$\mu(P)$	2	0.0113	0.0124	0.0128
		3	0.0064	0.0087	0.0104
	$\sigma(P)$	2	0.0130	0.0147	0.0151
		3	0.0051	0.0075	0.0092

Cases (*a*), (*b*) and (*c*) are defined in terms of the following environmental conditions:

(*a*) $V_{wind} = 5$ m/s, $H_s = 1.78$ m, $T_p = 6.26$ s, $\omega_0 = 1$ s^{-1}, $V_{curr} = 0.5$ m/s,

(*b*) $V_{wind} = 10$ m/s, $H_s = 3.21$ m, $T_p = 8.41$ s, $\omega_0 = 0.75$ s^{-1}, $V_{curr} = 0.5$ m/s,

(*c*) $V_{wind} = 15$ m/s, $H_s = 5.07$ m, $T_p = 10.56$ s, $\omega_0 = 0.59$ s^{-1}, $V_{curr} = 0.5$ m/s.

CURRICULUM VITAE

Short biography

Marko Valčić was born on 26 November 1976 in Zadar, Croatia, where he completed both elementary and secondary school, i.e. mathematics gymnasium "Franjo Petrić". Afterwards, he received the Dipl.Ing. (M.Eng.) and Ph.D. degrees in Marine engineering and Maritime transport technology from the Faculty of Maritime Studies, University of Rijeka, Croatia, in 2008 and 2015, respectively.

Currently, he is employed as an Assistant Professor at Department of Naval architecture and Ocean engineering, Faculty of Engineering, University of Rijeka, where he is teaching courses related to guidance and control of marine vehicles, marine and offshore operations, offshore structures and vessels, ship dynamics, seakeeping and manoeuvrability. He is also engaged as an external associate at the Faculty of Maritime Studies, University of Rijeka, where he is teaching courses related to decision support systems, guidance, navigation and control of marine vehicles, and computational data analysis with machine learning methods.

His research interests lie in the areas of marine hydrodynamics (environmental loads, vessel responses, ship speed loss estimation) and marine control systems (propulsion systems, dynamic positioning systems, guidance and navigational systems, autonomous navigation), green eco-friendly maritime transportation, decision support and knowledge-based systems, machine learning, computational intelligence, estimation and nonlinear optimization.

From 2015 to 2017, he was a visiting researcher at the Centre for Autonomous Marine Operations and Systems (AMOS), Department of Marine Technology, Norwegian University of Science and Technology (NTNU), Trondheim, Norway, and in 2018 at the Graduate School of Maritime Sciences, Faculty of Maritime Sciences, Kobe University, Kobe, Japan.

He has co-authored 1 university textbook, 1 book chapter and 37 research papers, 17 of which have been published in scientific journals and 20 in proceedings of international and national conferences. He was the editor of two conference proceedings and is the co-chair of the Baška GNSS Conference and Workshop on Smart Blue and Green Maritime Technologies. As a reviewer, he serves for the top international journals like Ocean Engineering, Applied Ocean Research, Applied Sciences, Mathematics, Energies, Journal of Navigation, etc., as well as for domestic journals like Brodogradnja, Transactions of FAMENA, Engineering Review, Scientific Journal of Maritime Research and Journal of Maritime and Transportation Sciences.

He is an expert user of MATLAB & Simulink software and various Kongsberg Maritime and Transas simulation systems. From a coding point of view, he programs at intermediate to expert level in MATLAB and Python programming languages, and at basic level in R, C/C++ and FORTRAN. From 2009, he is a full member of the international society IEEE (Oceanic Engineering, Computational Intelligence, Intelligent Transportation Systems).

Research projects

- Decision Support System for Green and Safe Ship Routing (Croatian Science Foundation, Researcher, 2019-2023)
- The Impact of Environmental Loads on the Characteristics of Dynamic Positioning Systems for Marine Vessels (University of Rijeka, Head researcher, 2018-2021)

- Uncertainties of Ship Speed Loss Evaluation under Real Weather Conditions (University of Rijeka, Researcher, 2018-2021)
- Energy Efficiency, Safety and Autonomy of Modern Marine Vessels (Faculty of Maritime Studies and University of Rijeka, Head researcher, 2017-2019)
- Greener Approach to Ship Design and Optimal Route Planning (Croatian Science Foundation, Researcher, 2014-2018)
- Numerical Modelling of Hydrodynamic Loads and Responses of Marine Structures (University of Rijeka, Researcher, 2014-2018)
- Information and Communication Technologies in ITS (University of Rijeka, Researcher, 2014-2018)
- Information-Communication Technologies in Smart Maritime Systems (Ministry of Science, Education and Sports in Croatia, Researcher, 2009-2013)

Selected publications

Book chapters

[1] **Valčić, M.**, Prpić-Oršić, J., Vučinić, D. (2020). *Application of Pattern Recognition Method for Estimating Wind Loads on Ships and Marine Objects*. In: Advances in Visualization and Optimization Techniques for Multidisciplinary Research, Trends in Modelling and Simulations for Engineering Applications, Eds. Vucinic, D., Rodrigues Leta, F., Janardhanan, S., Springer, Singapore. doi:10.1007/978-981-13-9806-3_5

Journal papers

[1] **Valčić, M.**, Prpić-Oršić, J. (2020). *Derivative Free Optimal Thrust Allocation in Ship Dynamic Positioning Based on Direct Search Algorithms*. TransNav – International Journal on Marine Navigation and Safety of Sea Transportation (accepted).

[2] Rudan, I., Frančić, V., **Valčić, M.**, Sumner, M. (2020). *Early Detection of Vessel Collision Situations in a VTS Area*. Transport (accepted). doi:10.3846/transport.2019.11464

[3] Prpić-Oršić, J., Sasa, K., **Valčić, M.**, Faltinsen, O.M. (2020). *Uncertainties of ship speed loss evaluation under real weather conditions*. Journal of offshore mechanics and arctic engineering - Transactions of the ASME, 142 (3), 031106, 5. doi:10.1115/1.4045790

[4] Sasa, K., Takeuchi, K., Chen, C., Faltinsen, O.M., Prpić-Oršić, J., **Valčić, M.**, Mrakovčić, T., Herai, N. (2019). *Evaluation of Speed Loss in Bulk Carriers with Actual Data from Rough Sea Voyages*. Ocean engineering, 187, pp. 1-19. doi:10.1016/j.oceaneng.2019.106162

[5] Brčić, D., Filjar, R., Kos, S., **Valčić, M.** (2019). *On Global Ionospheric Maps based winter-time GPS ionospheric delay with reference to the Klobuchar model: Case study of the Northern Adriatic*. Pomorstvo - Scientific journal of maritime research, 33 (2), pp. 210-221. doi:10.31217/p.33.2.11

[6] **Valčić, M.**, Prpić-Oršić, J., Vučinić, D. (2017). *Application of a pattern recognition method to estimate wind loads on ships and marine objects*. Materialwissenschaft und Werkstofftechnik, 48 (5), pp. 387-399. doi:10.1002/mawe.201700009

[7] **Valčić, M.**, Prpić-Oršić, J. (2016). *Hybrid method for estimating wind loads on ships based on elliptic Fourier analysis and radial basis neural networks*. Ocean engineering, 122, pp. 227-240. doi:10.1016/j.oceaneng.2016.06.031

[8] **Valčić, M.**, Dejhalla, R. (2015). *Neural Network Prediction of Open Water Characteristics of Ducted Propeller*. Journal of Maritime and Transportation Sciences, 49-50, pp. 101-115.

[9] **Valčić, M.**, Antonić, R., Tomas, V. (2011). *ANFIS Based Model for Ship Speed Prediction*. Brodogradnja, 62 (4), pp. 373-382.

[10] Komadina, P., Tomas, V., **Valčić, M.** (2011). *Combinatorial Neural Networks Based Model for Identification of Marine Steam Turbine Clustered Parameters*. Promet - Traffic & Transportation, 23 (1), pp. 1-9.

Conference papers

[1] **Valčić, M.**, Prpić-Oršić, J. (2019). *Derivative Free Optimal Thrust Allocation in Ship Dynamic Positioning Based on Direct Search Algorithms*. 13th International Conference on Marine Navigation and Safety of Sea Transportation - TransNav 2019, Gdynia, Poland.

[2] Šakan, D., Žuškin, S., **Valčić, M.**, Pavletić, D. (2019). *Challenges of adaptive coastal voyage planning*. In: Proceedings of the 13th Annual Baška GNSS Conference, Baška, Island of Krk, Croatia, pp. 87-106.

[3] Prpić-Oršić, J., Sasa, K., **Valčić; M.**, Faltinsen, O.M. (2018). *Uncertainties of Ship Speed Loss Evaluation under Real Weather Conditions.* In: Proceedings of the ASME 2018 37th International Conference on Ocean, Offshore and Arctic Engineering - OMAE 2018, Madrid, Spain.

[4] Braidotti, L., Prpić-Oršić, J., **Valčić, M.**, Trincas, G., Bucci, V. (2018). *Fuzzy Analytical Hierarchical Process to Assess Weights of Importance in Ship Operation Risk Assessment*. In: Proceedings of NAV 2018: 19th International Conference on Ship & Maritime Research - Technology and Science for the Ships of the Future, Trieste, Italy, pp. 88-96.

[5] **Valčić, M.**, Prpić-Oršić, J. (2017). *Forbidden zone handling in optimal thrust allocation of DP vessels*. In: Proceedings of the 17th International Congress of the International Maritime Association of the Mediterranean IMAM 2017 - Maritime Transportation and Harvesting of Sea Resources, Lisbon, Portugal, pp. 1043-1050.

[6] Prpić-Oršić, J., **Valčić, M.** (2016). *Sensitivity analysis of wind load estimation method based on elliptic Fourier descriptors*. In: Proceedings of the 3rd International Conference on Maritime Technology and Engineering (MARTECH 2016), Lisbon, Portugal, pp. 151-160.

[7] **Valčić, M.**, Prpić-Oršić, J. (2016). *The effect of forbidden zone handling on optimal thrust allocation*. In: Proceedings of the 22nd Symposium on Theory and Practice of Shipbuilding, In Memoriam prof. Leopold Sorta (SORTA 2016), Trogir, Croatia, pp. 163-173.

[8] **Valčić, M.**, Prpić-Oršić, J. (2015). *Wind load estimation method based on Elliptic Fourier Descriptors*. In: Proceedings of the 16th International Congress of the International Maritime Association of the Mediterranean IMAM 2015 - Towards Green Marine Technology and Transport, Pula, Croatia, pp. 883-890.

[9] Prpić-Oršić, J., Faltinsen, O.M., **Valčić, M.**, Vučinić, D. (2014). *Energy efficiency approach to ship design and route planning*. In: Proceedings of the 8th AIGE National Conference Reggio Emilia: Universita di Modena e Reggio Emilia, Modena, Italy.

[10] Nabergoj, R., Prpić-Oršić, J., **Valčić, M.** (2014). *Sensitivity of Thrust Efficiency Loss in Dynamic Positioning Predictions*. In: Proceedings of the 2nd International Symposium on Naval Architecture and Maritime INT-NAM 2014, Istanbul, Turkey, pp. 81-90.

[11] Prpić-Oršić, J., Faltinsen, O.M., **Valčić, M.** (2014). *Development Strategies for Greener Shipping*. In: Proceedings of ELMAR-2014, Zadar, Croatia, pp. 83-86.

[12] **Valčić, M.**, Prpić-Oršić, J., Nabergoj, R. (2014). *Impact of Thruster Interaction Effects on Optimal Thrust Allocation in Dynamic Positioning Systems*. In: Proceedings of the 21st Symposium on Theory and Practice of Shipbuilding, In Memoriam prof. Leopold Sorta (SORTA 2014), Baška, Island of Krk, Croatia, pp. 347-356.

[13] **Valčić, M.**, Dejhalla, R. (2014). *Determination of Hydrodynamic Characteristics of Ducted Propeller Using an Artificial Neural Network*. In: Proceedings of the 21st Symposium on Theory and Practice of Shipbuilding, In Memoriam prof. Leopold Sorta (SORTA 2014), Baška, Island of Krk, Croatia, pp. 357-368.